A new e^N database method for transition prediction

by

J.L. van Ingen
Emeritus professor of aerodynamics
Delft Aerospace
Faculty of Aerospace Engineering
Delft University of Technology

with contributions from
J. Bongers

Delft
September 2006

Preface

It is 50 years ago that the present author (van Ingen, 1956a,b, 📄)[1] and Smith and Gamberoni (Smith, 1956; Smith and Gamberoni, 1956) independently and simultaneously introduced their first versions of the e^9 (later e^N) method for the practical prediction of transition of incompressible two-dimensional boundary layers, based on linear stability theory. Over the last 50 years the method has proved its value and remained a useful tool in engineering aerodynamics. Because the present author's first publication, although still referenced in the literature, is not easily accessible anymore, and some other, older publications might still be of interest, it was decided to collect a series of these publications on a CD-ROM.

Different versions of the method have been used for airfoil design at the Low Speed Laboratory (LSL) of Delft Aerospace, notably by L.M.M. Boermans (Boermans) The close co-operation between design oriented engineers and students on the one hand and more fundamental boundary layer researchers at LSL on the other hand, has proved to be very fruitful over the years. The present author had the pleasure to be the Head of LSL for most of his working life at Delft Aerospace from 1952 (student-assistant) until 1997 (Dean). In this period it was shown that the e^N method could be applied successfully to two-dimensional boundary layers with pressure gradient including separation and suction. At the Delft Aerospace Low Speed Laboratory for a long time airfoil design has been performed using a computer program developed at LSL. This program included earlier versions of the present authors e^N method. More information on these earlier versions can be found in various reports on the CD-ROM. At present the group of Associate Professor L.M.M. Boermans employs Drela's XFOIL program. In this program the envelope version of the e^N method by Drela has been replaced by earlier versions of the present author's method.

Recently L.M.M. Boermans started work on the design of low-speed airfoils with laminarisation by suction, in first instance to be applied to sailplanes and general aviation aircraft. It was realized that the available e^N method, although capable of including the effect of suc-

---

[1]The icon depicted here and further on in the report can be used in the electronic version of the report to link directly to the corresponding article on the CD-ROM. Also all text in the electronic version of the report shown in blue links directly to the referred location in the report. In Acrobat Reader 8 or higher a toolbar called the "Navigation Toolbar" (see in the menu "View", then "Toolbars", and then "Navigation") can be used to have a "back" button available to return to the link in the report. For the bibliography such a feature is implemented by including linked pagenumbers (see, Bibliography) at which reference to the specific publication is given. Furthermore the CD-ROM includes a set of MATLAB programs and datafiles. One of these programs named "N_factor_show.m" is discussed in some detail in chapter 13. With this program the information given in the report can be supplemented.

tion, was in the first place aimed at calculating the amplification of unstable disturbances and predicting transition and less on the possible re-laminarisation that occurs for strong suction. Therefore prof. Boermans asked the present author to develop a new version of the method, better suited to design suction distributions. Stimulated by the presently available computational facilities, unimaginable 50 years ago, the present author agreed to take a fresh look at the method. The discussion in the present report is restricted to two-dimensional incompressible flow.

The later stages of the development of the new data base method have been done in the same period that the author assisted in the tutoring of Mr Jeroen Bongers during his Master Thesis work at the Delft Aerospace Low Speed Laboratory in the group of Prof. Boermans. The subject of the thesis was the implementation of the new data base method into the FORTRAN environment of the XFOIL program. In addition suction distributions had to be designed for the practical application to an ASW-28 standard class sailplane. While transferring the preliminary version of the new method into the XFOIL system, its handling and performance were thoroughly scrutinized by Jeroen Bongers which resulted in many suggestions for improvement. The great help this has provided to the author is gratefully acknowledged. Jeroen graduated from Delft University in August 2006 after his final examination on the thesis "Implementation of a new transition prediction method in XFOIL, *Predicting transition in suction boundary layers*" (Bongers, 2006, 🗐). The author is very pleased that both Jeroen Bongers and Prof. Boermans gave permission to include the Master Thesis on the CD-ROM, showing the possibilities for practical application of the new method. Jeroen has also been a great help during the preparation of the final text of the present report in LaTeX and the design and realisation of the CD-ROM.

The new database method was derived using a set of linear stability data that were published by Arnal, Arnal (1986). The author is indebted to Dr. Arnal for his permission to include these tables in the present digital form on the CD-ROM.

The author would be pleased to receive remarks, observed errors and suggestions for improvement by email at: prof.J.L.van.Ingen@planet.nl with a cc to B.W.vanOudheusden@TUDelft.nl. Information on possible further developments, correction of errors, answers to questions etc. will be made available at www.lr.tudelft.nl/aerodynamics/e-to-the-N

The developement of the new method was mostly done using the student version of MATLAB 5. The various splines therefore are in the MATLAB 5 format. These, however, are also accepted by MATLAB 7. Appendix A contains some information on how to translate these splines into other formats. Because the allowable array size in the student version of MATLAB is limited the "T_{ss}" splines had to be stored in "cell arrays".

List of Symbols

a	wave amplitude	[-]
a_0	wave amplitude at $x = x_0$ (spatial), or $t = t_0$ (temporal)	[-]
C_q	suction flow coefficient	[-]
c	airfoil chord	[m]
c	$= \frac{\omega}{\alpha}$	[-]
$c_{q_{red}}$	$10^4 \, C_q$	[-]
$\overline{c}$	$\frac{c}{U}$	[-]
F	$\frac{\omega \nu}{U^2}$	[-]
F_∞	$\frac{\omega \nu}{U_\infty^2}$	[-]
f	nondimensional streamfunction	[-]
H	shapefactor, $\frac{\delta^*}{\theta}$	[-]
l	$\frac{\tau_o \theta}{\mu U}$	[-]
M	$\frac{x}{U} \frac{dU}{dx}$	[-]
m_T	$\left(\frac{\partial^2 \bar{u}}{\partial \bar{y}^2} \right)_0$	[-]
N	amplification factor, envelope of all n	[-]
n	amplification factor for discrete frequencies	[-]
Re_c	Reynolds number with respect to chord length	[-]
Re_θ	Reynolds number with respect to momentum thickness	[-]
$Re_{\theta_{crit}}$	critical Reynolds number with respect to momentum thickness	[-]
r	$^{10}log(Re_\theta) - {}^{10}log(Re_{\theta_{crit}})$	[-]
r_{grid}	not equidistant grid of 59 points for $0 \le r \le 2.5$	[-]
r_{top}	r corresponding to T_{maxmax}	[-]
s	coordinate along (airfoil) surface	[m]
T	amplification of unstable disturbances (eq. 2.13)	[-]
T_{max}	maximum value of T at specific Re_θ	[-]
T_{maxmax}	global maximum value of T at specific $Re_{\theta_{crit}}$	[-]
Tu	Turbulence level	[%]
t_0	time at which a discrete frequency disturbance becomes unstable in the temporal mode	[-]
U	boundary layer edge velocity, parallel to surface	$\left[\frac{m}{s} \right]$
U_∞	freestream velocity	$\left[\frac{m}{s} \right]$
$\bar{U}$	$\frac{U}{U_\infty}$	[-]

u	tangential velocity in boundary layer	$\left[\frac{m}{s}\right]$
$\overline{u}$	$\frac{u}{U}$	[-]
v	normal velocity in boundary layer	$\left[\frac{m}{s}\right]$
v_0	normal velocity at the wall	$\left[\frac{m}{s}\right]$
x	distance along wall	[m]
x_0	wall coordinate at which a discrete frequency disturbance becomes unstable in the spatial mode	[-]
$\overline{x}$	$\frac{x}{c}$	[-]
y	distance normal to surface	[m]
$\overline{y}$	$\frac{y}{\theta}$	[-]

Greek symbols

α	$\alpha_r + i\alpha_i$	[-]
$-\alpha_i$	spatial growth rate of disturbances	[-]
α_r	wave number	[-]
β	Hartree shapefactor	[-]
β	$\beta_r + i\beta_i$	[-]
β_i	temporal growth rate of disturbances	[-]
β_r	frequency	[Hz]
δ	boundary layer thickness	[m]
δ	infinitesimal change	[-]
δ^*	displacement thickness of the boundary layer	[m]
η	nondimensionalized y-coordinate in boundary layer	[-]
θ	momentum loss thickness of the boundary layer	[m]
μ	viscosity	$[Pa \cdot s]$
ν	kinematic viscosity	$\left[\frac{m^2}{s}\right]$
ξ	nondimensionalized x-coordinate	[-]
ρ	(air) density	$\left[\frac{kg}{m^3}\right]$
σ_a	amplification factor (old notation for n)	[-]
τ	shear stress	[Pa]
τ_0	wall shear stress	[Pa]
ψ	streamfunction	[m s]
ω	frequency	[Hz]
$\overline{\omega}$	$= \left(\frac{\frac{\omega\theta}{U} - \frac{\omega\theta}{U}\,axis}{scale}\right)$ same as ω_{scaled}	[-]

Subscripts

0	at wall or at start of instability
∞	freestream
$axis$	position in $\frac{\omega\theta}{U}$ or F for "max"
c	chord
$crit$	instability point
i	i-th interval
j	j-th interval
max	local maximum at specific Re_θ
$maxmax$	global maximum
$scale$	frequency difference expressed in $\frac{\omega\theta}{U}$ between upper neutral curve and global maximum see figs. 2.3 - 2.5
ω_{scaled}	$= \left(\frac{\frac{\omega\theta}{U} - \frac{\omega\theta}{U}_{axis}}{scale} \right)$ same as $\overline{\omega}$
top	position of global maximum

Contents

List of Figures

List of Tables

Chapter 1

Introduction

The new data base method is based on a one parameter series of stability diagrams calculated by Arnal (Arnal, 1986). Scanned versions of the tables are provided on the CD-ROM (see appendix B). The velocity profiles used are 11 Hartree profiles as attached flow solutions of the Falkner-Skan equation for similar flows and 4 Stewartson second branch solutions of the Falkner-Skan equation for separated flow. All profiles are for zero suction. They will be characterized by the velocity profile shape parameter H. The Falkner-Skan equation and its solutions will be briefly discussed in chapter 3.

With strong suction H may assume values less than the Hartree stagnation point value (2.216); for instance the value 2 for the asymptotic suction profile. This specific boundary layer will be briefly discussed in section 3.2. It will be shown that the shape of the asymptotic suction profile is strongly related to the Hartree profiles. As will be shown in chapter 9 the stability diagram for the asymptotic suction profile can be estimated by extrapolation from that for the profiles used by Arnal. Hence it is easy to extend the stability data base to $H = 2$.

An important question to answer is whether the e^N method can be based on a one parameter family of stability diagrams only. Because in the literature there were no more extensive families of stability diagrams available, in earlier methods often the shape factor H has been used as a single parameter characterising all possible stability diagrams with and without suction. Chapter 4 of the present report will discuss this important aspect in some detail. It is concluded that also in the present fresh look it seems unavoidable and can even be recommended to use H as the basic parameter.

In chapter 5 a short study is made to see whether the asymptotic suction profile can be extrapolated from the Hartree profiles without suction.

The Arnal data will be analysed in detail in chapter 6. It will be shown that by proper scaling and shifting much of the variation with H can be removed from the stability diagrams. The resulting data base contains $15 \times 59 = 885$ splines representing 59 cross sections at constant values of $r = {}^{10}\log(Re_\theta) - {}^{10}\log(Re_{\theta_{crit}})$ (the "r_grid") for each of the 15 basic stability

diagrams; in total the database contains about 150,000 numbers.

Chapter 7 will give a comparison of stability diagrams according to the database with the original Arnal data.

It is shown in chapter 8 that the 6 scaled and shifted diagrams for $2.216 \leq H \leq 2.591$ (that is from stagnation point to flat plate boundary layer) are so very nearly equal that it can reasonably be assumed that the (scaled and shifted) diagram for the stagnation point flow is also applicable to the asymptotic suction profile. Chapter 9 will describe the estimation of the stability diagram for the asymptotic suction profile based on this assumption.

The most important element of the data base method is the MATLAB function cross_cut.m. This function generates the cross section at constant Re_θ for an arbitrary value of $^{10}log(Re_{\theta_{crit}})$ (hence an arbitrary value of the shape factor H). This function is described in some detail in chapter 10. A slightly altered, faster (but less accurate) version using some approximations is described in chapter 11.

The amplification of unstable disturbances can be calculated using the MATLAB m-file amplification.m; this function will be described in chapter 12. In various chapters of the present report the reader is referred to the MATLAB m-file "N_factor_show.m". This is a collection of MATLAB programs that are discussed in the text. By running these programs the information given in the text and the figures in the report can be supplemented. This program is discussed in chapter 13.

The necessary boundary layer calculations for some examples have been made by a finite difference method that was developed by the author (van Ingen, 1998,). A brief description is given in chapter 3.5.

Applications to airfoil design of the XFOIL (FORTRAN77) version of the present method can be consulted in the Master thesis of Jeroen Bongers *Implementation of a new transition prediction method in* XFOIL, *Predicting transition in suction boundary layers* ( )

The work described in the present report has been performed by the author on his home PC after his formal retirement from Delft Aerospace. All computations were done using the Student Version 5 of MATLAB. All relevant MATLAB m-files and the data files are mentioned in Appendix B and C respectively and provided on the present CD-ROM. All splines are in the format of the MATLAB 5 student version. For easy translation to other formats a translation procedure is described in appendix A.

Chapter 2

Basics of linear stability theory and the e^N method

The stability theory considers a given laminar main flow upon which small disturbances are superimposed. The present report will discuss only two-dimensional incompressible flow. To simplify the problem the boundary layer is locally approximated by a parallel flow with constant velocity profile (shape and thickness) in downstream direction. It is assumed that both the undisturbed and the disturbed flow satisfy the Navier-Stokes equations. The disturbance is assumed to be two-dimensional because it can be shown that the onset of instability is determined by the two-dimensional disturbances and not by the three-dimensional ones, which of course may also occur (Schlichting, 1978, chapter XVI) A suitable more recent textbook is White (2006). An extensive modern treatment of stability theory can be found in Schmid and Henningson (2000).

After linearization and non-dimensionalising, assuming small disturbances, the following Orr-Sommerfeld equation is obtained. (primes denote differentation w.r.t. $\overline{y}$)

$$(\overline{u} - \overline{c})(\phi'' - \alpha^2 \phi) - \overline{u}''\phi = \frac{-i}{\alpha Re} \left[\phi'''' - 2\alpha^2 \phi'' + \alpha^4 \phi \right] \tag{2.1}$$

This homogeneous linear equation in the disturbance amplitude function ϕ of course has the trivial zero solution representing the original undisturbed flow. The resulting eigenvalue problem may under certain circumstances also possess unstable solutions. A more detailed description of the derivation of the Orr-Sommerfeld equation can be consulted in (van Ingen, 1965, 📄) and the books mentioned above. Note that the velocity profile and its curvature play a prominent role in the equation. Since the curvature of the velocity profile is influenced by pressure gradient, suction and blowing, heating and cooling at the wall, etc. these factors have a strong influence on the solutions of the Orr-Sommerfeld equation and therefore on boundary layer stability. Furthermore the Reynolds number and the frequency of the imposed disturbances are found to be very important.

In the present report we will only discuss the effects of pressure gradient and suction/blowing at the wall.

In the derivation of the Orr-Sommerfeld equation a disturbance stream function ψ is defined as:

$$\psi(y) = \phi(y)e^{i(\alpha x - \omega t)} \tag{2.2}$$

In the so-called spatial mode of the stability analysis we take the circular frequency ω to be real and the wave number α to be complex. Also ϕ and ψ are complex but in the present report we will only need to specify α.

$$\alpha = \alpha_r + i\alpha_i \tag{2.3}$$

and:

$$c = \frac{\omega}{\alpha} \tag{2.4}$$

Introducing (2.3) into (2.2) leads to:

$$\psi(y) = \phi(y)e^{-\alpha_i x}e^{i(\alpha_r x - \omega t)} \tag{2.5}$$

It follows from (2.5) that disturbances grow, remain constant or decrease with x for $\alpha_i < 0, = 0$ and > 0 respectively, meaning that the given flow is unstable, neutral or stable against the given disturbance. Which case occurs depends on the shape of the velocity profile, the frequency and the Reynolds number Re_θ.

The results of stability calculations are normally presented in a "stability diagram" (fig. 2.1). Below the so-called critical Reynolds number $Re_{\theta_{crit}}$ the boundary layer is stable to small disturbances of all frequencies. At higher Reynolds numbers there is a range of frequencies for which instability occurs. As can be seen from equation (2.5) the rate of amplification or damping is determined by $-\alpha_i$. From numerical computations it is found that the shape of the stability diagram is strongly dependent upon the shape of the velocity profile (fig. 2.2). For a convex profile, such as occurs for a "favourable" pressure gradient near the leading edge of an airfoil the critical Reynolds number is high (type (b)). For a concave profile such as occurs for increasing pressure in downstream direction the critical Reynolds number is low(type (a)). Moreover for type (b) near a stagnation point the rate of amplification is orders of magnitude smaller than for type (a) near separation. Figures 2.3, 2.4 and 2.5 show as examples the neutral curves according to Arnal and the database representation for $\beta = 1$ (stagnation point), $\beta = 0$ (flat plate) and $\beta = -0.198838$ (separation). For $\beta \geq 0$ we have type (b) diagrams, for $\beta < 0$ type (a) diagrams occur. The effects of suction or blowing are similar to those for favourable and adverse pressure gradients respectively.

For the flow over an airfoil both the thickness of the boundary layer and its velocity profile shape may change in streamwise direction. Therefore, strictly speaking, the stability theory as developed for a parallel flow is not applicable. It has been shown however that the local stability can be determined with sufficient accuracy from the results of the Orr-Sommerfeld equation for the local profile. For each x-station then a cross section through the stability diagram should be computed for the local velocity profile and Reynolds number Re_θ.

Since even in the present computer era the numerical solution of the Orr-Sommerfeld equation is rather involved, it is customary for design computations to use a set of pre-computed results for a series of boundary layer velocity profiles. In general the Hartree and Stewartson solutions
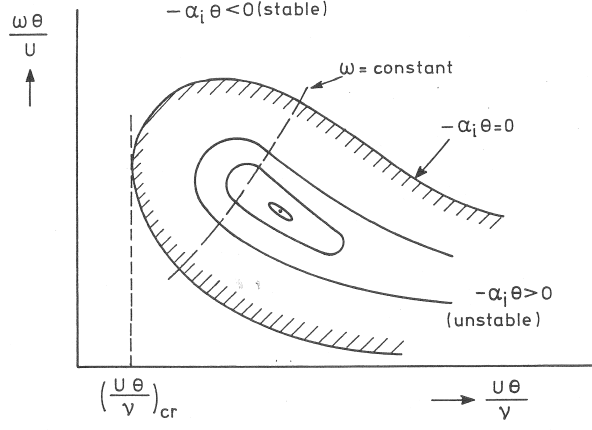
Figure 2.1: Principle of the stability diagram
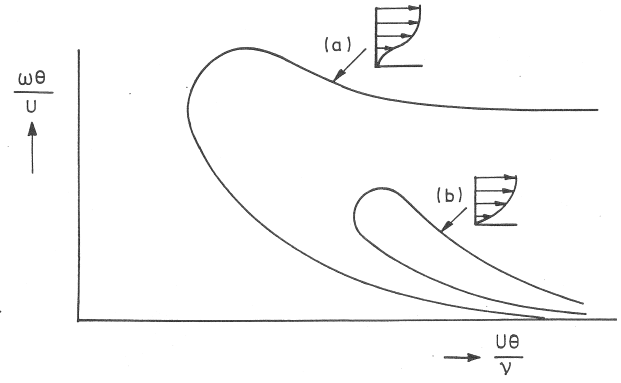
Figure 2.2: Type (a) and type (b) stability diagrams
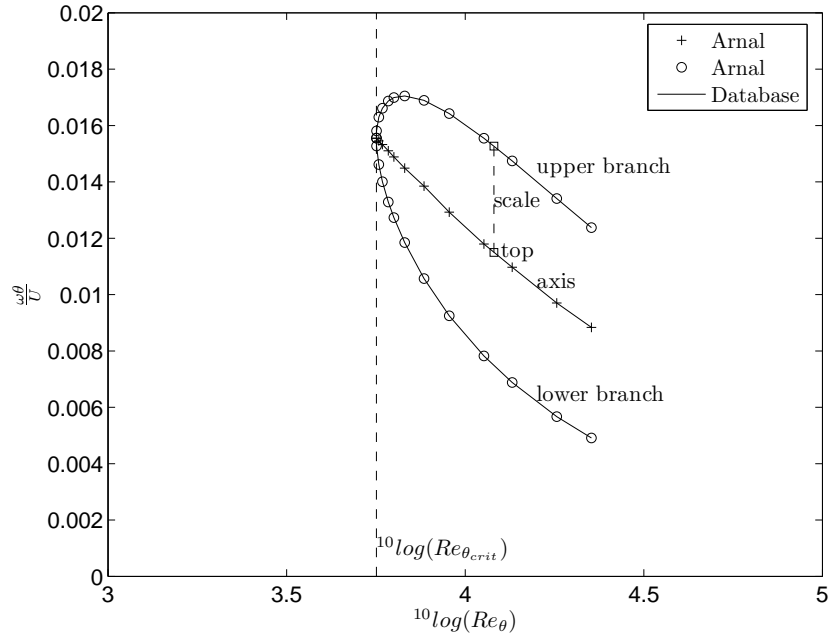
Figure 2.3: Neutral curve for $\beta = 1$ (stagnation point)
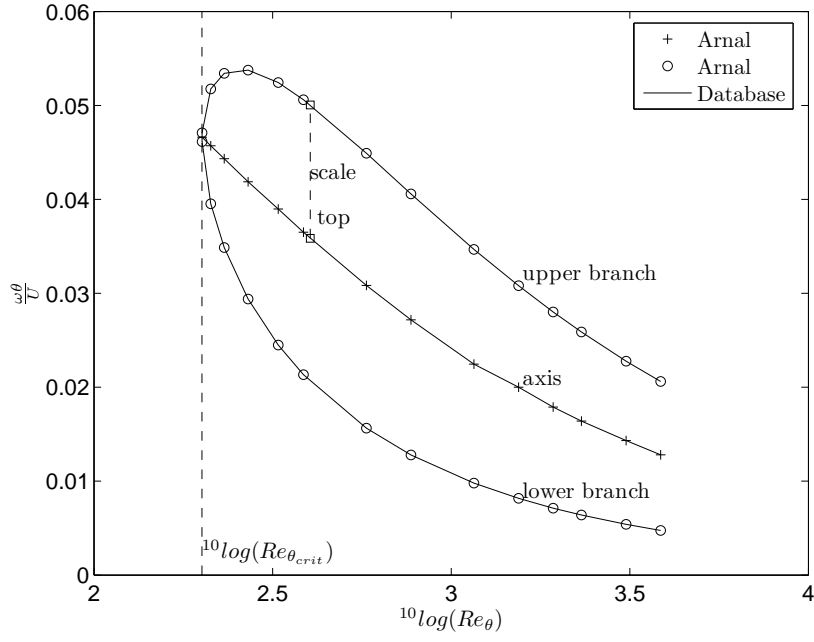
Figure 2.4: Neutral curve for $\beta = 0$ (flat plate)
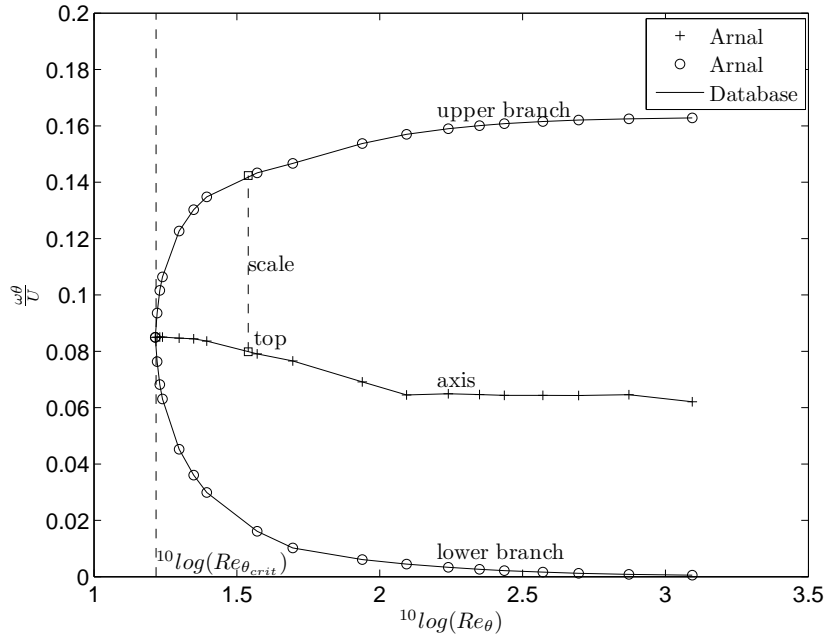
Figure 2.5: Neutral curve for $\beta = -0.198838$ (separation)

of the Falkner-Skan equation are used for this purpose (see section 3.4). The solutions that will be used in this report are for zero suction/blowing. In chapter 4 we will argue that they also may, with some confidence, be applied to suction cases. Fig. 2.6 shows a typical distribution of Re_θ and $Re_{\theta_{crit}}$ over an airfoil. The intersection of these two curves gives the instability point, downstream of which for certain frequencies the amplitude will start growing. Provided that stability diagrams are available for a sufficient number of streamwise
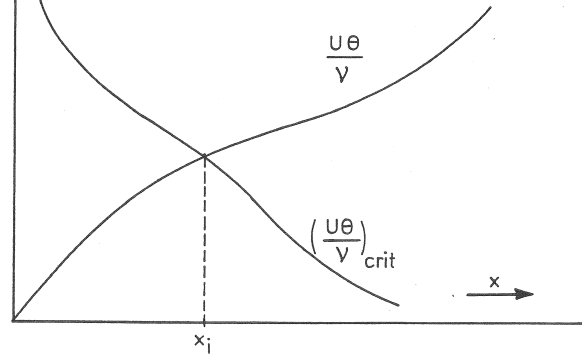
Figure 2.6: Typical $^{10}log(Re_\theta)$ and $^{10}log(Re_{\theta_{crit}})$ distribution over an airfoil

x-stations the amplitude a of the disturbance can be computed as a function of x. Using equation (2.5) it follows that the ratio of the amplitudes a and $a + da$ at x and $x + dx$ is given by

$$\frac{a + da}{a} = \frac{e^{-\alpha_i(x+dx)}}{e^{-\alpha_i x}} = e^{-\alpha_i dx} \tag{2.6}$$

or

$$ln(a + da) - ln(a) = -\alpha_i dx \tag{2.7}$$

$$d\left(ln(a)\right) = -\alpha_i dx \tag{2.8}$$

and after integration

$$n = ln\left(\frac{a}{a_0}\right) = \int_{x_0}^{x} -\alpha_i dx \tag{2.9}$$

where x_0 is the station where the disturbance with frequency ω and amplitude a_0 first becomes unstable. The quantity

$$n = ln\left(\frac{a}{a_0}\right) \tag{2.10}$$

will be denoted by "amplification factor" while $-\alpha_i$ is the "amplification rate" Then e^n gives the "amplification ratio". In applications we will write equation (2.10) as follows:

$$n(x,\omega) = \int_{x_0}^{x} -\alpha_i dx \tag{2.11}$$

$$n(x,\omega) = 10^{-6} \cdot \frac{U_\infty c}{\nu} \int_{\bar{x}_0}^{\bar{x}} 10^6 \cdot \frac{-\alpha_i \theta}{Re_\theta} \frac{U}{U_\infty} d\left(\frac{x}{c}\right) \tag{2.12}$$

Or denoting by T:

$$T = 10^6 \cdot \frac{-\alpha_i \theta}{Re_\theta} \tag{2.13}$$

and

$$\overline{x} = \frac{x}{c}; \qquad \overline{U} = \frac{U}{U_\infty}; \qquad Re_c = \frac{U_\infty c}{\nu}; \qquad Re_{c_{reduced}} = 10^{-6} \cdot \frac{U_\infty c}{\nu} \tag{2.14}$$

$$n(x,\omega) = Re_{c_{reduced}} \int_{\overline{x}_0}^{\overline{x}} T\overline{U} d\overline{x} \tag{2.15}$$

The factors 10^6 and 10^{-6} have been introduced for convenience.

If we calculate n as a function of x for a range of frequencies we get a set of n-curves as illustrated in fig. 2.7; the envelope of these curves gives the maximum amplification factor N which occurs at any x.
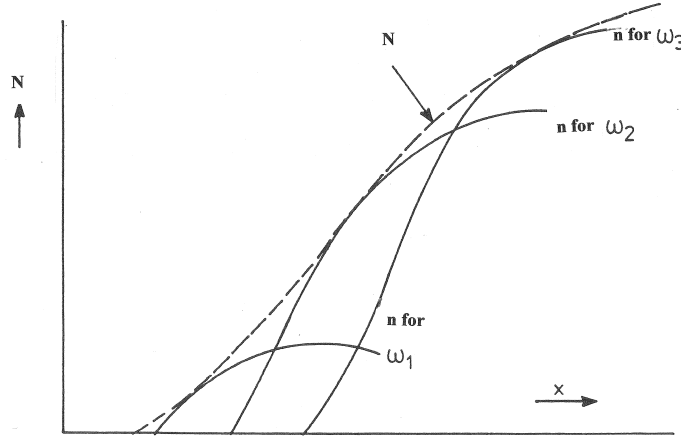
Figure 2.7: N-factor

Figure 2.8 shows as an example the n-factor calculation for the flat plate without suction using the database developed in later chapters. From the famous Schubauer and Skramstad experiment (figure 2.9) it follows that at low turbulence levels a transition region is found that extends from $Re_x = 2.8 \cdot 10^6$ to $Re_x = 3.9 \cdot 10^6$. From figure 2.8 it follows that at these Reynolds numbers N-factors of $N_1 = 8.22$ respectively $N_2 = 10.30$ are calculated. Van Ingen (van Ingen, 1956a, 🗎) found values for N_1 and N_2 of 7.8 and 10 respectively using the Pretsch stability diagrams. For airfoils the N-vs-x curve is rather steep near transition so that in those cases a transition <u>point</u> can be defined rather than a transition <u>region</u>. In their first version of the e^N-method Smith and Gamberoni (Smith and Gamberoni, 1956) concluded from a series of experimental results for airfoils that an N-factor of 9 very well correlated the experiments. It is in fact remarkable that after 50 years the calculated critical N-factor has remained nearly the same despite the availability of more accurate stability diagrams.

If the value $N = 9$ is assumed to be universally valid, we can "predict" transition for a new case by assuming that transition occurs as soon as the calculated N-factor has reached the value of 9. Later it has been shown by Van Ingen that the method is also valid for boundary
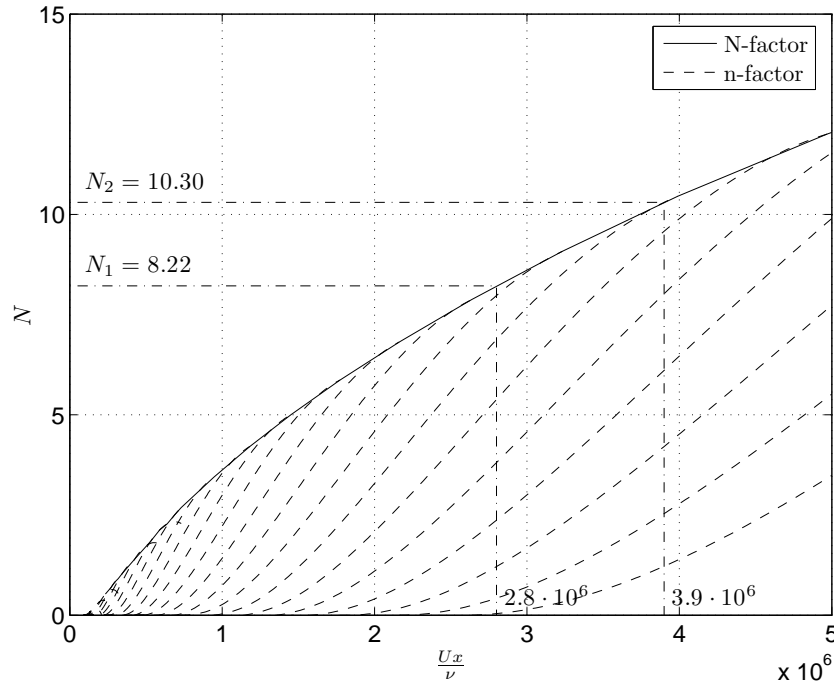
Figure 2.8: N-factor for flat plate
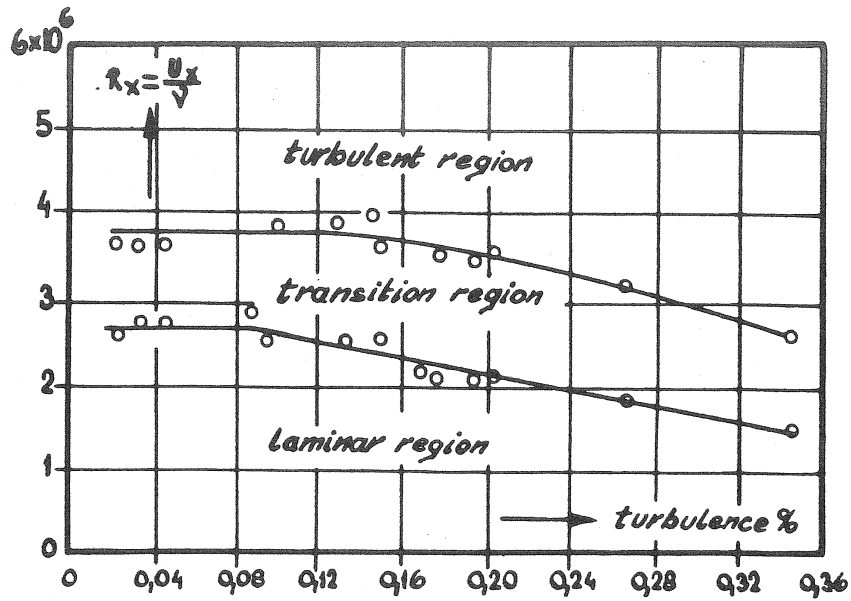
Figure 2.9: Influence of Tu on Reynolds number for transition on a flat plate according to Schubauer and Skramstad

layers with suction and for laminar separation bubbles. (See: (van Ingen, 1965, 📄), (van Ingen, 1977, 📄), (van Ingen, 1978, 📄), and (van Ingen, 1990, 📄)). Since suction makes the velocity profile more convex it increases stability and hence decreases the N-factor and thus

delays transition.

Further research has shown that the critical amplification factor N_{crit} depends on the free stream disturbances (level as well as spectrum) Therefore the method is now known as the e^N method for transition prediction. The critical N-factor has thus become a measure for the quality of a wind tunnel or for the atmospheric circumstances in free flight. From a series of measurements on flat plates, known from the literature, the transition position on the flat plate can be related to the turbulence level in the wind tunnel. Using these results and the calculated N-factors for the flat plate, the critical N factor for beginning and end of the transition region was made a function of the "effective turbulence level" Tu in %. (See figure 2.10, and (van Ingen, 1977, 📄)) For $Tu > 0.1\%$ the following relations can be used:

$$N_1 = 2.13 - 6.18^{10}log(Tu) \tag{2.16}$$
$$N_2 = 5.00 - 6.18^{10}log(Tu) \tag{2.17}$$

For values of $Tu < 0.1\%$ there is much scatter because in this region sound disturbances may become the factor controlling transition rather than turbulence. We may also use relations 2.16 and 2.17 for $Tu < 0.1\%$, but then we should define an "effective" value for Tu.

As far as the author can remember the history behind 2.16 and 2.17 is as follows. Eq. 2.16 was derived by the author around 1975 from a collection of published measurements on transition on flat plates with different free stream turbulence levels. These data included some tabular values taken from a paper by Mack (probably Mack (1975)). The N_2 curve was just made parallel to that for N_1. Later Mack himself has published the following equation:

$$N = -8.43 - 2.4ln(T) \tag{2.18}$$

Note that while our Tu is in % and we use ^{10}log, Mack uses T in absolute value and the natural logarithm. But in fact 2.16 for N_1 and 2.18 are very nearly equal, because they are based on essentially the same data. See also Mack (1977), Mack (1978) and Mack (1984).

Note that the turbulence level alone is not a sufficient characterization of the disturbance environment in a wind tunnel or in free flight. From stability theory it is known that the frequency spectrum of the disturbances should be taken into account. Therefore the critical N-factor for a certain disturbance environment, such as in a wind tunnel, can be determined only from an experiment in that facility. Since most modern low speed, low turbulence wind tunnels have been built after the same recipe they tend to have comparable critical N-factors.

The question should be asked why the e^N method has enjoyed so much success in the last 50 years. The theory used is a linear one while it is clear that transition to turbulence itself is a highly non-linear phenomenon. It should be observed however that the method is only used to "predict" the position of transition and not the physical transition process itself. From experiments it is known that the initial disturbances in low turbulence wind tunnels are so low that up to an N-factor of 7 the linear theory gives a good description of the disturbance development (Obremski et al., 1969), see also the paper by Wubben, Passchier and Van Ingen (1989) (Wubben et al., 1989, 📄). Hence extrapolation is only needed from N=7 to N=9 to "predict" the transition position.
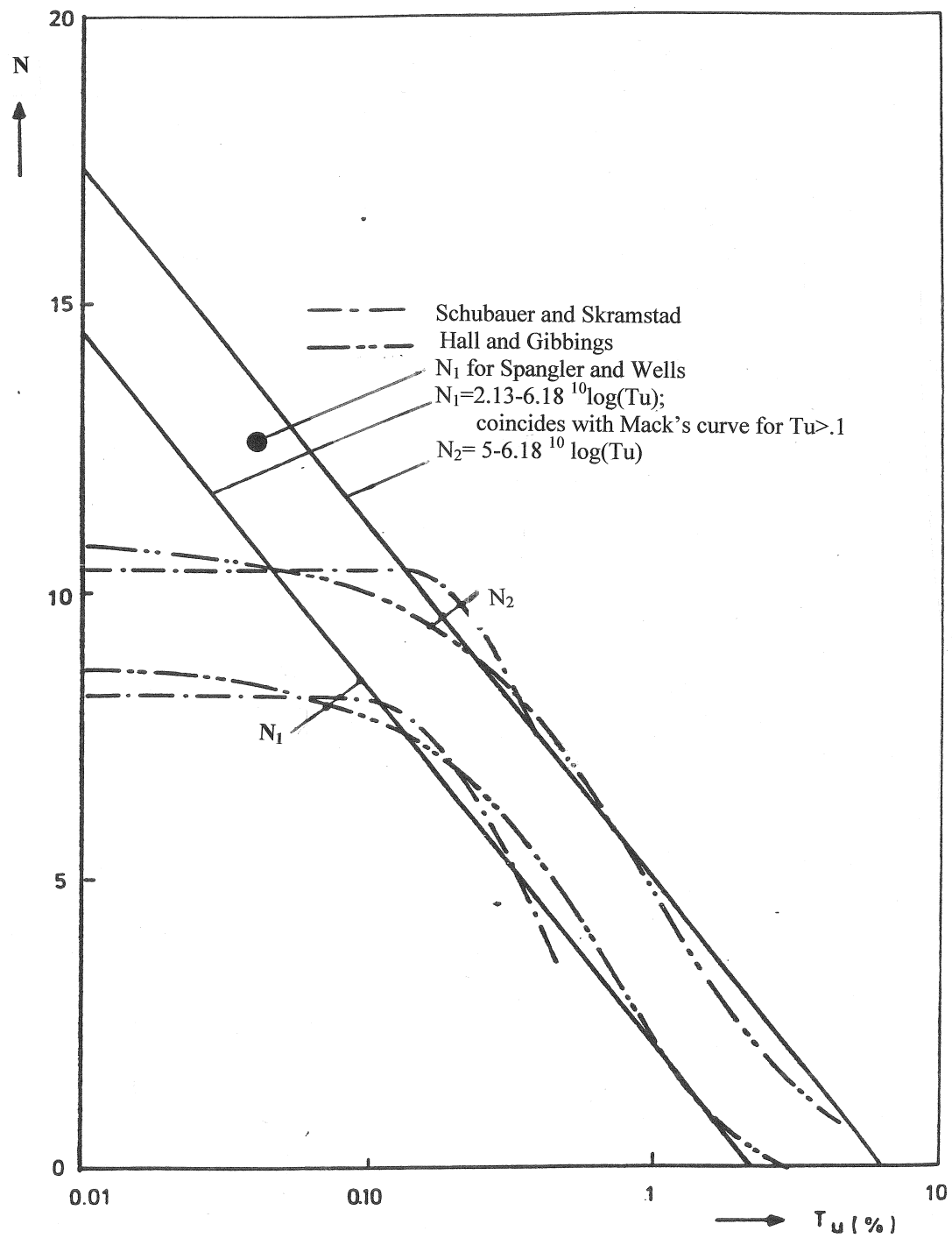
Figure 2.10: N-factor for various flat plate experiments

Chapter 3

Laminar boundary layers for two-dimensional incompressible flow

3.1 The laminar boundary layer equations

The laminar boundary layer equations can be derived from the Navier-Stokes equations under the assumption that the boundary layer thickness δ is small w.r.t. a typical length coordinate (say the chord of an airfoil). As long as δ is also small w.r.t. the radius of curvature (r) of the surface and moreover $\frac{dr}{dx}$ remains small, the resulting equations are equally valid for flat and curved surfaces. We will restrict our discussion to steady, laminar, two-dimensional, incompressible flows. Then we have the following equation (Schlichting, 1978, chapter VII):

$$u\frac{\partial u}{\partial x} + v\frac{\partial u}{\partial y} = -\frac{1}{\rho}\frac{dp}{dx} + \nu\frac{\partial^2 u}{\partial y^2} \tag{3.1}$$

Also the continuity equation should be satisfied:

$$\frac{\partial u}{\partial x} + \frac{\partial v}{\partial y} = 0 \tag{3.2}$$

The pressure is, in this approximation, constant across the boundary layer and satisfies the Bernoulli equation outside the boundary layer.

$$p + \frac{1}{2}\rho U^2 = constant \tag{3.3}$$

or

$$-\frac{1}{\rho}\frac{dp}{dx} = U\frac{dU}{dx} \tag{3.4}$$

When calculating the boundary layer, $p(x)$ is assumed to be known from experiment or a potential flow calculation, sometimes including the influence of the displacement effect of the boundary layer on the pressure distribution through "weak" or "strong" interaction. The development of the boundary layer depends to a large extent on the pressure gradient and

the amount of suction or blowing. Boundary conditions for (3.1) and (3.2) are (subscript zero always denotes values at the wall, $y = 0$):

$$y \quad = \quad 0 \qquad u = 0 \qquad v = v_0 \quad (v_0 < 0 \; for \; suction) \tag{3.5}$$

$$y \quad \rightarrow \quad \infty \qquad u \rightarrow U(x) \tag{3.6}$$

Furthermore a velocity profile should be known at some starting position x_0. For porous walls $v_0 \neq 0$; $v_0 > 0$ gives blowing, $v_0 < 0$ gives suction. Note that by keeping $u(0) = 0$ it is implied that suction is applied normal to the wall. This is strictly speaking not necessary. One could imagine a suction surface with oblique suction. However, we will conform to the usual assumption of "normal to the wall suction". It should be observed that $y \rightarrow \infty$ in (3.6) is only related to the thin boundary layer; for the outer flow the "edge of the boundary layer" is still very near to the wall. Using (3.1) and (3.5) it follows that at the wall the curvature of the velocity profile is determined by the pressure gradient and v_0 via the so called "first compatibility condition":

$$v_0 \left(\frac{\partial u}{\partial y} \right)_0 = -\frac{1}{\rho} \frac{dp}{dx} + \nu \left(\frac{\partial^2 u}{\partial y^2} \right)_0 = U \frac{dU}{dx} + \nu \left(\frac{\partial^2 u}{\partial y^2} \right)_0 \tag{3.7}$$

Hence for the no suction case, when the pressure decreases in stream wise direction (as on the forward part of an airfoil), the velocity profile is convex near the wall. With increasing pressure the profile is concave near the wall. At zero pressure gradient the profile is straight near the wall. Suction ($v_0 < 0$) has the same effect as a "favourable pressure gradient" ($\frac{dp}{dx} < 0$). This determines the effect of pressure gradient and suction on stability and hence on transition. From chapter 2 we know that convex velocity profiles have a much greater stability than concave profiles and hence tend to delay transition. Similar effects are due to heating and cooling at the wall. In air, cooling the wall is stabilising while in water it is destabilising (Wazzan et al., 1981). The effects of heating and cooling will not be discussed in the present report.

If we first differentiate (3.1) w.r.t. y and use (3.2) and (3.5), we find the "second compatibility condition":

$$v_0 \left(\frac{\partial^2 u}{\partial y^2} \right)_0 = \nu \left(\frac{\partial^3 u}{\partial y^3} \right)_0 \tag{3.8}$$

Note that for $v_0 = 0$ the third derivative of u w.r.t. y at the wall is zero, independent of the pressure gradient.

The velocity $u(y)$ tends to the value U only asymptotically; therefore the definition of the boundary layer thickness δ is rather arbitrary. Two well-defined thickness parameters are the displacement thickness:

$$\delta^* = \int_0^\infty \left(1 - \frac{u}{U} \right) dy \tag{3.9}$$

and the momentum loss thickness:

$$\theta = \int_0^\infty \frac{u}{U} \left(1 - \frac{u}{U} \right) dy \tag{3.10}$$

It can be shown that δ^* is related to the outward displacement of the streamlines due to viscosity. An improved pressure distribution is obtained from an inviscid flow calculation for a corrected body where a thickness δ^* is added to the contour (so called "weak interaction"). This method fails at separation; there a more involved procedure is necessary ("strong interaction").

Some more parameters, to be used in later sections, will be defined here.

The "shape factor":

$$H = \frac{\delta^*}{\theta} \qquad (3.11)$$

For the asymptotic suction profile (see chapter 3.2) the very low value of $H = 2$ is obtained. For the stagnation point $H = 2.216$; for the flat plate $H = 2.591$; at separation H assumes a value of about 4 and for velocity profiles downstream of separation H can reach values as high as 35.

The wall shear stress follows from:

$$\tau_0 = \mu \left(\frac{\partial u}{\partial y} \right)_0 \qquad (3.12)$$

A very often used non-dimensional form is

$$\ell = \frac{\tau_0 \theta}{\mu U} = \left(\frac{\partial \overline{u}}{\partial \overline{y}} \right)_0 \qquad (3.13)$$

where $\overline{u} = \frac{u}{U}$ and $\overline{y} = \frac{y}{\theta}$. The non-dimensional curvature of the velocity profile at the wall will be denoted by:

$$m_T = \left(\frac{\partial^2 \overline{u}}{\partial \overline{y}^2} \right)_0 \qquad (3.14)$$

The subscript T refers to Thwaites who first introduced ℓ and m_T as parameters to characterise laminar boundary layers. The non-dimensional pressure gradient will be denoted by the Pohlhausen parameter

$$K = \frac{\theta^2}{\nu} \frac{dU}{dx} \qquad (3.15)$$

For a non-dimensional suction parameter we will use

$$w = \frac{v_0 \theta}{\nu} \qquad (3.16)$$

Using these notations the first compatibility condition (3.7) can be rewritten as:

$$\frac{v_0 \theta}{\nu} \left(\frac{\partial \overline{u}}{\partial \overline{y}} \right)_0 = \frac{\theta^2}{\nu} \frac{dU}{dx} + \left(\frac{\partial^2 \overline{u}}{\partial \overline{y}^2} \right)_0 \qquad (3.17)$$

or:

$$m_T = w\ell - K \qquad (3.18)$$

The second compatibility condition (3.8) can now be rewritten as:

$$w \left(\frac{\partial^2 \overline{u}}{\partial \overline{y}^2} \right)_0 = \left(\frac{\partial^3 \overline{u}}{\partial \overline{y}^3} \right)_0 \qquad (3.19)$$

From (3.18) it can be seen that the curvature at the wall (m_T) can be influenced by the pressure gradient and suction/blowing. In chapter 4 we will introduce the assumption that pressure gradient and suction/blowing are to a large extent interchangeable so that stability diagrams calculated for velocity profiles at zero suction but with pressure gradient can be applied to the case of suction.

For special forms of the function $U(x)$ the set of partial differential equations (3.1) and (3.2) can be reduced to an ordinary differential equation. The resulting velocity profiles at all values of x are similar in shape. Some of these similar solutions will be discussed in sections 3.3 and 3.4. For other, more general functions $U(x)$ in the pre-computer era we had to use approximate "integral relation methods" to be able to design airfoils. (see e.g. (Schlichting, 1978), (Rosenhead, 1961), XFOIL (Drela, 1989), and (van Ingen, 1965, 🖹, 🖹, 🖹). We will not discuss these methods here. For some of the examples to be discussed in chapter 12 we will use a finite difference method developed by the author. A brief description will be given in section 3.5, an introduction to this method can be found in (van Ingen, 1998, 🖹).

3.2   The asymptotic suction boundary layer

A simple exact analytical solution of the boundary layer equations (in fact also of the full Navier-Stokes equations) is given by the "asymptotic suction boundary layer" (Meredith and Griffith, 1936), (Rosenhead, 1961). This solution is found for $x \to \infty$ on a flat plate with constant suction velocity v_0. The development of this asymptotic solution from $x = 0$ was already given by (Iglish, 1944). The Iglisch solution will be discussed in chapter 12; See also (van Ingen, 1965, 🖹) The asymptotic solution follows easily from (3.1) and (3.2) by stating that for $x \to \infty$ the boundary layer may be assumed to have a constant thickness and a constant velocity profile. From equation (3.2) then follows, with $\frac{\partial u}{\partial x} = 0$:

$$\frac{\partial v}{\partial y} = 0 \tag{3.20}$$

and since v_0 (v at the wall) is taken constant for all x it follows that $v = constant = v_0$ throughout the whole boundary layer. Then the boundary layer equation (3.1) simplifies to the following ordinary linear differential equation

$$v_0 \frac{\partial u}{\partial y} = \nu \frac{\partial^2 u}{\partial y^2} \tag{3.21}$$

The exact solution of (3.21) satisfying the boundary conditions (3.5) and (3.6) is easily found to be

$$\frac{u}{U} = 1 - e^{\left(\frac{v_0 y}{\nu}\right)} \tag{3.22}$$

Note that the boundary condition at $y \to \infty$ can only be satisfied for $v_0 < 0$, that is for suction. From (3.22) and the definitions (3.9), (3.10) and (3.11) for δ^*, θ and H it follows that:

$$-\frac{v_0 \delta^*}{\nu} = 1 \qquad -\frac{v_0 \theta}{\nu} = 0.5 \qquad H = \frac{\delta^*}{\theta} = 2 \tag{3.23}$$

That $H = 2$ means that the velocity profile for the asymptotic suction profile is much more convex and hence much more stable than the stagnation point profile without suction. A complete stability diagram for the asymptotic suction profile is not known to the author. Therefore we will, in chapter 9, "compose" such a diagram through extrapolation from the stagnation point diagram.

3.3   The laminar boundary layer on a flat plate

Another relatively simple solution of the boundary layer equations is provided by the case of a thin flat plate placed in the direction of a parallel flow with constant velocity U. The first potential flow approximation for the velocity outside the boundary layer is $U = constant$ and hence $\frac{dp}{dx} = 0$. Then (3.1) reduces to:

$$u\frac{\partial u}{\partial x} + v\frac{\partial u}{\partial y} = \nu\frac{\partial^2 u}{\partial y^2} \tag{3.24}$$

And the continuity equation remains:

$$\frac{\partial u}{\partial x} + \frac{\partial v}{\partial y} = 0 \tag{3.25}$$

The boundary conditions for zero suction then are:

$$y \quad = \quad 0 \qquad u = 0 \qquad v = 0 \tag{3.26}$$
$$y \quad \to \quad \infty \qquad u \to U \tag{3.27}$$

The equations (3.24) and (3.25) form a set of partial differential equations. The solution becomes relatively easy through the principle of "similarity" which means that we look for a solution where the velocity $u(y)$ can be made independent of x by introducing a properly scaled new variable η in y-direction. After introducing a stream function, the equations (3.24) and (3.25) can then be reduced to one ordinary differential equation. (For details see (Schlichting, 1978, chapter VII); we will here only present the main features of this problem.) The appropriate new variable η is:

$$\eta = \frac{y}{x}\sqrt{\frac{Ux}{\nu}} \tag{3.28}$$

A suitable expression for a non-dimensional stream function ψ is:

$$\psi = \sqrt{\nu x U}f(\eta) \tag{3.29}$$

With

$$u = \frac{\partial\psi}{\partial y} \qquad v = -\frac{\partial\psi}{\partial x} \tag{3.30}$$

it follows that

$$\frac{u}{U} \quad = \quad f'(\eta) \tag{3.31}$$

$$v \quad = \quad \frac{1}{2}\sqrt{\frac{\nu U}{x}}(\eta f' - f) \tag{3.32}$$

where primes denote differentiation w.r.t η. Introducing these new variables leads to the well-known Blasius equation

$$f''' + \frac{1}{2}f f'' = 0 \tag{3.33}$$

The corresponding boundary conditions are:

$$\eta = 0 \qquad f(\eta) = 0 \qquad f'(\eta) = 0 \tag{3.34}$$
$$\eta \to \infty \qquad\qquad\qquad f'(\eta) \to 1 \tag{3.35}$$

For suction or blowing $f(0)$ will be $\neq 0$. It should be observed that (3.33) is indeed a (non-linear) ordinary differential equation for $f(\eta)$. Since the boundary conditions (3.34) and (3.35) are given at two sides of an infinitely long interval a special procedure is needed to solve the equation. The boundary condition at infinity may be transferred to a finite but sufficiently large distance δ from the wall. Using a finite difference method this boundary condition is satisfied simultaneously with that at $\eta = 0$. The so-called "shooting method" transforms the problem into an initial value problem by assuming an additional boundary condition at the wall; for instance guessing a value for $f''(0)$ and iterating this value until the boundary condition at $\eta = \delta$ is also satisfied. Since the Blasius equation (3.33) can easily be differentiated a number of times it is easy to develop a Taylor series method for the shooting procedure. The results for the Blasius equation and the Falkner-Skan equation (to be discussed in section 3.4) were obtained by a Taylor series method of order h^8 (with steplength h). Note that the customary Runge-Kutta method is equivalent to a Taylor series developement of order h^4. The velocity profile follows from equation (3.31) Resulting values for δ^*, θ and H are:

$$\frac{\delta^*}{x}\sqrt{\frac{Ux}{\nu}} = 1.7208 \qquad \frac{\theta}{x}\sqrt{\frac{Ux}{\nu}} = 0.6641 \qquad H = \frac{\delta^*}{\theta} = 2.591 \tag{3.36}$$

3.4   The Hartree and Stewartson similar solutions of the Falkner-Skan equation

It can be shown that similar solutions are also possible for the more general flow

$$U = u_1 x^M \tag{3.37}$$

where u_1 and M are constants. This flow occurs near the apex of a wedge with angle $\pi\beta$, where

$$\beta = \frac{2M}{M+1} \tag{3.38}$$

It should be observed that the flat plate flow, discussed in section 3.3, is obtained for $\beta = 0$; $M = 0$. Introducing η and ψ as for the flat plate by (3.28) and (3.29) (but now for $U = U(x) = \ not\ constant$) we obtain the Falkner-Skan equation:

$$f''' + \frac{M+1}{2}f f'' + M(1 - f'^2) = 0 \tag{3.39}$$

With boundary conditions

$$\eta = 0 \qquad f = f(0) \qquad f'(0) = 0 \tag{3.40}$$

$$\eta \rightarrow \infty \qquad\qquad f' = \frac{u}{U}(\eta) \rightarrow 1 \tag{3.41}$$

(Note that $f(0) > 0$ for suction, $f(0) < 0$ for blowing)

The velocity profile follows from

$$\frac{u}{U} = f'(\eta) \tag{3.42}$$

When suction or blowing is involved a requirement for similarity, in addition to (3.37) is:

$$v_0 \sim x^{\frac{M-1}{2}} \tag{3.43}$$

The relation between v_0 and the non-dimensional streamfunction at the wall follows from:

$$\psi_{wall} = \int\limits_{x=0}^{x} -v_0 dx \quad and \quad \psi_{wall} = \sqrt{\nu x U} f(x,0) \tag{3.44}$$

For similar flows we have

$$f(0) = constant \tag{3.45}$$

Solutions of (3.39) have first been obtained by Hartree for attached flows (Hartree, 1937) and zero suction. A stagnation point flow is obtained for $\beta = 1$; the flat plate for $\beta = 0$ and a separation flow for $\beta = -.198838$. Hartree found that for $\beta \geq 0$ a unique solution exists. However, for $-.198838 \leq \beta < 0$ an infinite number of solutions exists that all satisfy the boundary conditions. He introduced the "Hartree condition" to single out the relevant solution, that is the one approaching $\overline{u} = 1$ from below as fast as possible without making an overshoot. (for a detailed discussion of this phenomenon see (van Ingen, 1965, 📄)).

It was shown by Stewartson (1954) that also solutions with backflow exist for $-.198838 \leq \beta \leq 0$. Solutions of (3.39) can, as for the Blasius equation, be obtained from a finite difference method or by shooting. Table 3.1 gives some details of the velocity profiles for which Arnal obtained the solutions of the Orr-Sommerfeld equation. For later convenience also the asymptotic suction profile is included.

3.5 A finite difference method to solve the laminar boundary layer equations

In the beginning of the 20th century it was still too complicated to calculate the boundary layer for arbitrary pressure distributions. Hence at first only similar flows could be calculated, such as the flat plate ((Prandtl, 1904), (Blasius, 1908)), the plane stagnation point flow (Hiemenz, 1911) and the wedge-type flows ((Falkner and Skan, 1930), (Hartree, 1937)) and the reversed flow solutions by (Stewartson, 1954). Some of these have been discussed in previous chapters. Non-similar solutions could be obtained for special pressure distributions for which the partial

Table 3.1: Overview of the Hartree-Stewartson profiles analysed by Arnal and re- analysed data for $Re_{\delta^*_{crit}}$. The value for $Re_{\delta^*_{crit}}$ for the asymptotic suction profile was derived from (Hughes and Reid, 1965)

icase	β	H	$\frac{\delta^*}{x}\sqrt{\frac{Ux}{\nu}}$	$\frac{\theta}{x}\sqrt{\frac{Ux}{\nu}}$	$Re_{\delta^*_{crit}}$ (Arnal, table 1)	$Re_{\delta^*_{crit}}$ (re-analysed)
1	1.00	2.216	.6479	.2924	12510	12501
2	.50	2.297	.9854	.4290	7750	7745
3	.20	2.411	1.3204	.5477	2860	2857
4	.10	2.481	1.4981	.6002	1390	1388
5	.05	2.529	1.5943	.6304	872	871
6	.00	2.591	1.7208	.6641	520	520
7	-.05	2.676	1.8789	.7021	315	315
8	-.10	2.802	2.0905	.7461	198	198
9	-.15	3.023	2.4146	.7987	126	126
10	-.185	3.378	2.8536	.8448	89	88.4
11	-.1988	4.029	3.4978	.8682	67	66.5
12	-.16	6.752	5.185	.7679	46.3	46.2
13	-.12	10.056	6.405	.6369	40.5	40.2
14	-.08	16.467	7.902	.4799	36.5	36.5
15	-.04	35.944	10.385	.2889	33.0	32.9
Asymptotic suction profile		2.000				46270

differential equations could be reduced to a series of ordinary differential equations ((Blasius, 1908); (Howarth, 1938); (Görtler, 1957)). All of these series solutions failed to converge sufficiently near separation and hence some kind of continuation procedure had to be devised which was either based on the momentum integral equation of von Kármàn ((Howarth, 1938); (Tani, 1949)) or on a direct numerical solution (Leigh, 1955). This work, especially that of Hartree, led to the notion of a singularity at separation. Later on this singularity was clarified by (Goldstein, 1948) and (Stewartson, 1954); a further numerical evaluation was given by (Terrill, 1960) [1]

At first these discussions of the singularity gave rise to the idea that the boundary layer equations ceased to be valid at separation. Later on it has become clear that the equations can be used through separation for a suitable pressure distribution (for instance a measured one), but that the result is extremely sensitive to small changes in this pressure distribution. Instead of prescribing the pressure distribution one should prescribe a regular behaviour through separation of a quantity such as the skin friction or the displacement thickness from which the pressure distribution follows. At present it is customary to use the concept of strong interaction where the boundary layer is calculated simultaneously with the pressure distribution. Both are coupled through the distribution of the displacement thickness.

Until 1921 boundary layer theory was not of much use to practical aerodynamicists. The practical application of boundary layer theory became possible through the use of the von Kármàn momentum integral equation and the Pohlhausen method, based on it. Hence, for a long time the practical application of boundary layer theory was through approximate methods such as Pohlhausens (Pohlhausen, 1921). It was only in the nineteen-sixties that direct numerical calculations became feasible, see for instance (Smith and Clutter, 1963). In his lectures at Delft University the author introduced a numerical solution procedure using a finite difference method based on the following simple second-order linear ordinary differential equation with non-constant coefficients as a standard form:

$$\overline{u}'' + P(\eta)\overline{u}' + Q(\eta)\overline{u} = R(\eta) \tag{3.46}$$

With boundary conditions:

$$\overline{u} = 0 \;\; at \;\; y = 0; \qquad \overline{u} = \overline{u}_{max} \to 1 \;\; at \;\; \eta_{max} \to \infty \tag{3.47}$$

Where $\overline{u}$ represents the non-dimensional velocity in the boundary layer. η is a non-dimensional distance to the wall, to be specified later. For certain applications where the exact solution is known, the exact value for $\overline{u}_{max}$ at a finite η_{max} can be used in order to be able to evaluate the quality of the numerical procedure. Equation (3.46) can be solved by shooting, but we use a 3-point finite difference method with application of the Thomas algorithm to solve the resulting linear algebraic equations. Using the simple Thomas algorithm the accuracy is of order h^2 where h is the (constant) step length. By using n, 2 n and 4 n intervals with step length h, $\frac{1}{2}h$ and $\frac{1}{4}h$ a Richardson type extrapolation can be used, increasing the accuracy to h^4 and h^6 respectively. For practical applications order h^4 is in general sufficient, which is equivalent to the customary Runge-Kutta result.

---

[1]To avoid a too lengthy list, well known references that can be found in the 7th edition of (Schlichting, 1978), (Rosenhead, 1961) or the reference list of the author's PhD thesis, also found on the CD-ROM, 📄, will not be listed in the present report.

As a first example we use the asymptotic suction boundary layer that was already discussed in section 3.2. Equation (3.21) can be brought in the form of our standard equation (3.46) by writing

$$P(\eta) = 1, \qquad Q(\eta) = 0, \qquad R(\eta) = 0, \qquad \eta = -\frac{v_0 y}{\nu} \tag{3.48}$$

The exact solution is:

$$\overline{u} = 1 - e^{-\eta} = 1 - e^{\frac{v_0 y}{\nu}} \tag{3.49}$$

A second example is Stokes first problem (accelerating infinite flat plate in a fluid at rest, (Schlichting, 1978, chapter V). Writing this problem in a frame of reference fixed to the plate, where the wall is stationary and the outer flow is moving, the boundary layer equation reduces to:

$$\overline{u}'' + 2\eta \overline{u}' = 0 \tag{3.50}$$

Where η is $\frac{y}{2\sqrt{\nu t}}$. The exact solution is:

$$\overline{u} = erf(\eta) \tag{3.51}$$

Where $erf(\eta)$ is the well known error function:

$$erf(\eta) = \frac{2}{\sqrt{\pi}} \int_0^\eta e^{-\eta^2} d\eta \tag{3.52}$$

Because of the known exact solutions for the two preceding cases they can be used to get some feeling for the influence of varying η_{max} and the number of steps through the boundary layer.

The boundary layer for the flat plate was shown in section 3.3 to lead to the following Blasius equation for the non-dimensional stream function f:

$$f''' + \frac{1}{2} f f'' = 0 \tag{3.53}$$

with

$$f \quad = \quad 0 \qquad f' = 0 \qquad at \; \eta = 0 \tag{3.54}$$
$$f' \to 1 \qquad for \; \eta \to \infty \tag{3.55}$$

The Blasius equation can be brought in the form of our standard equation (3.46) by substituting $f(\eta) = \overline{u}$ which leads to:

$$\overline{u}'' + \frac{1}{2} f \overline{u}' = 0 \tag{3.56}$$

Apparently we have to take $R = 0$ and $Q = 0$ while $P(\eta) = \frac{1}{2} f$. This is a complicating factor because now $P(\eta)$ is not known and the equation is not linear anymore. This problem is solved by using an iterative procedure where f is obtained from a previous iterate $\tilde{u}$ using:

$$f = \int_0^\eta \tilde{u} d\eta \tag{3.57}$$

(f is zero at the wall for the no-suction case) and taking $\overline{u} = 1 - e^{-\eta}$ as a first estimate for $\tilde{u}$. A few iterations using the Thomas algorithm and (half of) the Richardson extrapolation scheme are found to be sufficient.

The Falkner-Skan equation was introduced in section 3.4. Equation (3.39) can also be brought in the form of our standard equation (3.46) but has some complicating non-linear terms, namely ff'' and $(f')^2$ .The first one is treated as in the Blasius equation while the second one is linearised using:

$$f' = \overline{u}, \qquad \overline{u} - \tilde{u} = \delta\overline{u}, \qquad (\delta\overline{u}^2) \cong 0 \tag{3.58}$$

Where $\tilde{u}$ is the value of $\overline{u}$ from a previous iteration. An iterative solution is easily obtained from a first guess such as $\overline{u} = 1 - e^{-\eta}$. This procedure will not be discussed in further detail here. Non-similar boundary layers can be calculated from a form of the boundary layer equations which to a large extent resembles the Falkner-Skan equation. This form was first introduced by (Görtler, 1957); see also (Schlichting, 1978, chapter IX) and (Smith and Clutter, 1963). Introducing

$$\eta = \frac{y}{x}\sqrt{\frac{Ux}{\nu}} \tag{3.59}$$

and the non-dimensional streamfunction $f(x, \eta)$ by

$$\psi(x, \eta) = \sqrt{\nu x U} f(x, \eta) \tag{3.60}$$

we can transform equation (3.1) and (3.2) into

$$f''' + \frac{M+1}{2}ff'' + M\left(1 - (f')^2\right) = x\left[f'\frac{\partial f'}{\partial x} - f''\frac{\partial f}{\partial x}\right] \tag{3.61}$$

Where

$$M = \frac{x}{U}\frac{dU}{dx} \tag{3.62}$$

See also (Schlichting, 1978, chapter IX) and (Smith and Clutter, 1963). Equation (3.61) is now a partial differential equation because of the derivatives w.r.t. x in the right hand side which complicates its solution. The equation has the advantage that for $x \to 0$ the Falkner-Skan equation is obtained, hence the starting solution at $x = 0$ is known already. A marching procedure in x-direction can be obtained by replacing the derivatives with respect to x by finite differences based on a few points in x-direction (Hartree-Womersley method). The resulting ordinary differential equation in η can be solved by the shooting method or can be brought in the standard form (3.46), using the same procedures as for the Falkner-Skan equation. As in all direct numerical calculations singular behaviour near separation is observed. A good estimate for the position of separation is obtained by assuming that the singularity is of the simple Goldstein type where the wall shear stress approaches zero as the square root of the distance to separation. Hence a linear extrapolation of the square of the wall shear stress to zero provides an estimate of the separation position that is sufficiently accurate for practical purposes. The effects of suction can be taken into account by specifying the stream function $f(x, 0)$ at the wall. With normal velocity at the wall v_0 we can write the stream function at the wall as:

$$\psi = \int\limits_0^x -v_0 dx \tag{3.63}$$

Which leads to the following expression for f at the wall:

$$f(x,0) = \frac{1}{\sqrt{\nu x U}} \int\limits_{x=0}^{x} -v_0 dx \qquad (3.64)$$

Some applications of the finite difference method will be used in chapter 12.

Chapter 4

Choice of a parameter to characterise stability diagrams

4.1   Some early stability data

Stability diagrams are determined by the Eigensolutions of the Orr-Sommerfeld equation 2.1. The solutions depend on the shape of the velocity profile through $u(y)$ and $u''(y)$ in the left hand side of the equation. Especially u'' is known to have an important effect on the stability diagram. The occurrence of an inflexion point leads to a low critical Reynolds number and a high amplification rate. It was already mentioned in chapter 2 that curvature and hence the stability is dependent on pressure gradient, suction/blowing, heating or cooling, etc. Note that the reciprocal value of the Reynolds number occurs in the right hand side of the Orr-Sommerfeld equation as the coefficient of the highest (4th) derivative of the amplitude function ϕ. This makes numerical solutions of the equation, even in the present computer era, rather cumbersome and computer intensive. For infinite Reynolds number the right hand side disappears, lowering the order of the equation to 2. Solutions of this so called "Rayleigh equation" are only interesting for velocity profiles with an inflexion point. The $-\alpha_i\theta$ vs $\frac{\omega\theta}{U}$ cross section is then independent of the Reynolds number which has certain consequences for the shape of the stability diagram, to be discussed later.

Because of the relatively large computational effort it is not practical to solve the equation "on the fly" for all velocity profile at a large series of x-stations on an airfoil at a range of angles of attack and chord Reynolds numbers as would be needed for an airfoil design computer program. Therefore it is still customary to use pre-computed solutions for a standard series of velocity profiles at a number of Re_θ values in a data base method. In general, the Hartree and Stewartson solutions of the Falkner-Skan equation without suction/blowing are used for this purpose. The shape factor H is generally used to characterise the shape of the velocity profiles and hence the stability diagrams.

In the early days of the e^N method there was not much choice for the stability diagrams.

Although a number of neutral curves were available for flows with pressure gradient and suction, the only diagrams including amplification rates were those calculated by Pretsch, (see (Pretsch, 1941, 1942, 1945)) for six Hartree profiles from stagnation point to separation (see figure 4.1). In his first version of the method (van Ingen, 1956a, 📄) used the Pohlhausen method to calculate the boundary layer on an airfoil. The Pohlhausen pressure gradient parameter $\frac{\theta^2}{\nu}\frac{dU}{dx}$ was related to the Hartree β by calculating the Hartree boundary layers with the Pohlhausen method. Because Pretsch could not yet use numerical solution procedures for the Orr-Sommerfeld equation he had to rely on a (semi) analytical method that was not applicable at the low Reynolds number for the separation profile. Therefore he was unable to calculate the critical Reynolds number for this profile. Therefore, and also due to the limited accuracy of the Pohlhausen method near separation, no conclusion as to the validity of the e^N method near separation could be drawn. Figure 4.2 shows the critical Reynolds number for a series of boundary layer flows with and without suction. These data are rather well correlated by the following approximation due to (Wieghardt, 1954).

$$Re_{\theta_{crit}} = e^{26.3-8H} \tag{4.1}$$

From figure 4.3, to be discussed later, it follows that this good correlation is only true for a restricted range of H, namely $2.2 \leq H \leq 2.7$ In 1965 (van Ingen, 1965, 📄) used Lin's approximate formula for the critical Reynolds number of the velocity profiles that were used in his 2-parameter integral relation method for boundary layers with suction. The Pretsch diagram for which the critical Reynolds number was equal to Lin's value then was applied to the local boundary layer profile. Lin's equation is derived as a first crude approximation to the critical Reynolds number. In fact there are two formula's, namely:

$$-\pi \, \overline{u}'(0) \left(\frac{\overline{u} \, \overline{u}''}{\overline{u}'^3} \right)_c = 0.58 \tag{4.2}$$

$$Re_{crit} = 25\frac{u'(0)}{\overline{c}^4} \tag{4.3}$$

$\overline{c}$ is the value of $\overline{u}$ for which equation 4.2 is satisfied. We apply these formulae for $\overline{u} = \frac{u}{U}$ where the primes denote differentation w.r.t. $\overline{y} = \frac{y}{\theta}$, hence $u'(0) = \ell$.

The first equation determines a characteristic velocity $\overline{c}$ in the boundary layer. Once this value of $\overline{c}$ is known the second equation gives the critical Reynolds number. From this second equation it follows that the critical Reynolds number becomes zero at separation and would be negative for separated flows. This is certainly not in agreement with the presently known numerical solutions of the Orr-Sommerfeld equation. Figure 4.3 gives a comparison between the critical Reynolds numbers for the Hartree flows as calculated by Arnal and according to our database, and for the asymptotic suction profile according to (Hughes and Reid, 1965) ($Re_{\delta^*_{crit}} = 46270$; $Re_{\theta_{crit}} = 23135$; $^{10}log(Re_{\theta_{crit}}) = 4.3643$), Lin's approximation for these cases and also the curve fit of equation (4.1).

It can be seen that Lin's approximation and Wieghardts curve fit give reasonable results between $H = 2.2$ and $H = 2.7$ but are far off for flows approaching separation.

It has to be concluded that it is not simple to define a suitable parameter to characterize stability diagrams and moreover it is not clear whether it is permissible to use a single para-
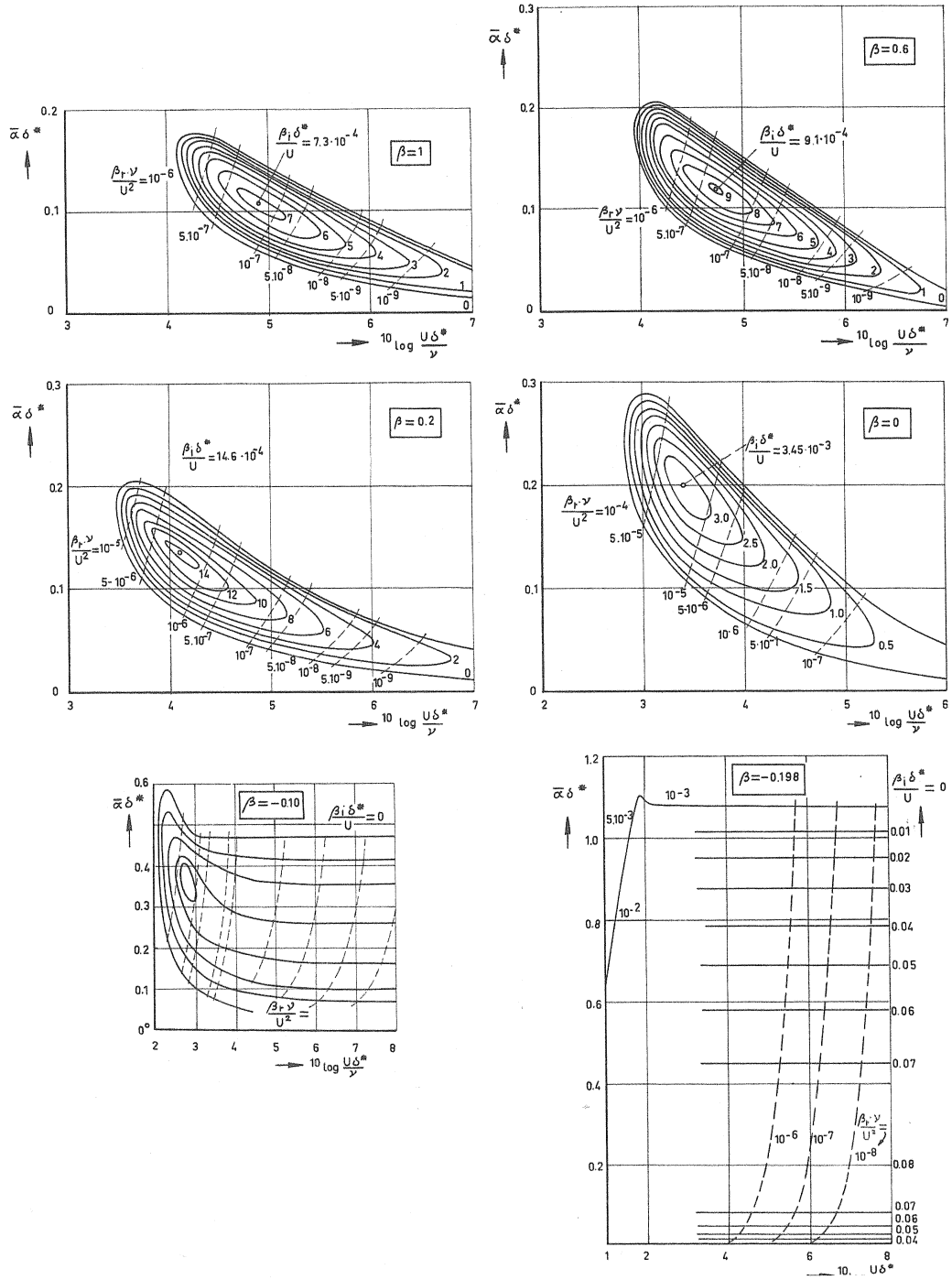
Figure 4.1: Pretsch diagrams
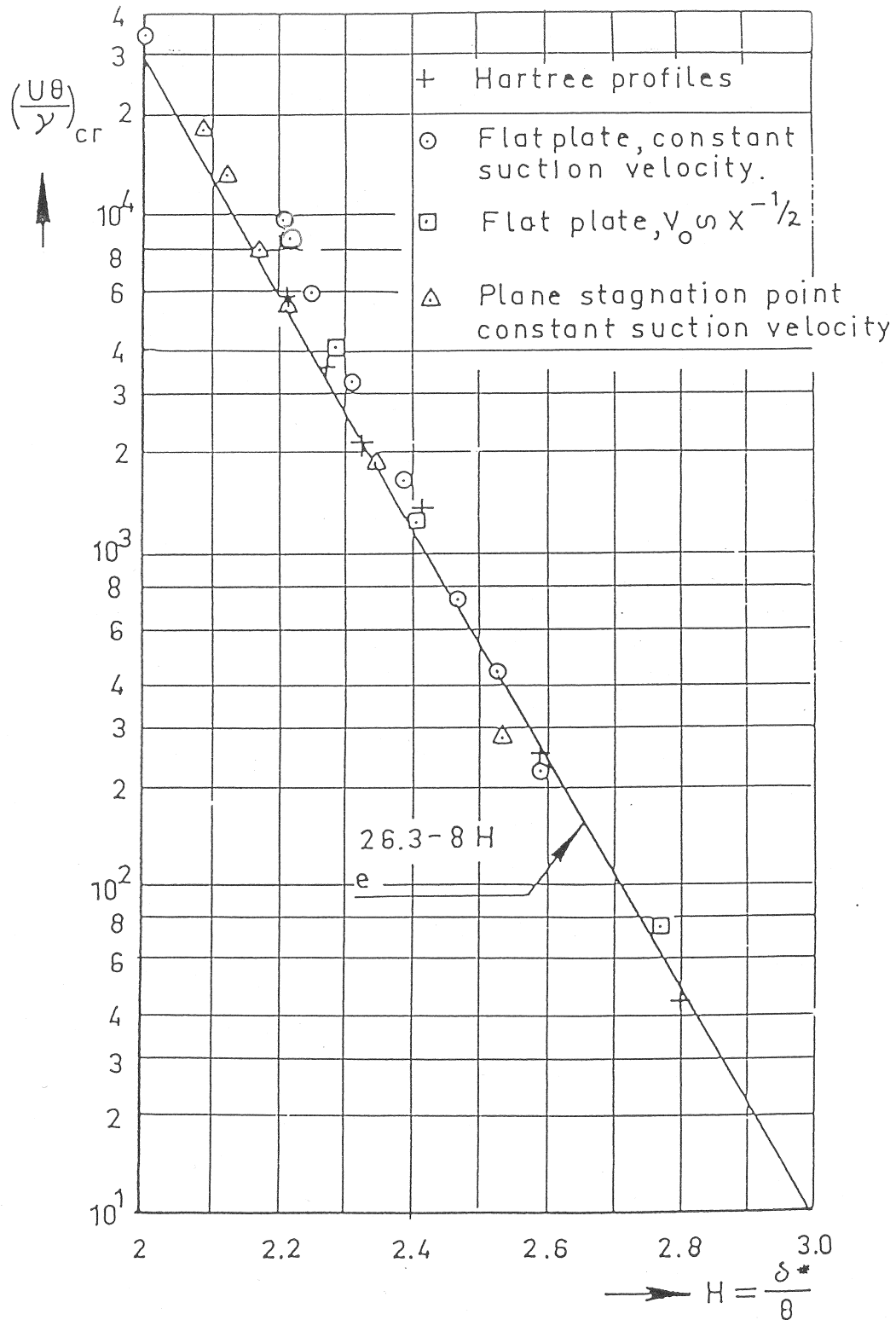
Figure 4.2: $Re_{\theta_{crit}}$ vs H for several velocity profiles and the Wieghardt correlation
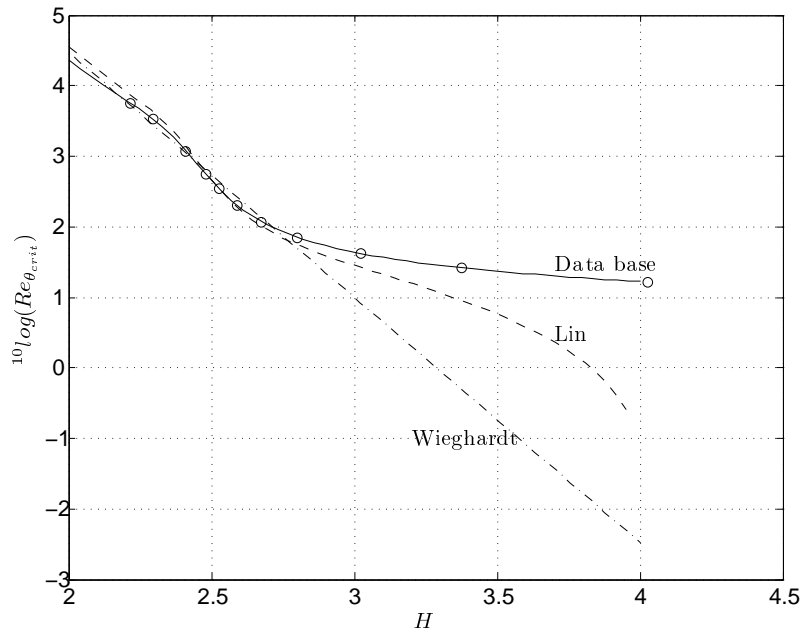
Figure 4.3: Lin's approximation for Falkner-Skan profiles without suction compared to Wieghardt's correlation and our database. Arnal's values are denoted by ○

meter to describe all possible stability diagrams with pressure gradient and suction. In his PhD thesis (van Ingen, 1965, 📄) made the following observations:

1. The results of different authors for the flat plate neutral curve showed appreciable differences (see figure 4.6) due to:

    a. using different analytical approximations to the Blasius profile. Although the profiles looked reasonable, the curvature was sometimes quite different.

    b. Using different (analytical) methods to solve the Orr-Sommerfeld equation.

2. In addition to the Pretschs complete diagrams for the Hartree profiles a number of neutral curves were available for boundary layers with pressure gradient/suction/blowing (Ulrich, 1944) (see figures 4.4, 4.5 and 4.6)

From these figures, taken from (van Ingen, 1965, 📄), it followed that if such an amount of suction is applied to a flat plate boundary layer that the critical Reynolds number becomes equal to that for the stagnation point flow, then also the remaining parts of the neutral curves look rather similar. A similar conclusion was valid for such an amount of blowing at the stagnation point that the critical Reynolds number for the flat plate was obtained. In order to be able to proceed at that time (1965) it was assumed (maybe rather boldly) that:
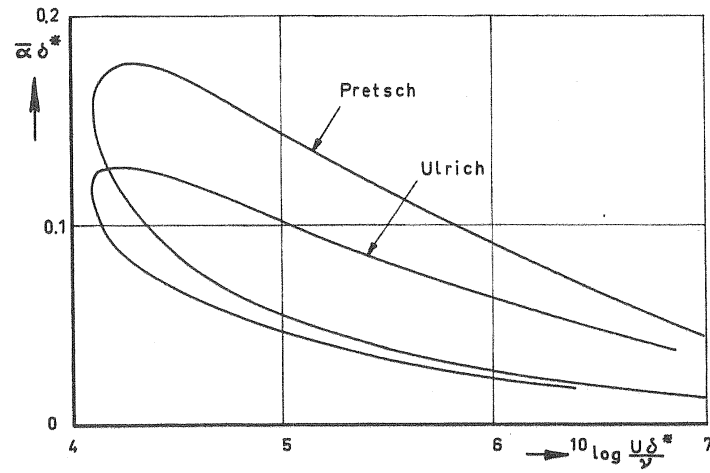
Figure 4.4: Plane stagnation point, Ulrich & Pretsch
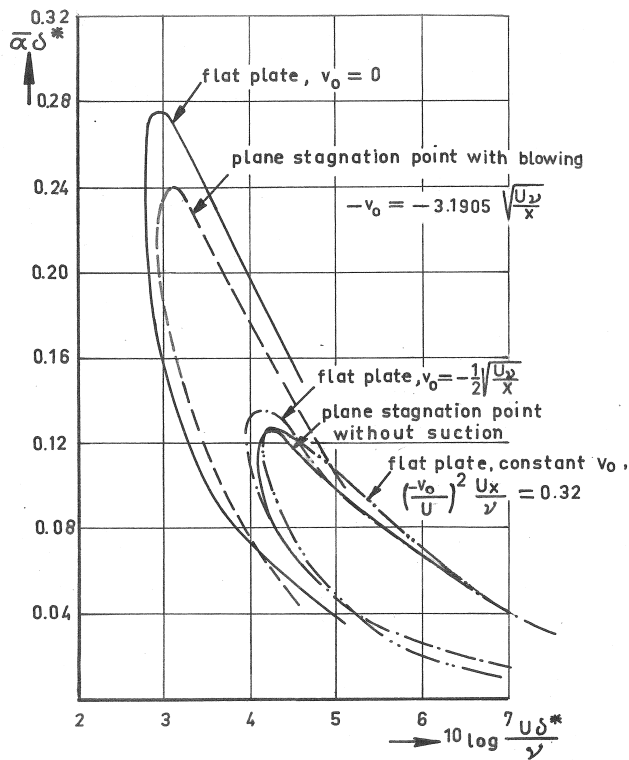
Figure 4.5: Some neutral curves for suction/blowing and pressure gradient
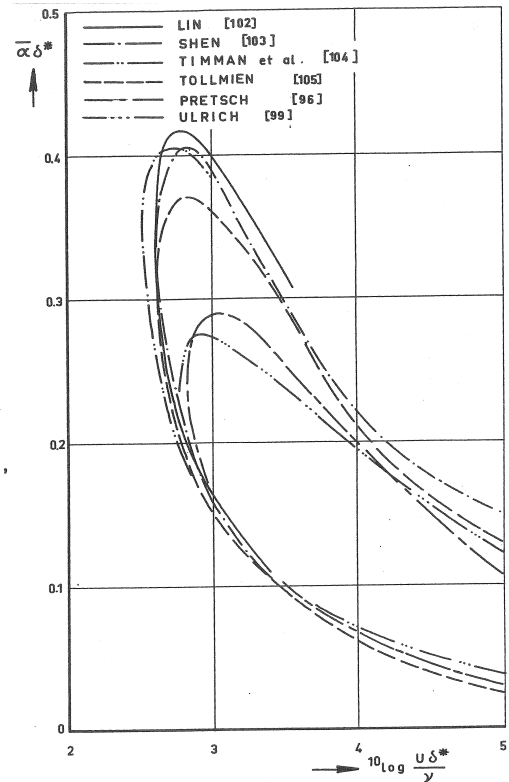
Figure 4.6: Neutral curves for the flat plate boundary layer

> *All possible stability diagrams for arbitrary pressure gradients and suction/blowing form a one-parameter family with the critical Reynolds number as parameter. This implies that it is assumed that the effects of pressure gradient and suction/blowing are interchangeable.*

Extensive use of this assumption has shown that application of the resulting e^N method gave good results for pressure gradient, suction blowing and even for separation bubbles. In later years very often the shape factor H has been used as the parameter characterising the critical Reynolds number (Rosenhead, 1961; van Ingen, 1965). Also the approximation due to Wieghart often has been used. In the present work we also will use H; in the next section we will give some more background to this choice. Similar work on the interchangeability of pressure gradient and suction has been done by (Stock, 1980; Stock and Degenhart, 1989). Because it is known that the curvature of the velocity profile has a strong effect on the stability diagram one might argue that the relevant parameter should be based on curvature rather than on the velocity profile shape parameter H. In chapter 3 we defined the parameter m_T as the non-dimensional curvature at the wall. Therefore m_T would present itself as a suitable parameter. However, the Hartree profiles cover only a limited range of m_T values with a maximum at separation as shown in figure 4.7. Here the $\ell - m_T$ relation for the Hartree profiles is compared with a number of non-similar boundary layers. Since non-dimensional wall shear stress (f"(0)) as a function of m_T is double valued for the Hartree-Stewartson profiles between $\beta = 0$ and $\beta = -0.1988$ (see figure 4.8) there seems not much choice to be left except using H.
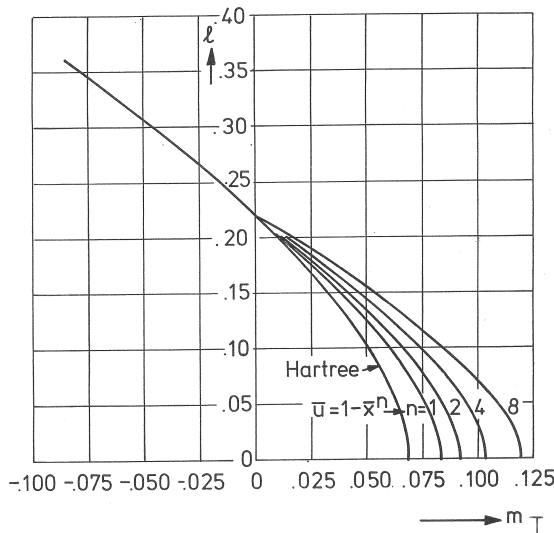
Figure 4.7: ℓ vs m_T
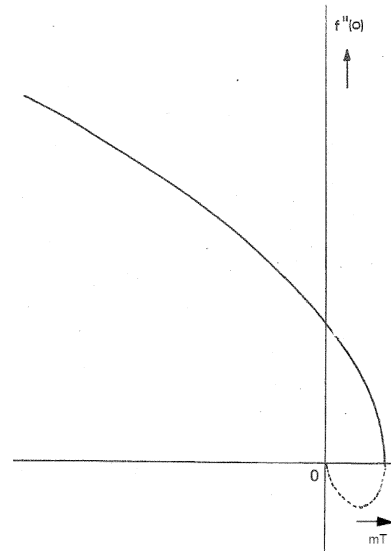
Figure 4.8: $f''(0)$ vs m_T for Hartree & Stewartson boundary layers

4.2   Comparison of solutions of the Falkner-Skan equation with and without suction

To see whether H might be used to characterise the distributions of $u(y)$ and $u''(y)$ and hence the stability diagram we calculated a series of 23 solutions of the Falkner-Skan equation for the flat plate with varying amounts of suction and blowing, shown in table 4.1. Note that case nr. 18 represents the flat plate without suction or blowing.

Table 4.1: Falkner-Skan solutions for flat plat with suction/blowing

	$f(0)$	$f''(0)$	η_{max}	ℓ	m_T	H
Asymptotic suction				0.5000	-0.2500	2.0000
Falkner-Skan						
1	10	5.0485	5.0000	0.4894	-0.2372	2.0153
2	1.6000	0.9897	8.0000	0.3755	-0.1140	2.2024
3	1.5000	0.9454	8.0000	0.3695	-0.1083	2.2138
4	1.4000	0.9014	8.0000	0.3632	-0.1024	2.2261
5	1.3000	0.8578	8.0000	0.3564	-0.0963	2.2394
6	1.2000	0.8144	8.0000	0.3493	-0.0899	2.2539
7	1.1000	0.7715	8.0000	0.3417	-0.0832	2.2696
8	1.0000	0.7289	8.0000	0.3336	-0.0764	2.2866
9	0.9000	0.6867	8.0000	0.3251	-0.0692	2.3053
10	0.8000	0.6450	8.0000	0.3160	-0.0619	2.3257
11	0.7000	0.6037	8.0000	0.3064	-0.0544	2.3481
12	0.6000	0.5630	8.0000	0.2961	-0.0467	2.3727
13	0.5000	0.5228	8.0000	0.2853	-0.0389	2.3999
14	0.4000	0.4833	10.0000	0.2738	-0.0310	2.4300
15	0.3000	0.4443	10.0000	0.2616	-0.0231	2.4636
16	0.2000	0.4061	12.0000	0.2486	-0.0152	2.5011
17	0.1000	0.3687	12.0000	0.2350	-0.0075	2.5433
18	0	0.3321	12.0000	0.2205	0	2.5911
19	-0.2000	0.2616	12.0000	0.1892	0.0137	2.7080
20	-0.4000	0.1956	12.0000	0.1547	0.0245	2.8658
21	-0.6000	0.1349	12.0000	0.1173	0.0306	3.0909
22	-0.8000	0.0808	14.0000	0.0777	0.0299	3.4419
23	-1.0000	0.0355	16.0000	0.0380	0.0204	4.0995

The amounts of suction/blowing were chosen in such a way that for most cases H for these flat plate flows was in the range from 2.2162 to 4.0292 ; that is the same range as for the no-suction case from stagnation point to separation. To show that for very strong suction the asymptotic suction profile is approached, we added case number 1 with $f(0) = 10$. The resulting value for H $(= 2.0153)$ shows that this boundary layer is already very near to the asymptotic suction state. For comparison also some data for the asymptotic suction profile are added to the table. Values in the table that are outside the range of the regular no-suction

Hartree boundary layers between stagnation point and separation are printed underlined. Figure 4.9 shows the 23 Falkner-Skan velocity profiles and the asymptotic suciton profile. Indeed profile number 1 is very close to the asymptotic suction profile. Figures 4.10 and 4.11 respectively show the shear stress and curvature profiles.
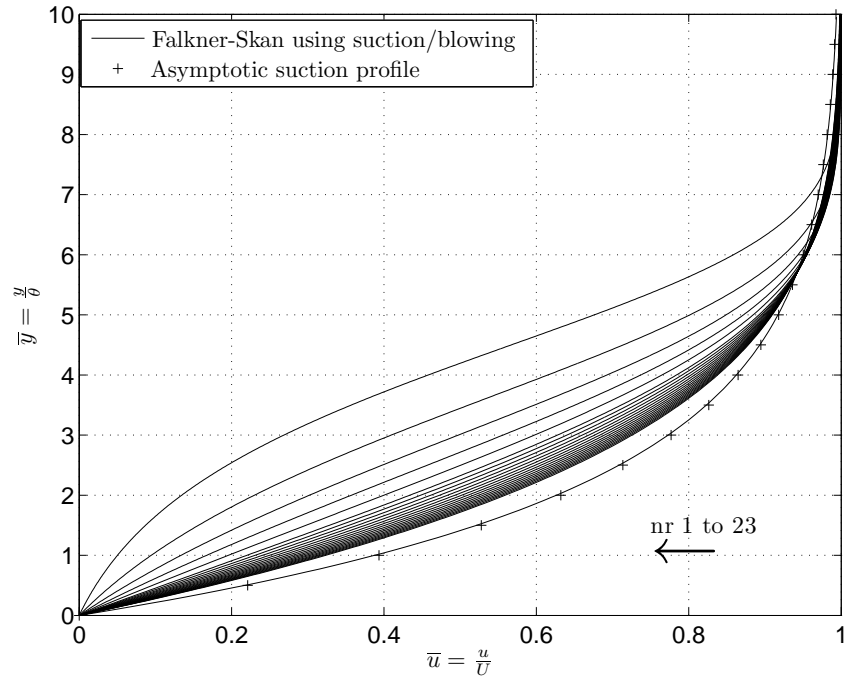
Figure 4.9: Falkner-Skan velocity profiles with blowing and suction for the flat plate and the asymptotic suction profile

For each of the not underlines cases in table 4.1 the corresponding Hartree profile with pressure gradient and no-suction can be calculated with the same value of ℓ, m_T or H as for the profiles in the table.(See the MATLAB program `comp_Hartree_suc_nosuc.m`; option 1 in `N_factor_show.m`. Using this program, the values for ℓ, m_T and H underlined in the table should be avoided, because here no comparable Hartree profile without suction can be found. Some cases for comparisons at equal H are shown in the figures 4.12 through 4.23. Note that u and y have been made non-dimensional with U and θ respectively.
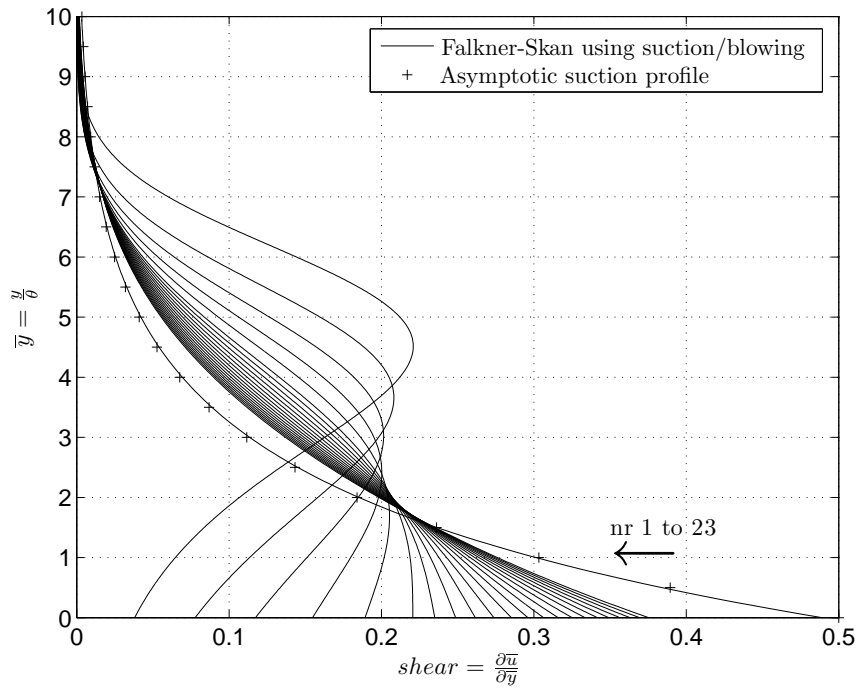
Figure 4.10: Falkner-Skan shear stress profiles with blowing and suction for the flat plate and the asymptotic suction profile
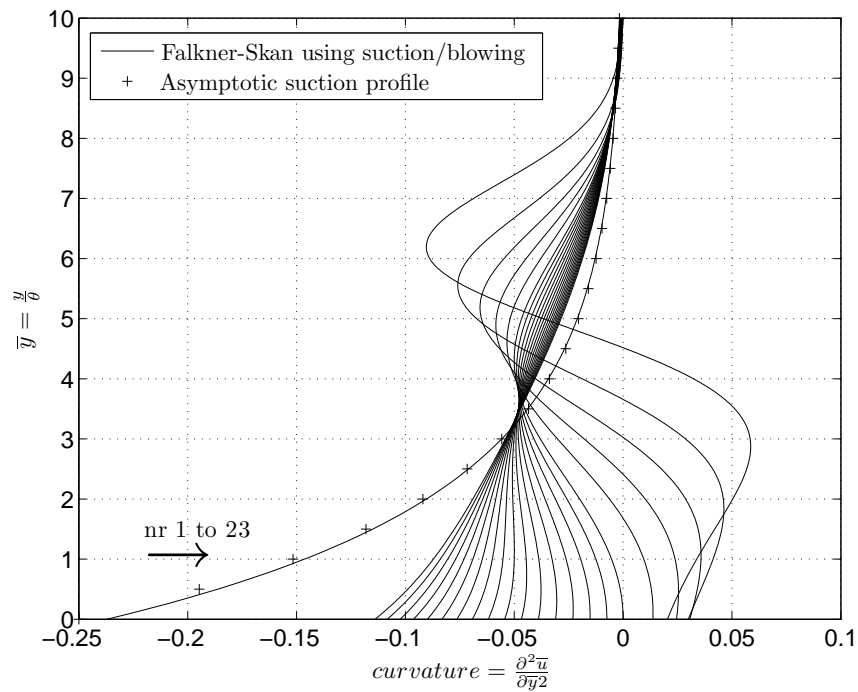
Figure 4.11: Falkner-Skan curvature profiles with blowing and suction for the flat plate and the asymptotic suction profile

From results not presented here, but easily checked with the computer program, we concluded that making m_T equal should not be recommended because of the restricted range of m_T for the Hartree profiles. Also making ℓ equal does not bring an advantage. It can be seen that at the same H the effects of suction/blowing and pressure gradient are indeed reasonably well interchangeable. What is remarkable, is that also the curvature profile at the same H is rather similar. Differences should be expected because of the consequences of the "compatibility conditions" for the 3rd derivative of u w.r.t. y as discussed in section 3.1. It is interesting to see however that these differences mainly show up near the wall. To show the consequences of this interesting result we calculated, for all regular cases in the table, the critical Reynolds number with Lin's approximate method that was discussed in chapter 4.1. Figure 4.24 shows the results in comparison with the data for the regular Hartree profiles. It follows that the results at equal H are rather close despite the differences in curvature. Why this is so follows from figures 4.12 through 4.23 where with a $\bigtriangledown$ or a $\bigtriangleup$ the position is indicated where the first of Lin's equations (4.2) and (4.3) is satisfied. In most cases this occurs at a height above the region where most of the differences in curvature occur. In the first place it should be noted that $\overline{u}(\overline{y})$ and $u'(\overline{y})$ are in most cases very nearly equal for the two profiles. Moreover, from Lin's equations (4.2) and (4.3) it follows that the curvature only influences the determination of the $\overline{y}$ value for which equation (4.2) is satisfied. It is seen that in general these $\overline{y}$ values are nearly equal for the original and comparison profiles. The $\overline{u}$ value $\overline{c}$ at this $\overline{y}$ value enters to the 4th power in equation (4.3) and hence, even if the $\overline{y}$ values are rather close, there still may be differences in the resulting critical Reynolds number as is visible in figure 4.24. This may also be caused by the differences in the wall shear stress ($\overline{u}'(0)$) for both profiles. Although it was shown in section 4.1 that Lin's method is not always accurate, it gives some support for choosing H as the characterising parameter.

Another factor that may contribute to the lesser importance of the curvature term than expected is the following. In the Orr-Sommerfeld equation 2.1 the curvature term ($\overline{u}''$) is multiplied by the amplitude function ϕ. At the wall both ϕ and ϕ' are zero because they represent the v and u component of the disturbance velocity. Therefore ϕ and hence the curvature term remains small over some distance near the wall. Some further remarks on this may be found in Obremski et al. (1969) and van Ingen (2008).

The MATLAB program `Hartree_zpg_pg.m` (N_factor_show.m, option 15) gives some more support to the conclusion that H is a more suitable parameter than l or m_T.

It should also be kept in mind that at not extremely high Reynolds numbers the required amount of suction to maintain laminar flow is relatively modest so that the resulting values of H may remain > 2.4.

It would be interesting to accurately calculate stability diagrams for a set of corresponding cases to see to what extent the differences in curvature near the wall have an influence on the stability diagram and compare these results to Lin's. Not being able to perform these calculations at present we decided to stick to the custom of using H as the parameter to correlate the critical Reynolds number. The correspondence in $u(y)$ and $u''(y)$ as discussed above gives some confidence. But maybe we should say that we accept this choice for lack of something better, just as in the past.
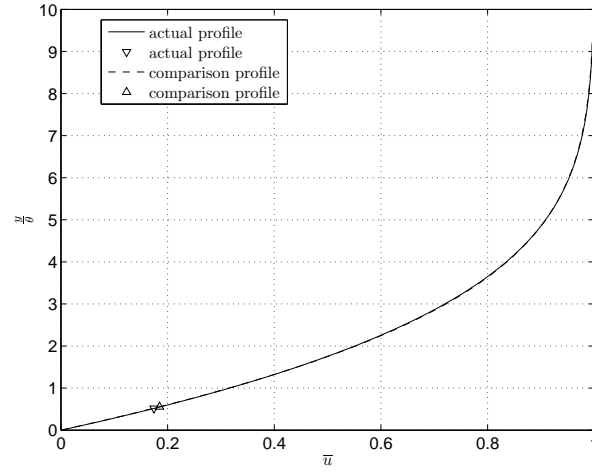
Figure 4.12: Velocity profile, equal H comparison of flat plate with suction/blowing to Hartree $v_0 = 0$, for $H = 2.2261$
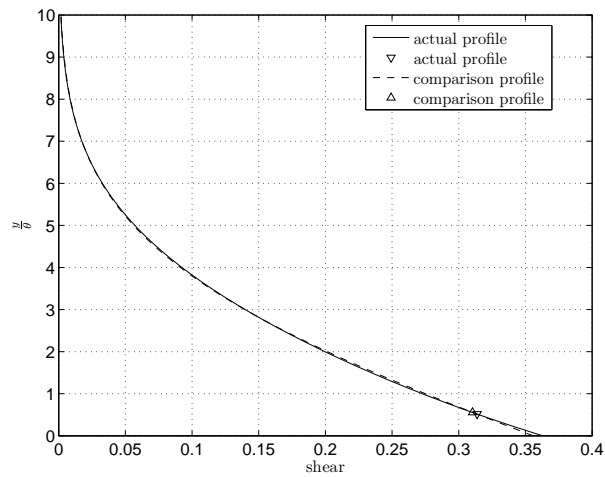
Figure 4.13: Shear stress profile, equal H comparison of flat plate with suction/blowing to Hartree $v_0 = 0$, for $H = 2.2261$
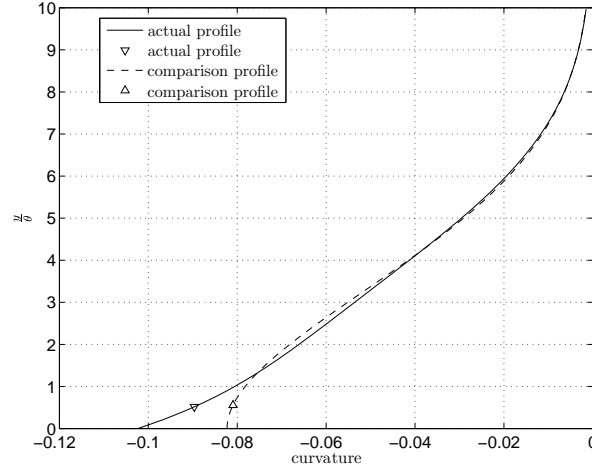
Figure 4.14: Curvature profile, equal H comparison of flat plate with suction/blowing to Hartree $v_0 = 0$, for $H = 2.2261$
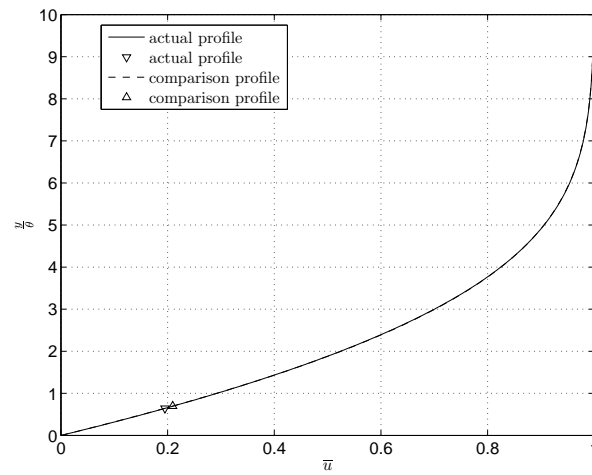
Figure 4.15: Velocity profile, equal H comparison of flat plate with suction/blowing to Hartree $v_0 = 0$, for $H = 2.3053$
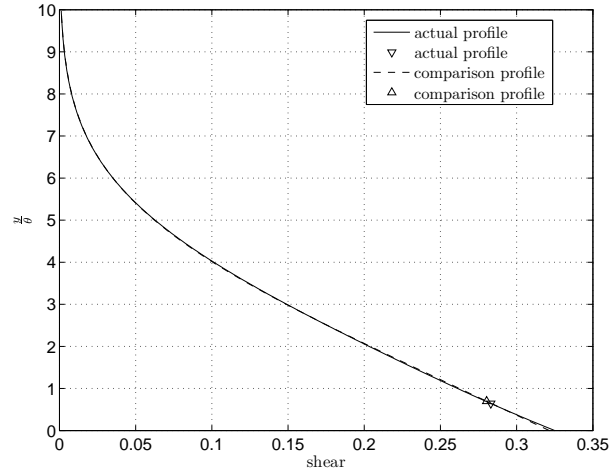
Figure 4.16: Shear stress profile, equal H comparison of flat plate with suction/blowing to Hartree $v_0 = 0$, for $H = 2.3053$
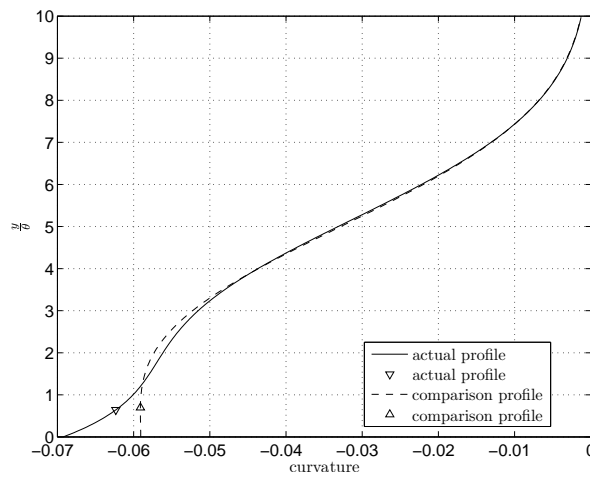
Figure 4.17: Curvature profile, equal H comparison of flat plate with suction/blowing to Hartree $v_0 = 0$, for $H = 2.3053$
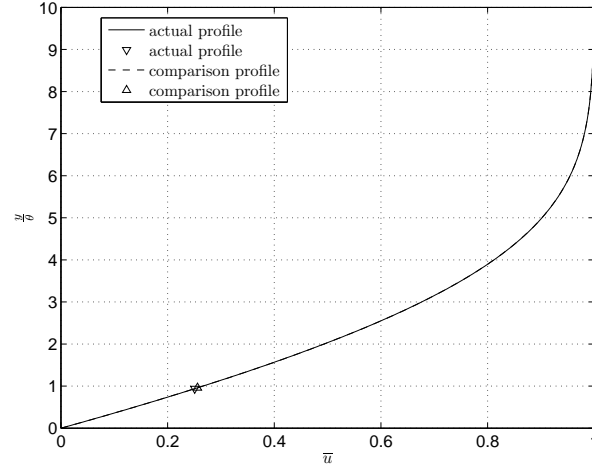
Figure 4.18: Velocity profile, equal H comparison of flat plate with suction/blowing to Hartree $v_0 = 0$, for $H = 2.3999$
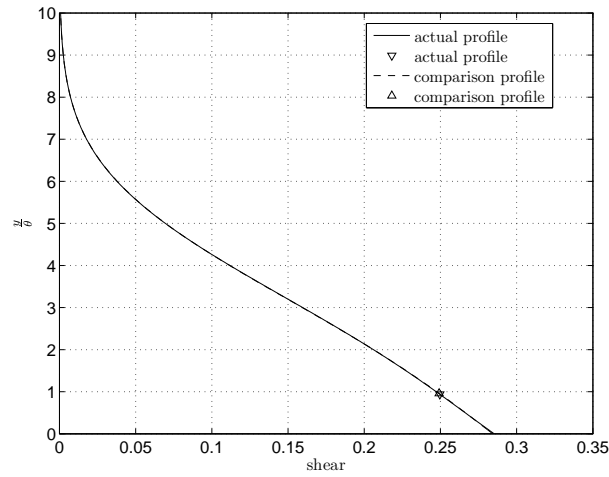
Figure 4.19: Shear stress profile, equal H comparison of flat plate with suction/blowing to Hartree $v_0 = 0$, for $H = 2.3999$
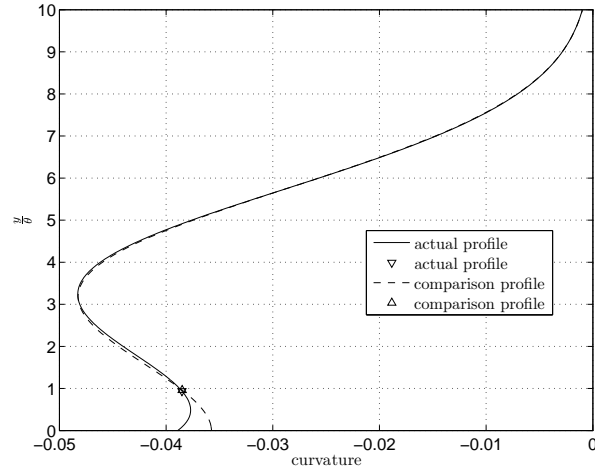
Figure 4.20: Curvature profile, equal H comparison of flat plate with suction/blowing to Hartree $v_0 = 0$, for $H = 2.3999$
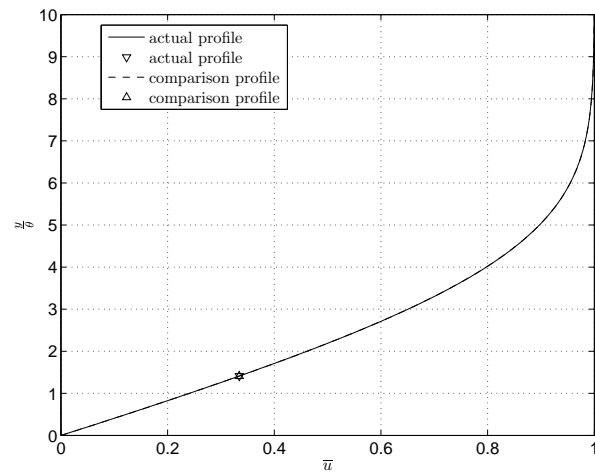
Figure 4.21: Velocity profile, equal H comparison of flat plate with suction/blowing to Hartree $v_0 = 0$, for $H = 2.5011$
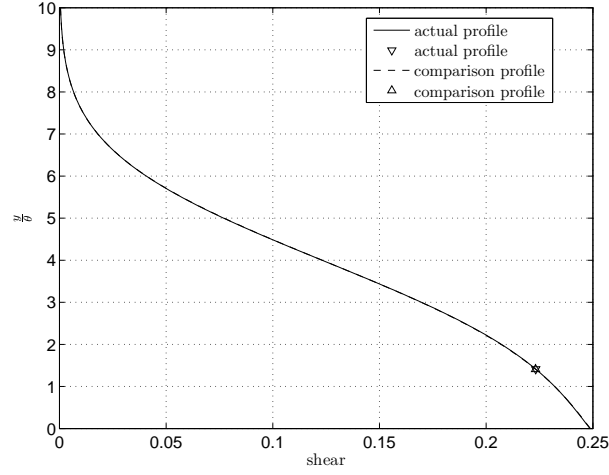
Figure 4.22: Shear stress profile, equal H comparison of flat plate with suction/blowing to Hartree $v_0 = 0$, for $H = 2.5011$
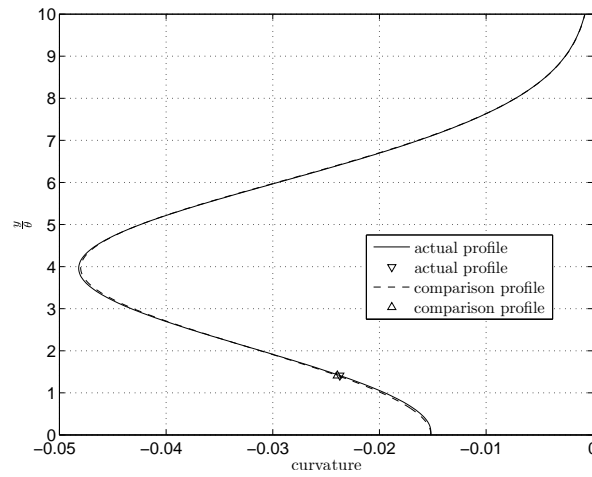
Figure 4.23: Curvature profile, equal H comparison of flat plate with suction/blowing to Hartree $v_0 = 0$, for $H = 2.5011$
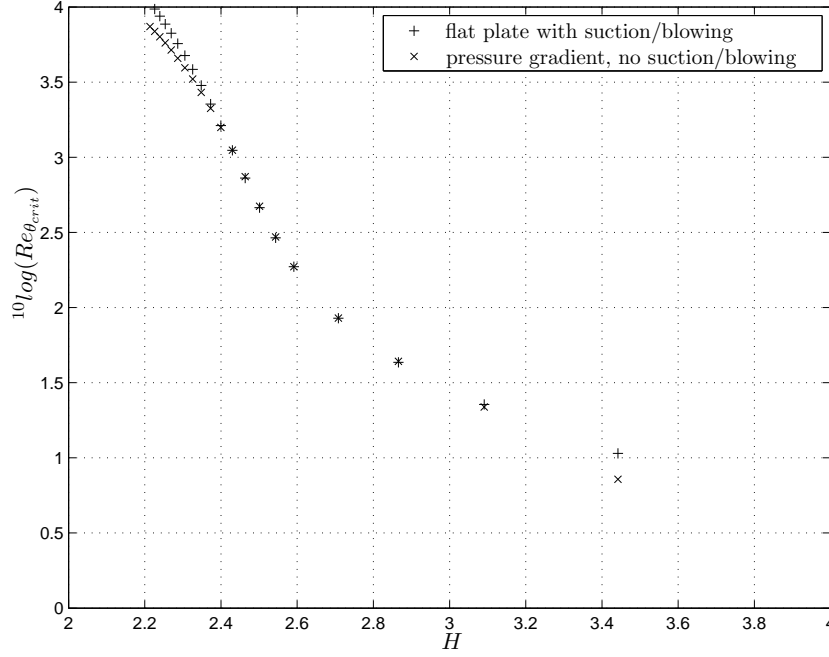
Figure 4.24: $^{10}log(Re_{\theta_{crit}})$ for flat plate with suction/blowing compared to Hartree profile with equal H

A possibility to compare arbitrary velocity profiles with the corresponding regular Hartree profile at the same value of H has also been introduced into the finite difference program that was discussed in chapter 3.5. At selected x-stations a subroutine is called to find the Hartree profile without suction with the same H as the local profile. It is found that also here H presents itself as a suitable parameter. As an example the potential flow pressure distribution around a circular cilinder $U(\overline{x}) = sin(\overline{x})$ without and with suction was used. (Terrill, 1960) has presented an accurate numerical solution for both cases and moreover gave a detailed analytical discussion of the solution near separation. The suction distribution in the second case was given by:

$$v_s = \frac{-v_0}{U_\infty \sqrt{R_c}} \tag{4.4}$$

with $v_s = constant = .5$ For the position of separation with and without suction (Terrill, 1960) found $\overline{x} = 1.822983$ and 2.00164 respectively while our finite difference calculation gave 1.8226 and 2.0028. The result of our calculation is presented as $H(\overline{x})$ in figure 4.25. At $\overline{x} = 1.92$ for the suction case $H = 2.6282$ as indicated in figure 4.25 with o. For this station we also calculated the comparison profile with equal H. Results are shown in figures 4.26, 4.27 and 4.28 for $\overline{u}$, u' and u''. Again the $\overline{u_c}$ and $\overline{y_c}$ values are rather close so that the difference in $Re_{\theta_{crit}}$ is mainly caused by the difference in shear stress at the wall (see equation (4.3) and figure 4.27) The critical Reynolds number $Re_{\theta_{crit}}$ according to Lin for the actual profile and the comparison profile is 117.3 and 139.2 respectively; again rather close.
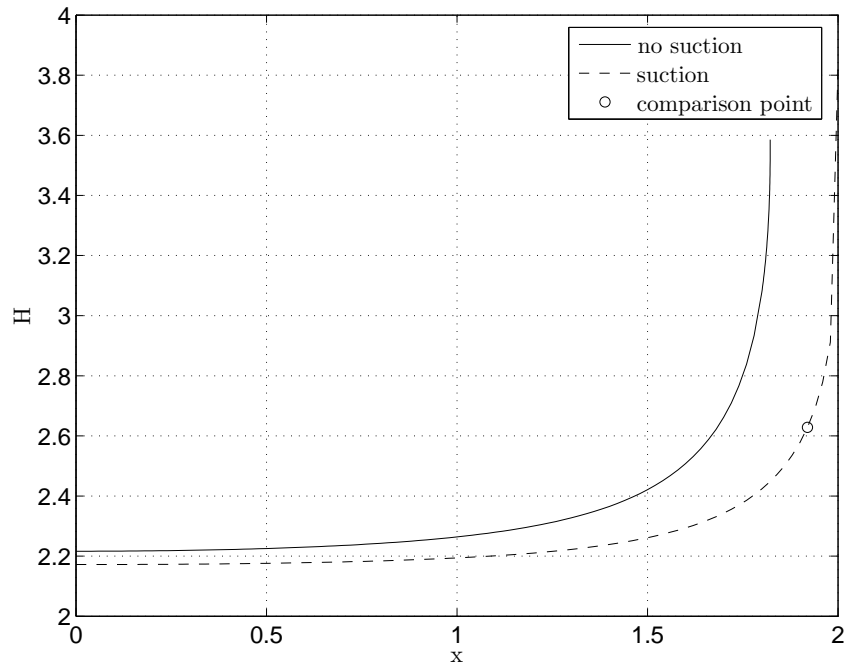
Figure 4.25: H for $\bar{U} = sin(\bar{x})$ with and without suction
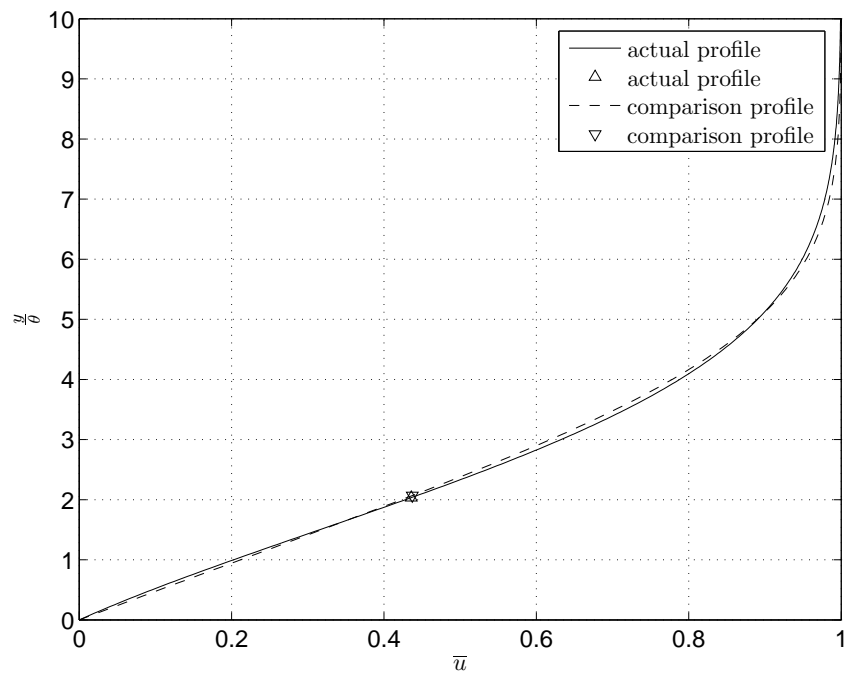
Figure 4.26: Velocity profile for $\bar{U} = sin(\bar{x})$ at $\bar{x} = 1.92$ with suction and comparison Hartree profile without suction at equal $H = 2.6282$
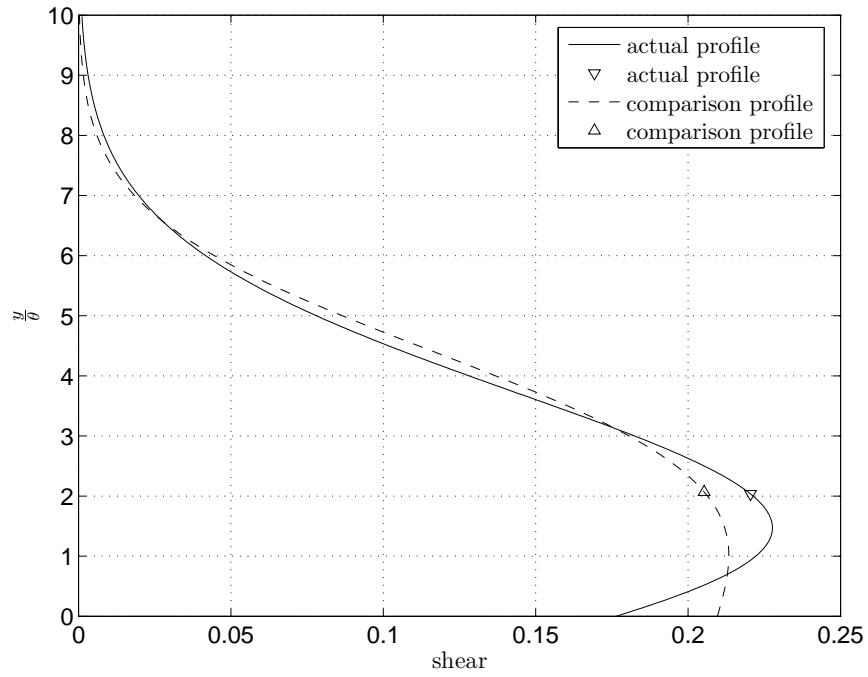
Figure 4.27: Shear stress profile for $\bar{U} = sin(\bar{x})$ with suction and comparison Hartree profile without suction at equal $H = 2.6282$
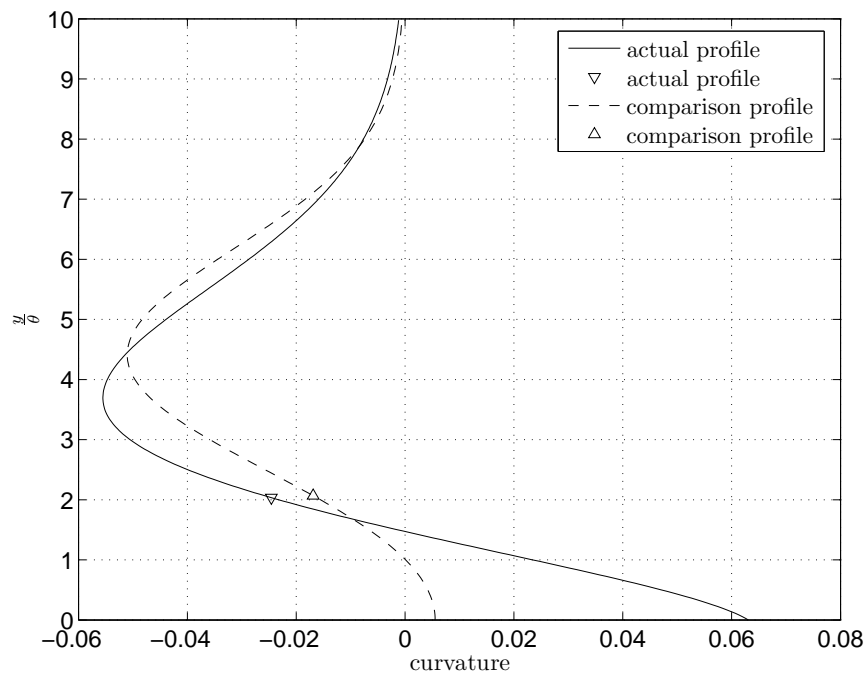
Figure 4.28: Curvature profile for $\bar{U} = sin(\bar{x})$ with suction and comparison Hartree profile without suction at equal $H = 2.6282$

Chapter 5

Comparing the asymptotic suction profile to the Hartree profiles without suction

We now want to investigate whether it can be expected that the stability diagram for the asymptotic suction profile can be derived from an extrapolation of the Arnal tables for the Hartree profiles. Figure 5.1 shows the 6 Hartree profiles for $\beta = 1$ to $\beta = 0$, from Arnal's series and the asymptotic suction profile. All profiles have been made non-dimensional by U and θ. In addition the figure shows the asymptotic suction profile in comparison with a quadratic extrapolation in $^{10}log(H)$ from the first 3 Hartree profiles nearest to the stagnation point. Figures 5.2 and 5.3 show similar results for the shear stress and curvature profiles. Hence it is concluded that the asymptotic suction profile can, with some confidence, be added to the series of Hartree profiles without an inflexion point.

Figures 5.4 and 5.5 show some results for similar boundary layers with suction/blowing and heating taken from (Wazzan et al., 1981). Also here H presents itself as a suitable parameter to characterise $Re_{\delta^*_{crit}}$, $Re_{x_{crit}}$ and Re_x for $N = 9$.
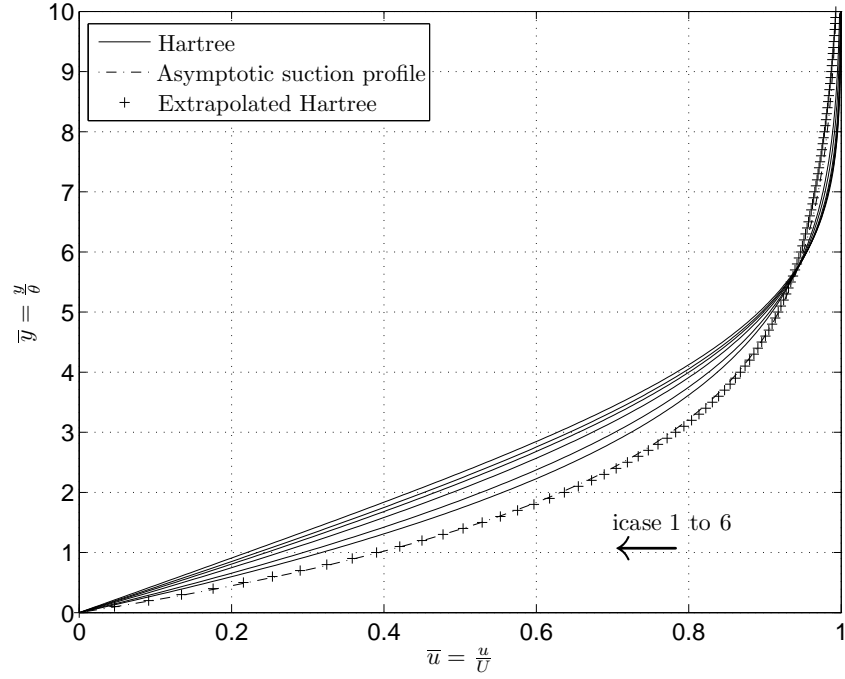
Figure 5.1: Velocity profiles for Hartree, asymptotic suction and extrapolation in $^{10}log(H)$ from icase=1:3 to $^{10}log(2)$
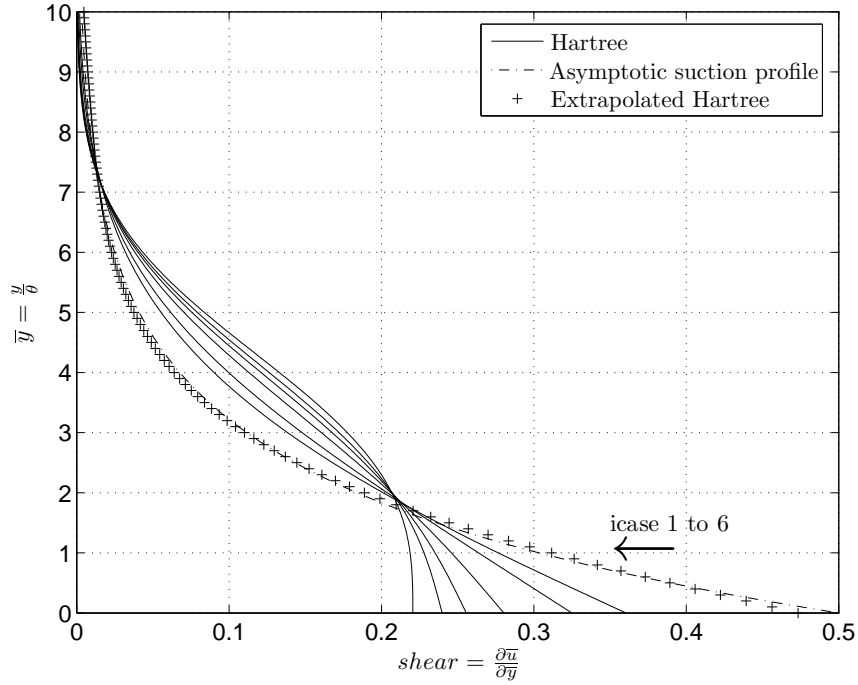
Figure 5.2: Shear profiles for Hartree, asymptotic suction and extrapolation in $^{10}log(H)$ from icase=1:3 to $^{10}log(2)$
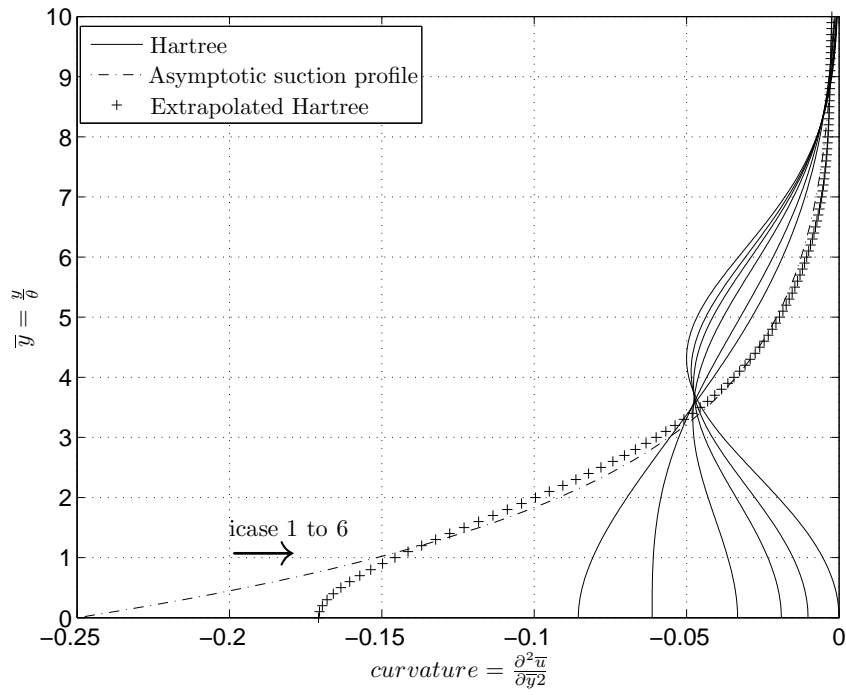
Figure 5.3: Curvature profiles for Hartree, asymptotic suction and extrapolation in $^{10}log(H)$ from icase=1:3 to $^{10}log(2)$
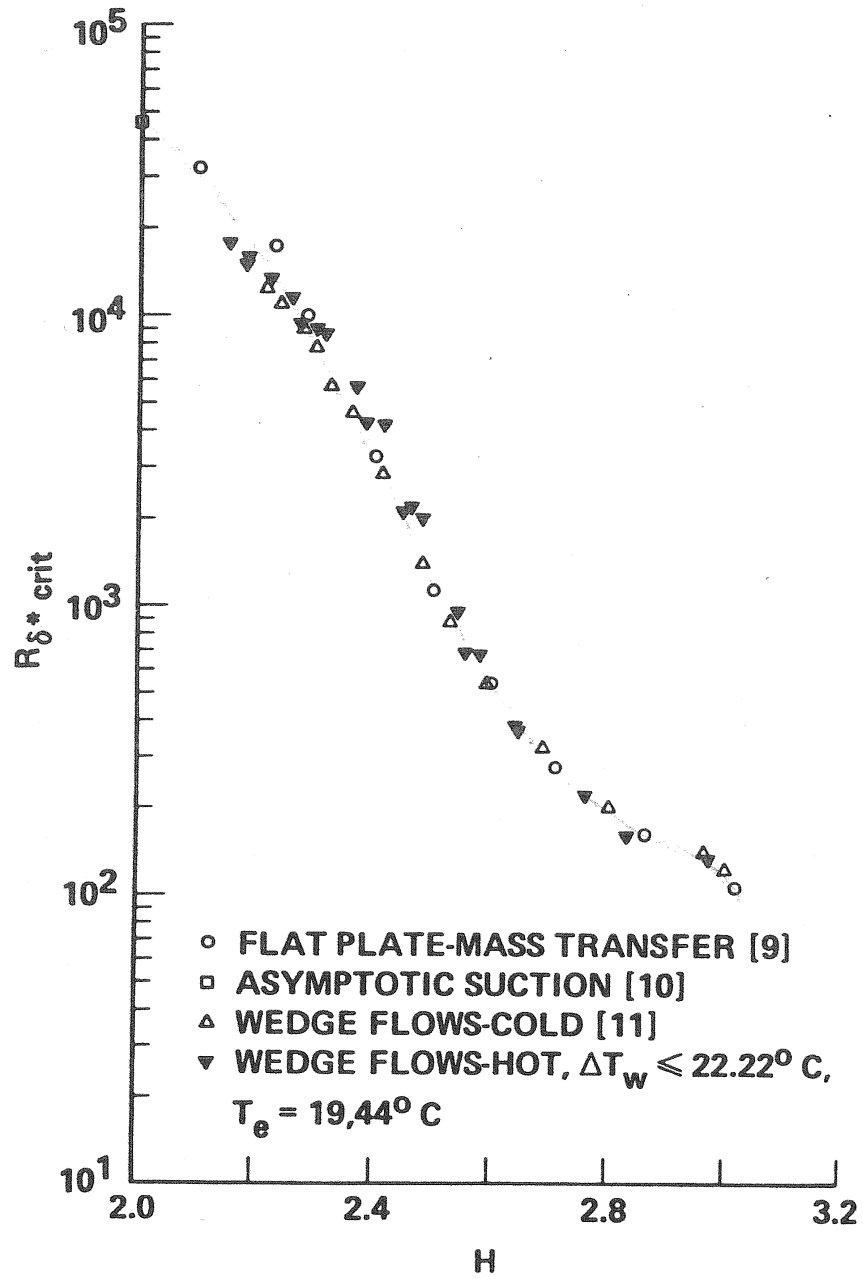
Figure 5.4: $Re_{\delta^*_{crit}}$ for flows with suction, blowing, cooling and heating plotted against H, from (Wazzan et al., 1981)
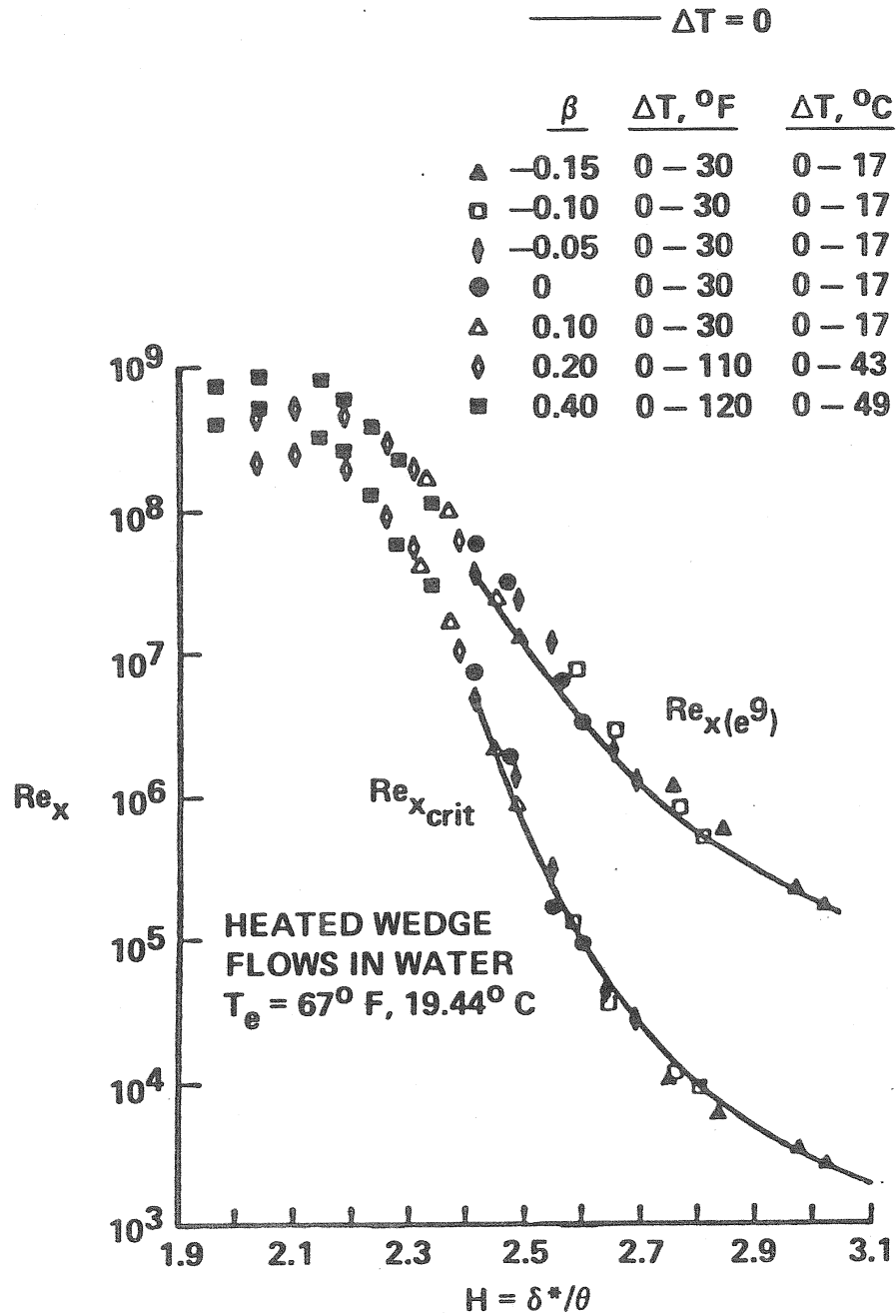
Figure 5.5: $Re_{x_{crit}}$ and Re_x for $N = e^9$ for heated (=stabilised) wedge flows in water, from (Wazzan et al., 1981)

Chapter 6

Overview of the Arnal data and development of the database method

Arnal (1986) presents solutions of the Orr-Sommerfeld equation for 15 Hartree velocity profiles without suction. An overview was given in table 3.1 where for convenience also the asymptotic suction profile is added. The critical Reynolds number for this additional case is taken from Hughes and Reid (1965). Table 6.1 (page 56) presents additional stability data for the Arnal profiles that are included in our database. The various Arnal cases are indicated in the following text and in the MATLAB programs with "icase=1:15". From the renewed analysis of the Arnal data in some cases a slightly different value for the critical Reynolds number was found; this is indicated in table 3.1. The tables that were derived from scanning the original Arnal tables can be found in the MATLAB m-files `Arnal_table_01.m` through `Arnal_table_15.m`. Note that Arnal used δ^* to make the data non-dimensional. We will use θ but left the data unchanged in the files mentioned above. For each velocity profile Arnal presents cross sections through the stability diagram for 13 to 19 values of the Reynolds number. This results in a total of 242 cross sections. In our description of the Arnal tables we have used for unification a format assuming a maximum number of 19 cross-sections per case; non-relevant entries in tables are filled in with easily recognised numbers such as 999. The number of frequencies per cross section may vary.

As an example figure 6.1 gives the Arnal table for the flat plate boundary layer at $Re_{\delta^*} = 600$. For the derivation of our data base we only need the 2nd and 3rd column, containing $\alpha_i \delta^*$ and $\frac{\omega \delta^*}{U}$ respectively. Furthermore observe that the 5th column contains $F = \frac{\omega \nu}{U^2}$ and hence should be equal to the 3rd column divided by Re_{δ^*}. To check for possible errors resulting from the scanning process our first job was to run all Arnal tables through a program that plots for each cross section the values of $-\alpha_i \delta^*$ versus $\frac{\omega \delta^*}{U}$; any gross errors immediately showed up in this way and could easily be corrected after a comparison with the original tables. **It should be noted that the other columns are not used in the present data base and hence have not been checked in this way. Future users of additional columns**

```
RDELTA1 = 0.60000E+03
*********************

alphar    alphai    omega     cr        F

0.209E+00 0.318E-02 0.750E-01 0.360E+00 0.125E-03
0.220E+00 0.200E-02 0.800E-01 0.364E+00 0.133E-03
0.231E+00 0.958E-03 0.850E-01 0.368E+00 0.142E-03
0.242E+00 0.618E-04 0.900E-01 0.372E+00 0.150E-03
0.253E+00 -.683E-03 0.950E-01 0.376E+00 0.158E-03
0.264E+00 -.127E-02 0.100E+00 0.379E+00 0.167E-03
0.275E+00 -.169E-02 0.105E+00 0.382E+00 0.175E-03
0.286E+00 -.195E-02 0.110E+00 0.385E+00 0.183E-03
0.297E+00 -.203E-02 0.115E+00 0.387E+00 0.192E-03
0.308E+00 -.194E-02 0.120E+00 0.390E+00 0.200E-03
0.319E+00 -.166E-02 0.125E+00 0.392E+00 0.208E-03
0.329E+00 -.120E-02 0.130E+00 0.395E+00 0.217E-03
0.340E+00 -.551E-03 0.135E+00 0.397E+00 0.225E-03
0.351E+00 0.291E-03 0.140E+00 0.399E+00 0.233E-03
0.362E+00 0.133E-02 0.145E+00 0.401E+00 0.242E-03
0.372E+00 0.257E-02 0.150E+00 0.403E+00 0.250E-03
0.383E+00 0.400E-02 0.155E+00 0.405E+00 0.258E-03
```

Figure 6.1: Note: alphar $= \alpha_r \delta^*$; alphai $= \alpha_i \delta^*$; omega $= \frac{\omega \delta^*}{U}$; cr $= \frac{c_r}{U}$; F$= \frac{\omega \nu}{U^2}$

of the scanned tables should make their own checks.

To extract the data for our database we have run the Arnal tables through various programs; each time calling a different routine from the positions marked in `Arnal_table_01.m` through `Arnal_table_15.m`. These m-files were only used to derive our database and will not be reproduced here. In the following sections the process of defining the data base will be discussed in some detail. Only a limited number of figures will be included. The reader can easily follow the process by loading the database and running the various options of the MATLAB program `N_factor_show.m` concurrent with reading the text and following the explanations given below.

First the amplification rate $-\alpha_i \theta$ is converted into the quantity T:

$$T = \frac{-\alpha_i \theta}{Re_\theta} \cdot 10^6 \qquad (6.1)$$

as introduced in chapter 2. The disturbance frequency will be non-dimensionalised in two ways; each of which has its own merits as will be shown later. We will be using:

$$\frac{\omega \theta}{U} \quad and \quad F = \frac{\omega \nu}{U^2} = \frac{\frac{\omega \theta}{U}}{Re_\theta} \qquad (6.2)$$

Neutral curves for $\beta = 1$ (icase=1; stagnation point); $\beta = 0$ (icase=6; flat plate) and $\beta = -.198838$ (icase=11; separation profile) were shown in figs. 2.3 through 2.5. The complete diagrams for these values of β and in addition for the separated profile with H=35.944 are shown in figs. 6.2 through 6.5. All 15 diagrams can be viewed by running `N_factor_show.m` and selecting option 7.

Note the characteristic difference for profiles without (icase=1:6) and with inflexion point (icase=7:15). In order to bring the Arnal data into a form which allows easy and accurate interpolation between the various icase and Re_θ we try to scale and shift the diagrams in such
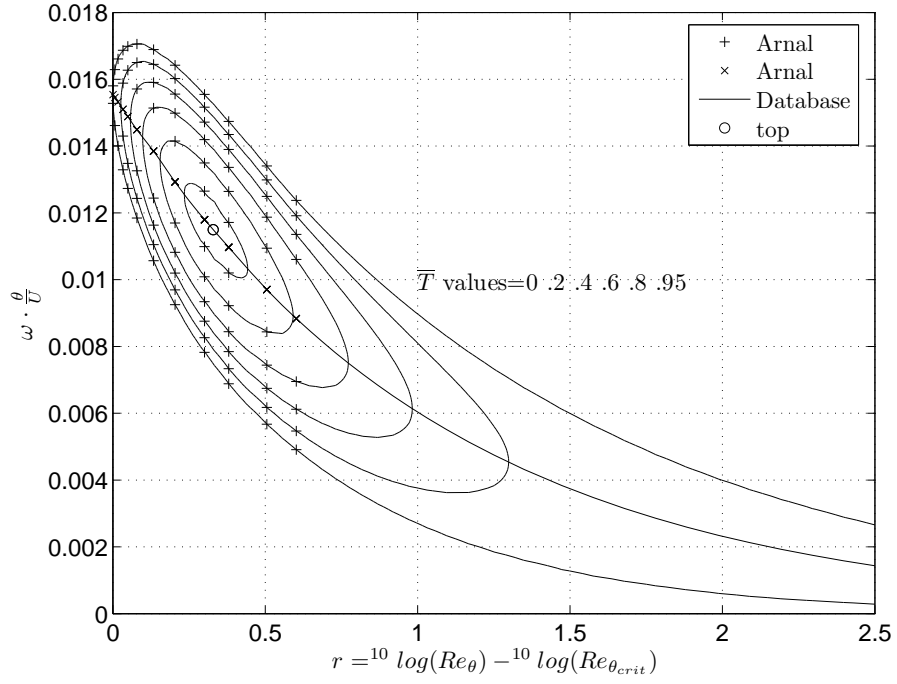
Figure 6.2: Classic stability diagram; icase $= 1$ ($\beta = 1$, stagnation point); $\overline{T} = \frac{T}{T_{maxmax}}$
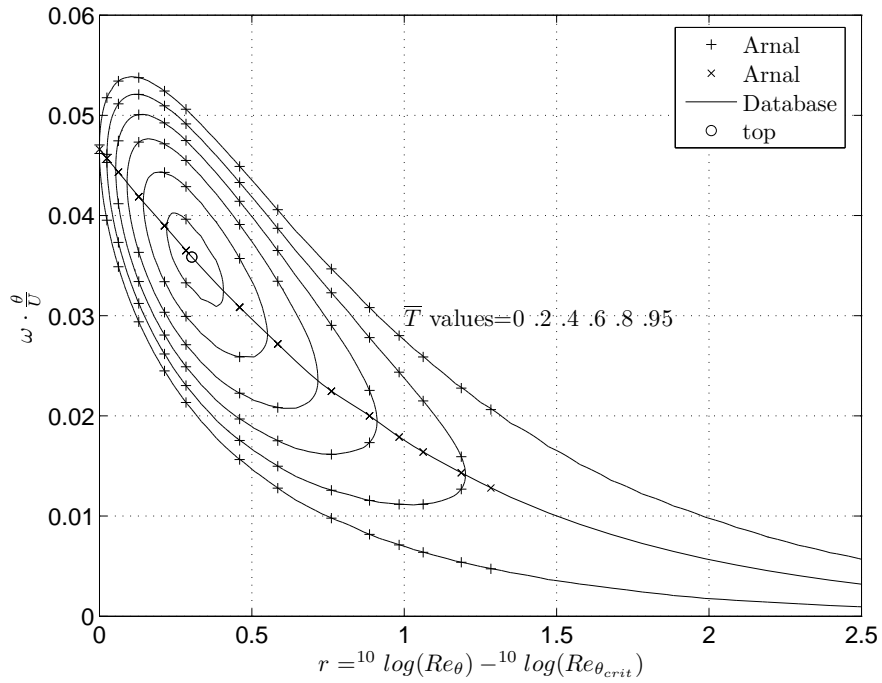
Figure 6.3: Classic stability diagram; icase $= 6$ ($\beta = 0$, flat plate); $\overline{T} = \frac{T}{T_{maxmax}}$
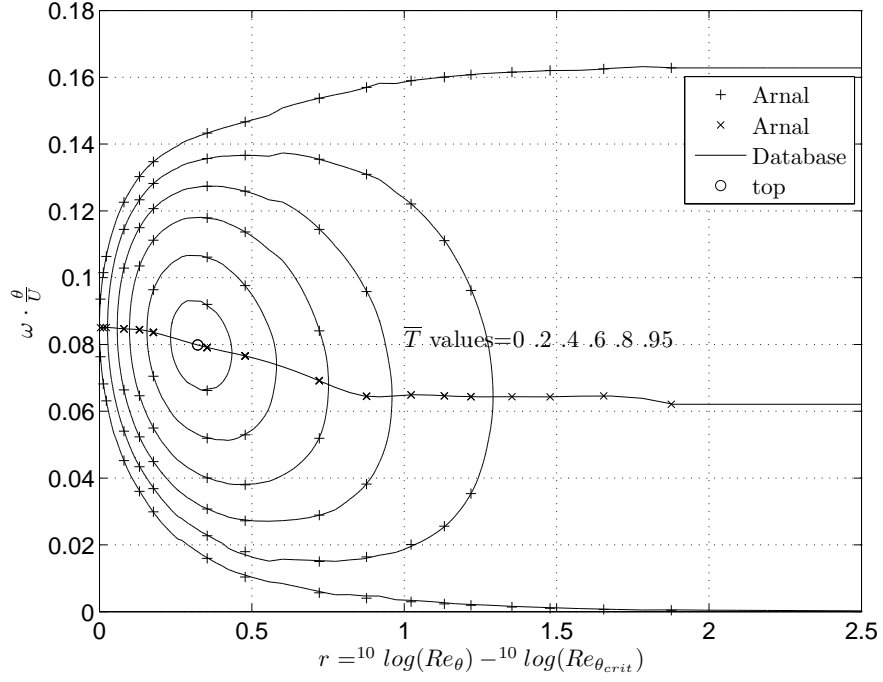
Figure 6.4: Classic stability diagram; icase = 11 ($\beta = -0.198838$, separation); $\overline{T} = \frac{T}{T_{maxmax}}$
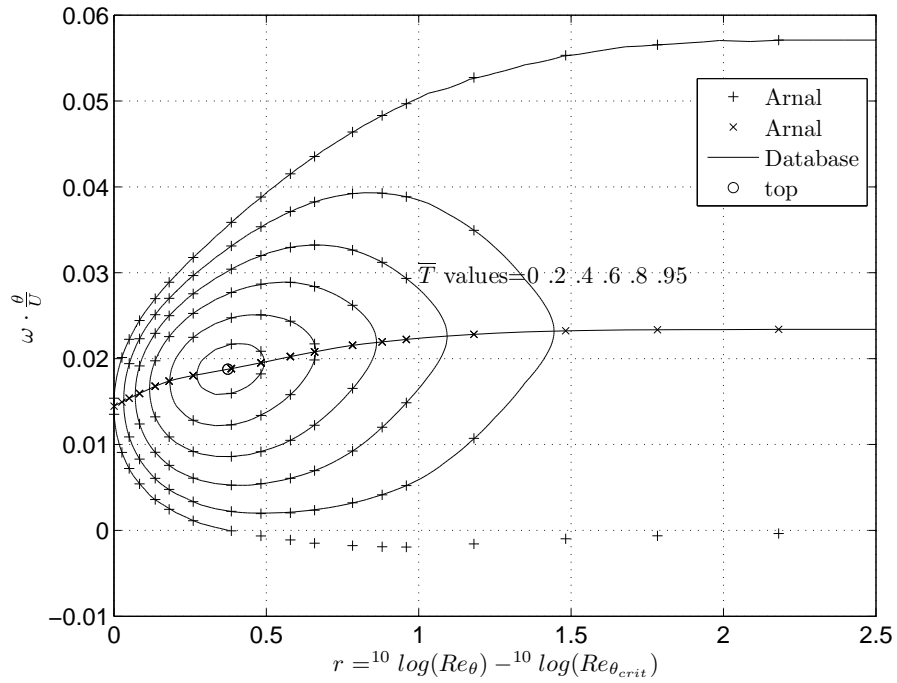
Figure 6.5: Classic stability diagram; icase = 15 ($\beta = -0.04$, $H = 35.944$); $\overline{T} = \frac{T}{T_{maxmax}}$

a way that as much as possible from the variation is removed. A first shifting of the diagrams by introducing:

$$r =^{10} log(Re_\theta) -^{10} log(Re_{\theta_{crit}}) \tag{6.3}$$

was already done in figs. 6.2 through 6.5. Points for which T reaches its maximum value T_{max} in a certain cross section form the "axis". The absolute maximum of T for the whole diagram is denoted by T_{maxmax} and is given in table 6.1(next page) for all icase. From the table it follows that T_{maxmax} varies with several orders of magnitude from icase=1 to 15; in our plots we will use $^{10}log(T_{maxmax})$.

Table 6.1: Data for the 15 Arnal profiles

icase	β	H	number of crossections	r_{top}	$scale^*$	T_{maxmax}	^{10}log (T_{maxmax})	$Re_{\theta_{crit}}$	^{10}log $(Re_{\theta_{crit}})$
1	1.	2.216	13	0.3291	0.003767	0.1185	-0.92628	5641.57	3.7514
2	0.5	2.297	13	0.3259	0.004037	0.1931	-0.71422	3372.09	3.5279
3	0.2	2.411	15	0.3197	0.00556	0.615	-0.21112	1185.22	3.0738
4	0.1	2.481	18	0.3145	0.007802	1.6103	0.20691	559.62	2.7479
5	0.05	2.529	16	0.3074	0.010101	3.2333	0.50965	344.42	2.5371
6	0.	2.591	15	0.3032	0.014209	7.487	0.87431	200.63	2.3024
7	-0.05	2.676	16	0.3063	0.020793	18.258	1.2614	117.78	2.0711
8	-0.1	2.802	17	0.303	0.030183	45.867	1.6615	70.58	1.8487
9	-0.15	3.023	17	0.31	0.043024	119.42	2.0771	41.66	1.6198
10	-0.185	3.378	17	0.3187	0.055643	274.53	2.4386	26.17	1.4179
11	-0.1988	4.029	18	0.3224	0.062504	577.37	2.7615	16.49	1.2174
12	-0.16	6.752	16	0.342	0.05551	1695.9	3.2294	6.42	0.83523
13	-0.12	10.056	14	0.3546	0.042963	2599.2	3.4148	3.99	0.60191
14	-0.08	16.467	18	0.3567	0.030196	3668.9	3.5645	2.21	0.34552
15	-0.04	35.944	19	0.3735	0.016734	5148.2	3.7117	0.91	-0.037824

(*) as defined in figures 2.3 through 2.5
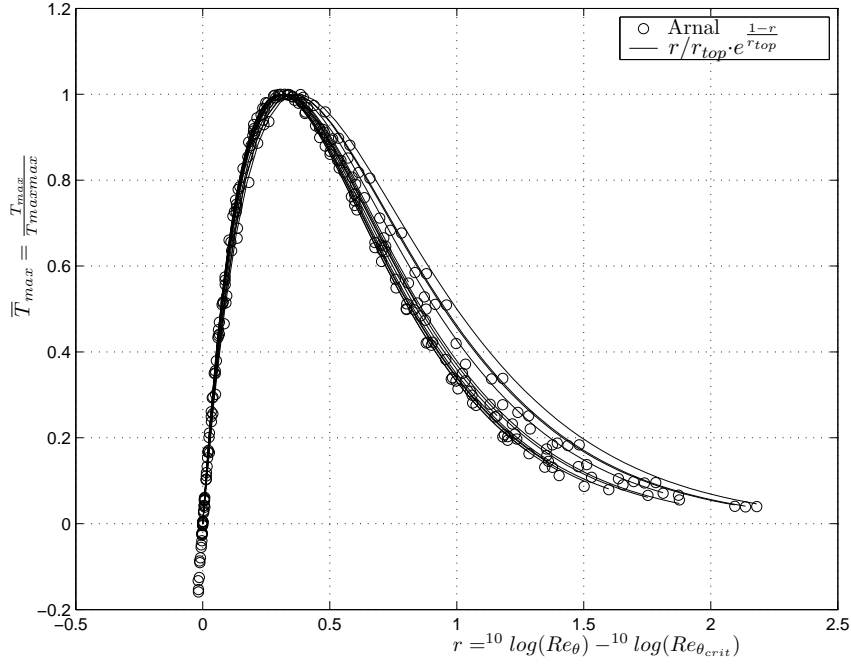
Figure 6.6: $\overline{T_{max}}$ vs r for icase 1-15

T will be non-dimensionalized with T_{maxmax} reducing the maximum value for each diagram to 1. Non-dimensional values of $T = T_{max}$ on the axis will be denoted by $\overline{T_{max}}$. From fig. 6.6 and program `review_Tbar.m` (option 5 in the "N_factor_show)" it follows that $\overline{T_{max}}$ vs r is a nearly universal curve for all 15 cases. If we introduce r_{top} as the value for r at which T_{max} reaches T_{maxmax}, and plot $\overline{T_{max}}$ as a function of $\overline{r} = \frac{r}{r_{top}}$ all curves very nearly collapse. See fig. 6.7 and `review_scaling.m` (`N_factor_show.m` option 6) Moreover this universal curve is very well approximated by

$$\overline{T_{max}} = \overline{r}e^{1-\overline{r}} \tag{6.4}$$

The "axis", as locus of T_{max}, is found to be better plotted as $^{10}log(F_{axis})$, where

$$F = \frac{\omega\nu}{U^2} = \frac{\omega\theta}{U}\frac{1}{Re_\theta} \tag{6.5}$$

Results are shown in fig. 6.8. The axes in this format turn out to be nearly straight and rather evenly distributed and hence well suited for later extrapolation and interpolation. The kinks in the axes for icase > 6 at higher values of r are due to the appearance of Rayleigh instability for velocity profiles with an inflexion point. Because for Rayleigh instability $\frac{\omega\theta}{U}$ for the upper branch of the neutral curve and for the axis become constant the slope of these curves in the $^{10}log(F)$ format vs r becomes -1. The slope for cases without inflexion point appears to be near to $-\sqrt{2}$; whether this is exact and could be proved is unknown to the author. The coordinates of the "top of the amplification mountain" are denoted by r_{top} and $^{10}log(F_{for\ top})$. As an average value for r_{top} we will sometimes use $r_{top} = \frac{1}{3}$. The values for $^{10}log(F_{axis})$ at $r = \frac{1}{3}$ for icase = 1:15 are shown in figure 6.9 as function of $^{10}log(Re_{\theta_{crit}})$. It is easy to extrapolate the 15 values to the value of $^{10}log(Re_{\theta_{crit}})$ for the asymptotic suction profile. (indicated by + in the figure).
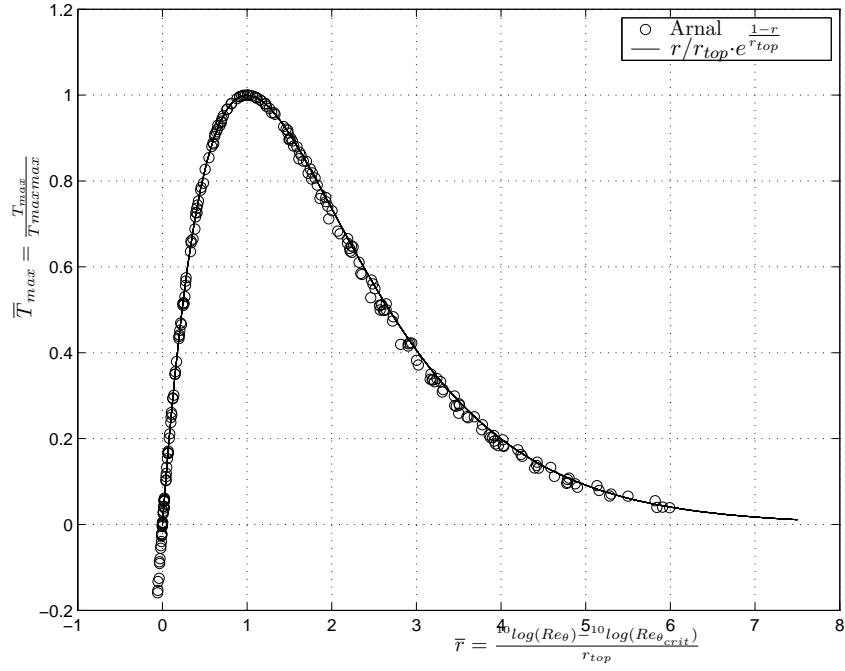
Figure 6.7: $\overline{T_{max}}$ vs $\bar{r}$ for icase 1-15
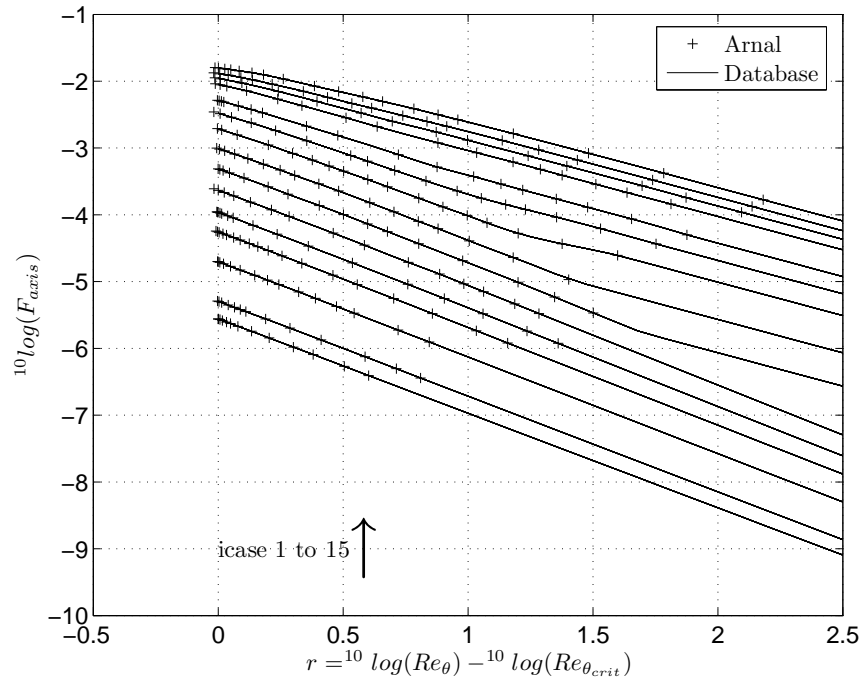
Figure 6.8: $^{10}log(F_{axis})$ as function of r for Arnal data $(+)$ and for the data base
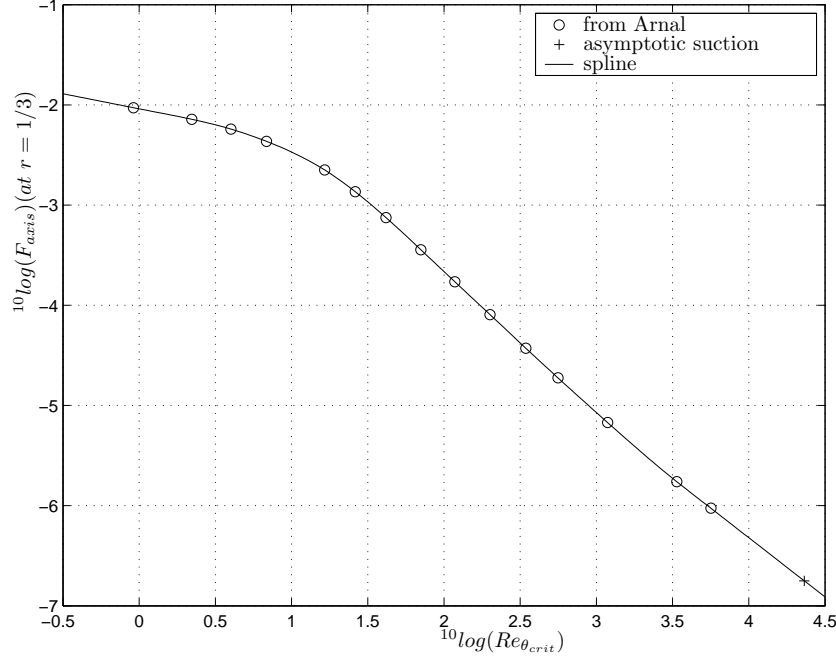
Figure 6.9: $^{10}log(F_{axis})$ at $r = \frac{1}{3}$ vs $^{10}log(Re_{\theta_{crit}})$

The coordinates of the 242 cross sections given by Arnal are plotted in fig. 6.10 as values of $^{10}log(Re_{\theta_{crit}})$ vs. r. This plot will later be used as a "road map" to trace a developing boundary layer from the stable region ($r < 0$), possibly into the unstable region ($r > 0$) and sometimes due to sufficient suction back into the stable region ($r < 0$).

In order to further reduce the variation we will scale $\frac{\omega\theta}{U}$ with the scale as defined in figures 2.3 through 2.5. Using this scale the frequencies in each crosssection are finally scaled as :

$$\overline{\omega} = \frac{\frac{\omega\theta}{U} - \frac{\omega\theta}{U}\,axis}{scale} \tag{6.6}$$

All interesting Arnall values are now found in the region $-2 \leq \overline{\omega} \leq 3$. Fig 6.11 shows, as an example, all T for all cross sections for the flat plate diagram vs $\frac{\omega\theta}{U}$. Figure 6.12 shows the same results but now in the form $\frac{T}{T_{maxmax}}$ vs $\overline{\omega}$ so that all maxima are found at $\overline{\omega} = 0$. See also `N_factor_show.m`, option 6.

A final shifting is performed by moving the curves in fig. 6.12 in vertical direction so that the local maximum value of the shifted $\overline{T}$ becomes zero. (fig. 6.13) The values of T thus obtained will be denoted by T_{ss} (ss stands for shifted and scaled). To show to what extent the Arnal data have been prepared for interpolation all 242 T_{ss} plotted versus $\overline{\omega}$ can be viewed using `review_scaling.m` . (option 6 in the `N_factor_show.m`)

A number of results obtained thus far have been curve-fitted by splines and plotted in figures 6.9 and 6.14 through 6.18. In these figures the 15 Arnal cases (indicated by a 0) are supplemented by known or extrapolated values for the asymptotic suction profile (indicated by +).
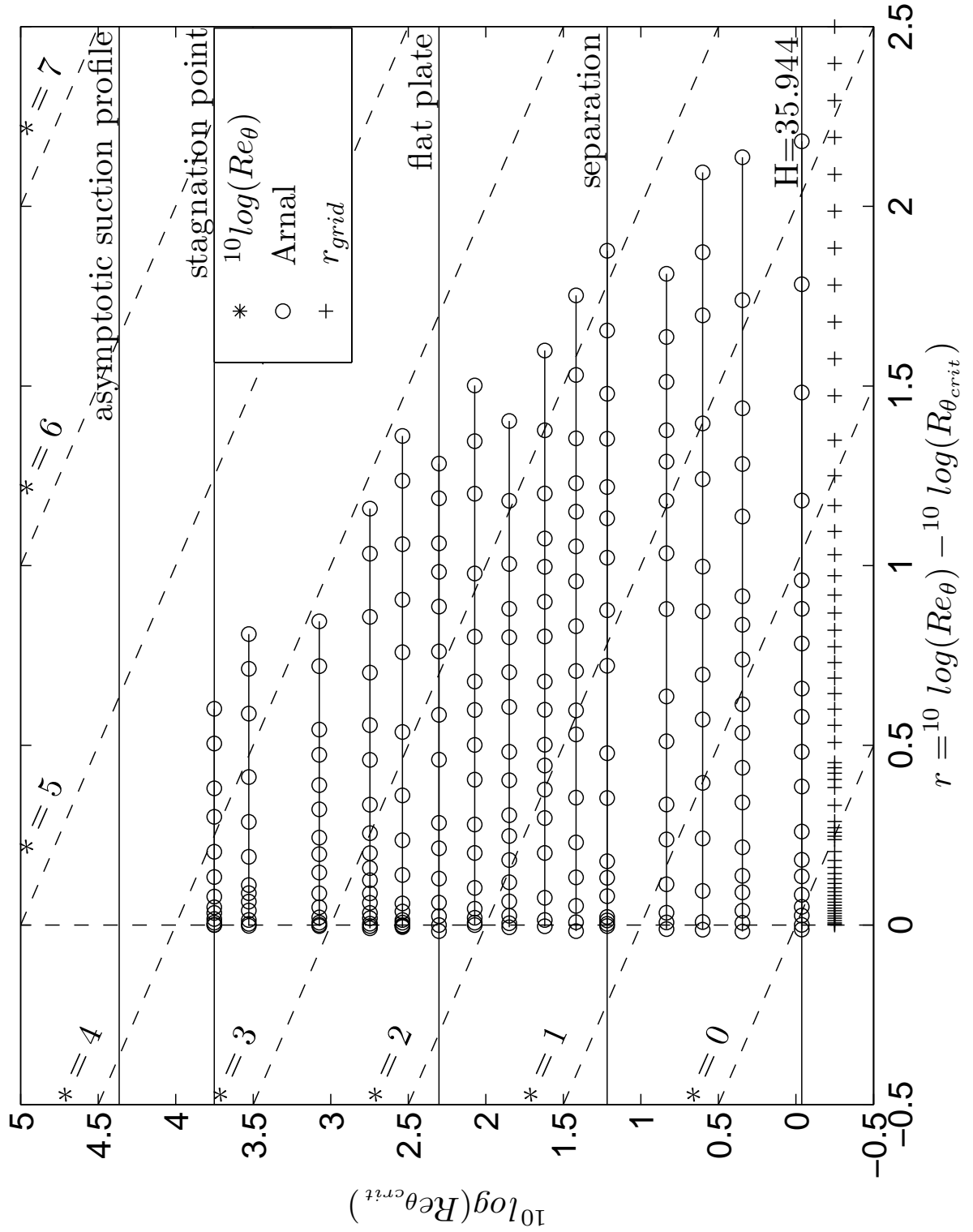
Figure 6.10: Roadmap showing $^{10}log(Re_{\theta_{crit}})$ vs $r =^{10} log(R_\theta) -^{10} log(R_{\theta_{crit}})$
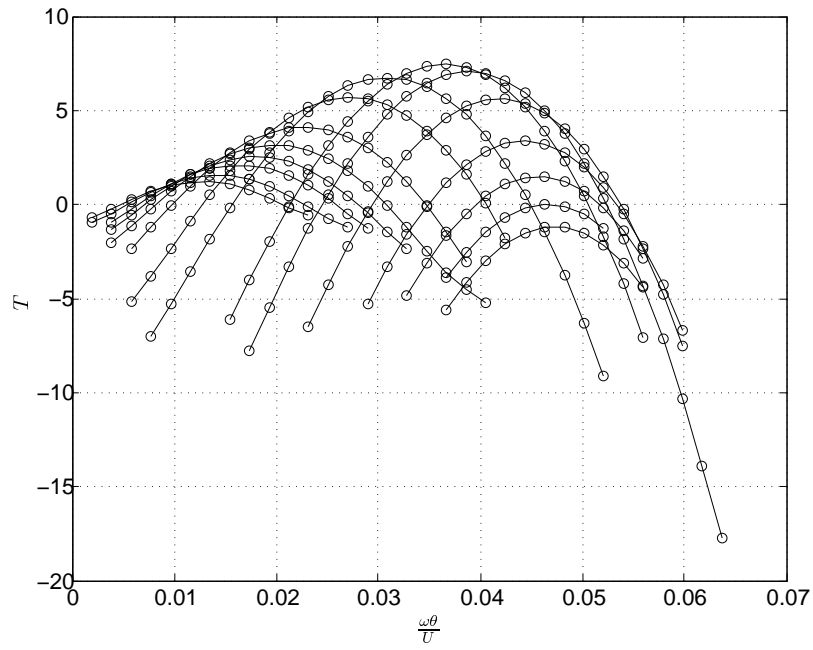
Figure 6.11: T vs $\frac{\omega\theta}{U}$ for flat plate
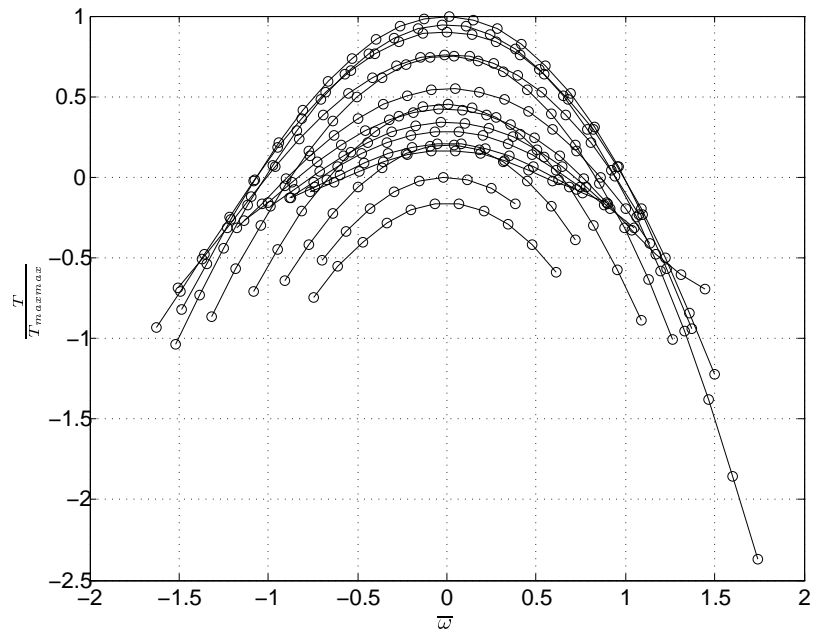
Figure 6.12: $\frac{T}{T_{maxmax}}$ vs $\overline{\omega}$ for flat plate
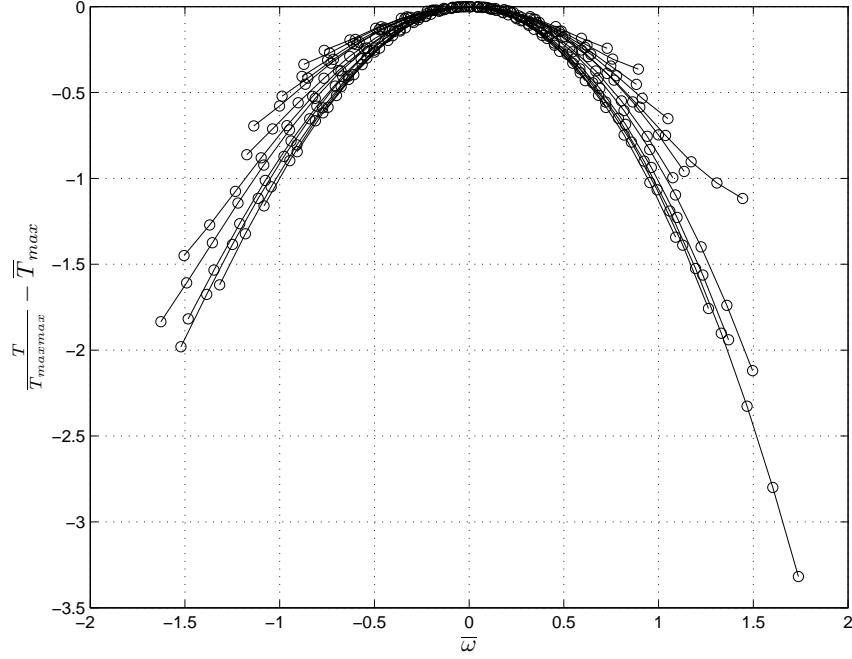
Figure 6.13: $\frac{T}{T_{maxmax}} - \overline{T_{max}}$ vs $\overline{\omega}$ for flat plate

All splines can be inspected by running `review_splines.m`. (option 4 in the `N_factor_show.m`) All splines are in the format used in the Student version of MATLAB 5. Appendix A gives an explanation of this format and contains a function to translate these MATLAB 5 splines into other spline formats.

Inspecting the "road map" in figure 6.10 shows that the Arnal data points are distributed rather irregular and moreover have an upper limit at a variable value of r. This makes interpolation in this area rather cumbersome. To ease interpolation and possibly extrapolation we introduced a 59 point non-equidistant "r_{grid}" in the region $0 \le r \le 2.5$. Because variations are fast near $r = 0$ and slow near $r = 2.5$, the density of the r-grid has been chosen accordingly. In all 15 x 59 =885 points a T_{ss} spline has been defined; either by quadratic Lagrange interpolation within the Arnal region for constant icase or by extrapolation to the right from the last Arnal point until $r = 2.5$. The extrapolation will not be described in detail because this region is less important. In practice it will seldom be used because it can be expected that transition will occur within the Arnal covered range. To illustrate this, figure 6.19 shows the roadmap with curves for constant N-factors of 1 through 15 that were calculated for the Hartree and Stewartson similar flows. Of course the vertical axis $r = 0$ corresponds to $N = 0$. In applications of the database method we will use the roadmap shown in figure 6.20 where only the curve for $N = 9$ is shown. Note that for similar boundary layers the interpolation of T_{ss} is done along horizontal lines for constant H and hence constant $^{10}log(Re_{\theta_{crit}})$. For non-similar flows the curves for N are not valid. Imagine a trace in the roadmap approaching the $N = 9$ curve from the left after which such a distribution of suction with x is applied that the $N = 9$ curve is not crossed. Because still being in the unstable region for $r > 0$ it should be expected that transition may occur to the left of the $N = 9$
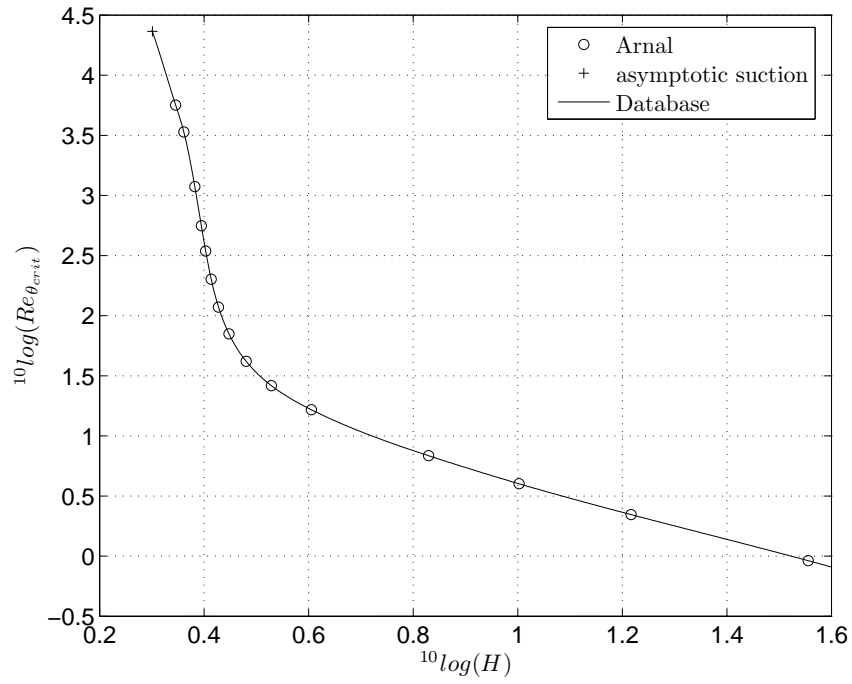
Figure 6.14: $^{10}log(Re_{\theta_{crit}})vs^{10}log(H)$
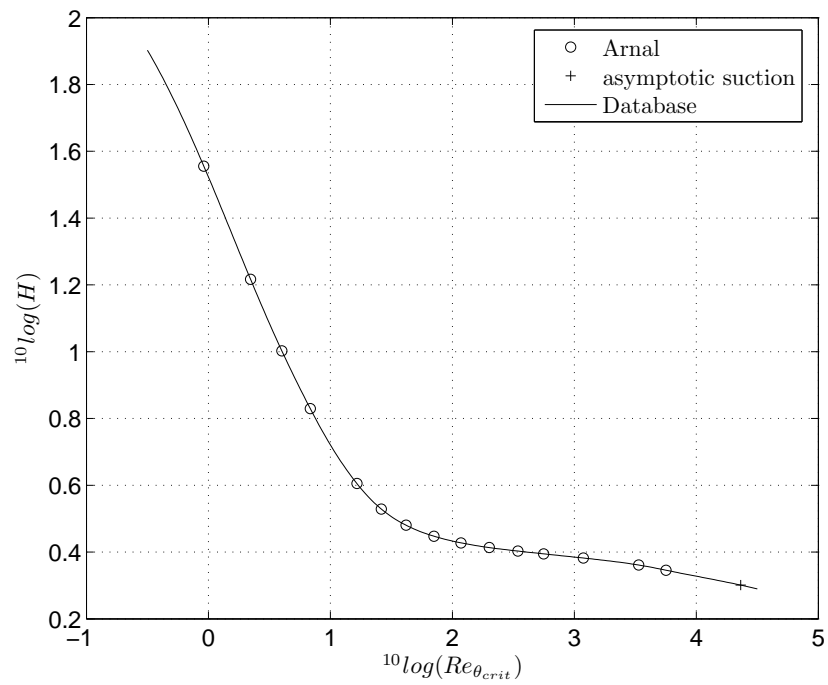
Figure 6.15: $^{10}log(H)vs^{10}log(Re_{\theta_{crit}})$
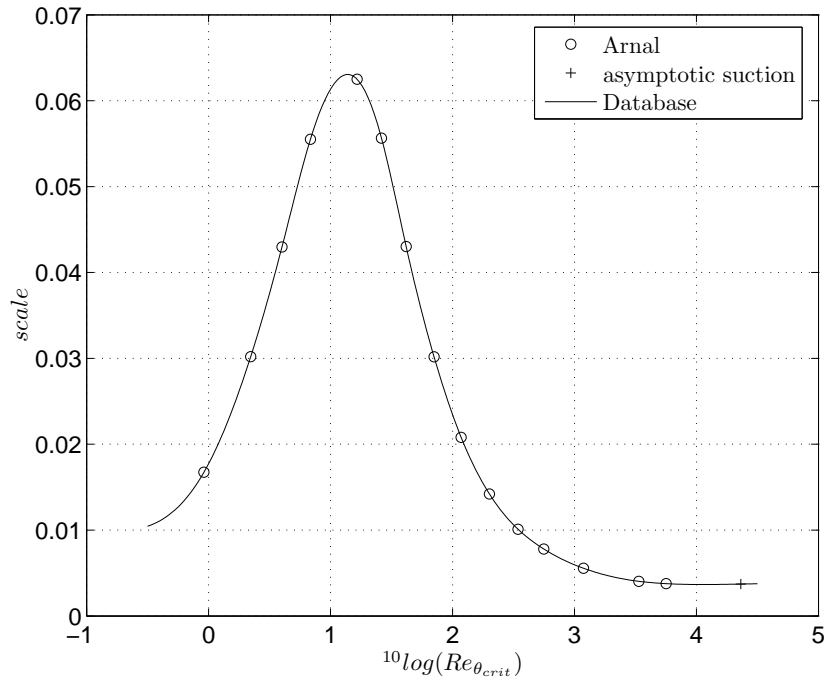
Figure 6.16: *Scale* vs $^{10}log(Re_{\theta_{crit}})$
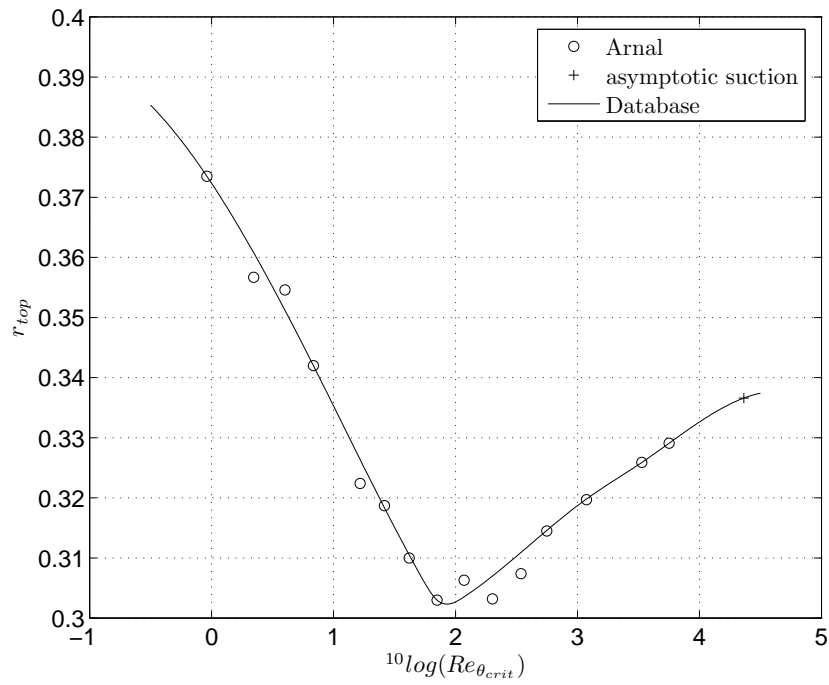
Figure 6.17: r_{top} vs $^{10}log(Re_{\theta_{crit}})$
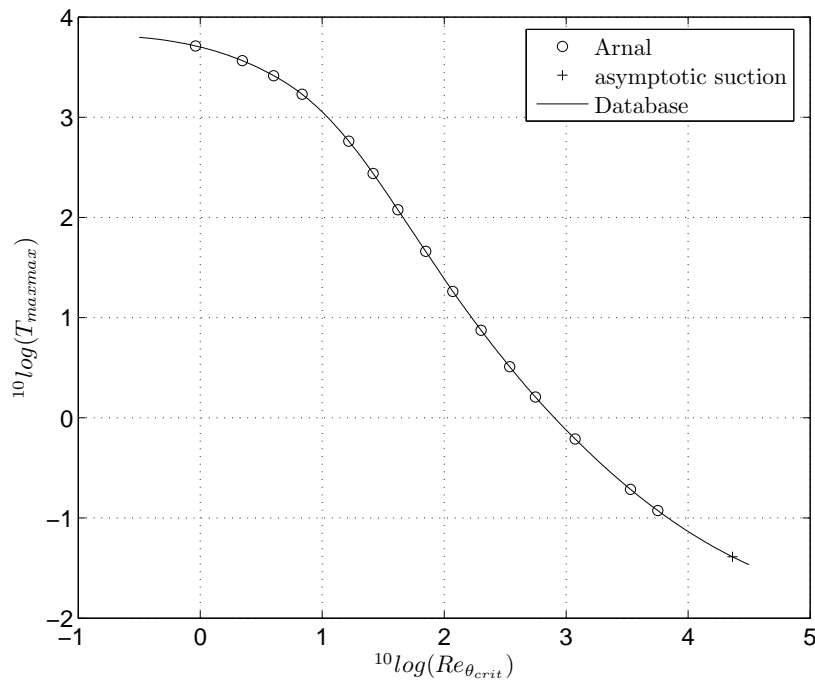
Figure 6.18: $^{10}log(T_{maxmax})$ vs $^{10}log(Re_{\theta_{crit}})$

curve.

The T_{ss} splines have been defined in 34 points in the interval $-2 \leq \overline{\omega} \leq 3$. It may occur in certain extreme cases that the splines are extrapolated beyond the boundaries -2 and $+3$. Cubic spline polynomials may behave badly when used too far outside their definition region. Therefore care was taken to ensure that the first and last spline polynomials reduced exactly to a linear function avoiding bad behaviour. Because the student version of MATLAB 5 limits arrays to a maximum of 16384 elements the T_{ss} splines were put into cell-arrays. A function `cross_cut.m` was written that uses a two-dimensional quadratic Lagrange interpolation in the nearest 9 points in the 15 x 59 grid to find the T_{ss} spline at arbitrary values of $^{10}log(Re_{\theta_{crit}})$ and r. Because the spline format in MATLAB allows linear operations (like the Lagrange interpolation) on the whole spline at once, `cross_cut.m` works very fast. Furthermore it should be mentioned that the MATLAB 5 spline format contains some integer "identification numbers". After the interpolation these may have become classified as "reals" and may have to be restored. The function `rectify_Tss.m` does this and also restores the linear ends of the spline after interpolation. Figure 6.21 shows a schematic of the road map area divided in certain regions. Note that region 5 is covered by the (extrapolated) Arnal data as described earlier. In coming applications we also want to be able to enter the regions for $r < 0$ to calculate the stabilising effects of strong suction. This will be explained in chapter 10 when the working of `cross_cut.m` is explained in some detail. The comment lines in the m-file itself can also be consulted for further explanations. With strong suction we may also enter the region for $H < 2.2$, approaching $H = 2$ for the asymptotic suction profile. Chapter 10 will also go into this extrapolation in some more detail.

Late in the present study it has become clear that the variation of the T_{ss} splines with varying
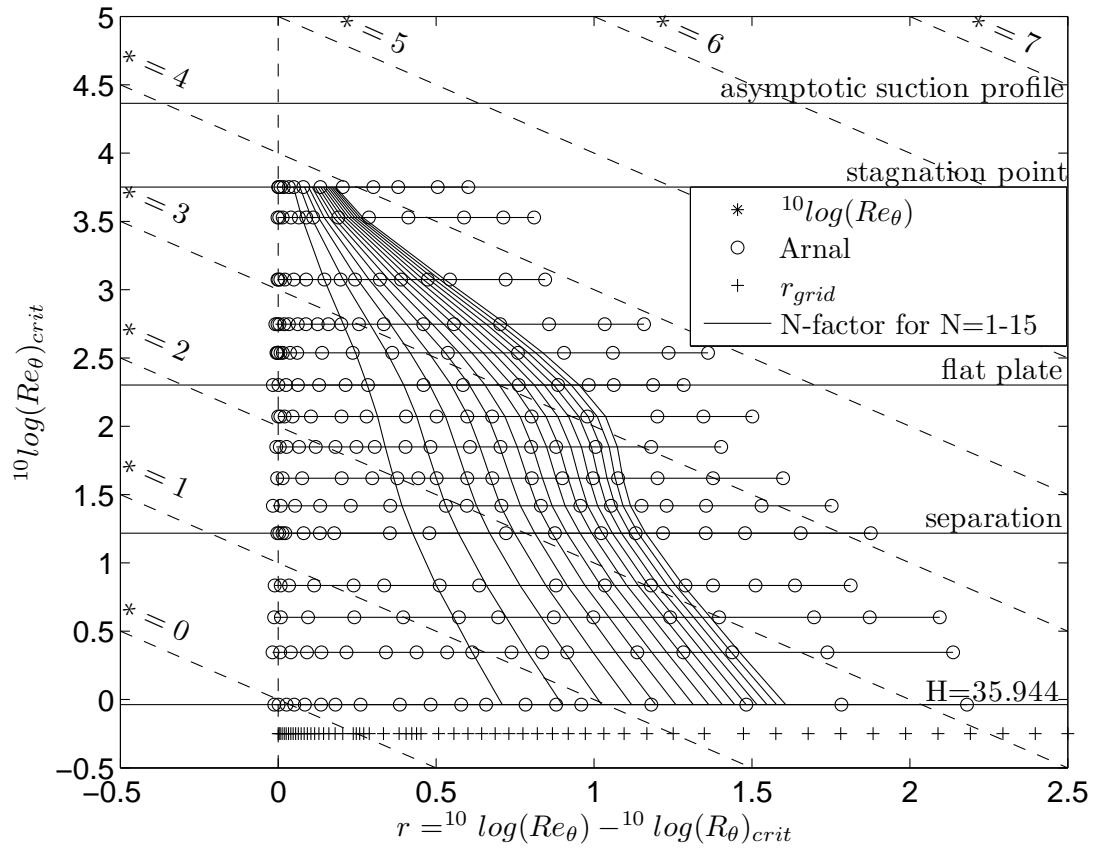
Figure 6.19: *N*-factor in roadmap, *N*=1-15
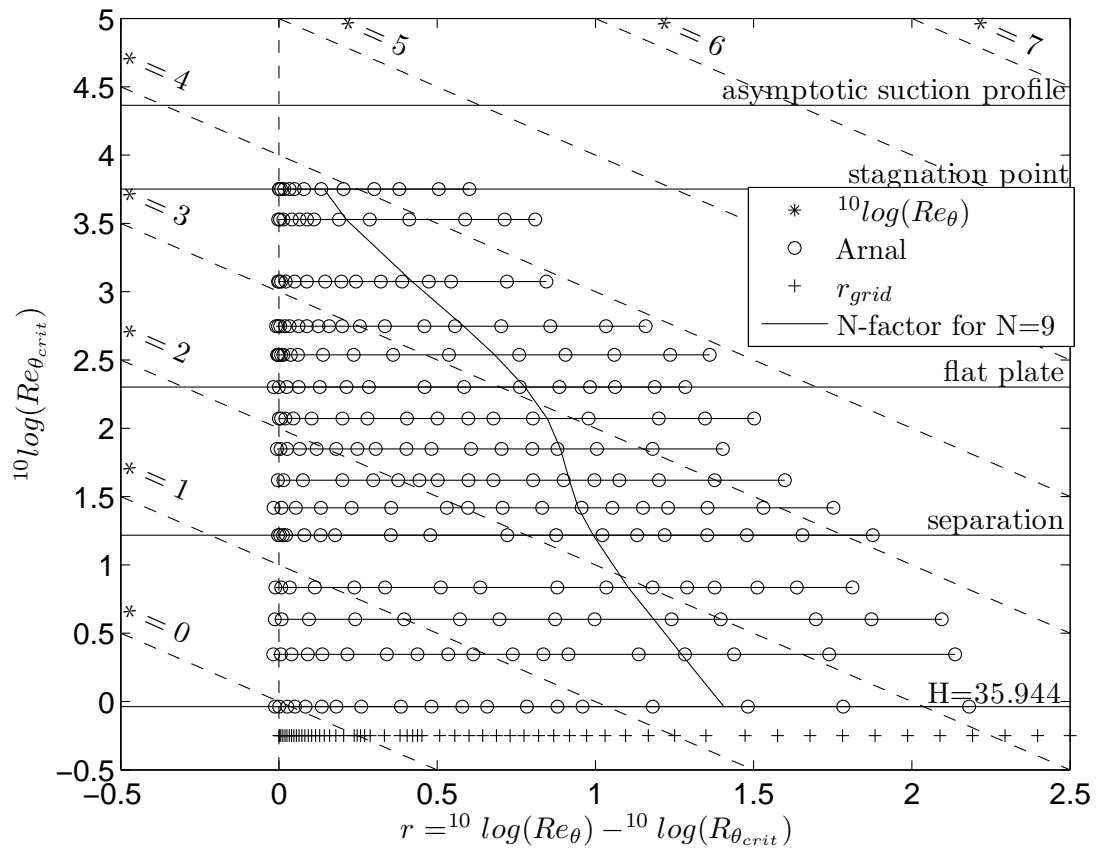
Figure 6.20: *N*-factor in roadmap, $N = 9$

icase but at constant r, is rather small. Based on this observation a function cross_cut_fast.m has been developed that is much faster than cross_cut.m but also somewhat less accurate. This faster version will be discussed in chapter 11.
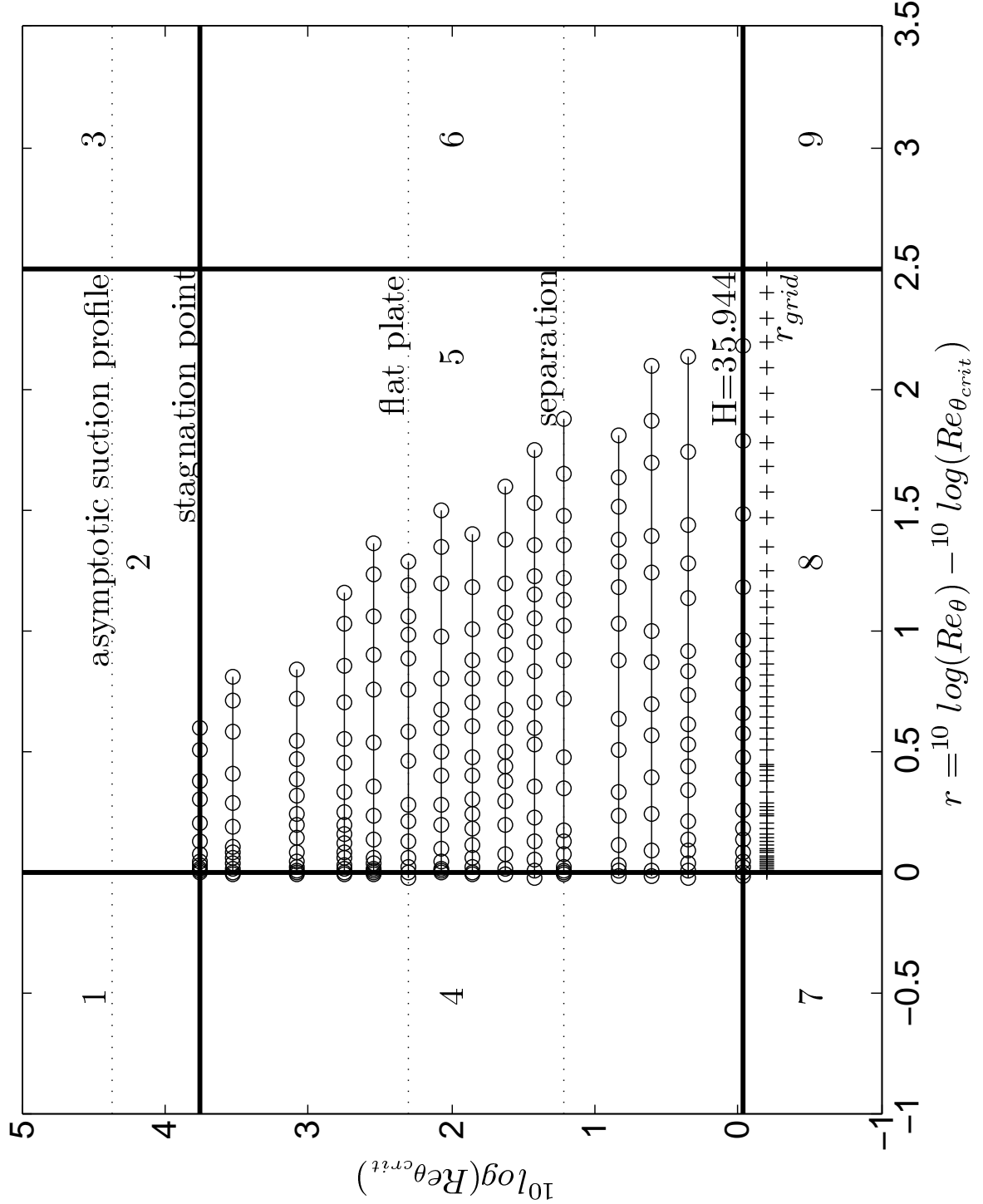
Figure 6.21: Schematic roadmap with 9 regions (the circles represent the Arnal points

Chapter 7

Comparison of stability diagrams according to Arnal and the database

Once the database has become available it is rather easy to generate the stability diagram for an arbitrary value of the shape factor H in the range $2.216 \leq H \leq 35.944$ as covered by the Arnal data and its extrapolation to $r = 2.5$. We will first as a check demonstrate how well the database reproduces the Arnal data. The program `comp_data_base_to_Arnal.m` (option 2 in the `N_factor_show.m`) shows, for values of icase that can be selected, all Arnal cross sections and its approximation by the T_{ss} spline. Fig 7.1 through 7.4 give some typical examples namely for icase=1 (stagnation point, $H = 2.216$), icase=6 (flat plate, $H = 2.591$), icase=11 (separation profile, $H = 4.029$) and icase=15 ($H = 35.944$). The correspondence is seen to be excellent. In all cases the crosssection nearest the top has been selected. Complete stability diagrams for values of icase that can be selected can be calculated in various forms by the following programs that are part of the `N_factor_show.m`

1. `plot_stability_diagrams.m` (option 7 in `N_factor_show.m`) gives the diagrams in the classical form and also the scaled and shifted version. This last form gives contour plots for $\overline{T} = \frac{T}{T_{maxmax}}$ in the variables r along the horizontal axis and $\overline{\omega}$ as defined by equation (6.6) along the vertical axis. In all cases full curves denote the database result; symbols are for the Arnal data. In the program the choice can be made to superimpose various shifted and scaled diagrams. It follows that the scaled and shifted diagrams for icase=1 to 6, that is from stagnation point to flat plate, are very similar if not identical. Figure 7.5 through 7.10 show some examples. It should be observed that the extrapolated righthand "tails" of the scaled and shifted diagrams do not collapse as well as the left hand parts. However these extrapolations were made before the similarity was realised. Had this been known earlier the extrapolations would have been made in the scaled and shifted form imposing the similarity. In chapter 8 we will show that this similarity will allow us to generate a very good approximation for the diagrams for icase=2 to
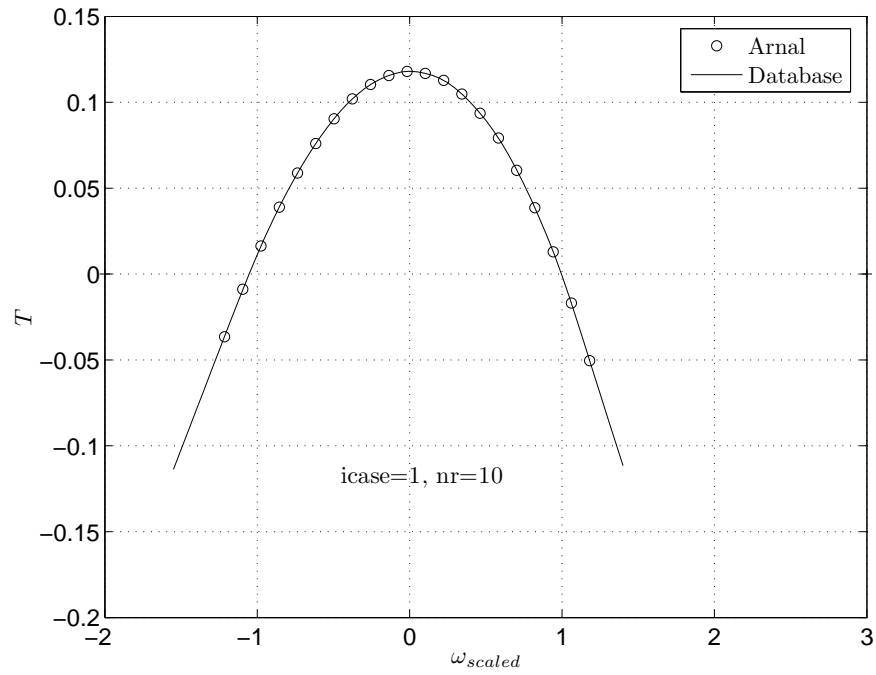
Figure 7.1: T vs ω_{scaled}, icase $= 1$ ($\beta = 1$, stagnation point)
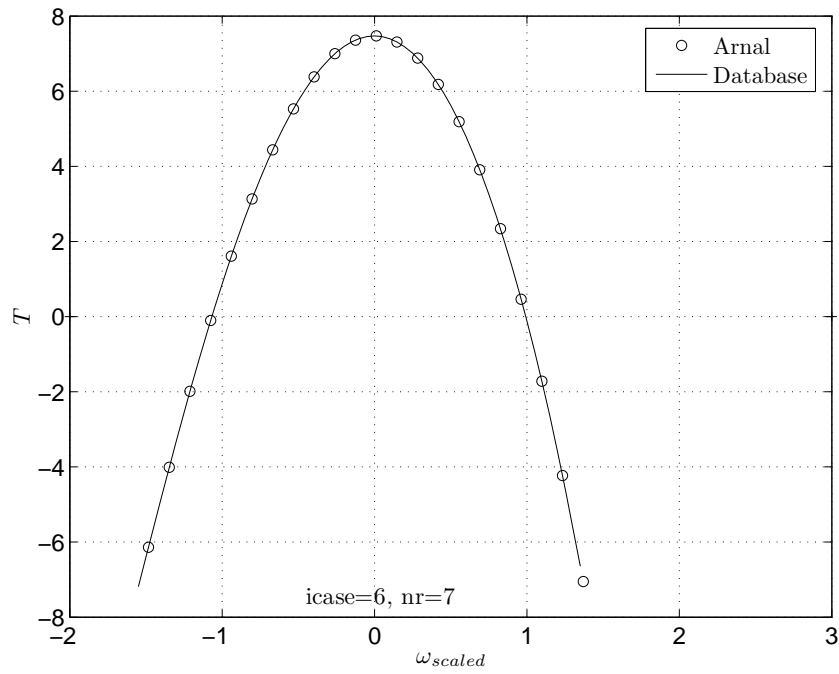
Figure 7.2: T vs ω_{scaled}, icase $= 6$ ($\beta = 0$, flat plate)
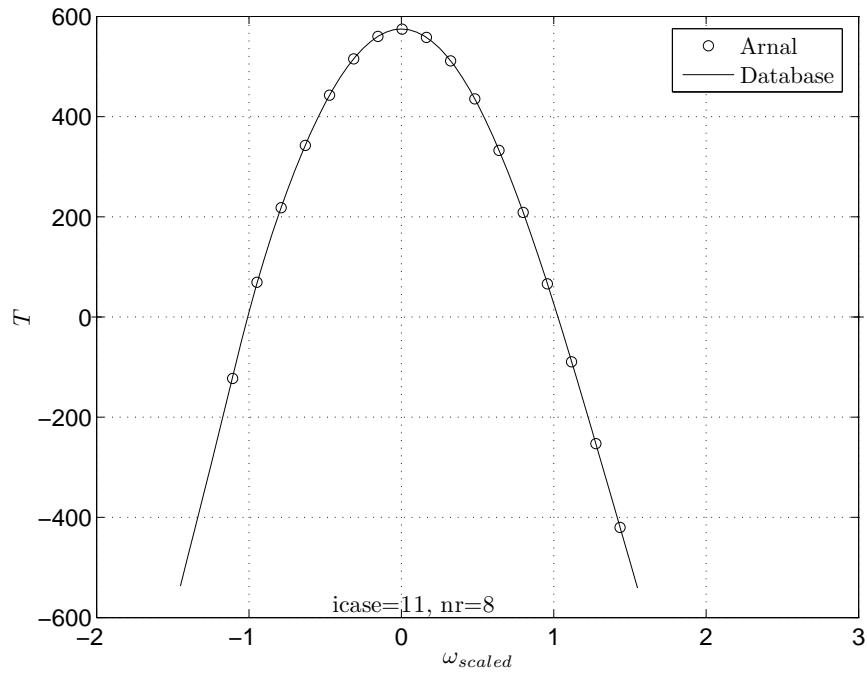
Figure 7.3: T vs ω_{scaled}, icase $= 11$ ($\beta = -0.198838$, separation)
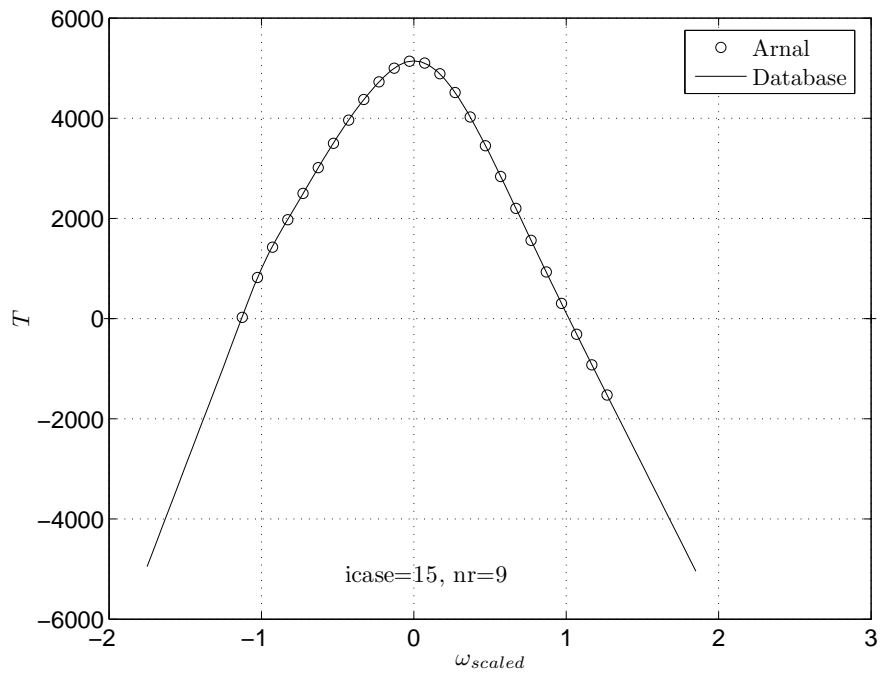
Figure 7.4: T vs ω_{scaled}, icase $= 15$ ($\beta = -0.04$, $H = 35.944$)

6 starting from the diagram for icase=1. In chapter 9 we will use this similarity to generate an approximation for the stability diagram of the asymptotic suction profile from that for the stagnation point flow.
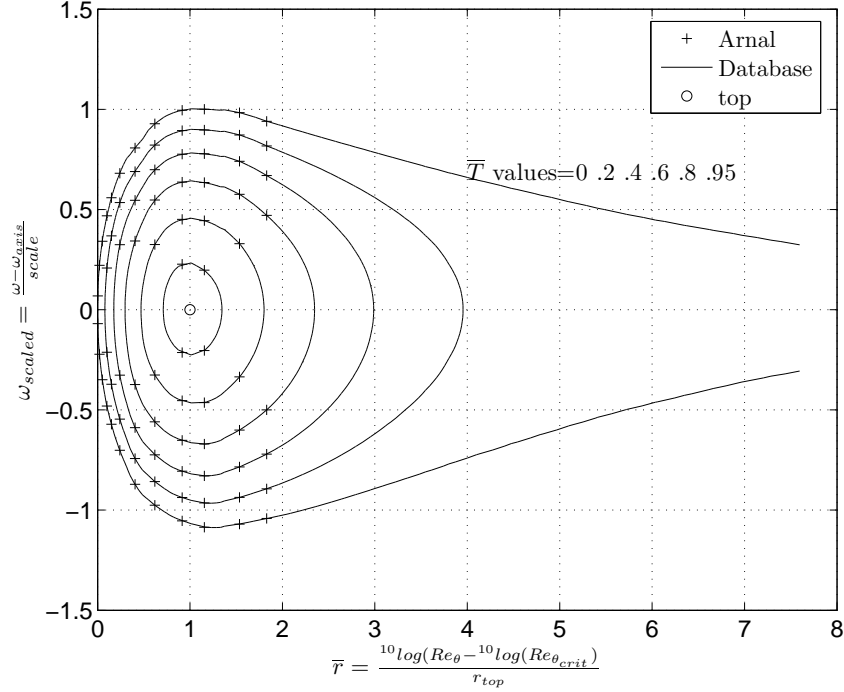
Figure 7.5: Scaled and shifted diagram; icase = 1 ($\beta = 1$, stagnation point)

2. Stability diagrams in the classical form also follow from option 7 and are given as contour plots for $\overline{T}$ in a plane with $^{10}log(Re_\theta)$ or r (to be selected) along the horizontal axis and $\frac{\omega\theta}{U}$ along the vertical axis. A few examples are given in figures 7.11 through 7.14. Note that especially for icase=1 (stagnation point) the data base curves have been extrapolated over a rather large r-region. This was already apparent from the road-map shown in figure 6.10.

3. Stability diagrams in the form where the frequencies are given as $^{10}log(F) = {}^{10}log(\frac{\omega\nu}{U^2})$ are produced by the program `logF_stability_diagrams.m` (option 8 in `N_factor_show.m`). This log form is only possible for positive values of ω. Hence certain parts of the diagram have to be excluded from these plots because the Arnal data show negative values for the lower branch of the neutral curve at higher values of the Reynolds number for icase > 11. Note that because of the use of the log-value of F small irregularities that are not visible in the other forms are exaggerated. Since these are in a region that can be expected not to be used in applications, we refrained from a cosmetic operation by applying further smoothing. Examples are given in figures 7.15 through 7.18.

Stability diagrams for arbitrary values of $2 \leq H \leq 35.944$ can be calculated using the program `make_diagram_for_H` (option 11 in the `N_factor_show`). Examples for $H = 2$ and 2.591 are
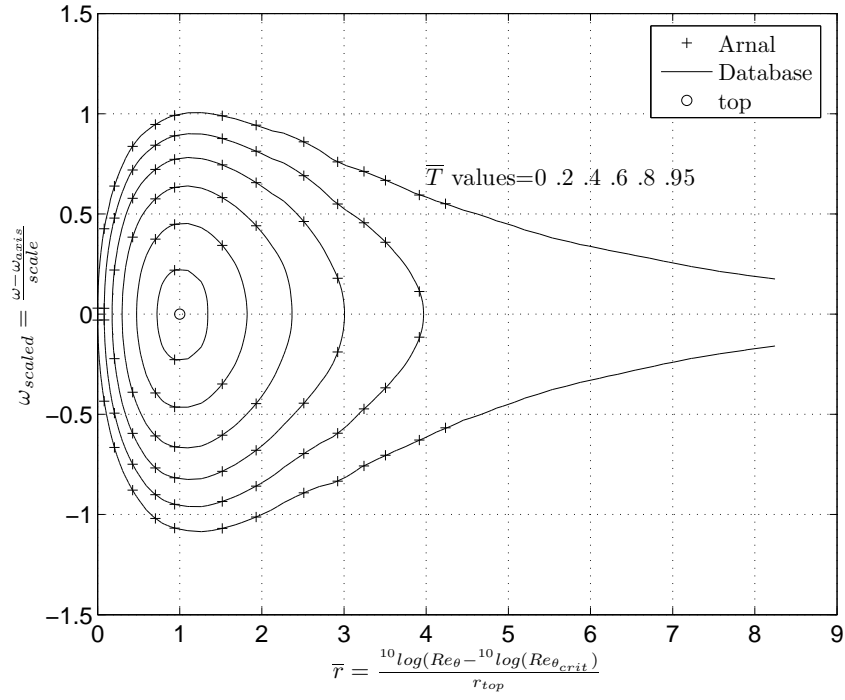
Figure 7.6: Scaled and shifted stability diagram; icase = 6 ($\beta = 0$, flat plate)
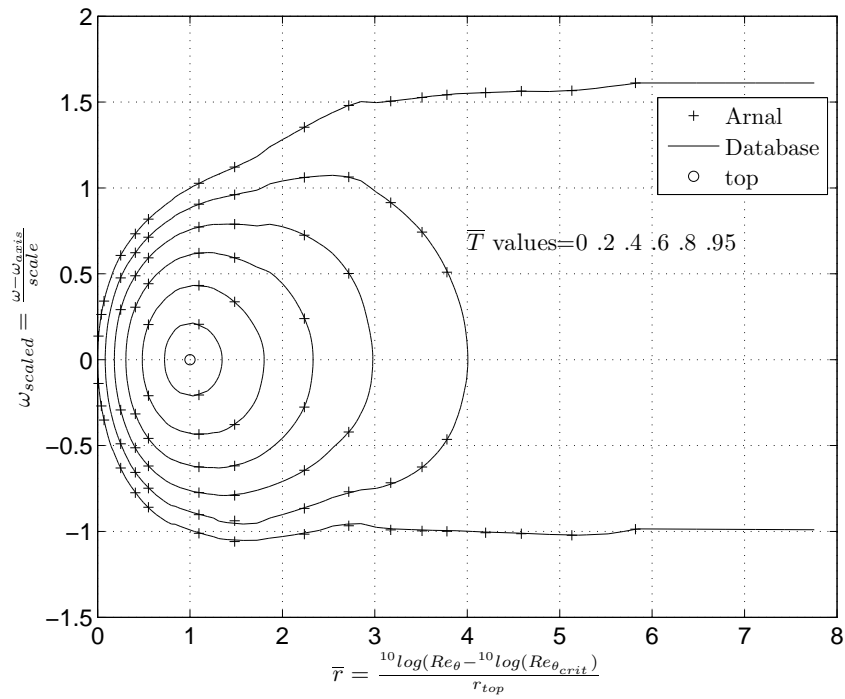
Figure 7.7: Scaled and shifted stability diagram; icase = 11 ($\beta = -0.198838$, separation)
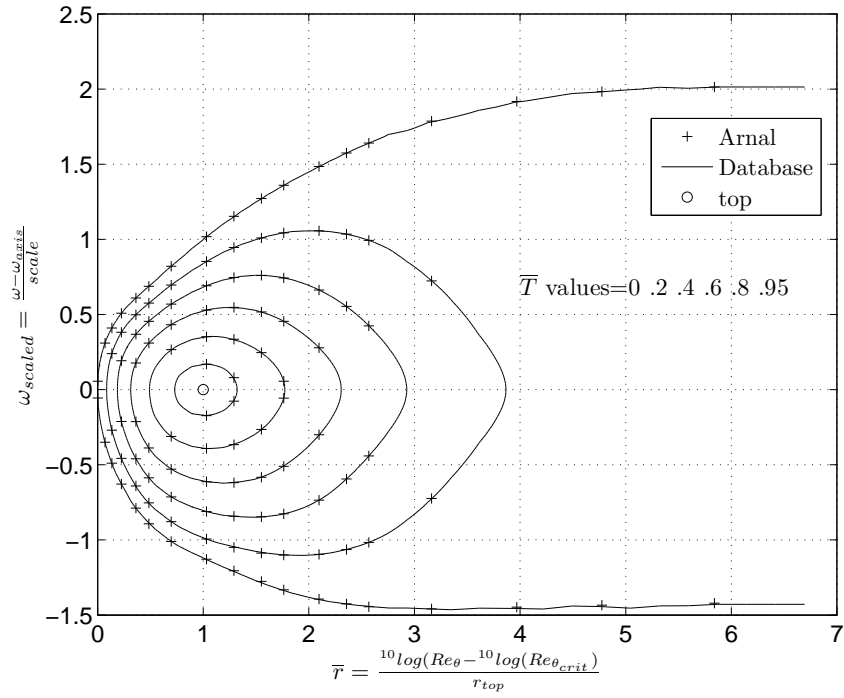
Figure 7.8: Scaled and shifted stability diagram; icase $= 15$ ($\beta = -0.04$, $H = 35.944$)
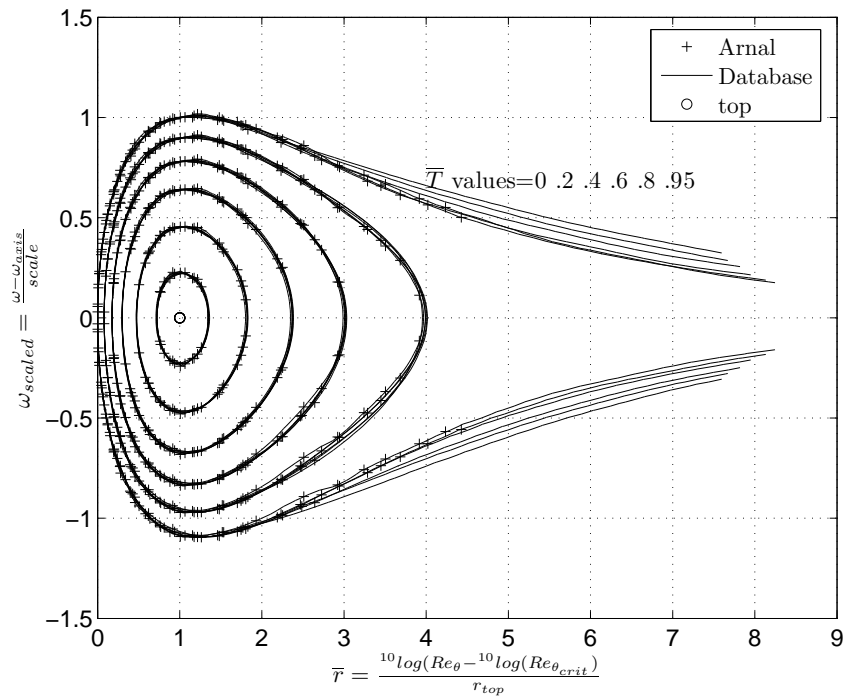
Figure 7.9: Scaled and shifted stability diagram; icase $= 1:6$, superimposed
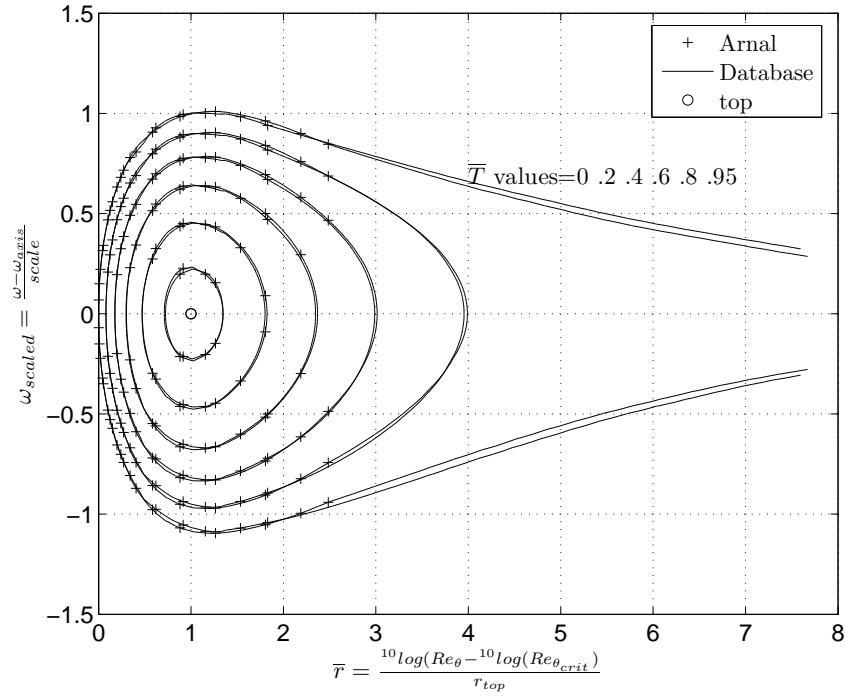
Figure 7.10: Scaled and shifted stability diagram; icase = 1-2, superimposed
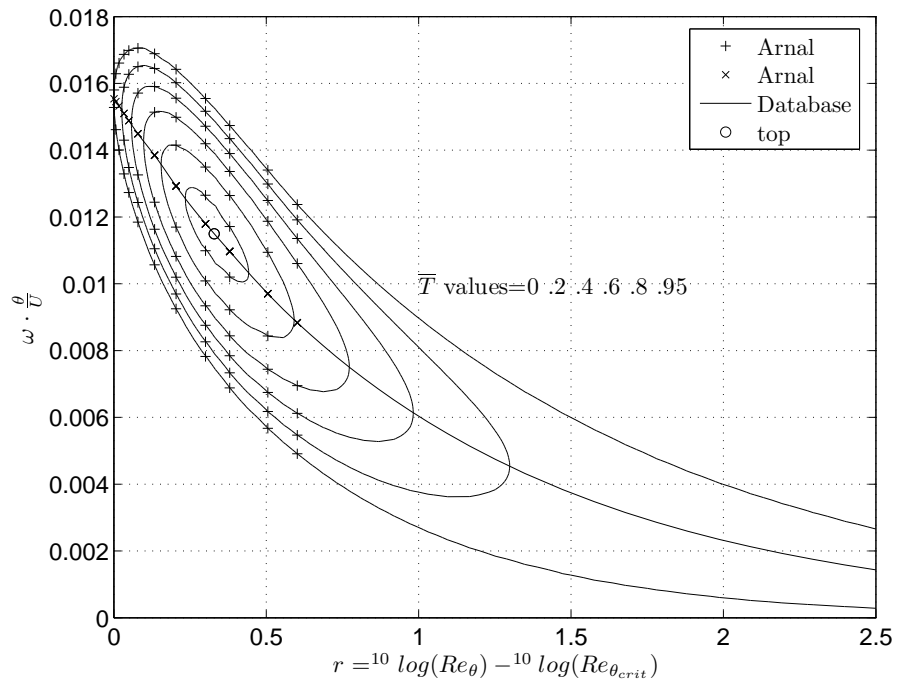
Figure 7.11: Classic stability diagram; icase = 1 ($\beta = 1$, stagnation point)
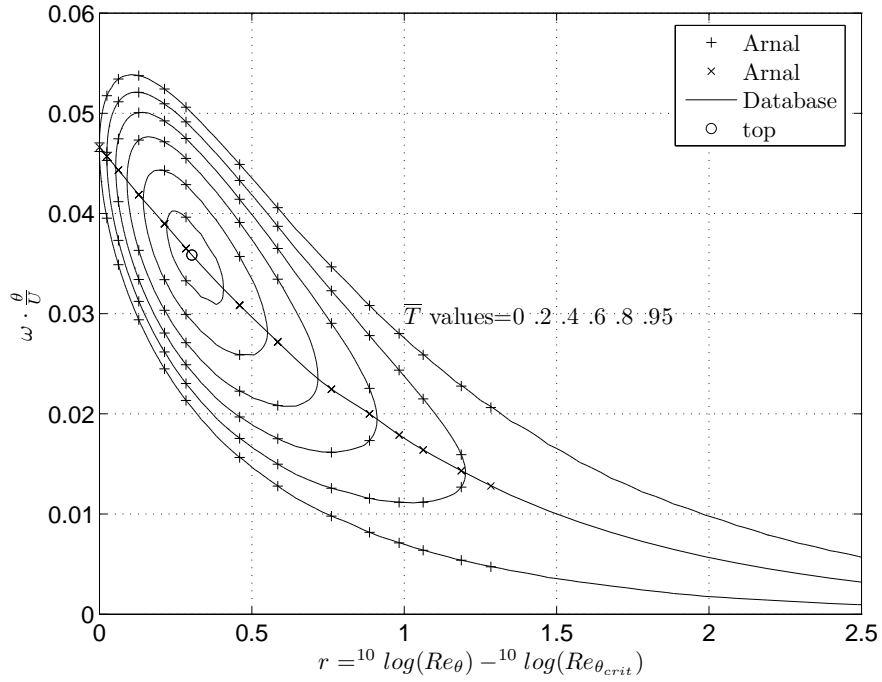
Figure 7.12: Classic stability diagram; icase = 6 ($\beta = 0$, flat plate)
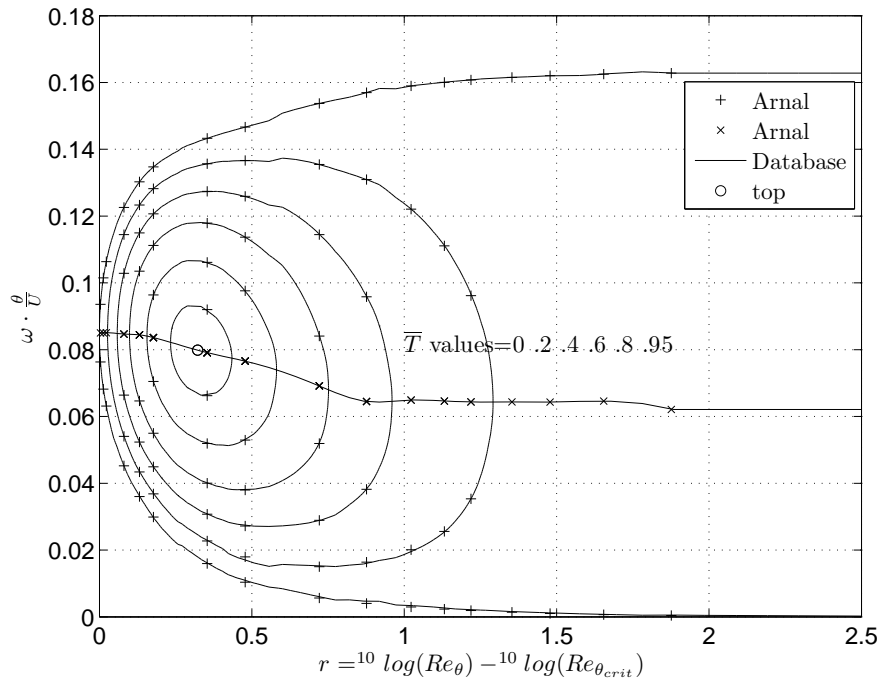
Figure 7.13: Classic stability diagram; icase = 11 ($\beta = -0.198838$, separation)
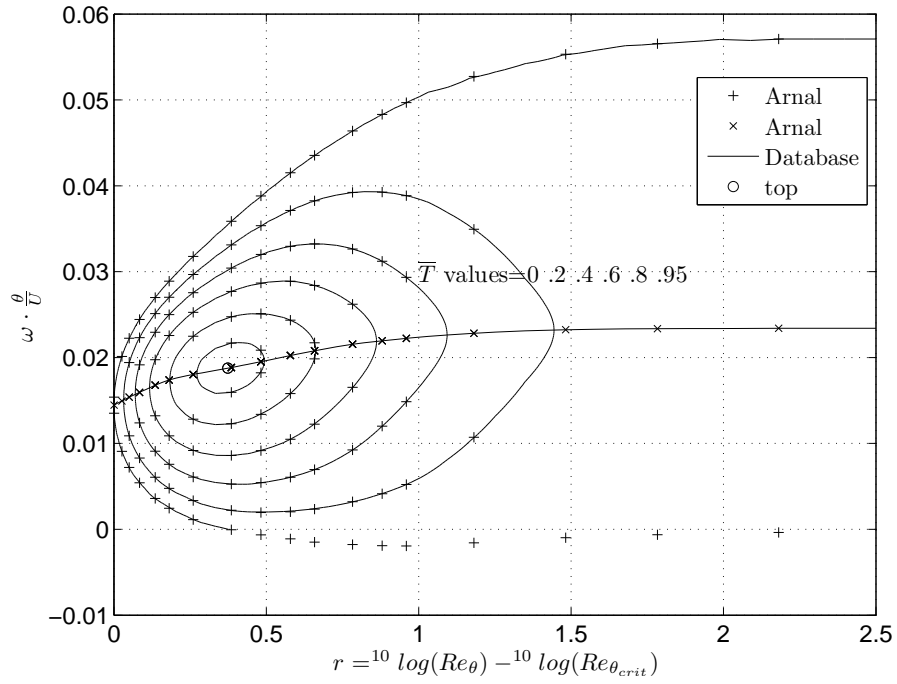
Figure 7.14: Classic stability diagram; icase = 15 ($\beta = -0.04$, $H = 35.944$)

shown in figure 7.19 and 7.20 respectively. The first one should represent the asymptotic suction diagram, the second one represents the flat plate.
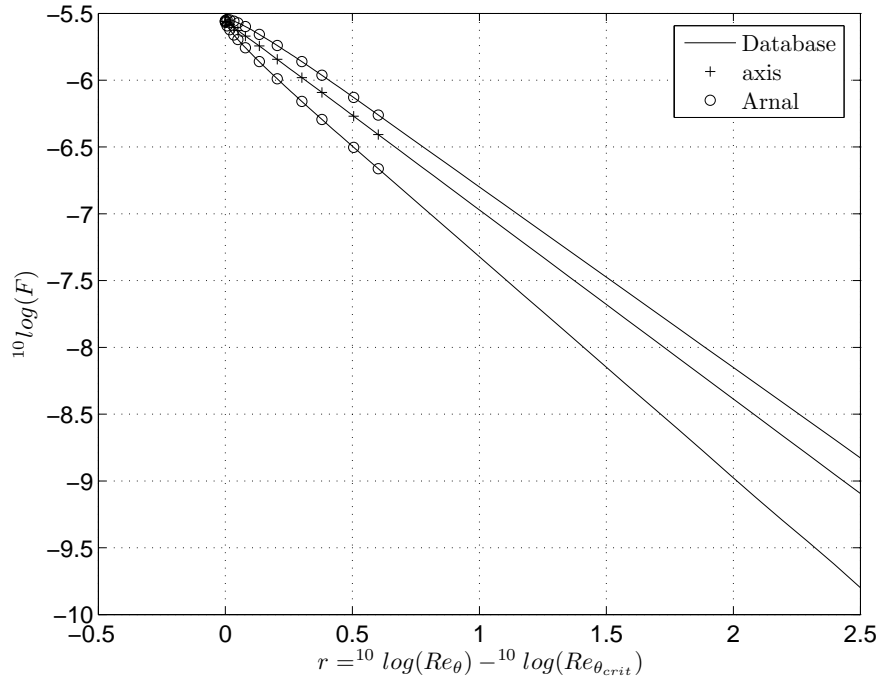
Figure 7.15: $^{10}log(F)$ stability diagram; icase = 1 ($\beta = 1$, stagnation point)
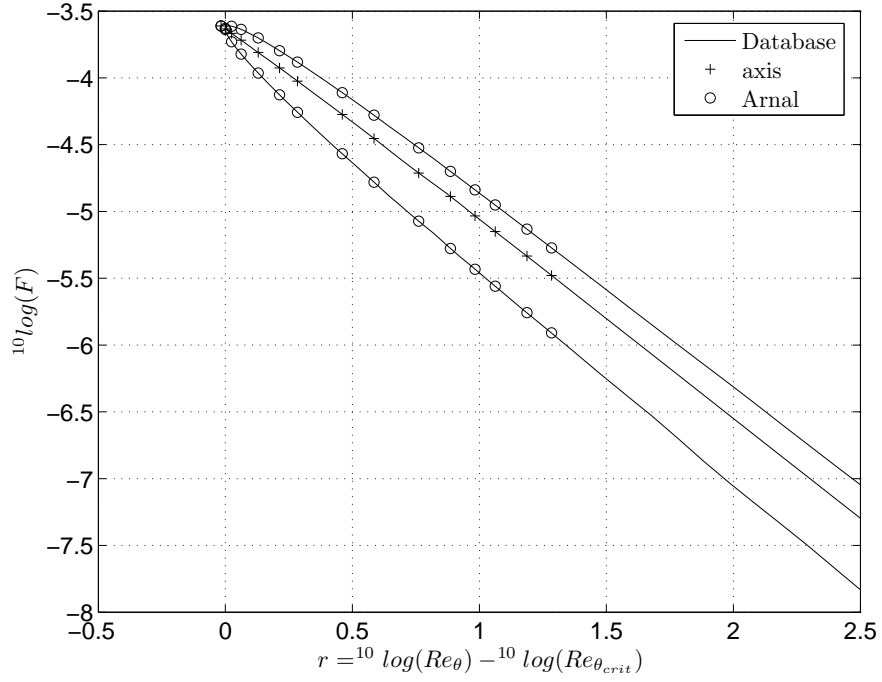
Figure 7.16: $^{10}log(F)$ stability diagram; icase = 6 ($\beta = 0$, flat plate)
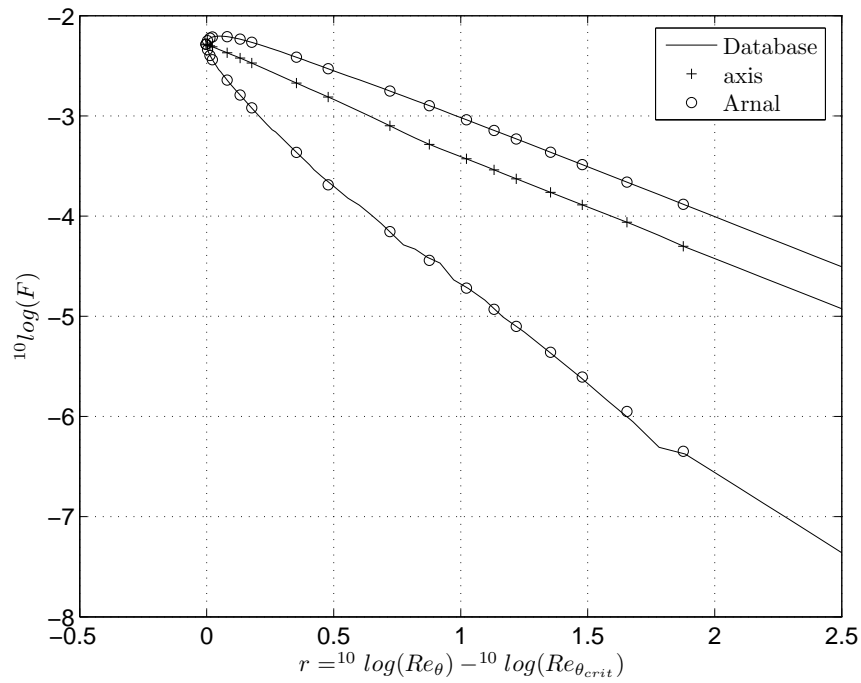
Figure 7.17: $^{10}log(F)$ stability diagram; icase = 11 ($\beta = -0.198838$, separation)
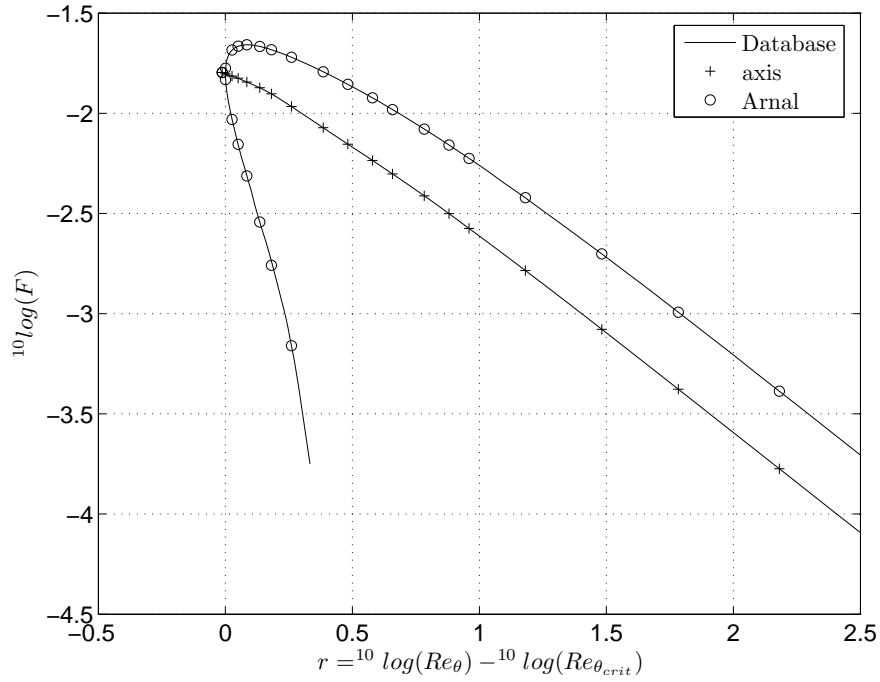
Figure 7.18: $^{10}log(F)$ stability diagram; icase = 15 ($\beta = -0.04$, $H = 35.944$)
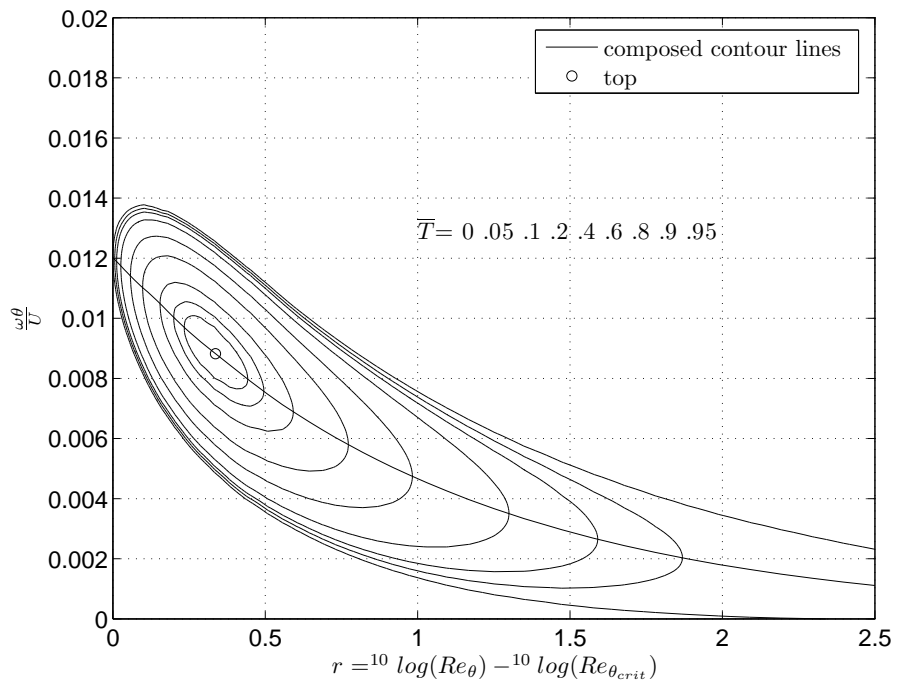
Figure 7.19: Composed stability diagram for H=2 (asymptotic suction)
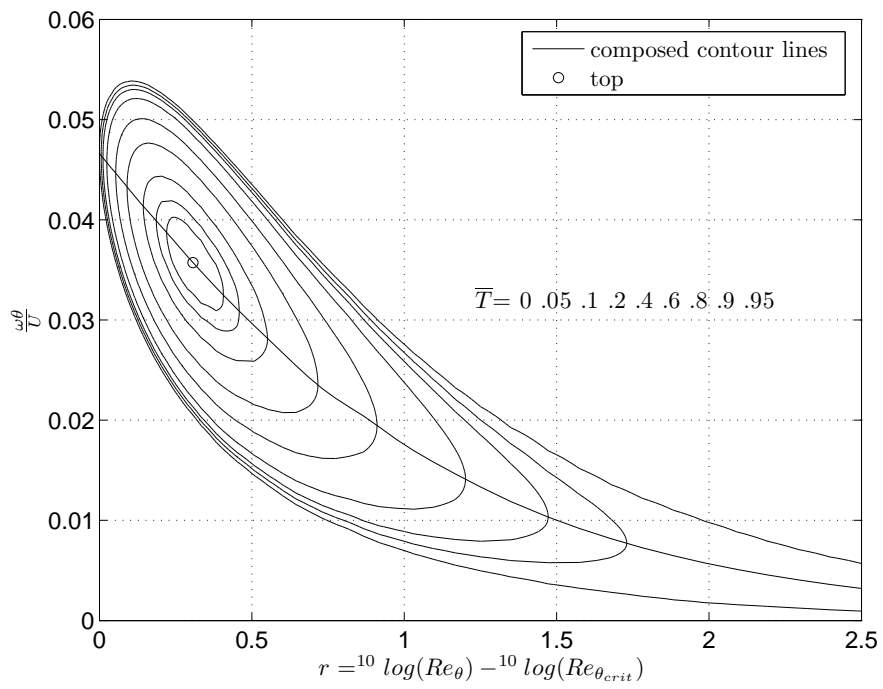
Figure 7.20: Composed stability diagram for H=2.591 ($\beta = 0$, flat plate)

Chapter 8

Deriving stability diagrams for icase = 2 to 6 from that for the stagnation point (icase=1)

To further exploit the similarity of the diagrams that was observed in chapter 7 we will now demonstrate that it is easy to estimate the diagram for icase=2:6 from that for icase=1. We only have to assume that the scaled and shifted diagrams, as described in chapter 7, are identical for $1 \leq$ icase ≤ 6 (that is for all Hartree velocity profiles without an inflexion point). In addition it is only necessary to know for values of icase from 2 to 6 :

- The value of H

- $^{10}log(Re_{\theta_{crit}})$ from the `logcrit_vs_logH_spline`.

- The scale for omega from the `scale_domega_vs_logcrit_spline`

- The position of the top from the `log_Ftop_spline`

Fig. 8.1 through 8.7 show the results for icase=1:7; these figures can be generated by the program `make_icase_from_1.m` (option 9 in `N_factor_show.m`). The diagram for icase=1 is included to check the program because this case should be reproduced exactly; icase=7 is included to show that for this velocity profile with an inflexion point the good comparison is only maintained near the critical Reynolds number. The full curves follow from the extrapolation from icase=1; the symbols denote the Arnal data for the case being estimated. From the figures it can be seen that especially for icase=2 and 3 the estimated diagram compares very well with the Arnal values. In the next chapter we will derive the diagram for the asymptotic suction profile, assuming that the same similarity will hold at "the other side of the stagnation point"
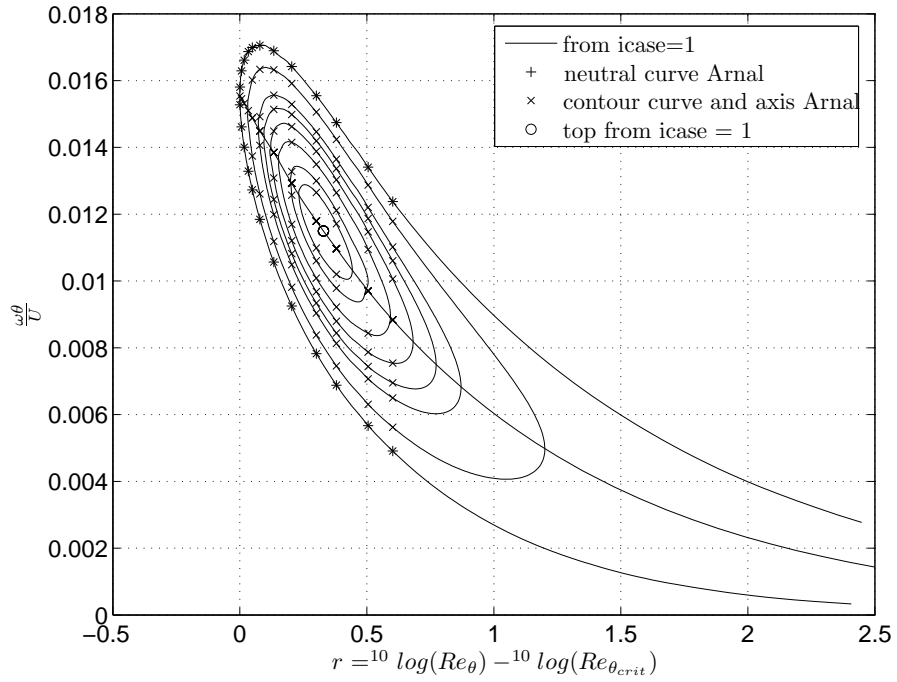
Figure 8.1: Stability diagram for icase = 1 derived from icase = 1
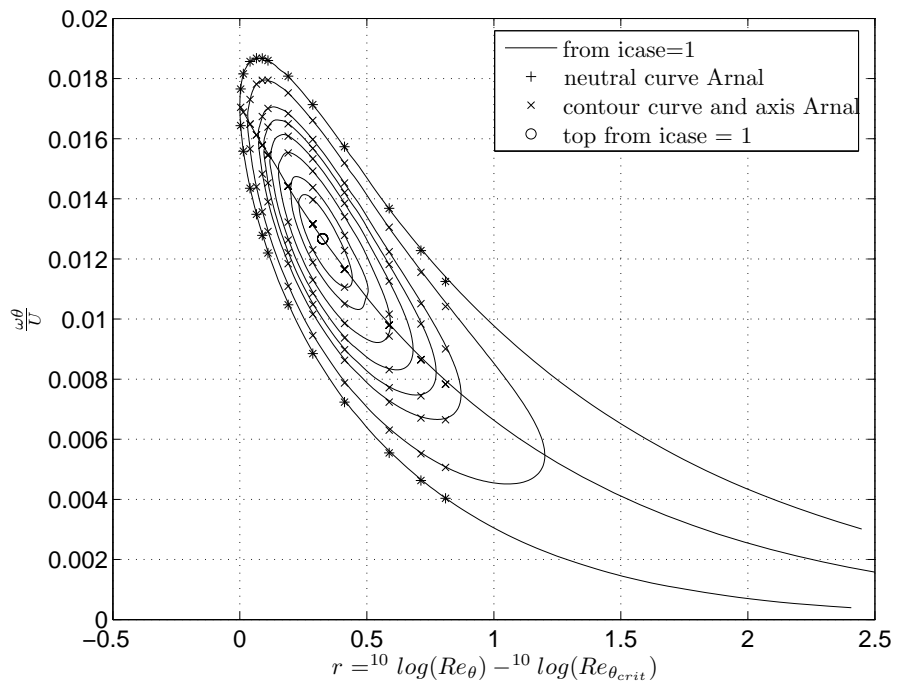
Figure 8.2: Stability diagram for icase = 2 derived from icase = 1
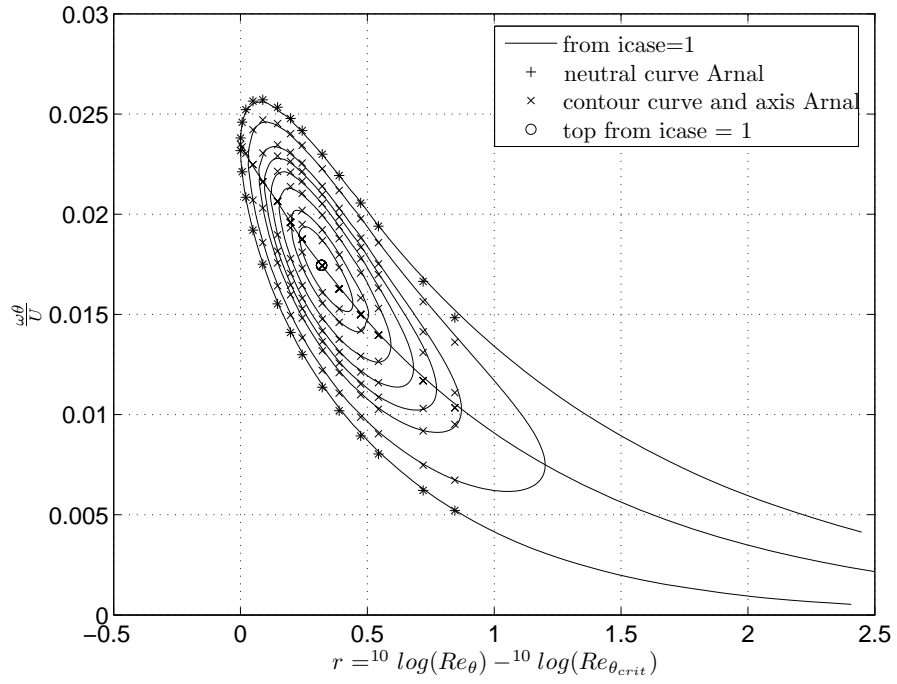
Figure 8.3: Stability diagram for icase = 3 derived from icase = 1
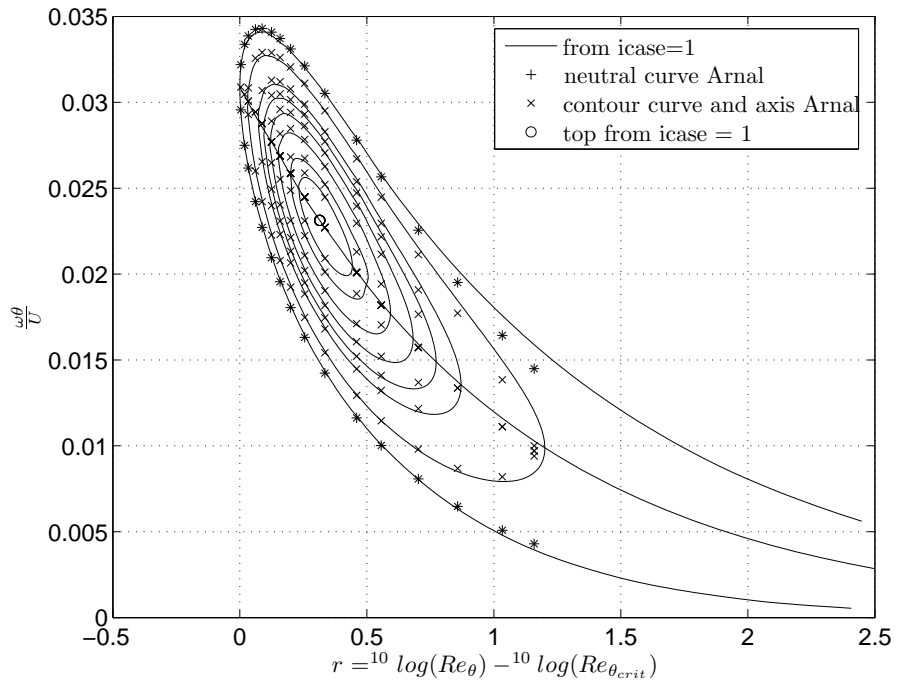
Figure 8.4: Stability diagram for icase = 4 derived from icase = 1
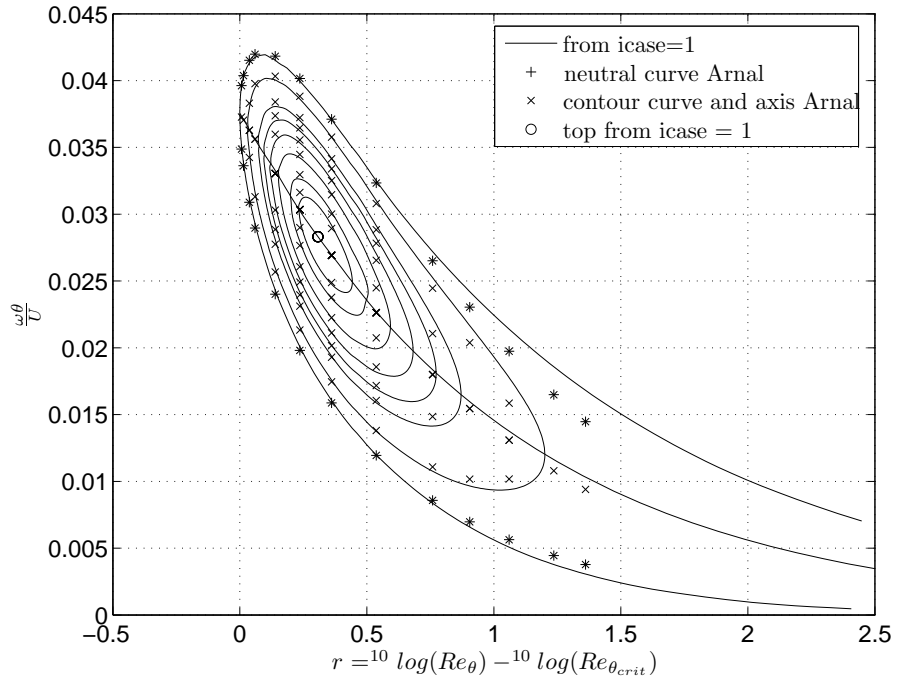
Figure 8.5: Stability diagram for icase = 5 derived from icase = 1
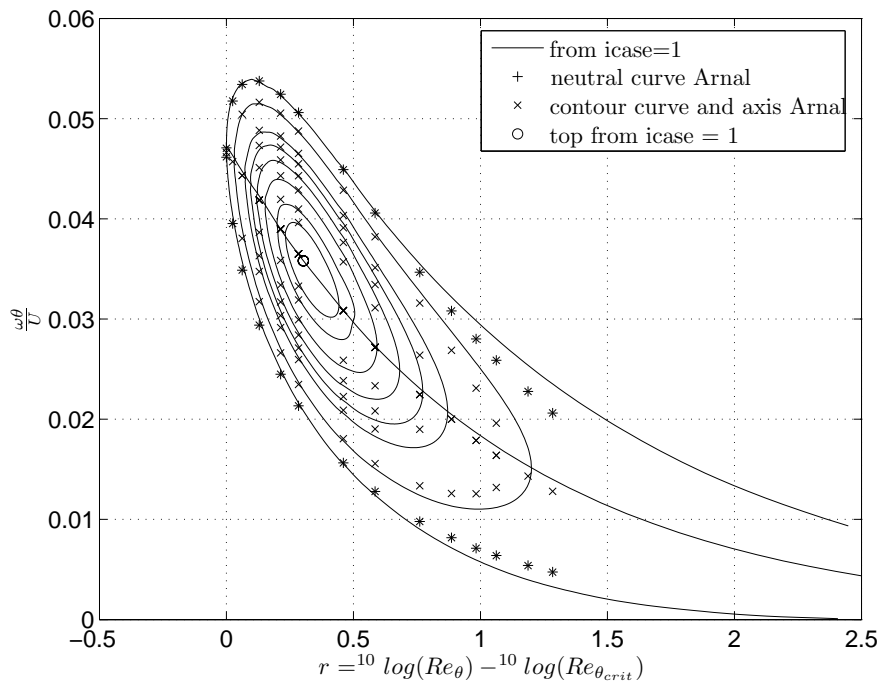
Figure 8.6: Stability diagram for icase = 6 derived from icase = 1
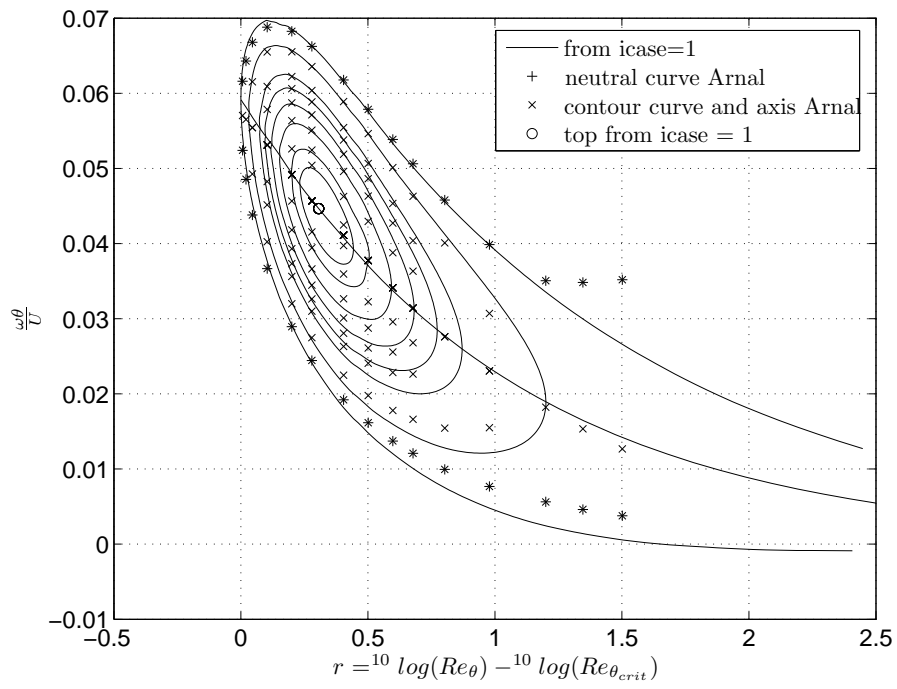
Figure 8.7: Stability diagram for icase = 7 derived from icase = 1

Chapter 9

Composing the diagram for the asymptotic suction profile from that for the stagnation point

The results of the preceding chapter suggest that a good estimate for the stability diagram of the asymptotic suction profile can be obtained from that for the stagnation point flow by assuming that the non-dimensional scaled and shifted diagrams for both cases are identical. In the present chapter we will discuss the "composing" of a complete stability diagram for the asymptotic suction profile. First we summarise what we already know about this case.

- $H = 2$

- The critical Reynolds number $Re_{\delta*}$ follows from Hughes and Reid (1965) as 46270 that means $Re_{\theta_{crit}} = 23135$ and $^{10}log(Re_{\theta_{crit}}) = 4.3643$.

- T_{maxmax} follows from an extrapolation of the Arnal data versus $^{10}log(Re_{\theta_{crit}})$ through the spline `logMaxMaxT_vs_logcrit_spline` as shown in figure 6.18. Judging from the shape of this curve it is assumed that the extrapolation can not be far off. We find $^{10}log(T_{maxmax}) = -1.3871$ and hence $T_{maxmax} = 0.041$

- From figure 6.8 it can be seen that the "axes" in $^{10}log(F)$ form are rather straight and regularly spaced. The value of $^{10}log(F_{axis})$ at $r_{grid}(27) = 0.3333$ is approximated by `log_Ftop_spline` as shown in figure 6.9 with o for the Arnal data. Again extrapolation to $^{10}log(Re_{\theta_{crit}})$ for the asymptotic suction profile is straightforward (+ in figure 6.9).

- The scale for omega was already defined in figures 2.3 through 2.5 and splined in `scale_domega_vs_logcrit_spline`, again extrapolation is straight-forward.

- When we look at the non-dimensional scaled and shifted stability diagrams for the first 6 Arnal cases; that means velocity profiles without inflexion point; we see a great similarity. (See chapter 8 and the `N_factor_show` (option 7) and especially by choosing the option to superimpose the diagrams.)

- In chapter 5 it was shown that the asymptotic suction profile fits nicely into the Hartree series.

Based on these observations we dare to assume that the scaled and shifted diagram for the asymptotic suction profile is identical to that for the stagnation point profile (icase = 1, $\beta = 1$, see figure 9.1). The program `make_asuc_diagram.m` (see `N_factor_show` (option 10)) gives the resulting diagram in the classical form. (figure 9.2). Tables 9.1 through 9.5 present $\frac{\omega\theta}{U}$, $-\alpha_i\theta$ and T for a few cross-sections through the diagram. Tables are given for $r = 0$, (0.25),1 that means for $^{10}log(Re_\theta) = r +^{10} log(Re_{\theta_{crit}}) = r + 4.3643$. The MATLAB program "make_table_for_H.m" generates stability data in tables for arbitrary values of H and Reynolds number. Results may be presented in terms of δ^* or θ. When using δ^* a comparison with the Arnal tables is easy. The program uses the function cross_cut.m

The tables for the asymptotic suction profile, as presented in the present chapter, were made with this program for H=2 and the values for r listed above.

Of course the diagram in fig. 9.2 may also be generated by using `make_diagram_for_H.m` for $H = 2$. In this program we use the function `cross_cut.m` to be described in chapter 10.
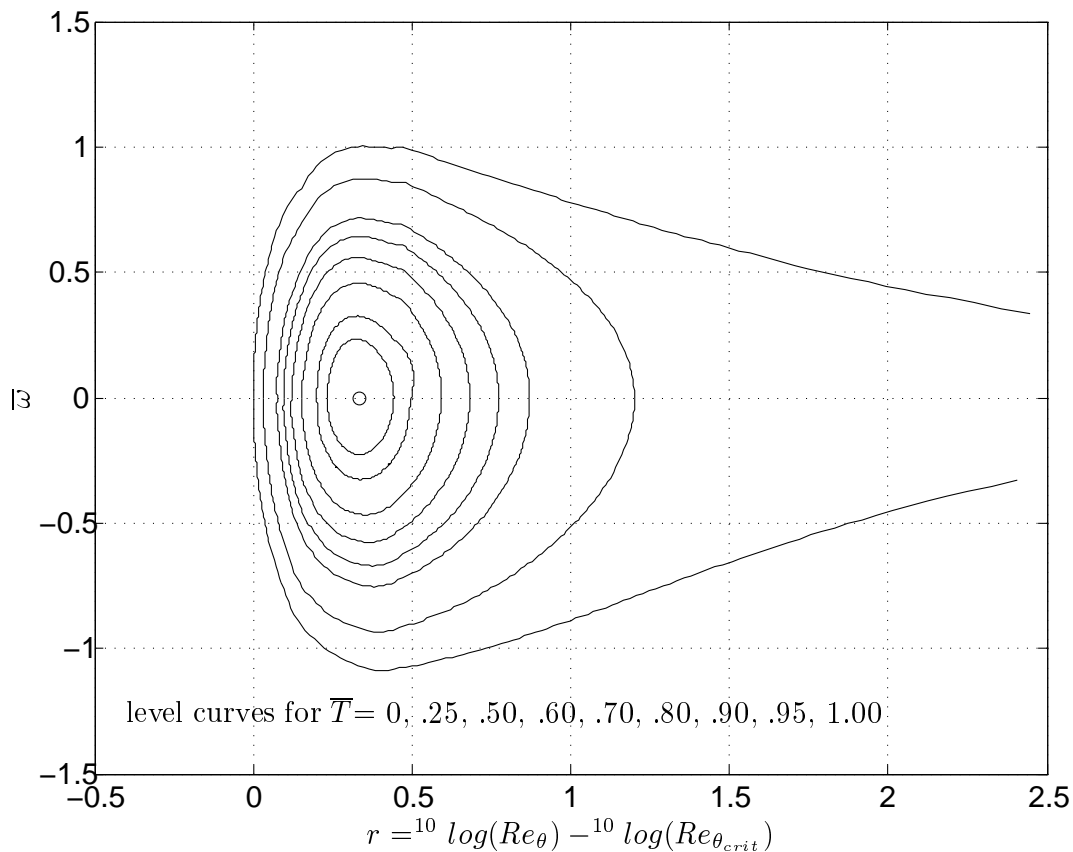
Figure 9.1: The shifted and scaled diagram for the stagnation point profile; assumed to be valid for the asymptotic suction profile.
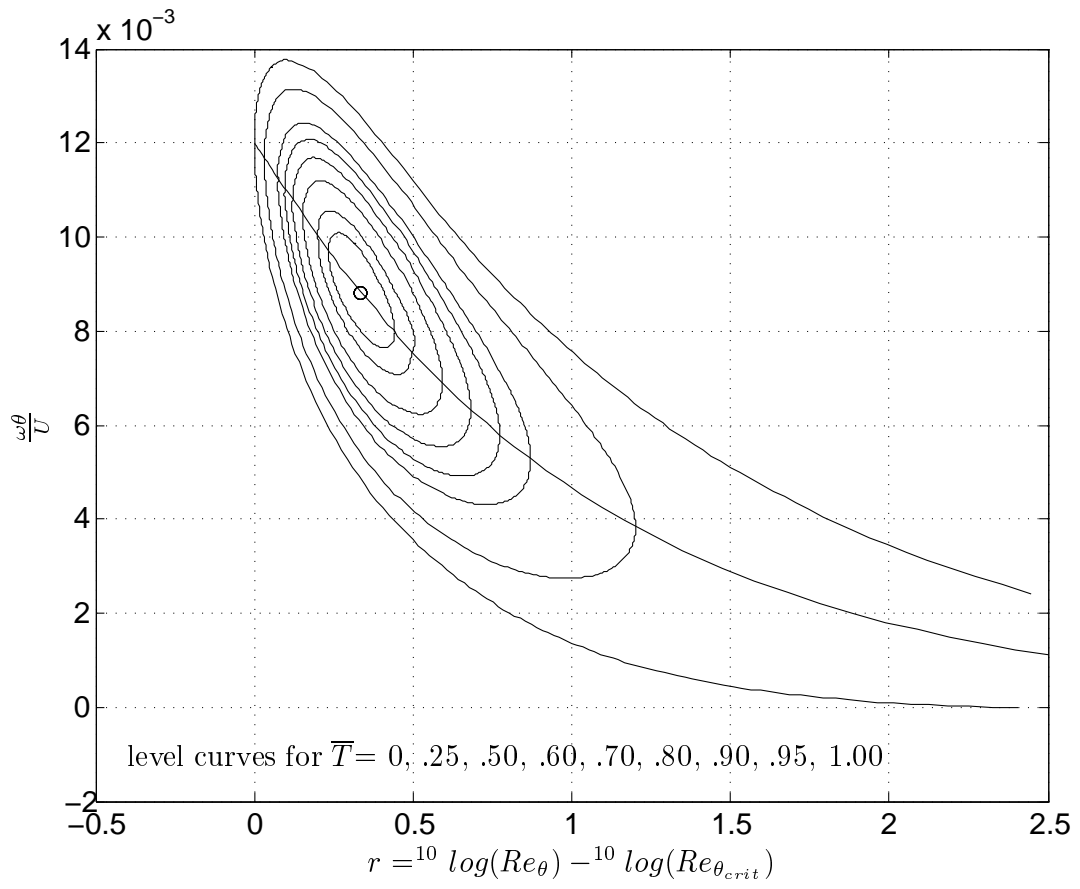
Figure 9.2: Stability diagram for the asymptotic suction profile derived from fig. 9.1

Table 9.1: Cross cut of the stability diagram for the asmptotic suction profile at $r = 0$

$\overline{\omega}$	$\frac{\omega\theta}{U}$	$\overline{T}$	$-\alpha_i\theta$	F
-2.0000	$4.5730{\cdot}10^{-3}$	-1.4226	$-1.3484{\cdot}10^{-3}$	$1.9766{\cdot}10^{-7}$
-1.8000	$5.3170{\cdot}10^{-3}$	-1.2671	$-1.2010{\cdot}10^{-3}$	$2.2983{\cdot}10^{-7}$
-1.6000	$6.0611{\cdot}10^{-3}$	-1.1116	$-1.0536{\cdot}10^{-3}$	$2.6199{\cdot}10^{-7}$
-1.4000	$6.8052{\cdot}10^{-3}$	$-9.5612{\cdot}10^{-1}$	$-9.0625{\cdot}10^{-4}$	$2.9415{\cdot}10^{-7}$
-1.2000	$7.5492{\cdot}10^{-3}$	$-8.0062{\cdot}10^{-1}$	$-7.5886{\cdot}10^{-4}$	$3.2631{\cdot}10^{-7}$
-1.0000	$8.2933{\cdot}10^{-3}$	$-6.4509{\cdot}10^{-1}$	$-6.1145{\cdot}10^{-4}$	$3.5847{\cdot}10^{-7}$
$-8.0000{\cdot}10^{-1}$	$9.0374{\cdot}10^{-3}$	$-4.8966{\cdot}10^{-1}$	$-4.6412{\cdot}10^{-4}$	$3.9064{\cdot}10^{-7}$
$-6.0000{\cdot}10^{-1}$	$9.7814{\cdot}10^{-3}$	$-3.3403{\cdot}10^{-1}$	$-3.1660{\cdot}10^{-4}$	$4.2280{\cdot}10^{-7}$
$-4.0000{\cdot}10^{-1}$	$1.0525{\cdot}10^{-2}$	$-1.7808{\cdot}10^{-1}$	$-1.6879{\cdot}10^{-4}$	$4.5496{\cdot}10^{-7}$
$-2.0000{\cdot}10^{-1}$	$1.1270{\cdot}10^{-2}$	$-4.4464{\cdot}10^{-2}$	$-4.2145{\cdot}10^{-5}$	$4.8712{\cdot}10^{-7}$
$-1.6000{\cdot}10^{-1}$	$1.1418{\cdot}10^{-2}$	$-2.8671{\cdot}10^{-2}$	$-2.7175{\cdot}10^{-5}$	$4.9355{\cdot}10^{-7}$
$-1.2000{\cdot}10^{-1}$	$1.1567{\cdot}10^{-2}$	$-1.6216{\cdot}10^{-2}$	$-1.5370{\cdot}10^{-5}$	$4.9999{\cdot}10^{-7}$
$-8.0000{\cdot}10^{-2}$	$1.1716{\cdot}10^{-2}$	$-7.2122{\cdot}10^{-3}$	$-6.8360{\cdot}10^{-6}$	$5.0642{\cdot}10^{-7}$
$-4.0000{\cdot}10^{-2}$	$1.1865{\cdot}10^{-2}$	$-1.7906{\cdot}10^{-3}$	$-1.6972{\cdot}10^{-6}$	$5.1285{\cdot}10^{-7}$
0.0000	$1.2014{\cdot}10^{-2}$	$1.7204{\cdot}10^{-6}$	$1.6307{\cdot}10^{-9}$	$5.1928{\cdot}10^{-7}$
$4.0000{\cdot}10^{-2}$	$1.2162{\cdot}10^{-2}$	$-1.8032{\cdot}10^{-3}$	$-1.7092{\cdot}10^{-6}$	$5.2572{\cdot}10^{-7}$
$8.0000{\cdot}10^{-2}$	$1.2311{\cdot}10^{-2}$	$-7.3176{\cdot}10^{-3}$	$-6.9359{\cdot}10^{-6}$	$5.3215{\cdot}10^{-7}$
$1.2000{\cdot}10^{-1}$	$1.2460{\cdot}10^{-2}$	$-1.6562{\cdot}10^{-2}$	$-1.5698{\cdot}10^{-5}$	$5.3858{\cdot}10^{-7}$
$1.6000{\cdot}10^{-1}$	$1.2609{\cdot}10^{-2}$	$-2.9382{\cdot}10^{-2}$	$-2.7849{\cdot}10^{-5}$	$5.4501{\cdot}10^{-7}$
$2.0000{\cdot}10^{-1}$	$1.2758{\cdot}10^{-2}$	$-4.5620{\cdot}10^{-2}$	$-4.3241{\cdot}10^{-5}$	$5.5145{\cdot}10^{-7}$
$4.0000{\cdot}10^{-1}$	$1.3502{\cdot}10^{-2}$	$-1.8516{\cdot}10^{-1}$	$-1.7550{\cdot}10^{-4}$	$5.8361{\cdot}10^{-7}$
$6.0000{\cdot}10^{-1}$	$1.4246{\cdot}10^{-2}$	$-3.5865{\cdot}10^{-1}$	$-3.3994{\cdot}10^{-4}$	$6.1577{\cdot}10^{-7}$
$8.0000{\cdot}10^{-1}$	$1.4990{\cdot}10^{-2}$	$-5.2771{\cdot}10^{-1}$	$-5.0018{\cdot}10^{-4}$	$6.4793{\cdot}10^{-7}$
1.0000	$1.5734{\cdot}10^{-2}$	$-6.9932{\cdot}10^{-1}$	$-6.6285{\cdot}10^{-4}$	$6.8009{\cdot}10^{-7}$
1.2000	$1.6478{\cdot}10^{-2}$	$-8.7055{\cdot}10^{-1}$	$-8.2514{\cdot}10^{-4}$	$7.1225{\cdot}10^{-7}$
1.4000	$1.7222{\cdot}10^{-2}$	-1.0415	$-9.8722{\cdot}10^{-4}$	$7.4442{\cdot}10^{-7}$
1.6000	$1.7966{\cdot}10^{-2}$	-1.2127	$-1.1495{\cdot}10^{-3}$	$7.7658{\cdot}10^{-7}$
1.8000	$1.8710{\cdot}10^{-2}$	-1.3838	$-1.3117{\cdot}10^{-3}$	$8.0874{\cdot}10^{-7}$
2.0000	$1.9454{\cdot}10^{-2}$	-1.5550	$-1.4739{\cdot}10^{-3}$	$8.4090{\cdot}10^{-7}$
2.2000	$2.0198{\cdot}10^{-2}$	-1.7261	$-1.6361{\cdot}10^{-3}$	$8.7306{\cdot}10^{-7}$
2.4000	$2.0942{\cdot}10^{-2}$	-1.8972	$-1.7983{\cdot}10^{-3}$	$9.0523{\cdot}10^{-7}$
2.6000	$2.1686{\cdot}10^{-2}$	-2.0684	$-1.9605{\cdot}10^{-3}$	$9.3739{\cdot}10^{-7}$
2.8000	$2.2431{\cdot}10^{-2}$	-2.2395	$-2.1227{\cdot}10^{-3}$	$9.6955{\cdot}10^{-7}$
3.0000	$2.3175{\cdot}10^{-2}$	-2.4106	$-2.2849{\cdot}10^{-3}$	$1.0017{\cdot}10^{-6}$

Table 9.2: Cross cut of the stability diagram for the asmptotic suction profile at $r = 0.25$

$\overline{\omega}$	$\frac{\omega\theta}{U}$	$\overline{T}$	$-\alpha_i\theta$	F
-2.0000	$2.1111 \cdot 10^{-3}$	-1.9138	$-3.2257 \cdot 10^{-3}$	$5.1315 \cdot 10^{-8}$
-1.8000	$2.8552 \cdot 10^{-3}$	-1.5224	$-2.5660 \cdot 10^{-3}$	$6.9401 \cdot 10^{-8}$
-1.6000	$3.5992 \cdot 10^{-3}$	-1.1314	$-1.9070 \cdot 10^{-3}$	$8.7487 \cdot 10^{-8}$
-1.4000	$4.3433 \cdot 10^{-3}$	$-7.4025 \cdot 10^{-1}$	$-1.2477 \cdot 10^{-3}$	$1.0557 \cdot 10^{-7}$
-1.2000	$5.0874 \cdot 10^{-3}$	$-3.4913 \cdot 10^{-1}$	$-5.8846 \cdot 10^{-4}$	$1.2366 \cdot 10^{-7}$
-1.0000	$5.8314 \cdot 10^{-3}$	$3.4695 \cdot 10^{-2}$	$5.8479 \cdot 10^{-5}$	$1.4174 \cdot 10^{-7}$
$-8.0000 \cdot 10^{-1}$	$6.5755 \cdot 10^{-3}$	$3.5945 \cdot 10^{-1}$	$6.0586 \cdot 10^{-4}$	$1.5983 \cdot 10^{-7}$
$-6.0000 \cdot 10^{-1}$	$7.3196 \cdot 10^{-3}$	$6.1889 \cdot 10^{-1}$	$1.0431 \cdot 10^{-3}$	$1.7792 \cdot 10^{-7}$
$-4.0000 \cdot 10^{-1}$	$8.0636 \cdot 10^{-3}$	$8.0762 \cdot 10^{-1}$	$1.3613 \cdot 10^{-3}$	$1.9600 \cdot 10^{-7}$
$-2.0000 \cdot 10^{-1}$	$8.8077 \cdot 10^{-3}$	$9.2544 \cdot 10^{-1}$	$1.5599 \cdot 10^{-3}$	$2.1409 \cdot 10^{-7}$
$-1.6000 \cdot 10^{-1}$	$8.9565 \cdot 10^{-3}$	$9.4011 \cdot 10^{-1}$	$1.5846 \cdot 10^{-3}$	$2.1771 \cdot 10^{-7}$
$-1.2000 \cdot 10^{-1}$	$9.1053 \cdot 10^{-3}$	$9.5182 \cdot 10^{-1}$	$1.6043 \cdot 10^{-3}$	$2.2132 \cdot 10^{-7}$
$-8.0000 \cdot 10^{-2}$	$9.2541 \cdot 10^{-3}$	$9.6046 \cdot 10^{-1}$	$1.6189 \cdot 10^{-3}$	$2.2494 \cdot 10^{-7}$
$-4.0000 \cdot 10^{-2}$	$9.4029 \cdot 10^{-3}$	$9.6572 \cdot 10^{-1}$	$1.6277 \cdot 10^{-3}$	$2.2856 \cdot 10^{-7}$
0.0000	$9.5518 \cdot 10^{-3}$	$9.6746 \cdot 10^{-1}$	$1.6307 \cdot 10^{-3}$	$2.3217 \cdot 10^{-7}$
$4.0000 \cdot 10^{-2}$	$9.7006 \cdot 10^{-3}$	$9.6580 \cdot 10^{-1}$	$1.6279 \cdot 10^{-3}$	$2.3579 \cdot 10^{-7}$
$8.0000 \cdot 10^{-2}$	$9.8494 \cdot 10^{-3}$	$9.6115 \cdot 10^{-1}$	$1.6200 \cdot 10^{-3}$	$2.3941 \cdot 10^{-7}$
$1.2000 \cdot 10^{-1}$	$9.9982 \cdot 10^{-3}$	$9.5373 \cdot 10^{-1}$	$1.6075 \cdot 10^{-3}$	$2.4303 \cdot 10^{-7}$
$1.6000 \cdot 10^{-1}$	$1.0147 \cdot 10^{-2}$	$9.4347 \cdot 10^{-1}$	$1.5902 \cdot 10^{-3}$	$2.4664 \cdot 10^{-7}$
$2.0000 \cdot 10^{-1}$	$1.0296 \cdot 10^{-2}$	$9.2998 \cdot 10^{-1}$	$1.5675 \cdot 10^{-3}$	$2.5026 \cdot 10^{-7}$
$4.0000 \cdot 10^{-1}$	$1.1040 \cdot 10^{-2}$	$8.0980 \cdot 10^{-1}$	$1.3649 \cdot 10^{-3}$	$2.6835 \cdot 10^{-7}$
$6.0000 \cdot 10^{-1}$	$1.1784 \cdot 10^{-2}$	$6.0874 \cdot 10^{-1}$	$1.0260 \cdot 10^{-3}$	$2.8643 \cdot 10^{-7}$
$8.0000 \cdot 10^{-1}$	$1.2528 \cdot 10^{-2}$	$3.1832 \cdot 10^{-1}$	$5.3653 \cdot 10^{-4}$	$3.0452 \cdot 10^{-7}$
1.0000	$1.3272 \cdot 10^{-2}$	$-6.0750 \cdot 10^{-2}$	$-1.0240 \cdot 10^{-4}$	$3.2260 \cdot 10^{-7}$
1.2000	$1.4016 \cdot 10^{-2}$	$-5.3536 \cdot 10^{-1}$	$-9.0236 \cdot 10^{-4}$	$3.4069 \cdot 10^{-7}$
1.4000	$1.4760 \cdot 10^{-2}$	-1.0115	$-1.7049 \cdot 10^{-3}$	$3.5878 \cdot 10^{-7}$
1.6000	$1.5504 \cdot 10^{-2}$	-1.4897	$-2.5109 \cdot 10^{-3}$	$3.7686 \cdot 10^{-7}$
1.8000	$1.6248 \cdot 10^{-2}$	-1.9674	$-3.3161 \cdot 10^{-3}$	$3.9495 \cdot 10^{-7}$
2.0000	$1.6992 \cdot 10^{-2}$	-2.4452	$-4.1215 \cdot 10^{-3}$	$4.1303 \cdot 10^{-7}$
2.2000	$1.7736 \cdot 10^{-2}$	-2.9230	$-4.9268 \cdot 10^{-3}$	$4.3112 \cdot 10^{-7}$
2.4000	$1.8481 \cdot 10^{-2}$	-3.4008	$-5.7321 \cdot 10^{-3}$	$4.4921 \cdot 10^{-7}$
2.6000	$1.9225 \cdot 10^{-2}$	-3.8786	$-6.5374 \cdot 10^{-3}$	$4.6729 \cdot 10^{-7}$
2.8000	$1.9969 \cdot 10^{-2}$	-4.3564	$-7.3428 \cdot 10^{-3}$	$4.8538 \cdot 10^{-7}$
3.0000	$2.0713 \cdot 10^{-2}$	-4.8342	$-8.1481 \cdot 10^{-3}$	$5.0346 \cdot 10^{-7}$

Table 9.3: Cross cut of the stability diagram for the asmptotic suction profile at $r = 0.5$

$\overline{\omega}$	$\frac{\omega\theta}{U}$	$\overline{T}$	$-\alpha_i\theta$	F
-2.0000	$9.2128 \cdot 10^{-5}$	-1.5904	$-4.7670 \cdot 10^{-3}$	$1.2593 \cdot 10^{-9}$
-1.8000	$8.3619 \cdot 10^{-4}$	-1.2470	$-3.7377 \cdot 10^{-3}$	$1.1430 \cdot 10^{-8}$
-1.6000	$1.5803 \cdot 10^{-3}$	$-9.0259 \cdot 10^{-1}$	$-2.7054 \cdot 10^{-3}$	$2.1600 \cdot 10^{-8}$
-1.4000	$2.3243 \cdot 10^{-3}$	$-5.5866 \cdot 10^{-1}$	$-1.6745 \cdot 10^{-3}$	$3.1771 \cdot 10^{-8}$
-1.2000	$3.0684 \cdot 10^{-3}$	$-2.1391 \cdot 10^{-1}$	$-6.4116 \cdot 10^{-4}$	$4.1941 \cdot 10^{-8}$
-1.0000	$3.8125 \cdot 10^{-3}$	$1.0994 \cdot 10^{-1}$	$3.2954 \cdot 10^{-4}$	$5.2112 \cdot 10^{-8}$
$-8.0000 \cdot 10^{-1}$	$4.5565 \cdot 10^{-3}$	$3.8430 \cdot 10^{-1}$	$1.1519 \cdot 10^{-3}$	$6.2282 \cdot 10^{-8}$
$-6.0000 \cdot 10^{-1}$	$5.3006 \cdot 10^{-3}$	$6.0474 \cdot 10^{-1}$	$1.8126 \cdot 10^{-3}$	$7.2453 \cdot 10^{-8}$
$-4.0000 \cdot 10^{-1}$	$6.0446 \cdot 10^{-3}$	$7.6615 \cdot 10^{-1}$	$2.2964 \cdot 10^{-3}$	$8.2623 \cdot 10^{-8}$
$-2.0000 \cdot 10^{-1}$	$6.7887 \cdot 10^{-3}$	$8.6538 \cdot 10^{-1}$	$2.5938 \cdot 10^{-3}$	$9.2794 \cdot 10^{-8}$
$-1.6000 \cdot 10^{-1}$	$6.9375 \cdot 10^{-3}$	$8.7754 \cdot 10^{-1}$	$2.6303 \cdot 10^{-3}$	$9.4828 \cdot 10^{-8}$
$-1.2000 \cdot 10^{-1}$	$7.0863 \cdot 10^{-3}$	$8.8671 \cdot 10^{-1}$	$2.6578 \cdot 10^{-3}$	$9.6862 \cdot 10^{-8}$
$-8.0000 \cdot 10^{-2}$	$7.2352 \cdot 10^{-3}$	$8.9308 \cdot 10^{-1}$	$2.6769 \cdot 10^{-3}$	$9.8896 \cdot 10^{-8}$
$-4.0000 \cdot 10^{-2}$	$7.3840 \cdot 10^{-3}$	$8.9683 \cdot 10^{-1}$	$2.6881 \cdot 10^{-3}$	$1.0093 \cdot 10^{-7}$
0.0000	$7.5328 \cdot 10^{-3}$	$8.9807 \cdot 10^{-1}$	$2.6918 \cdot 10^{-3}$	$1.0296 \cdot 10^{-7}$
$4.0000 \cdot 10^{-2}$	$7.6816 \cdot 10^{-3}$	$8.9684 \cdot 10^{-1}$	$2.6881 \cdot 10^{-3}$	$1.0500 \cdot 10^{-7}$
$8.0000 \cdot 10^{-2}$	$7.8304 \cdot 10^{-3}$	$8.9315 \cdot 10^{-1}$	$2.6771 \cdot 10^{-3}$	$1.0703 \cdot 10^{-7}$
$1.2000 \cdot 10^{-1}$	$7.9792 \cdot 10^{-3}$	$8.8687 \cdot 10^{-1}$	$2.6582 \cdot 10^{-3}$	$1.0907 \cdot 10^{-7}$
$1.6000 \cdot 10^{-1}$	$8.1280 \cdot 10^{-3}$	$8.7771 \cdot 10^{-1}$	$2.6308 \cdot 10^{-3}$	$1.1110 \cdot 10^{-7}$
$2.0000 \cdot 10^{-1}$	$8.2768 \cdot 10^{-3}$	$8.6537 \cdot 10^{-1}$	$2.5938 \cdot 10^{-3}$	$1.1313 \cdot 10^{-7}$
$4.0000 \cdot 10^{-1}$	$9.0209 \cdot 10^{-3}$	$7.5932 \cdot 10^{-1}$	$2.2759 \cdot 10^{-3}$	$1.2331 \cdot 10^{-7}$
$6.0000 \cdot 10^{-1}$	$9.7650 \cdot 10^{-3}$	$5.7854 \cdot 10^{-1}$	$1.7341 \cdot 10^{-3}$	$1.3348 \cdot 10^{-7}$
$8.0000 \cdot 10^{-1}$	$1.0509 \cdot 10^{-2}$	$3.1816 \cdot 10^{-1}$	$9.5364 \cdot 10^{-4}$	$1.4365 \cdot 10^{-7}$
1.0000	$1.1253 \cdot 10^{-2}$	$-2.8457 \cdot 10^{-2}$	$-8.5295 \cdot 10^{-5}$	$1.5382 \cdot 10^{-7}$
1.2000	$1.1997 \cdot 10^{-2}$	$-4.6472 \cdot 10^{-1}$	$-1.3929 \cdot 10^{-3}$	$1.6399 \cdot 10^{-7}$
1.4000	$1.2741 \cdot 10^{-2}$	$-9.5014 \cdot 10^{-1}$	$-2.8479 \cdot 10^{-3}$	$1.7416 \cdot 10^{-7}$
1.6000	$1.3485 \cdot 10^{-2}$	-1.4316	$-4.2911 \cdot 10^{-3}$	$1.8433 \cdot 10^{-7}$
1.8000	$1.4229 \cdot 10^{-2}$	-1.9142	$-5.7374 \cdot 10^{-3}$	$1.9450 \cdot 10^{-7}$
2.0000	$1.4973 \cdot 10^{-2}$	-2.3965	$-7.1831 \cdot 10^{-3}$	$2.0467 \cdot 10^{-7}$
2.2000	$1.5717 \cdot 10^{-2}$	-2.8788	$-8.6289 \cdot 10^{-3}$	$2.1484 \cdot 10^{-7}$
2.4000	$1.6462 \cdot 10^{-2}$	-3.3612	$-1.0075 \cdot 10^{-2}$	$2.2501 \cdot 10^{-7}$
2.6000	$1.7206 \cdot 10^{-2}$	-3.8436	$-1.1520 \cdot 10^{-2}$	$2.3518 \cdot 10^{-7}$
2.8000	$1.7950 \cdot 10^{-2}$	-4.3259	$-1.2966 \cdot 10^{-2}$	$2.4535 \cdot 10^{-7}$
3.0000	$1.8694 \cdot 10^{-2}$	-4.8083	$-1.4412 \cdot 10^{-2}$	$2.5552 \cdot 10^{-7}$

Table 9.4: Cross cut of the stability diagram for the asmptotic suction profile at $r = 0.75$

$\overline{\omega}$	$\frac{\omega\theta}{U}$	$\overline{T}$	$-\alpha_i\theta$	F
-2.0000	-1.5174 $\cdot10^{-3}$	-1.2280	-6.5454 $\cdot10^{-3}$	-1.1663 $\cdot10^{-8}$
-1.8000	-7.7333 $\cdot10^{-4}$	-9.8401 $\cdot10^{-1}$	-5.2448 $\cdot10^{-3}$	-5.9442 $\cdot10^{-9}$
-1.6000	-2.9262 $\cdot10^{-5}$	-7.4033 $\cdot10^{-1}$	-3.9460 $\cdot10^{-3}$	-2.2492 $\cdot10^{-10}$
-1.4000	7.1480 $\cdot10^{-4}$	-4.9641 $\cdot10^{-1}$	-2.6459 $\cdot10^{-3}$	5.4944 $\cdot10^{-9}$
-1.2000	1.4589 $\cdot10^{-3}$	-2.5330 $\cdot10^{-1}$	-1.3501 $\cdot10^{-3}$	1.1214 $\cdot10^{-8}$
-1.0000	2.2029 $\cdot10^{-3}$	-8.1500 $\cdot10^{-3}$	-4.3440 $\cdot10^{-5}$	1.6933 $\cdot10^{-8}$
-8.0000 $\cdot10^{-1}$	2.9470 $\cdot10^{-3}$	2.1009 $\cdot10^{-1}$	1.1198 $\cdot10^{-3}$	2.2652 $\cdot10^{-8}$
-6.0000 $\cdot10^{-1}$	3.6911 $\cdot10^{-3}$	3.8801 $\cdot10^{-1}$	2.0681 $\cdot10^{-3}$	2.8371 $\cdot10^{-8}$
-4.0000 $\cdot10^{-1}$	4.4351 $\cdot10^{-3}$	5.1816 $\cdot10^{-1}$	2.7619 $\cdot10^{-3}$	3.4091 $\cdot10^{-8}$
-2.0000 $\cdot10^{-1}$	5.1792 $\cdot10^{-3}$	5.9794 $\cdot10^{-1}$	3.1871 $\cdot10^{-3}$	3.9810 $\cdot10^{-8}$
-1.6000 $\cdot10^{-1}$	5.3280 $\cdot10^{-3}$	6.0751 $\cdot10^{-1}$	3.2381 $\cdot10^{-3}$	4.0954 $\cdot10^{-8}$
-1.2000 $\cdot10^{-1}$	5.4768 $\cdot10^{-3}$	6.1494 $\cdot10^{-1}$	3.2777 $\cdot10^{-3}$	4.2098 $\cdot10^{-8}$
-8.0000 $\cdot10^{-2}$	5.6256 $\cdot10^{-3}$	6.2027 $\cdot10^{-1}$	3.3061 $\cdot10^{-3}$	4.3242 $\cdot10^{-8}$
-4.0000 $\cdot10^{-2}$	5.7744 $\cdot10^{-3}$	6.2350 $\cdot10^{-1}$	3.3233 $\cdot10^{-3}$	4.4385 $\cdot10^{-8}$
0.0000	5.9233 $\cdot10^{-3}$	6.2460 $\cdot10^{-1}$	3.3292 $\cdot10^{-3}$	4.5529 $\cdot10^{-8}$
4.0000 $\cdot10^{-2}$	6.0721 $\cdot10^{-3}$	6.2344 $\cdot10^{-1}$	3.3230 $\cdot10^{-3}$	4.6673 $\cdot10^{-8}$
8.0000 $\cdot10^{-2}$	6.2209 $\cdot10^{-3}$	6.1992 $\cdot10^{-1}$	3.3042 $\cdot10^{-3}$	4.7817 $\cdot10^{-8}$
1.2000 $\cdot10^{-1}$	6.3697 $\cdot10^{-3}$	6.1396 $\cdot10^{-1}$	3.2725 $\cdot10^{-3}$	4.8961 $\cdot10^{-8}$
1.6000 $\cdot10^{-1}$	6.5185 $\cdot10^{-3}$	6.0548 $\cdot10^{-1}$	3.2273 $\cdot10^{-3}$	5.0105 $\cdot10^{-8}$
2.0000 $\cdot10^{-1}$	6.6673 $\cdot10^{-3}$	5.9442 $\cdot10^{-1}$	3.1683 $\cdot10^{-3}$	5.1249 $\cdot10^{-8}$
4.0000 $\cdot10^{-1}$	7.4114 $\cdot10^{-3}$	5.0080 $\cdot10^{-1}$	2.6693 $\cdot10^{-3}$	5.6968 $\cdot10^{-8}$
6.0000 $\cdot10^{-1}$	8.1555 $\cdot10^{-3}$	3.4212 $\cdot10^{-1}$	1.8235 $\cdot10^{-3}$	6.2687 $\cdot10^{-8}$
8.0000 $\cdot10^{-1}$	8.8995 $\cdot10^{-3}$	1.1254 $\cdot10^{-1}$	5.9985 $\cdot10^{-4}$	6.8406 $\cdot10^{-8}$
1.0000	9.6436 $\cdot10^{-3}$	-1.9675 $\cdot10^{-1}$	-1.0487 $\cdot10^{-3}$	7.4126 $\cdot10^{-8}$
1.2000	1.0388 $\cdot10^{-2}$	-5.7937 $\cdot10^{-1}$	-3.0881 $\cdot10^{-3}$	7.9845 $\cdot10^{-8}$
1.4000	1.1132 $\cdot10^{-2}$	-9.8000 $\cdot10^{-1}$	-5.2235 $\cdot10^{-3}$	8.5564 $\cdot10^{-8}$
1.6000	1.1876 $\cdot10^{-2}$	-1.3766	-7.3377 $\cdot10^{-3}$	9.1284 $\cdot10^{-8}$
1.8000	1.2620 $\cdot10^{-2}$	-1.7746	-9.4587 $\cdot10^{-3}$	9.7003 $\cdot10^{-8}$
2.0000	1.3364 $\cdot10^{-2}$	-2.1721	-1.1578 $\cdot10^{-2}$	1.0272 $\cdot10^{-7}$
2.2000	1.4108 $\cdot10^{-2}$	-2.5698	-1.3697 $\cdot10^{-2}$	1.0844 $\cdot10^{-7}$
2.4000	1.4852 $\cdot10^{-2}$	-2.9674	-1.5817 $\cdot10^{-2}$	1.1416 $\cdot10^{-7}$
2.6000	1.5596 $\cdot10^{-2}$	-3.3651	-1.7936 $\cdot10^{-2}$	1.1988 $\cdot10^{-7}$
2.8000	1.6340 $\cdot10^{-2}$	-3.7627	-2.0056 $\cdot10^{-2}$	1.2560 $\cdot10^{-7}$
3.0000	1.7084 $\cdot10^{-2}$	-4.1604	-2.2175 $\cdot10^{-2}$	1.3132 $\cdot10^{-7}$

Table 9.5: Cross cut of the stability diagram for the asmptotic suction profile at $r = 1$

$\overline{\omega}$	$\frac{\omega\theta}{U}$	$\overline{T}$	$-\alpha_i\theta$	F
-2.0000	-2.7785 $\cdot10^{-3}$	-9.3963 $\cdot10^{-1}$	-8.9062 $\cdot10^{-3}$	-1.2010 $\cdot10^{-8}$
-1.8000	-2.0344 $\cdot10^{-3}$	-7.6996 $\cdot10^{-1}$	-7.2980 $\cdot10^{-3}$	-8.7938 $\cdot10^{-9}$
-1.6000	-1.2904 $\cdot10^{-3}$	-6.0117 $\cdot10^{-1}$	-5.6982 $\cdot10^{-3}$	-5.5776 $\cdot10^{-9}$
-1.4000	-5.4631 $\cdot10^{-4}$	-4.3260 $\cdot10^{-1}$	-4.1004 $\cdot10^{-3}$	-2.3614 $\cdot10^{-9}$
-1.2000	1.9775 $\cdot10^{-4}$	-2.6396 $\cdot10^{-1}$	-2.5019 $\cdot10^{-3}$	8.5478 $\cdot10^{-10}$
-1.0000	9.4182 $\cdot10^{-4}$	-9.5178 $\cdot10^{-2}$	-9.0213 $\cdot10^{-4}$	4.0710 $\cdot10^{-9}$
-8.0000 $\cdot10^{-1}$	1.6859 $\cdot10^{-3}$	6.8804 $\cdot10^{-2}$	6.5216 $\cdot10^{-4}$	7.2872 $\cdot10^{-9}$
-6.0000 $\cdot10^{-1}$	2.4299 $\cdot10^{-3}$	2.0351 $\cdot10^{-1}$	1.9289 $\cdot10^{-3}$	1.0503 $\cdot10^{-8}$
-4.0000 $\cdot10^{-1}$	3.1740 $\cdot10^{-3}$	3.0392 $\cdot10^{-1}$	2.8807 $\cdot10^{-3}$	1.3720 $\cdot10^{-8}$
-2.0000 $\cdot10^{-1}$	3.9181 $\cdot10^{-3}$	3.6540 $\cdot10^{-1}$	3.4634 $\cdot10^{-3}$	1.6936 $\cdot10^{-8}$
-1.6000 $\cdot10^{-1}$	4.0669 $\cdot10^{-3}$	3.7283 $\cdot10^{-1}$	3.5338 $\cdot10^{-3}$	1.7579 $\cdot10^{-8}$
-1.2000 $\cdot10^{-1}$	4.2157 $\cdot10^{-3}$	3.7858 $\cdot10^{-1}$	3.5883 $\cdot10^{-3}$	1.8222 $\cdot10^{-8}$
-8.0000 $\cdot10^{-2}$	4.3645 $\cdot10^{-3}$	3.8270 $\cdot10^{-1}$	3.6274 $\cdot10^{-3}$	1.8865 $\cdot10^{-8}$
-4.0000 $\cdot10^{-2}$	4.5133 $\cdot10^{-3}$	3.8519 $\cdot10^{-1}$	3.6510 $\cdot10^{-3}$	1.9509 $\cdot10^{-8}$
0.0000	4.6621 $\cdot10^{-3}$	3.8604 $\cdot10^{-1}$	3.6590 $\cdot10^{-3}$	2.0152 $\cdot10^{-8}$
4.0000 $\cdot10^{-2}$	4.8110 $\cdot10^{-3}$	3.8513 $\cdot10^{-1}$	3.6504 $\cdot10^{-3}$	2.0795 $\cdot10^{-8}$
8.0000 $\cdot10^{-2}$	4.9598 $\cdot10^{-3}$	3.8235 $\cdot10^{-1}$	3.6241 $\cdot10^{-3}$	2.1438 $\cdot10^{-8}$
1.2000 $\cdot10^{-1}$	5.1086 $\cdot10^{-3}$	3.7763 $\cdot10^{-1}$	3.5793 $\cdot10^{-3}$	2.2082 $\cdot10^{-8}$
1.6000 $\cdot10^{-1}$	5.2574 $\cdot10^{-3}$	3.7090 $\cdot10^{-1}$	3.5156 $\cdot10^{-3}$	2.2725 $\cdot10^{-8}$
2.0000 $\cdot10^{-1}$	5.4062 $\cdot10^{-3}$	3.6214 $\cdot10^{-1}$	3.4325 $\cdot10^{-3}$	2.3368 $\cdot10^{-8}$
4.0000 $\cdot10^{-1}$	6.1503 $\cdot10^{-3}$	2.8829 $\cdot10^{-1}$	2.7325 $\cdot10^{-3}$	2.6584 $\cdot10^{-8}$
6.0000 $\cdot10^{-1}$	6.8943 $\cdot10^{-3}$	1.6184 $\cdot10^{-1}$	1.5339 $\cdot10^{-3}$	2.9800 $\cdot10^{-8}$
8.0000 $\cdot10^{-1}$	7.6384 $\cdot10^{-3}$	-2.1907 $\cdot10^{-2}$	-2.0764 $\cdot10^{-4}$	3.3017 $\cdot10^{-8}$
1.0000	8.3825 $\cdot10^{-3}$	-2.7081 $\cdot10^{-1}$	-2.5668 $\cdot10^{-3}$	3.6233 $\cdot10^{-8}$
1.2000	9.1265 $\cdot10^{-3}$	-5.4998 $\cdot10^{-1}$	-5.2129 $\cdot10^{-3}$	3.9449 $\cdot10^{-8}$
1.4000	9.8706 $\cdot10^{-3}$	-8.2668 $\cdot10^{-1}$	-7.8356 $\cdot10^{-3}$	4.2665 $\cdot10^{-8}$
1.6000	1.0615 $\cdot10^{-2}$	-1.1043	-1.0467 $\cdot10^{-2}$	4.5881 $\cdot10^{-8}$
1.8000	1.1359 $\cdot10^{-2}$	-1.3817	-1.3096 $\cdot10^{-2}$	4.9098 $\cdot10^{-8}$
2.0000	1.2103 $\cdot10^{-2}$	-1.6591	-1.5726 $\cdot10^{-2}$	5.2314 $\cdot10^{-8}$
2.2000	1.2847 $\cdot10^{-2}$	-1.9366	-1.8356 $\cdot10^{-2}$	5.5530 $\cdot10^{-8}$
2.4000	1.3591 $\cdot10^{-2}$	-2.2140	-2.0985 $\cdot10^{-2}$	5.8746 $\cdot10^{-8}$
2.6000	1.4335 $\cdot10^{-2}$	-2.4914	-2.3615 $\cdot10^{-2}$	6.1962 $\cdot10^{-8}$
2.8000	1.5079 $\cdot10^{-2}$	-2.7689	-2.6245 $\cdot10^{-2}$	6.5179 $\cdot10^{-8}$
3.0000	1.5823 $\cdot10^{-2}$	-3.0463	-2.8874 $\cdot10^{-2}$	6.8395 $\cdot10^{-8}$

Chapter 10

The m-file function cross_cut.m

The CD-ROM that is presented with this report contains a number of MATLAB m-files and datafiles. The most important programs are discussed in some detail in chapter 10, 11, 12 and 13. All relevant programs and datafiles will be presented in appendix B and C respectively.

An important role in the new data base method is played by the MATLAB function `cross_cut.m` The present chapter first introduces the main aspects of this function. After that the function listing itself is reprinted, containing an ample number of comment lines.

The function `cross_cut` determines the "scaled and shifted" spline T_{ss} for arbitrary values of H and Re_θ within the limits of the road-map area covered by the Arnal data and the extrapolations we performed. As already discussed in chapter 6 we defined splines for the cross section through the stability diagram for the 15 values of icase (and hence of H and $^{10}log(Re_{\theta_{crit}})$) and 59 values of r defined by the "r-grid". Using suitable extrapolations we dare also to venture outside the road-map area defined in the rectangle $0 \le r \le 2.5$ and $-.0378 \le {}^{10}log(Re_{\theta_{crit}}) \le 3.7514$(equivalent to the range from $H = 35.944$ to 2.216). The extended road-map area is divided in 9 regions as shown in figure 6.21. In the `cross_cut` function first the value of H is used to find $^{10}log(Re\theta_{crit})$ from the spline `logcrit_vs_logH_spline` and then r is determined by

$$r = {}^{10}log(Re_\theta) - {}^{10}log(Re_{\theta_{crit}}) \tag{10.1}$$

These two values determine the coordinates in the road-map; for brevity we will denote $^{10}log(Re_{\theta_{crit}})$ by *logcriti*. We will discuss the 9 regions in turn, starting with region 5 because this is the basic region that is used in most cases. The other regions are discussed in turn in the listing.

Region 5
This region is fully covered by the 15x59 (not equally spaced) points in which the T_{ss} splines have been defined. We use a two-dimensional Lagrange quadratic interpolation in the 9 grid points that are nearest to the selected point. All points are within or at most at the bound-

aries of region 5. On the boundaries we could have used a one-dimensional interpolation in three points, but because of a better clarity of the program we allowed occasionally that the interpolating factors for 6 of the 9 points become zero. Because interpolation in the 9 splines in the MATLAB "pp-form" (piecewise polynomial) is a linear process it can be done fast using MATLAB array arithmatic. In the student version of MATLAB 5 that was used, the pp-form contains some integers that are used to identify an array as a MATLAB spline. These numbers retain their values after the interpolation but can have become classified as reals instead of integers. Therefore these numbers are restored to integers after the interpolation by using the function `rectify_Tss.m`. When defining the T_{ss} splines as a function of $\overline{\omega}$ in the range $-2 \le \overline{\omega} \le 3$ we have made sure that in both end intervals the cubic spline reduced to an exact linear function. This was done to ensure that any unexpected extrapolation outside the definition interval of the spline could not lead to a "wild explosion". The function `rectify_Tss.m` also restores the linearity after the interpolation. Further explanations on region 5 can be found in the comment lines of the program. In most cases for points in the other regions first the T_{ss} spline is found in the nearest point on the boundaries of region 5. After that an extrapolation is used that is specific for the region. The function listing below is thought to give a sufficient explanation.

Since all T_{ss} splines use the same breakpoints $\overline{\omega}$ the first 35 elements of these splines are always the same (see appendix A). These elements could have been stored only once and added to the spline after the interpolation. For simplicity of the program we refrained from this.

```
function Tss_local=cross_cut(Rt,H)    % (CD-ROM version)
% Function to find the cross section in Tss form of the stability diagram for
% arbitrary values of H (and hence of R-theta-crit) and Reynolds-theta.
% The m-file interpolates in a dataset that was derived from Arnal's tables
% by scaling and shifting in such a way that interpolation becomes easy and
% accurate. See chapters 6 and 10 of the report.
% The value of 10Log(Rtheta-crit) is found from a spline in log10(H).
% In this way T can be determined for a series of frequencies at a certain x-station.
% Repeating this procedure at a number of x-stations allows to compute the n-factor
% for each frequency.At each x-station the maximum n-factor gives N.
% A trace of the stability characteristics of the boundary layer can be plotted in a
% "road map" by the calling program. Sometimes the trace leaves the region covered by
% the Arnal data.It is advised to check this roadmap to keep an eye on the
% credibility of the extrapolated stability data.
% The roadmap shows a curve for N-factor=9 for the Hartree-Stewartson similar flows.
% These flows trace horizontal lines in the road map. Observe that the curve
% for N=9 is not necessarily valid for non-similar flows.
% Make sure that in the main program the necessary stability data were loaded
% by executing "load datafile_for_n_factor"
% Reynolds-theta should be given as a value for "Rt" in the calling program
% Also the value of the shape factor H should be provided.
% The following global statement may contain more variables then are really needed for
% the present function because we kept the globals the same for most m-files.
% ---------------------------------------------------------------------------------
global ...
ArMaxMaxT ArlogRtcrit r_grid Tbar Tss domega_saved dome   ...
logFax logMaxMaxT_vs_logcrit_spline logcrit_vs_logH_spline rtop_vs_logcrit_spline ...
```

```
scale_domega_vs_logcrit_spline ycentre_spline slope_left_vs_logcrit_spline   ...
ArNumberofReynolds ArH  Arscomega Arr omega_Arnal T_Arnal ome_ax fnr ri logcriti ...
omega_at_axis log_Ftop_spline scomega TMax TMaxMax omegatop ...
% ---------------------------------------------------------------end global-------
logRt=log10(Rt);
logH=log10(H);
logcrit_stag=ArlogRtcrit(1);
logcrit15=ArlogRtcrit(15);
log_Ftop_stag=ppval(log_Ftop_spline,logcrit_stag);
logcriti=ppval(logcrit_vs_logH_spline,logH);
log_Ftop_i=ppval(log_Ftop_spline,logcriti);
% ----------------------------------------------------------------------------------
if logcriti>=ArlogRtcrit(6) % This statement determines the slope of Log10(Faxis)
   slope_right=-sqrt(2);    % at the right-hand side of the roadmap.Different for
else                        % velocity profiles with (icase>6) or without (icase <=6)
   slope_right=-1;          % an inflexion point.
end
% ----------------------------------------------------------------------------------
logMaxMaxT=ppval(logMaxMaxT_vs_logcrit_spline,logcriti);
TMaxMax=10^logMaxMaxT;
scomega=ppval(scale_domega_vs_logcrit_spline,logcriti);
ri=logRt-logcriti;
% ----------------------------------------------------------------------------------
% Interpolation will be done with 3 values for r and 3 values for 10LogRtheta_crit
% First we locate 3 points in the r_grid
% Only points within or at the boundary of region 5 are used. See figure below.
% Outside region 5 extrapolations are used.
% ----------------------------------------------------------------------------------
if ri<=0
   nr2=2;
else
   nr2=max(find(r_grid <= ri));
end
if nr2>58
   nr2=58;
end
if (ri-r_grid(nr2)) > .5*(r_grid(nr2+1)-r_grid(nr2))      % to find the nearest point
    nr2=nr2+1;
end
if nr2<=2
   nr2=2;
elseif nr2>=58   % All 3 points should be in the interval r_grid(1)=0
   nr2=58;        % and r_grid(59)=2.5
end
% ------------------------The same values for r are used at the 3 values for logcrit
nr3=nr2+1;
nr1=nr2-1;
nr4=nr1;
nr5=nr2;
nr6=nr3;
nr7=nr1;
nr8=nr2;
nr9=nr3;
% now determine the icase values for interpolation and the corresponding logcrit values
icase_series=[1:15];
if logcriti>=ArlogRtcrit(2)
   icase2=2;
```

```
elseif logcriti<=ArlogRtcrit(14)
    icase2=14;
else
    icase2=interp1(ArlogRtcrit,icase_series,logcriti,'nearest');
end
% -------------------All icase values should remain in the interval 1:15 -----------
if icase2<=2
    icase2=2;
elseif icase2>=14
    icase2=14;
end
icase1=icase2-1;icase3=icase2+1;
icase123=[icase1 icase2 icase3];
logcrit123=ArlogRtcrit(icase1:icase3);
logcrit1=logcrit123(1);
logcrit2=logcrit123(2);
logcrit3=logcrit123(3);
logcrit_array=[logcrit123 logcriti];
rtop=ppval(rtop_vs_logcrit_spline,logcrit_array);
rtop1=rtop(1);rtop2=rtop(2);rtop3=rtop(3);rtopi=rtop(4);
rbi=ri/rtopi;
% --------------------------------------------------------------------------------
r1=r_grid(nr1);r2=r_grid(nr2);r3=r_grid(nr3);
r4=r1;
r5=r2;
r6=r3;
r7=r1;
r8=r2;
r9=r3;
r1_9=[r1 r2 r3 r4 r5 r6 r7 r8 r9];
% We now have defined 9 points and are ready to interpolate using Lagrange_2d
% The points are not equally spaced, however the 3 r_values are the same in the
% three rows
%
%    icase1 ----------- P1 ------- P2 ------  P3 ----------
%
%    icase2 ----------- P4 ------- P5 ------  P6 ----------
%
%    icase3 ----------- P7 ------- P8 ------  P9 ----------
%
%                      |          |           |
%                   r1=r4=r7    r2=r5=r8    r3=r6=r9
%
% We treat different regions separately (see figure below); region 5 is the
% standard.
% At the boundaries of region 5 interpolation could have been done simpler by
% 1-D Lagrange,but for clarity of the program it has been accepted that in some
% (not so often occurring) cases a number of zeros appear in the array of
% interpolating coefficients.
% The 9 points are always inside or (at most 3 or 6 of them) on the boundary
% of region 5
% For points outside region 5 special extrapolations are used, to be discussed later.
%
%                         |                        |
%                 1       |          2             |          3
%                         |                        |
%     H1=2.2160    -------A------------------------B---------------------
```

```
%                              |                    |
%                 4           |       region 5      |          6
%                              |                    |
%     H15=35.9440    ------C-------------------------D--------------------
%                              |                    |
%                 7           |         8           |          9
%                        E                        F
%                       r=0                       r=2.5
%
H1=ArH(1);      %= 2.2160
H15=ArH(15);    %=35.9440
% We first determine the region in which the point for later interpolation
% is located within or at the boundary of region 5.
% Region 5 is the normal situation.If we look for a point outside region 5 we
% arrive there later by extrapolation.
if ri>=0 & ri<=2.5 & H>=H1 & H<=H15
   region=5;
   r_array=[r1_9 ri];
   logcrit_array=[logcrit123 logcriti];
   facs=lagrange_2d(r_array,logcrit_array);
elseif  H<H1 & ri<0
   region=1;
   r_array=[r1_9 0];% we first find Tss at point A and later shift to the left and up
   logcrit_array=[logcrit123 logcrit_stag];
   facs=lagrange_2d(r_array,logcrit_array);
elseif H<H1 & ri>=0 & ri<=2.5
   region=2;
   r_array=[r1_9 ri];
   logcrit_array=[logcrit123 logcrit_stag];%we first find Tss at H1 (=along AB)and later
   %                                        extrapolate upwards as described for the
   %                                        asymptotic suction profile
   facs=lagrange_2d(r_array,logcrit_array);
elseif H<H1 & ri>2.5
   region=3;                 %We first find Tss at B and later shift to the right and up
   r_array=[r1_9 2.5];
   logcrit_array=[logcrit123 logcrit_stag];
   facs=lagrange_2d(r_array,logcrit_array);
elseif ri<0 & H>=H1 & H<=H15
   region=4;                          %We first find Tss at AC and later shift left
   r_array=[r1_9 0];
   logcrit_array=[logcrit123 logcriti];
   facs=lagrange_2d(r_array,logcrit_array);
elseif H>=H1 & H<=H15 & ri>2.5
   region=6;
   r_array=[r1_9 2.5];                     % we first find Tss at BD and later shift right
   logcrit_array=[logcrit123 logcriti];
   facs=lagrange_2d(r_array,logcrit_array);
elseif H>H15 & ri<0
   region=7;                 % We extrapolate linearly from icase=14 and 15 down at r=0
   rrr=[r1 r2 r3 0];         % and shift later to the left
   facr=lagrange(rrr);
   fact=(crit2-logcriti)/(logcrit2-logcrit3);
   facs(1)=0;
   facs(2)=0;
   facs(3)=0;
   facs(4)=(1-fact)*facr(1);
   facs(5)=(1-fact)*facr(2);
```

```
      facs(6)=(1-fact)*facr(3);
      facs(7)=fact*facr(1);
      facs(8)=fact*facr(2);
      facs(9)=fact*facr(3);
elseif H>H15 & ri>=0 & ri<=2.5
      region=8 ;                        % We find Tss at H15 (=along CD) by interpolation
      rrr=[r1 r2 r3 ri];                % in the r_grid and extrapolate linearly from
      facr=lagrange(rrr);               % icase=14 and 15 down
      fact=(logcrit2-logcriti)/(logcrit2-logcrit3);
      facs(1)=0;
      facs(2)=0;
      facs(3)=0;
      facs(4)=(1-fact)*facr(1);
      facs(5)=(1-fact)*facr(2);
      facs(6)=(1-fact)*facr(3);
      facs(7)=fact*facr(1);
      facs(8)=fact*facr(2);
      facs(9)=fact*facr(3);
else
      region=9;               % We extrapolate linearly from icase=14 and 15 down at r=2.5
      rrr=[r1 r2 r3 2.5];     % and shift later to the right
      facr=lagrange(rrr);
      fact=(logcrit2-logcriti)/(logcrit2-logcrit3);
      facs(1)=0;
      facs(2)=0;
      facs(3)=0;
      facs(4)=(1-fact)*facr(1);
      facs(5)=(1-fact)*facr(2);
      facs(6)=(1-fact)*facr(3);
      facs(7)=fact*facr(1);
      facs(8)=fact*facr(2);
      facs(9)=fact*facr(3);
end
% -------------------------------------------------------------------------------
% We now have the Lagrange interpolation factors to find Tss as follows.
% For region 1 at A
% For region 2 at AB and r
% For region 3 at B
% For region 4 at AC and logcriti
% For region 5 within ABDC and at ri and logcriti
% For region 6 at BD and logcriti
% For region 7 at CE and logcriti
% For region 8 at r and logcriti
% For region 9 at DF and logcriti
% -------------------------------------------------------------------------------
% Now follows the 2d Lagrange interpolation

Tss_local=facs(1)*Tss{icase1,nr1}+facs(2)*Tss{icase1,nr2}+ ...
          facs(3)*Tss{icase1,nr3}+facs(4)*Tss{icase2,nr4}+ ...
          facs(5)*Tss{icase2,nr5}+facs(6)*Tss{icase2,nr6}+ ...
          facs(7)*Tss{icase3,nr7}+ facs(8)*Tss{icase3,nr8}+ ...
          facs(9)*Tss{icase3,nr9};
Tss_local=rectify_Tss(Tss_local);

log10Fax=facs(1)*logFax(icase1,nr1)+ ...
         facs(2)*logFax(icase1,nr2)+ ...
         facs(3)*logFax(icase1,nr3)+ ...
```

```
            facs(4)*logFax(icase2,nr4)+ ...
            facs(5)*logFax(icase2,nr5)+ ...
            facs(6)*logFax(icase2,nr6)+ ...
            facs(7)*logFax(icase3,nr7)+ ...
            facs(8)*logFax(icase3,nr8)+ ...
            facs(9)*logFax(icase3,nr9);

  TMax=facs(1)*Tbar(icase1,nr1)+ ...  % Note that Tbar and hence TMax is T at the
       facs(2)*Tbar(icase1,nr2)+ ...  % axis divided by TMaxMax
       facs(3)*Tbar(icase1,nr3)+ ...
       facs(4)*Tbar(icase2,nr4)+ ...
       facs(5)*Tbar(icase2,nr5)+ ...
       facs(6)*Tbar(icase2,nr6)+ ...
       facs(7)*Tbar(icase3,nr7)+ ...
       facs(8)*Tbar(icase3,nr8)+ ...
       facs(9)*Tbar(icase3,nr9);


% We now make the final adjustments per region -----------------------------------
switch region  % -------------------------------------------------------------
case 1  % Is for region 1 etc.------------------------------------------------
    TMax=rbi*exp(1-rbi);   % We use the analytical approximation for r<0
    sl=ppval(slope_left_vs_logcrit_spline,logcrit_stag);% The axis in log form is
                                                        % extrapolated linear to the
                                                        % left with the appropriate slope
    log10Fax=log10Fax+ri*sl;
    log_Ftop_i=ppval(log_Ftop_spline,logcriti);
    log10Fax=log10Fax-log_Ftop_stag+log_Ftop_i;
 case 2 % ---------------------------------------
    log_Ftop_i=ppval(log_Ftop_spline,logcriti);
    log10Fax=log10Fax-log_Ftop_stag+log_Ftop_i;
 case 3 % ---------------------------------------
    a=2.5/rtopi;
    aa=a*exp(1-a)  % to keep T-bar continuous across r=2.5
    TMax=TMax*rbi*exp(1-rbi)/aa;
    log10Fax=log10Fax+(ri-2.5)*slope_right;% extrapolate axis with slope -1 or -sqrt(2)
    log_Ftop_i=ppval(log_Ftop_spline,logcriti);
    log10Fax=log10Fax-log_Ftop_stag+log_Ftop_i;    % extrapolate upwards
 case 4 % -----------------------------------------
    TMax=rbi*exp(1-rbi);
    sl=ppval(slope_left_vs_logcrit_spline,logcriti);
    log10Fax=log10Fax+ri*sl;
 case 5  % -----------------------------------------
    % no further action needed
 case 6  % -----------------------------------------
    a=2.5/rtopi;
    aa=a*exp(1-a)
    TMax=TMax*rbi*exp(1-rbi)/aa;  % As in region 3,but only extrapolation to the right.
    log10Fax=log10Fax+(ri-2.5)*slope_right;
 case 7  % -------------------------------------------------
    TMax=rbi*exp(1-rbi);
    sl=ppval(slope_left_vs_logcrit_spline,logcrit15);
    log10Fax=log10Fax+ri*sl;
 case 8  % -------------------------------------------------
        % no further action needed
 case 9  % -------------------------------------------------
    TMax=96.4274*TMax*rbi*exp(1-rbi);
    log10Fax=log10Fax+(ri-2.5)*slope_right;
```

```
end              %for switch region   -----------------------

Fax=10^log10Fax;
omega_at_axis=Fax*Rt;
% Note that Tss_local after the above interpolation should remain the
% MATLAB representation (for the version used)of a spline. Certain elements
% that should be integers, although having retained their values,may have
% become classified as floating point numbers after the interpolation.
% Furthermore we defined the splines such that the ends left and right should
% be linear to avoid problems if occasionally extrapolation far outside the
% definition range of the splines should occur.This linearity should also remain
% after extrapolation.
% Both aspects are taken care off bij the function "rectify"
```

Chapter 11

The m-file function cross_cut_fast.m

11.1 Introduction

In chapters 7 and 8 it was shown that the "scaled and shifted" stability diagrams for $1 \leq icase \leq 6$ show a great deal of similarity. These diagrams correspond to velocity profiles without an inflexion point for $2.2160 \leq H \leq 2.5910$. Even for $icase > 6$ ($H > 2.5910$) the low Reynolds number part of the diagram, where the Rayleigh instability is not yet manifest, shows this similarity. Because the similarity was only discovered in the later stages of the development of the new method it was also realised rather late that a drastic simplification of the function cross_cut.m might be possible, be it with a possible reduced accuracy. Such a faster routine could be very useful for the design of suction airfoils where it can be expected that the amount of suction that is necessary to prevent transition will result in velocity profiles without an inflexion point. For design purposes a reduced accuracy combined with a higher computational speed might be useful and acceptable. The present chapter describes such a simplified function cross_cut_fast.m. Chapter 12 will describe some applications of the new method. There the two versions of the function cross_cut will be compared with regard to speed and accuracy.

Another possibility to speed-up the cross_cut routine is to use a special function to evaluate a given spline at only one point. The MATLAB function ppval.m is designed to evaluate a spline in a whole array of points. If one needs only the evaluation at one point it pays to use equally spaced break points so that it is easy to find the interval in which the evaluation will take place and store the cubic polynomial coefficients ("coefs" in MATLAB language) separately for direct use. This procedure will be discussed in some more detail in section 11.4.

11.2   Approximation of the T_{ss}-splines by parabolic curves.

First of all the T_{ss} splines at given values of r for all icase were compared. It was found that the cross-sections in T_{ss} form were nearly identical for $icase \leq 6$ at the same value of r and also forsome $icase\_values > 6$ at the smaller values of the Reynoldsnumber, where the Rayleigh instability does not yet show up. Moreover it was observed that the curves are nearly parabolic (but not completely symmetrical). Then for all values of icase 1 through 6 and the r_{grid} points number 10 to 59 the Tss curves were approximated by:

$$T_{ss} = aa_{left} \cdot \overline{\omega}^2 \ for \ \overline{\omega} \leq 0 \tag{11.1}$$

$$T_{ss} = aa_{right} \cdot \overline{\omega}^2 \ for \ \overline{\omega} \geq 0 \tag{11.2}$$

$$\overline{\omega} = \frac{\frac{\omega\theta}{U} - \left(\frac{\omega\theta}{U}\right)_{axis}}{scale} \tag{11.3}$$

The coefficients aa_{left} and aa_{right} were determined by satisfying 11.1 and 11.2 for points near to the lower and upper branch of the neutral curve respectively. The first 9 points in the r_{grid} were not used because here the upper and lower branches are rather close and hence the $aa - coefficients$ showed more scatter. It was found that the coefficients aa_{left} and aa_{right} do depend on r but only to a small extent on icase. Therefore the (maybe bold) step was taken to fit a second degree polynomial in r to aa_{left} and aa_{right} separately but combined for all values of $icase \leq 6$. This resulted in the polynomials pp_overall_left and pp_overall_right that are contained in the database and used in `cross_cut_fast`.

These formulae are also applicable to the values of $0 \leq r \leq r_{grid}(10)$. For $r < 0$ the values at $r = 0$ are used. How well these approximations fit the T_{ss} splines and the original Arnal data follows from the program `comp_data_base_to_Arnal.m` (option 2 in the `N_factor_show.m`). It should be observed that the parabolic fit to T_{ss} was made for the region inside the neutral curve. Not much attention was paid to the tails of the T_{ss} curves because these had earlier been obtained by extrapolation of the Arnal data. The approximation is found to be surprisingly good. It is instructive to run the program also for $icase > 6$. It follows that also here a reasonable approximation is obtained as long as no Rayleigh instability is present. In general this means that for $icase > 6$ the region for r_grid point > 35 should be avoided (that is $r > 1.25$). From the roadmap, for example in figure 6.20, it follows that this region is well to the right of the $N = 9$ curve for similar flows. In practice this region will therefore not often be used when designing suction distributions to prevent transition.

11.3   Some further simplifications

When developing the fast version of `cross_cut.m` some additional (maybe bold) steps were taken. The value of log_Ftop=$^{10} log(F_{axis}$ at $r = \frac{1}{3})$ is found from the current version of the critical Reynolds number and the

$$log\_Ftop\_spline \tag{11.4}$$

The value of log_F_axis at an arbitrary value of r then follows from:

$$^{10}log(F_{axis} \ at \ r) = log\_Ftop - \sqrt{2} \cdot \left(r - \frac{1}{3} \right) \tag{11.5}$$

T_{maxmax} and r_{top} are determined from the relevant splines:

$$log\_MaxMaxT\_vs\_logcrit\_spline \tag{11.6}$$

$$rtop\_vs\_logcrit\_spline \tag{11.7}$$

Then with $\overline{r} = \frac{r}{r_{top}}$; $\overline{T}_{max}$ follows from the approximation that was discussed in chapter 6:

$$\overline{T}_{max} = \overline{r} \cdot e^{(1-\overline{r})} \tag{11.8}$$

The various splines are evaluated using the simplified form to be discussed in section 11.4.

11.4   A method for the fast evaluation of a spline if the result is only needed in one point.

It was noticed that evaluating an x-y spline at only one value of x using the MATLAB function y=ppval(spline,x) is rather time consuming. A method that is about 15 times faster if only a one point evaluation is needed can be obtained if one uses equally spaced break points and stores the MATLAB "coefs" separately instead of the complete MATLAB pp array. The new method can directly locate the interval in which x is contained and the corresponding cubic polynomial to be used. Therefore various existing splines were recast in a new form with new equally spaced breakpoints. The number of breakpoints was taken rather large suggesting a high accuracy. This, of course, is not true; the only justification is that we wanted to maintain consistency with the results of the original splines For the new splines it is only necessary to store the MATLAB "coefs" and to remember the x-range and the number of breakpoints. Details will become clear from the listing of the new function "cross_cut_fast" that will be discussed in section 11.5.

11.5   The new function cross_cut_fast(Rt,H)

The simplifications that were discussed in the preceding sections have been used to develop a new function to find the cross section through a stability diagram for arbitrary values of Re_{θ} and the shape factor H. The new version is about 8 times faster than the earlier one.A listing is given below; the comment lines give an adequate description. Note the much shorter program listing as compared to the one given in chapter 10.

```
function [aa_left,aa_right]=cross_cut_fast(Rt,H)% (CD-ROM version)
% Function to find the cross section in parabolic form of the stability diagram
```

```
% for arbitrary values of H (and hence of R-theta-crit) and Reynolds-theta.
% See chapter 11 of the report.
% The value of 10Log(Rtheta-crit) is found from coefs for a spline in log10(H).
% In this way T can be determined for a series of frequencies at a certain x-station
% in the calling program. Repeating this procedure at a number of x-stations allows
% to compute the n-factor for each frequency.
% At each x-station the maximum n-factor gives N.
% A trace of the stability characteristics of the boundary layer can be plotted in a
% "road map" by the calling program. Sometimes the trace leaves the region covered by
% the Arnal data.It is advised to check this roadmap to keep an eye on the credibility
% of the extrapolated stability data.
% The roadmap shows a curve for N-factor=9 for the Hartree-Stewartson similar flows.
% These flows trace horizontal lines in the road map. Observe that the curve
% for N=9 is not necessarily valid for non-similar flows.
% Make sure that in the main program the necessary stability data were loaded
% by executing "load datafile_for_n_factor".
% Reynolds-theta should be given as a value for "Rt" in the main program.
% Also the value of the shape factor H should be provided.
% The following global statement may contain more variables then are really needed for
% the present function because we kept the global statement the same for a number
% of m-files.
% ---------------------------------------------------------------------------------
global ...
ArMaxMaxT ArlogRtcrit r_grid Tbar Tss domega_saved dome  ...
logFax logMaxMaxT_vs_logcrit_spline logcrit_vs_logH_spline rtop_vs_logcrit_spline ...
scale_domega_vs_logcrit_spline  ycentre_spline  slope_left_vs_logcrit_spline ...
ArNumberofReynolds ArH  Arscomega Arr omega_Arnal T_Arnal ome_ax fnr ri logcriti ...
omega_at_axis log_Ftop_spline scomega TMax TMaxMax omegatop ...
pp_overall_left  pp_overall_right ...
coefs_log_Ftop  coefs_log_MaxMaxT   coefs_scale ...
coefs_rtop  coefs_slope_left  coefs_logcrit_vs_logH ...
breaks_log_Ftop  breaks_logMaxMaxT   breaks_scale ...
breaks_rtop  breaks_slope_left breaks_logcrit_vs_logH
% ------------------------------------------------------------------ end global
logRt=log10(Rt);
logH=log10(H);
% ----------first find logcriti; result should be the same as in cross_cut ------
xx=logH;
h=.005; % =interval for logH; 1/h=200
n=floor(200*(xx-.25));    % n is the number of complete intervals to the left of xx
if n<0
   n=0;
end
if n>300
   n=300;
end
t=xx-n*h-.25;
t2=t*t;
t3=t2*t;
coefspol=coefs_logcrit_vs_logH(n+1,:);
logcriti=coefspol(1)*t3+coefspol(2)*t2+coefspol(3)*t+coefspol(4);

% --------------now find other parameters from the splines in logcriti ------------
xx=logcriti;
h=.02;   % =interval length in logcriti 1/h=50 Is the same for all following splines
n=floor(50*(xx+1));        % n is the number of complete intervals to the left of xx
if n<0
```

```
   n=0;
end
if n>300
   n=300;
end
t=xx-n*h+1;
t2=t*t;
t3=t2*t;

coefspol=coefs_log_Ftop(n+1,:);
log_Ftop_i=coefspol(1)*t3+coefspol(2)*t2+coefspol(3)*t+coefspol(4);

coefspol=coefs_log_MaxMaxT(n+1,:);
logMaxMaxT=coefspol(1)*t3+coefspol(2)*t2+coefspol(3)*t+coefspol(4);

coefspol=coefs_scale(n+1,:);
scomega=coefspol(1)*t3+coefspol(2)*t2+coefspol(3)*t+coefspol(4);

coefspol=coefs_rtop(n+1,:);
rtop=coefspol(1)*t3+coefspol(2)*t2+coefspol(3)*t+coefspol(4);

slope=-sqrt(2);  % This is a rather bold approximation. Should be OK for all
% icase <=6 and for the other ones for r< r_top (=1/3). For the intended applications
% this is assumed to be sufficiently accurate.
% Future versions may be changed. Please check the web site mentioned on the CD-ROM.

TMaxMax=10^logMaxMaxT;
ri=logRt-logcriti;
rib=ri/rtop;
TMax=rib*exp(1-rib);
log10Fax=log_Ftop_i+slope*(ri-1/3);
Fax=10^log10Fax;
omega_at_axis=Fax*Rt;
if ri<0
   aa_left=-1.0482;
   aa_right=-1.1518;
else
   aa_left =polyval(pp_overall_left ,ri);
   aa_right=polyval(pp_overall_right,ri);
end
```

11.6   Concluding remarks on cross_cut_fast.m

In chapter 12 a set of example calculations will be made to see whether a useful acceleration of the computations has been realised by the new version of `cross_cut` without too much sacrifice in quality.

Chapter 12

Some applications of the new database method

12.1 Introduction

In the present chapter we will review some applications of the new database method for some typical boundary layers. Applications in the context of the design of airfoils with suction can be found in (Bongers, 2006, 🗎). The applications to be discussed here can be reviewed by running the MATLAB program `amplification.m` (option 13 in `N_factor_show.m`). The reader can familiarise himself with the method by running some applications with varying parameters. The program allows a comparison between the original and the later developed fast version of the function cross‑cut as described in chapters 10 and 11 respectively. Another version (ampli.m) gives a choice for either version. As an introduction we reproduce below some initial parts of the m-file amplification.m. The first comment lines would also appear in a MATLAB session following the command "help amplification"

```
% Amplification.m   (CD-ROM version)
% To calculate the N_factor for a given distribution of  x,U,H and R-theta.
% In this program we just calculate the N-factor. You may later introduce an "effective
% turbulence level" Tu to define the critical N-factor (Ncrit) to stop the calculation and
% switch to turbulent flow.
% In that case you may want to do the N-factor calculation step by step together with the
% laminar boundary layer calculation; it should not be difficult to adjust the program to
% your needs.
% We have predefined some typical cases; you can easily add your own case.
% Here we assume the laminar boundary layer to be known from a preceding calculation.
% After having built up experience with this program you may want to reduce the
% range of frequencies, and/or the number of frequencies within that range, to be used.
% At present this range is rather wide to accommodate applications in the upper right-hand
% corner of the roadmap area. Please observe the used frequencies in the detailed plots
% (figures 2 and 3).
% As soon as edge maxima for the n-factor as function of frequency occur you need to
```

```
% adjust the frequency range.
% We will denote the amplification factor as function of the frequency by n.
% We will denote the maximum amplification factor as function of x by N.
% For further explanations see chapter 12 of the report.
% Practical applications inserted into XFOIL can be found in the Masters thesis of
% J. Bongers (see report on the CD-ROM)
% No attempt has been made to optimise the MATLAB program. For routine (design)
% applications you may use an optimising (e.g. C-) compiler to speed up the computation.
% Also the "accelerator" for loops in later versions of MATLAB may be useful.
% The present version of the program allows you to use either:
%               1)   cross_cut
%               2)   cross_cut_fast
%               3)   both versions in parallel
% At each x-station detailed plots of T*U vs frequency and n-factor vs frequency are
% provided on request.Also the trace of the boundary layer in a "roadmap" and the growth
% of N with x may be followed.
% A companion program "ampli" lets you run either cross_cut or cross_cut_fast without
% the detailed plots.
% -----------------------------------------------------------------------------------
clear
close all
global ...
ArMaxMaxT ArlogRtcrit r_grid Tbar Tss  domega_saved logFax ...
logMaxMaxT_vs_logcrit_spline logcrit_vs_logH_spline rtop_vs_logcrit_spline ...
scale_domega_vs_logcrit_spline  slope_left_vs_logcrit_spline ...
ArNumberofReynolds ArH Arscomega Arr omega_Arnal T_Arnal ome_ax fnr ri ...
logcriti log_Ftop_spline TMax TMaxMax omega_at_axis scomega  coefs_log_Ftop ...
coefs_log_MaxMaxT  coefs_scale coefs_rtop  coefs_slope_left ...
coefs_logcrit_vs_logH  pp_overall_left  pp_overall_right
% The global statement above may contain more variables than really needed because
% we kept the global statement the same for a number of m-files.
% ------------------------------- end global  ------------------------------------
load datafile_for_n_factor
% -----------------------------------------------------------------------------------
disp ('You may use various versions of "cross_cut"               ')
disp ('1=The extensive one (cross_cut)                           ')
disp ('2=The fast approximate one (cross_cut_fast)               ')
disp ('3=Both at the same time to be able to compare the results ')
version_cross=input('give your choice:  1, 2 or 3                ')
close all
freqs=[-7 -1  601];% This is a rather wide range of frequencies. For practical
% applications you may want to reduce this range and/or the number of frequencies
% within that range after having built up experience with the method.
% Just keep an eye on the detailed plots.
f1=freqs(1);
f2=freqs(2);
fnr=freqs(3);
Finf=logspace(f1,f2,fnr);
xfr=[1:fnr];
% The N-factor calculations should be done for constant values of omega,
% that is constant Finf=omega*nu/Uinf^2. Other researchers have used for convenience
% constant F=omega*nu/U^2
% Our experience has shown that the final results show negligible differences
% because we use the envelope for a large number of frequencies.
% We will always use the first option.
% -----------------------------------------------------------------------------------
disp('------------------------------------------------- ----')
```

```
disp('       You have a choice from various cases        ')
disp('       1=PhD case van Ingen                        ')
disp('       2=flat plate                                ')
disp('       3=flat plate with oscillating H superimposed ')
disp('       4=flat plate with reduced H-region          ')
disp('       5=Rheinboldt 1.0                            ')
disp('       6=Iglisch                                   ')
disp('       7=simulated rooftop airfoil                 ')
disp('       8=you may add your own cases here           ')
disp('----------------------------------------------------')
my_choice=input('give the number of your choice;   1<= number <=7   ');
```

The predefined examples are listed below as presented in the program. For the more complicated cases the laminar boundary layer has been calculated separately with the finite difference method that was briefly discussed in section 3.5. The results were saved and loaded into the present program. These data files are available on the CD-ROM. For some simpler cases the boundary layer data are calculated within the present program. In some cases (3, 4 and 7 from the list below, a perturbation of the flat plate boundary layer was studied. Because changes in the stability characteristics are for the greater part due to changes in the critical Reynolds number (that is in H) and not in Re_θ, for simplicity Re_θ was taken equal to that for the basic flat plate. For the sake of the demonstration this was thought to be permissable. You have a choice from various cases:

1. PhD case van Ingen

2. flat plate

3. flat plate with oscillating H superimposed

4. flat plate with reduced H-region

5. Rheinboldt 1.0

6. Iglisch

7. simulated rooftop airfoil

8. you may add your own case here. Give the results of the boundary layer calculation as arrays for x, U, H and Re_θ as $xarr$, $Uarr$, $Harr$ and $Rtarr$ respectively. Also give the chord Reynolds number as $Rcred$, that is leave out a factor 10^6.

All examples calculated with `amplification.m` have a standardised output where the user can choose to follow the calculation step by step in the following 4 separate figures on the screen.

1. Figure 1, upper left, shows the progression of the calculation in the "roadmap" .

2. Figure 2, upper right, gives at each x-station the quantity $T \cdot U$ plotted versus a "frequency number"; remember that $T \cdot U$ has to be integrated to find the n-factor (see equation (2.15)).

3. Figure 3, lower left, shows at each x-station the n-factor as a function of the frequency number.

4. Figure 4, lower right, shows the chord wise distributions of $^{10}log(Re_\theta)$ and $^{10}log(Re_{\theta_{crit}})$ and the developing N-factor, clearly showing the stable and unstable regions. Of course these are also defined in the roadmap by the crossings with the $r = 0$ axis.

At the end of the calculation the final versions of figures 1 and 4 may be viewed and printed separately on a larger scale. We will now discuss examples in succession using the extensive version of cross_cut.m , referring to the format presented under 1-4 above. In section 12.9 we add the same examples run with both versions of cross_cut.

In the sections 12.2 through 12.7 the examples 1 through 6, run with the extensive version cross_cut, will be discussed. Section 12.9 presents for all examples the comparison between both versions.

12.2   Example 1: "PhD case van Ingen"

In his PhD thesis (van Ingen, 1965, 📄) the author presented an extensive theoretical and experimental research program on laminarisation by suction through a porous surface. For one of the experimental cases detailed data on the pressure- and suction distribution and various boundary layer parameters are available in the thesis (van Ingen, 1965, chapter 11 📄). It appeared in hindsight that in this case the suction distribution had been adjusted in such a way that a nearly fully stable boundary layer was achieved until laminar separation and subsequent transition occurred at the end of the porous region at the 90% chord position. The maximum N-factor near the beginning of the porous region is only about 0.2 . Many other suction distributions have been tested that would be interesting candidates for an N-factor calculation. This will have to wait however for a search in the 40 year old archives to find the data. Figure 12.1 shows the 4 sub plots that were generated during the calculation. On the upper left the roadmap can be seen as it was at the last calculated point (stopped because of nearing laminar separation). Figure 12.2 is an enlarged version that is plotted at the end of the calculation. Note that the trace first is in the stable region ($r < 0$), then enters very briefly into the unstable region ($r > 0$); then stays in the stable region for a long distance and near the end progresses with large steps into the unstable region again. The trace even crosses the N-factor $= 9$ line without transition illustrating that the $N = 9$ line is not valid for non-similar flows as we have here. Note that similar flows should produce a horizontal trace in the roadmap. In fact the maximum N-factor reached is just above .5 as follows from the lower right hand plot in figure 12.1 (shown enlarged in figure 12.3). The upper right hand plot of figure 12.1 shows $T \cdot U$ at the last station that was calculated. The reader is advised to choose the option "to view the results at each x-station" (certainly when an extreme situation is expected).
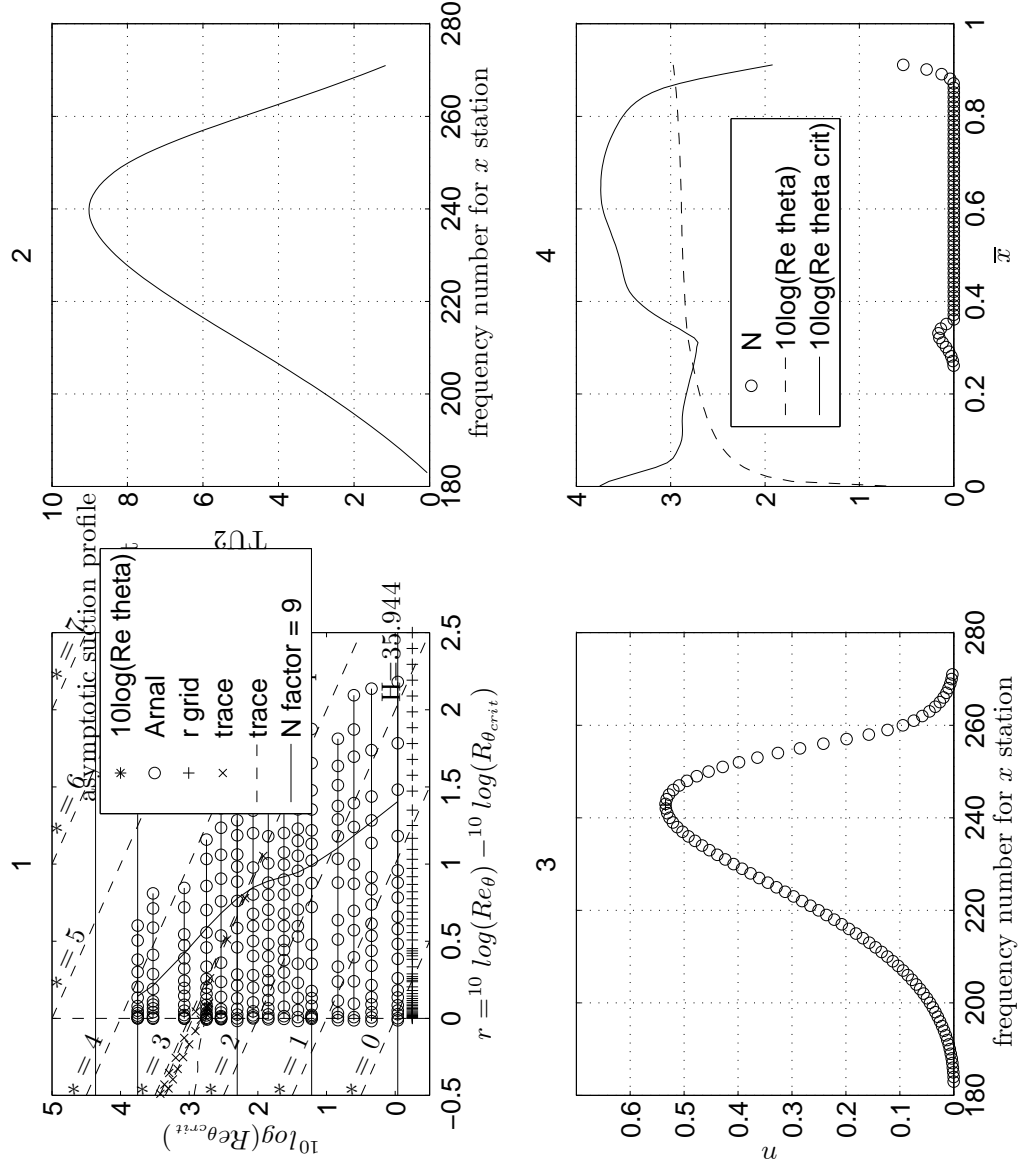
Figure 12.1: PhD case, 1) trace in roadmap, 2) TU w.r.t. frequency number for last x-station, 3) n w.r.t. frequency number for last x-station, 4) N, $^{10}log(Re_\theta)$ and $^{10}log(Re_{\theta_{crit}})$ vs x
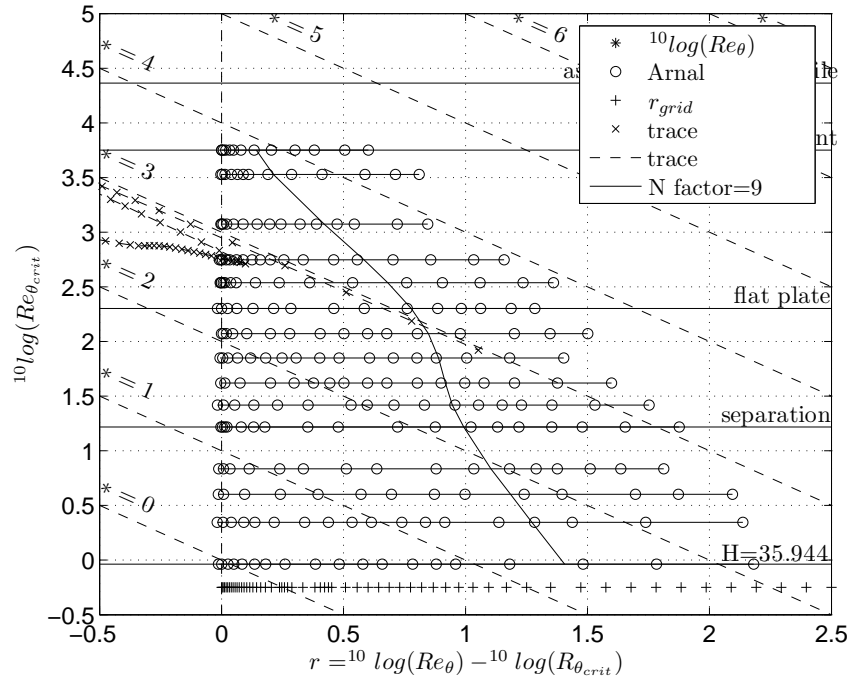
Figure 12.2: PhD case, trace in roadmap
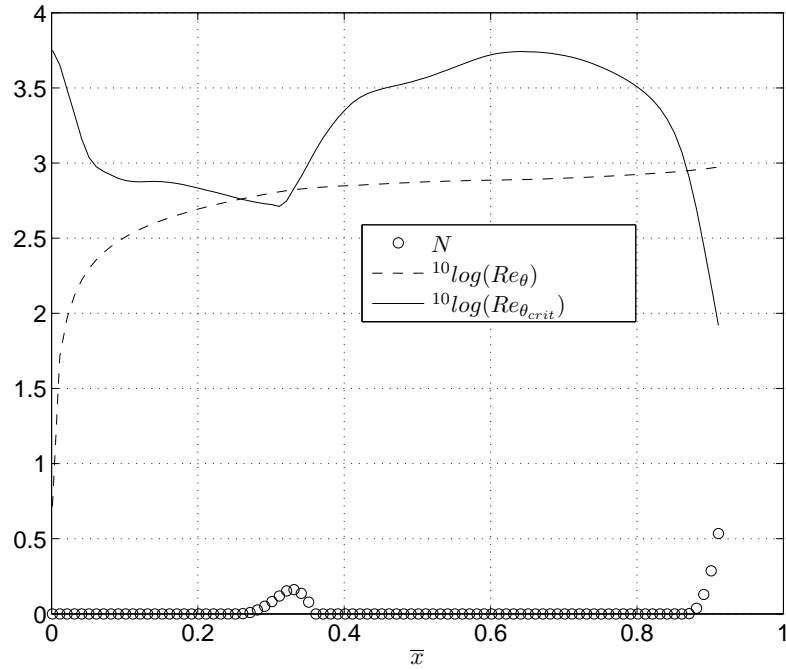
Figure 12.3: PhD case, N, $^{10}log(Re_\theta)$ and $^{10}log(Re_{\theta_{crit}})$ vs $\overline{x}$

12.3   Example 2: The flat plate

The results of this calculation were already presented in chapter 2. This case is shown here in the figures 12.4, 12.5 and 12.6. Since the chord Reynolds number was taken equal to $10 \cdot 10^6$, the critical N-factors N_1 and N_2 should be reached at $\overline{x} = 0.28$ and 0.39 respectively. Note that the trace in the roadmap follows the horizontal line labelled "flat plate" Here the crossing of the $N = 9$ line will indicate transition.
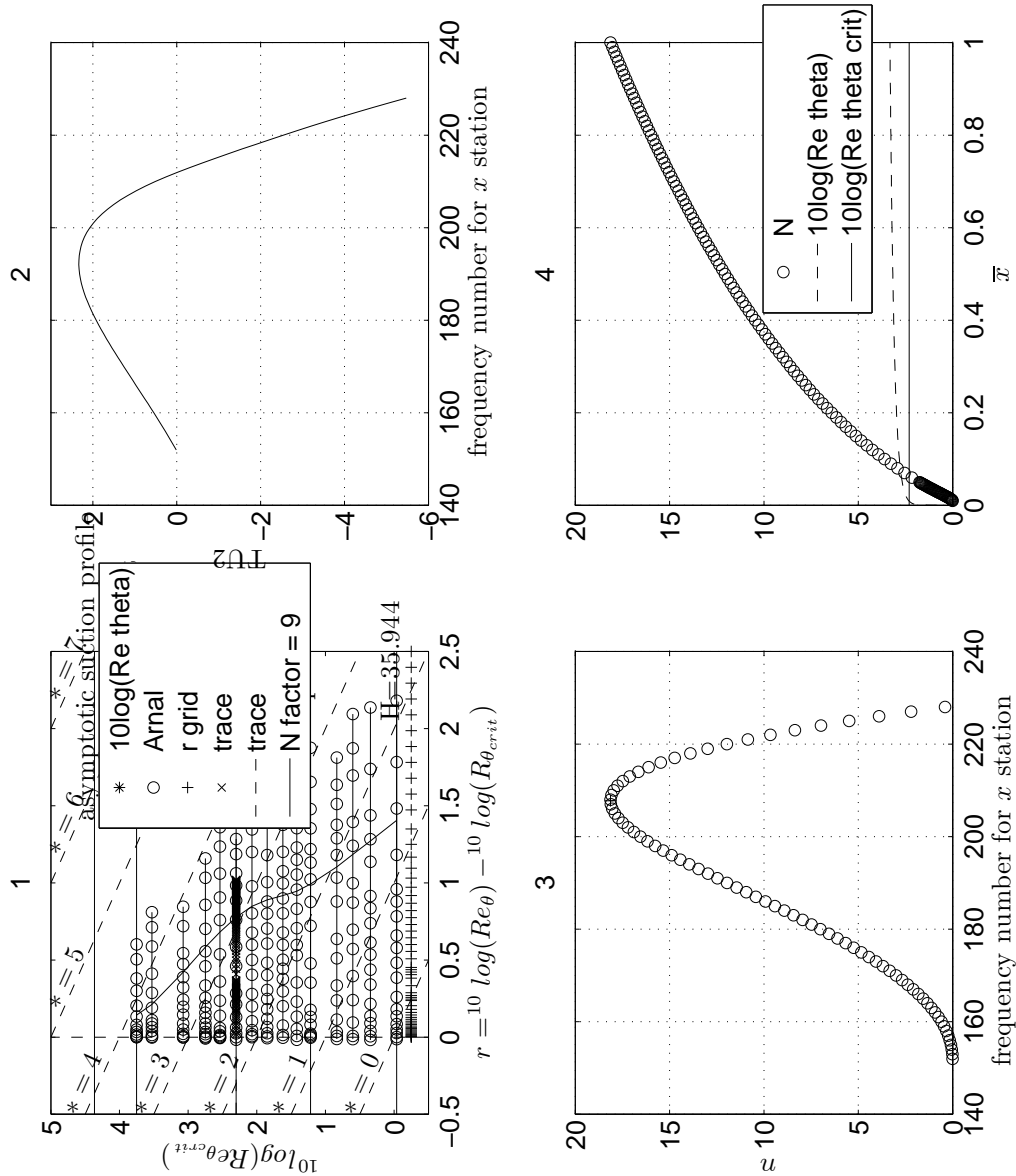
Figure 12.4: Flat plate, 1) trace in roadmap, 2) TU w.r.t. frequency number for last x-station, 3) n w.r.t. frequency number for last x-station, 4) N, $^{10}log(Re_\theta)$ and $^{10}log(Re_{\theta_{crit}})$ vs $\overline{x}$, $R_c = 10 \cdot 10^6$
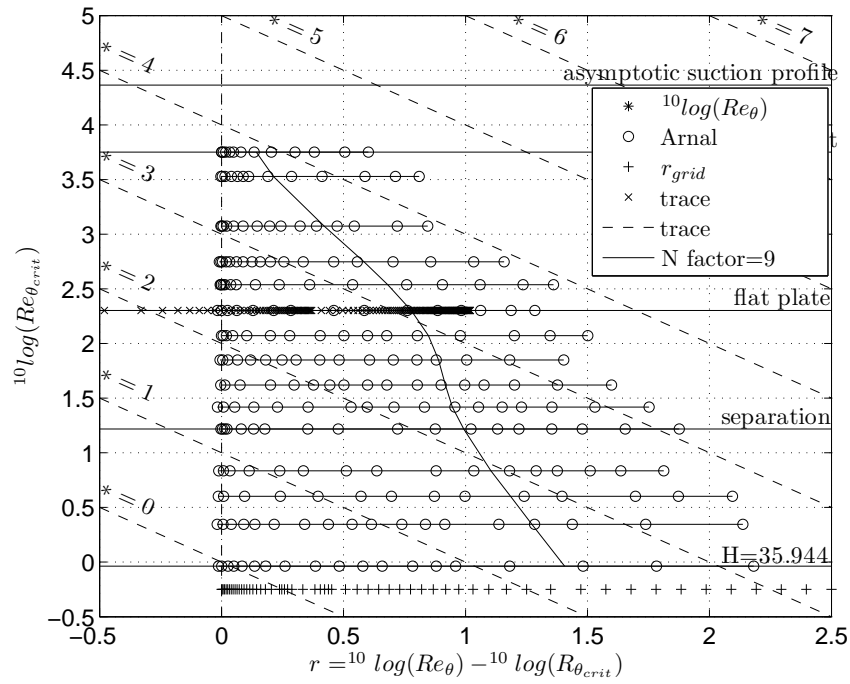
Figure 12.5: Flat plate, trace in roadmap
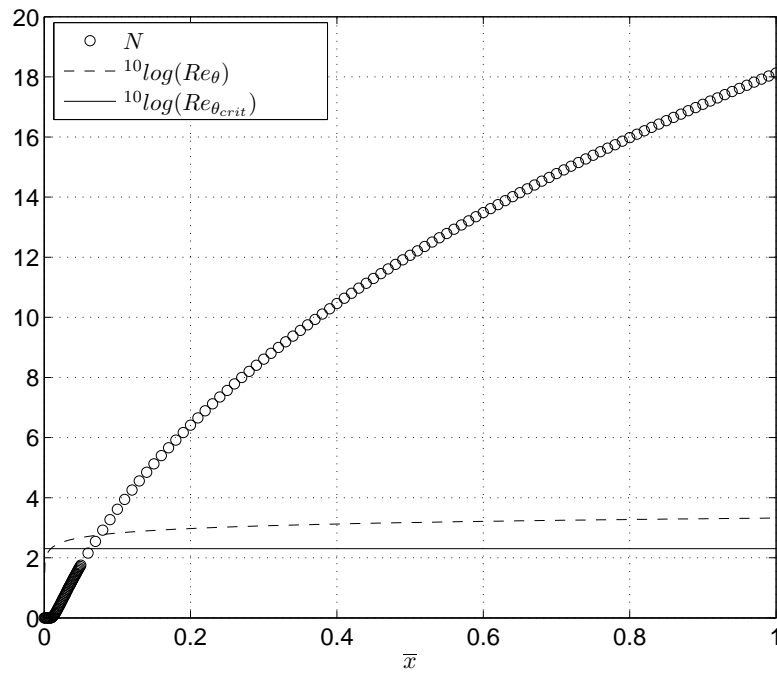
Figure 12.6: Flat plate, N, $^{10}log(Re_\theta)$ and $^{10}log(Re_{\theta_{crit}})$ vs $\overline{x}$

12.4 Example 3: The flat plate with oscillating H superimposed.

Here we take the flat plate with a sinusoidal variation of H between $\frac{x}{c} = .50$ and 1.0 superimposed on the constant value 2.591 to simulate the effect of suction and blowing. The amplitude (dH) may be chosen (positive or negative). Because experience has shown that with moderate suction the change in stability is nearly completely due to the change in H (and hence in critical Reynolds number) and not to the minor change in Re_θ, we took for convenience in this simple illustration the Re_θ distribution equal to the unsucked Blasius case for $Rc_{red} = 10$. In the present example we took the amplitude of the H-variation equal to $-.2$ which means that H is first decreased ($^{10}log(Re_{\theta_{crit}})$ increased, stabilisation) and then H is increased (de-stabilisation).The results are shown in figures 12.7 and 12.8.
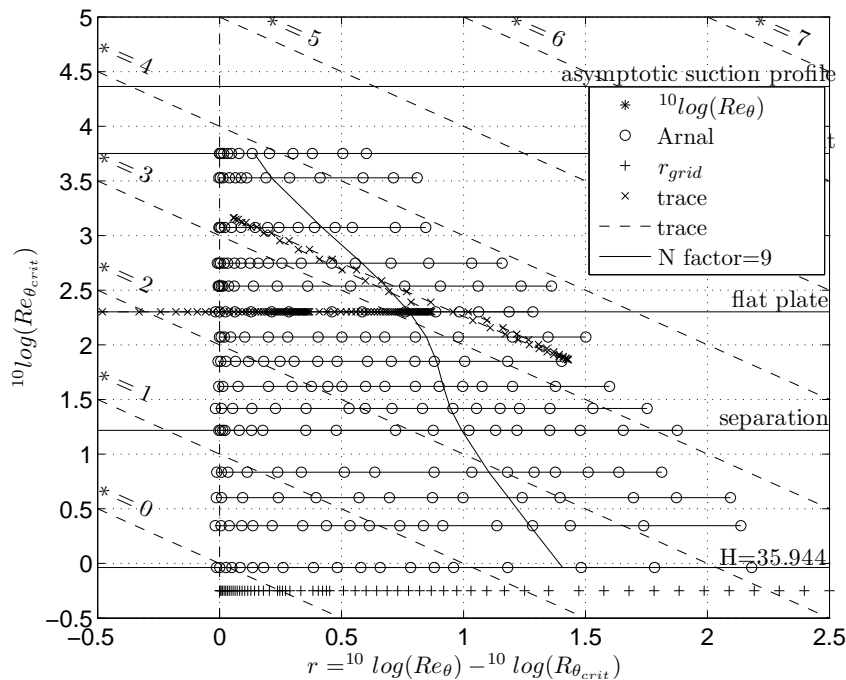
Figure 12.7: Flat plate with oscillating H with $dH = -.2$, trace in roadmap

12.5 Example 4: The flat plate with a reduced H region: a quadratic dip from $\frac{x}{c} = .20$ to .50.

We choose for a dip with maximum depth of .3; this first stabilises the flow until it is nearly stable again and then it becomes unstable again. For this case we only present the two large scale pictures as figure 12.9 and 12.10 respectively. Again Re_θ is kept equal to the Blasius value for $Rc_{red} = 10$.
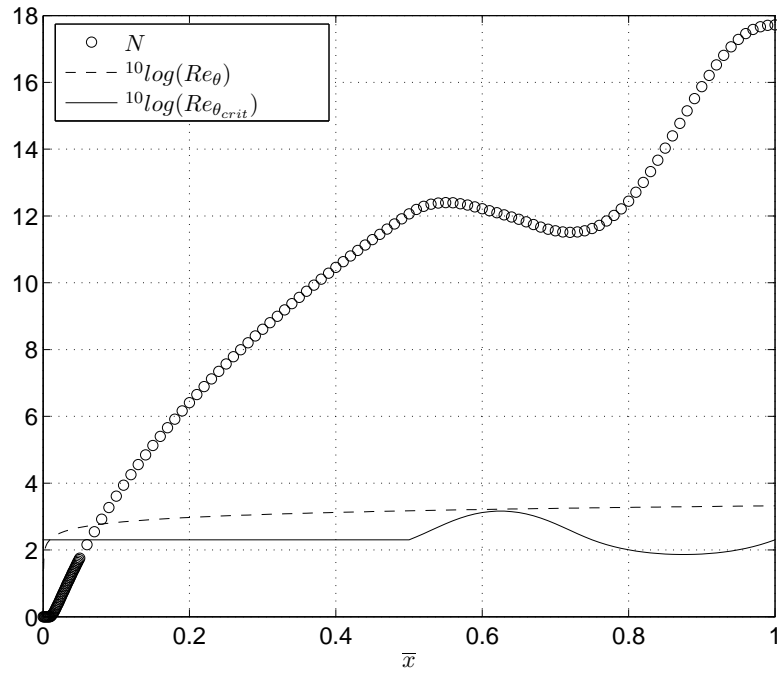
Figure 12.8: Flat plate with oscillating H with $dH = -.2$, N, $^{10}log(Re_\theta)$ and $^{10}log(Re_{\theta_{crit}})$ vs $\overline{x}$
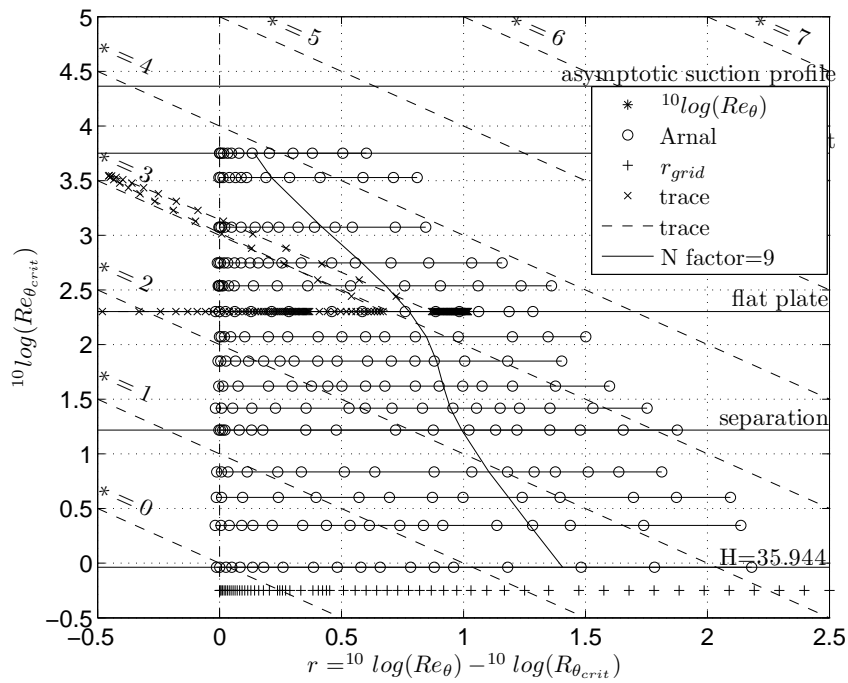
Figure 12.9: Flat plate with reduced H-region with $dH = .3$, trace in roadmap
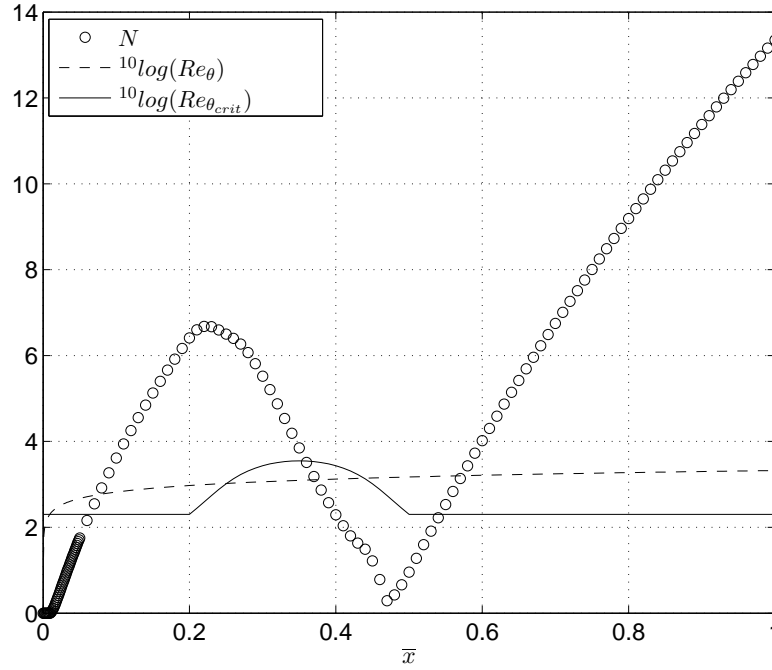
Figure 12.10: Flat plate with reduced H-region with $dH = .3$, N, $^{10}log(Re_\theta)$ and $^{10}log(Re_{\theta_{crit}})$ vs $\overline{x}$

12.6 Example 5: Rheinboldt's flat plate with discontinuous suction.

(Rheinboldt, 1956) designed a special procedure for the calculation of boundary layers with discontinuous suction. The method was illustrated with several examples. One of these examples is the boundary layer on a flat plate with non-porous entry length c followed by a porous region with constant suction velocity for $x > c$. See fig. 12.11. Of course it can be expected that for $x \rightarrow \infty$ the asymptotic suction boundary layer is obtained. Here we will discuss this case for a suction velocity given by $\frac{-v_0}{U}\sqrt{\frac{Uc}{\nu}} = 1.0$. In order to handle the discontinuity at $x = c$, we took a number of extremely small steps around $x = c$ and rounded the discontinuities. Further downstream the calculation reproduces Rheinboldt's results. The Reynolds number based on U and c was taken equal to 10^6 so that at $x = c$ (at the start of suction) the N-factor should remain well below 9. The results of our calculation are shown in figures 12.12 and 12.13. Note that in the roadmap the trace starts along the flat plate (zero suction) and then returns to the stable region ($r < 0$) along a path that is very nearly parallel to the constant Re_θ lines. The maximum N-factor is 3.5 at suction begin (figure 12.13).Stabilisation sets in a small distance before $\frac{x}{c} = 1$ due to the rounding of the discontinuity.
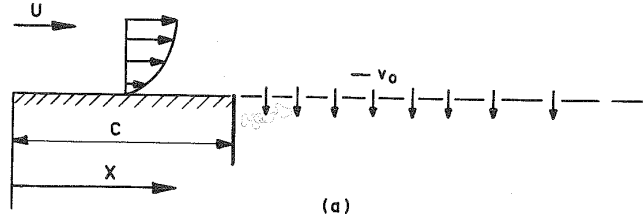
Figure 12.11: Rheinboldt's flat plate with discontinuous suction
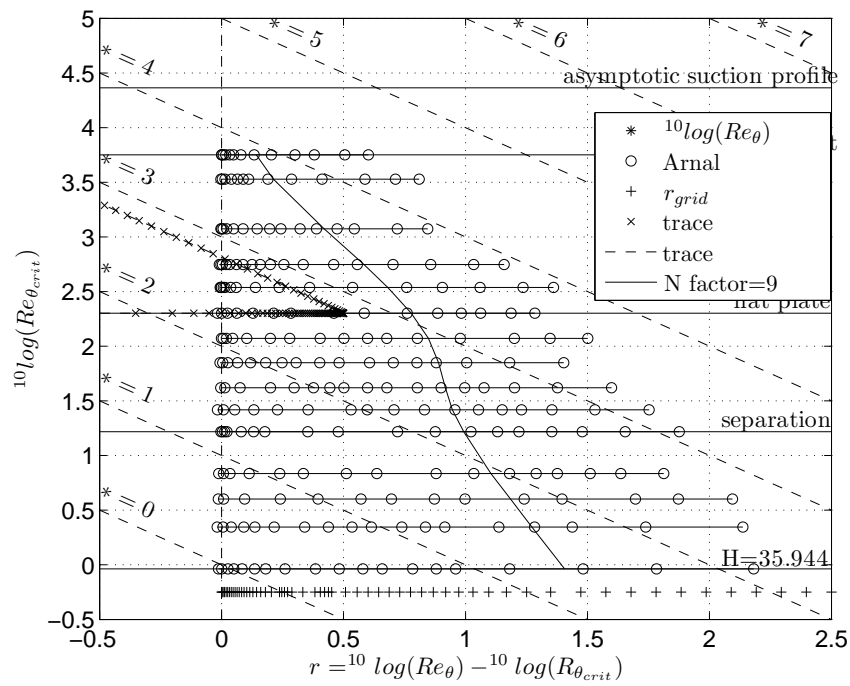
Figure 12.12: Rheinboldt's flat plate with discontinuous suction, trace in roadmap
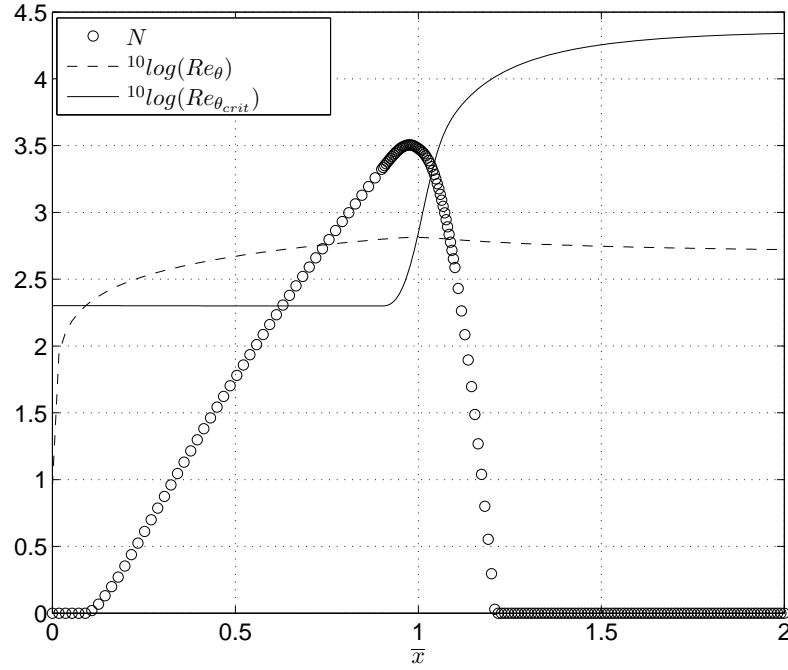
Figure 12.13: Rheinboldt's flat plate with discontinuous suction, N, $^{10}log(Re_\theta)$ and $^{10}log(Re_{\theta_{crit}})$ vs $\overline{x}$

12.7 Example 6: Iglisch boundary layer on a flat plate with constant suction.

For the flat plate with constant suction velocity an exact solution has been given by (Iglish, 1944). (see also (van Ingen, 1965, 📄)) In this solution a new independent variable $\overline{x}$ is introduced by

$$\overline{x} = \left(\frac{-v_0}{U} \right)^2 \frac{Ux}{\nu} \tag{12.1}$$

which implies that the "reference length" c is defined by

$$c = U \left(\frac{\nu}{-v_o^2} \right) \tag{12.2}$$

If for the reference speed U_∞ the constant mainstream velocity U is used it follows that $\overline{U} = \frac{U}{U_\infty} = 1$ and that "R_c"$=\left(\frac{U}{-v_0} \right)^2$

From Iglisch's solution it is known that at $\overline{x} = 0$ the boundary layer starts as the Blasius flat plate without suction and that for $x \to \infty$ the asymptotic suction boundary layer is obtained. It also is known that near $\overline{x} = 0$ more regular plots are obtained if $\sqrt{x}$ is used.

We used a power series solution for $f(x,y)$ in $\sqrt{\overline{x}}$ near $x = 0$ to start the finite difference calculation and saved the results as input to the present program. We will see that interesting
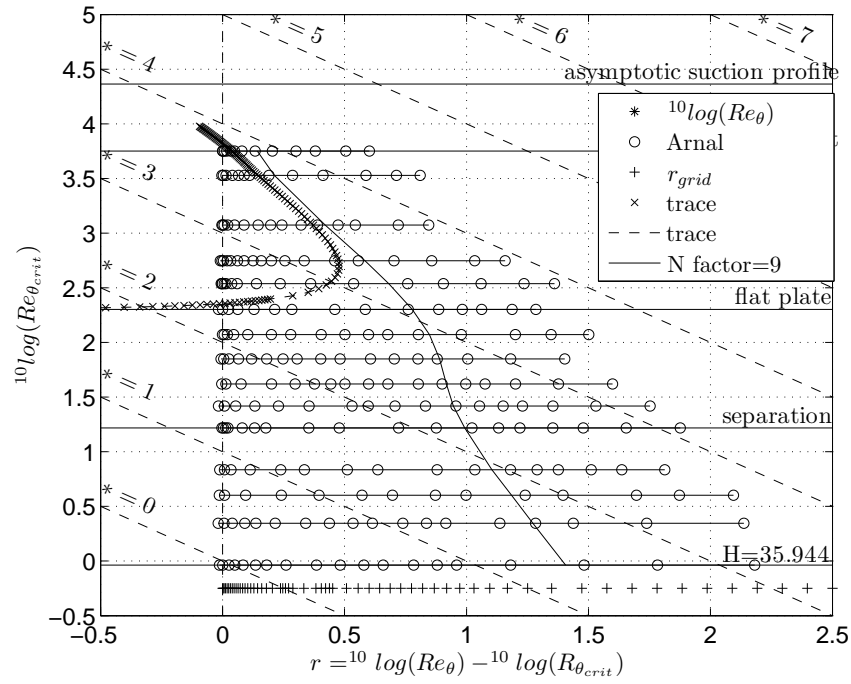
Figure 12.14: Iglisch flat plate with constant suction($c_{q_{red}} = .5$), trace in roadmap
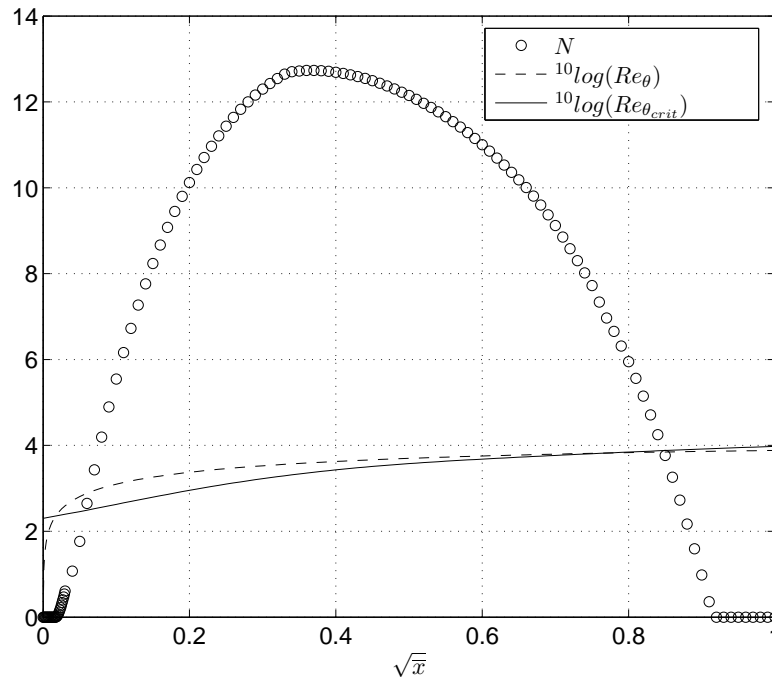
Figure 12.15: Iglisch flat plate with constant suction ($c_{q_{red}}$=.5, N, $^{10}log(Re_\theta)$ and $^{10}log(Re_{\theta_{crit}})$ vs $\sqrt{x}$)

values of $c_q = \frac{-v_0}{U}$ are of the order 10^{-4} and hence that the Reynolds number based on c is of the order 10^8. This may bring us in the upper right hand part of the roadmap where very high values of Re_θ occur. Figures 12.14 and 12.15 present results for $c_q = .5 \cdot 10^{-4}$. It follows that in this case the maximum N-factor is nearly 13 at $\sqrt{\overline{x}} = .35$ Note that the variable along the horizontal axis in figure 12.15 is $\sqrt{\overline{x}}$ which gives a better behaviour near $x = 0$. We have run the Iglisch case for 12 c_q values ranging from $.4 \cdot 10^{-4}$ to $1.5 \cdot 10^{-4}$ For the lowest value the maximum N-factor exceeds 9 so that transition will occur. For the highest value complete stabilisation is reached. This shows that extremely small suction velocities are sufficient for complete stabilisation. For just keeping the boundary layer laminar the maximum N-factor is allowed to grow until about 9. This has been found to reduce the required suction velocity to less than 50% of that for complete stabilization. Since the maximum N-factor is only reached locally a further reduction in suction quantity would follow from taking a non-constant suction velocity, adjusted to the stability characteristics of the boundary layer. (see (van Ingen, 1965, chapter 9,)).

The following figures in this chapter will present some detailed results for the Iglisch flow, that have been calculated with a separate program, not included on the CD-ROM. They are nearly self explanatory so that only a very brief discussion will be presented. Figures 12.16 and 12.17 show H vs $\overline{x}$ and $\sqrt{\overline{x}}$ respectively. It is clear that using $\sqrt{\overline{x}}$ is to be preferred for plotting. Note that the calculations with the finite difference method have been made with $\overline{x}$ as independent variable but that the calculation was started some distance away from $\overline{x} = 0$. The first part was done with a power series solution in $\sqrt{\overline{x}}$ for the streamfunction f. There is a good correspondence with the classical results by Iglisch. It is clear that the boundary layer starts as that for the Blasius case and asymptotically approaches the asymptotic suction boundary layer. Figure 12.18 shows the value of $\frac{-v_0\theta}{\nu}$. Figure 12.19 gives $^{10}log(Re_{\theta_{crit}})$ and the 12 curves for $^{10}log(Re_\theta)$ at $c_{q_{red}}$ from .4 to 1.5. It can be seen that complete stability is obtained for $c_{q_{red}}$ is 1.5. This is confirmed by figure 12.20 which is in fact the set of road map traces turned over 90 degrees. Figure 12.21 shows the N-factor vs $\sqrt{\overline{x}}$ confirming the earlier results; transition will occur at $\sqrt{\overline{x}}$ about .3 for $c_{q_{red}}$ between .5 and .6. Figure 12.22 shows the maximum N-factor as function of $c_{q_{red}}$. Figure 12.23 shows the same results as fig. 12.21 but now with the x-Reynolds number along the horizontal axis. Note the extremely high values of $\frac{Ux}{\nu}$; due to the relation between R_c and c_q; that is $R_c = (c_q)^{-2}$. Finally figure 12.24 shows the traces in the roadmap for all 12 $c_{q_{red}}$ values. Note that for the lowest value (.4) the trace just crosses the $N = 9$ curve. It should be remembered however that the Iglisch boundary layer is not a similar flow. Hence the $N = 9$ curve cannot be expected to indicate transition for this case. In the older literature it was mentioned that for the Iglisch flow a reduced suction coefficient of 1.18 was sufficient to obtain complete stability. We find the higher value 1.5. This appears to be due to the fact that the critical Reynolds numbers as used by Ulrich are higher than in our data base. This is illustrated by figure 12.25 were a comparison is made for different sets of data. It can be seen that also for some no-suction cases the Ulrich values are on the high side. Figure 12.26 shows the same results as figure 12.19 but now with Ulrich's values for the critical Reynolds number for the Iglisch flow. Now we also find a critical $c_{q_{red}}$ value just below 1.2.
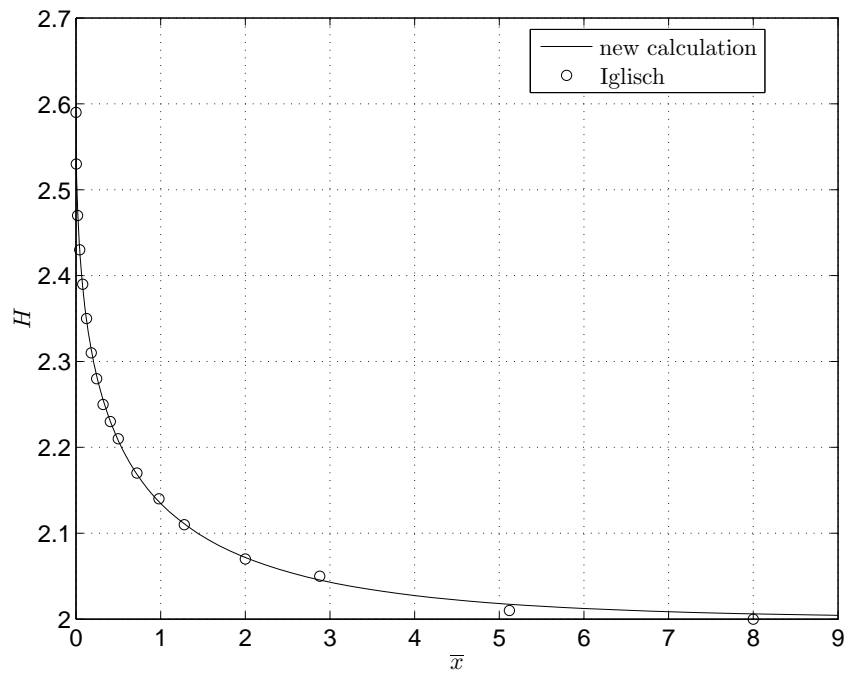
Figure 12.16: H vs $\overline{x}$ for the Iglisch boundary layer
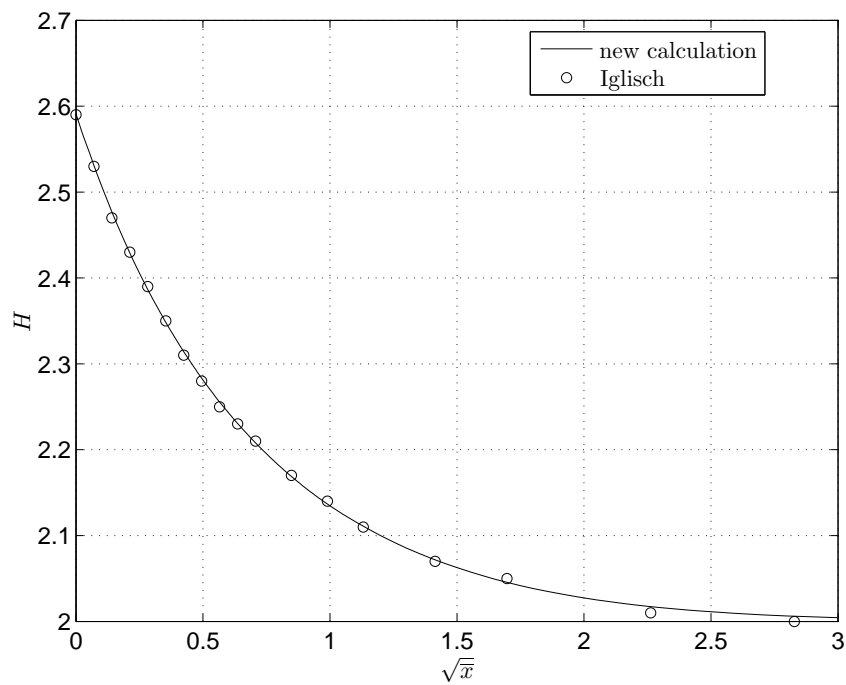
Figure 12.17: H vs $\sqrt{\overline{x}}$ for the Iglisch boundary layer
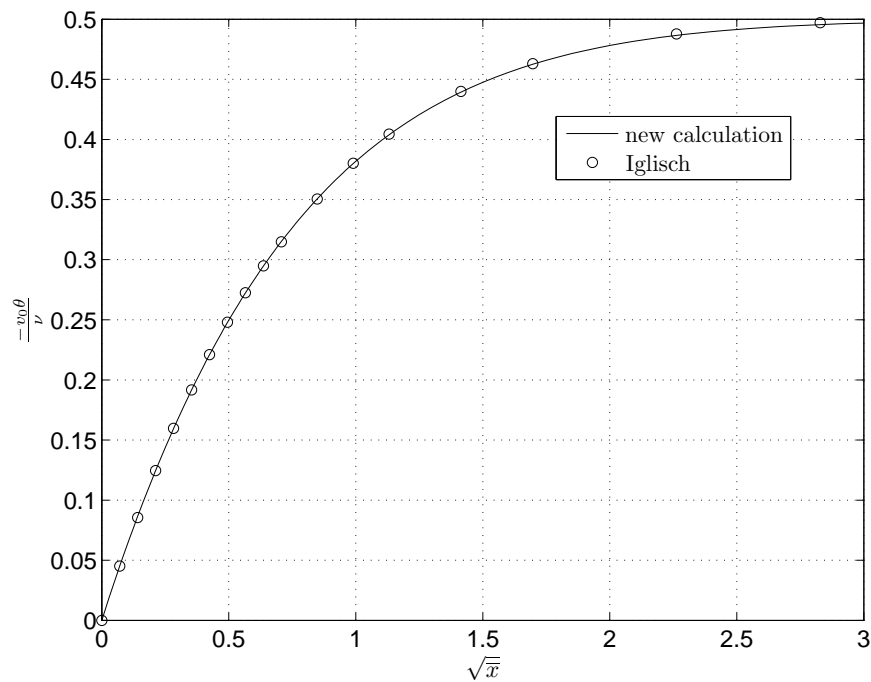
Figure 12.18: $\frac{-v_0\theta}{\nu}$ vs $\sqrt{x}$ for the Iglisch boundary layer
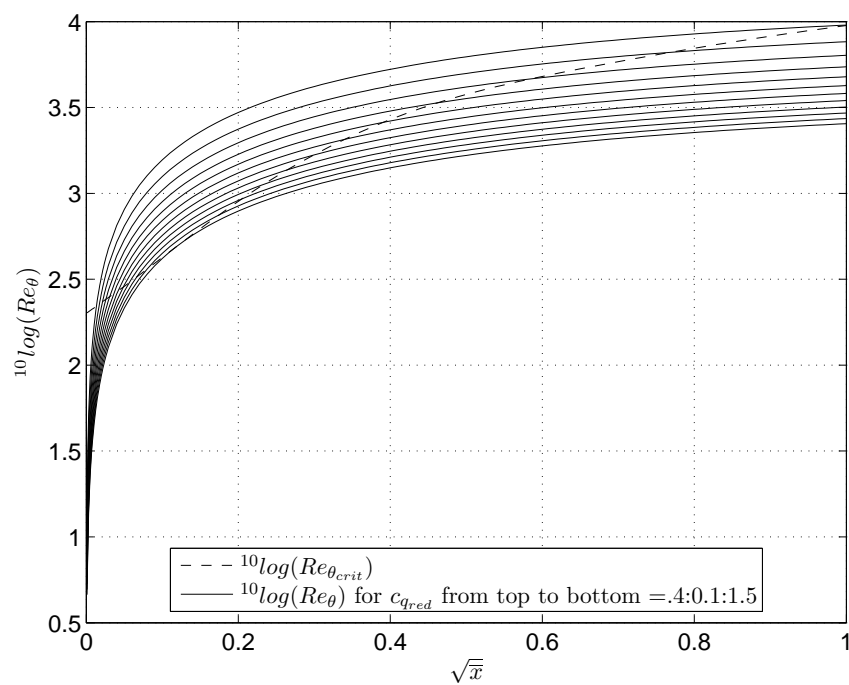
Figure 12.19: $^{10}log(Re_\theta)$ and $^{10}log(Re_{\theta_{crit}})$ for various c_q
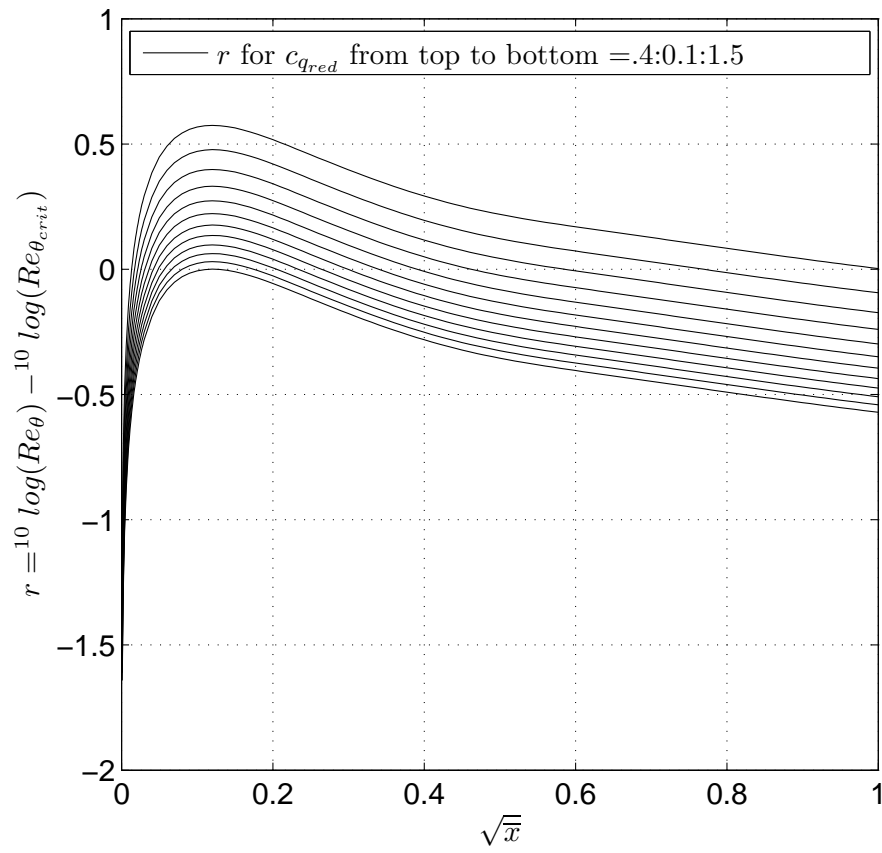
Figure 12.20: r vs $\sqrt{\overline{x}}$ for the Iglisch boundary layer at various values of $c_{q_{red}}$
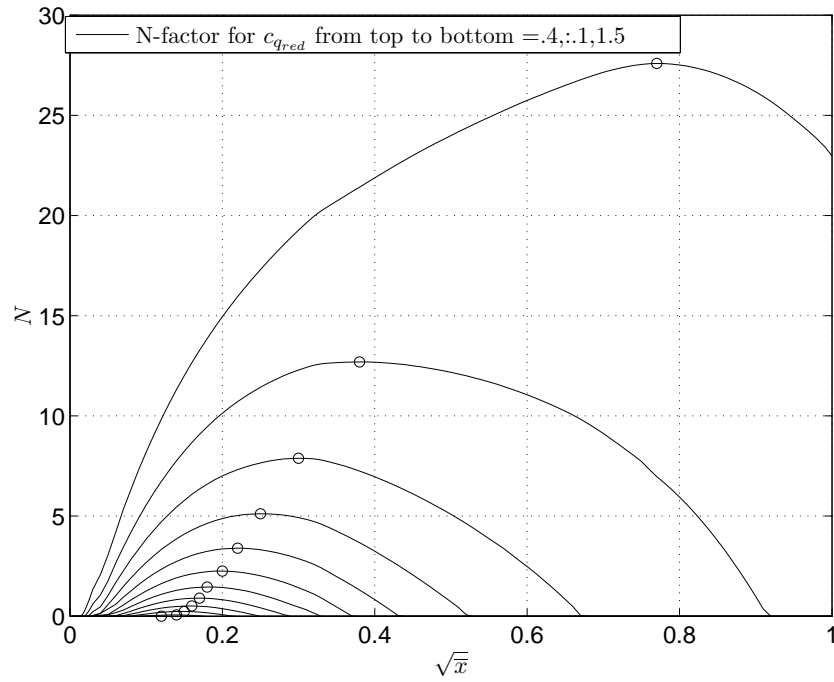
Figure 12.21: N-factor vs $\sqrt{\overline{x}}$ for the Iglisch boundary layer at various values of $c_{q_{red}}$
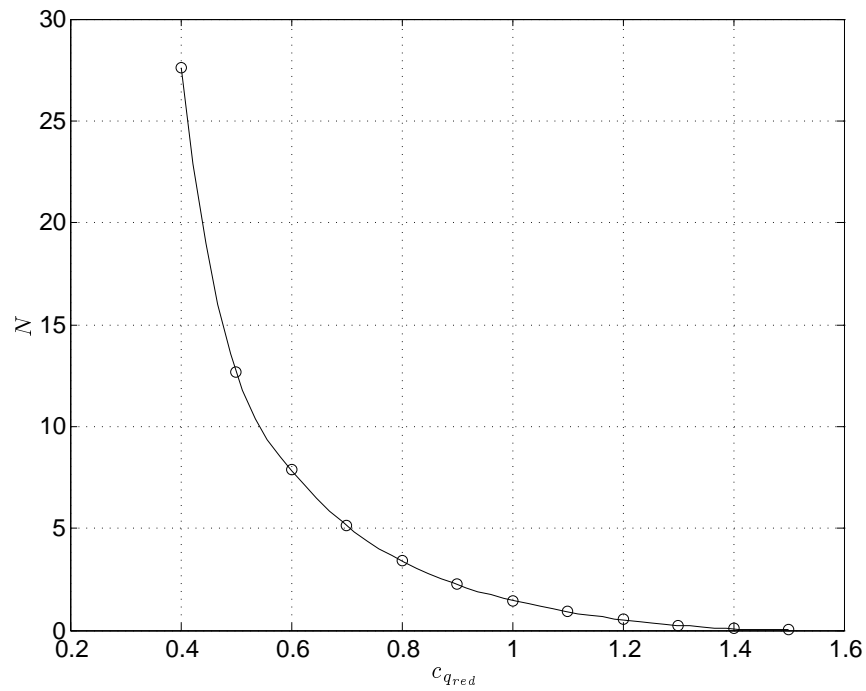
Figure 12.22: Maximum N-factor vs $c_{q_{red}}$ for the Iglisch boundary layer
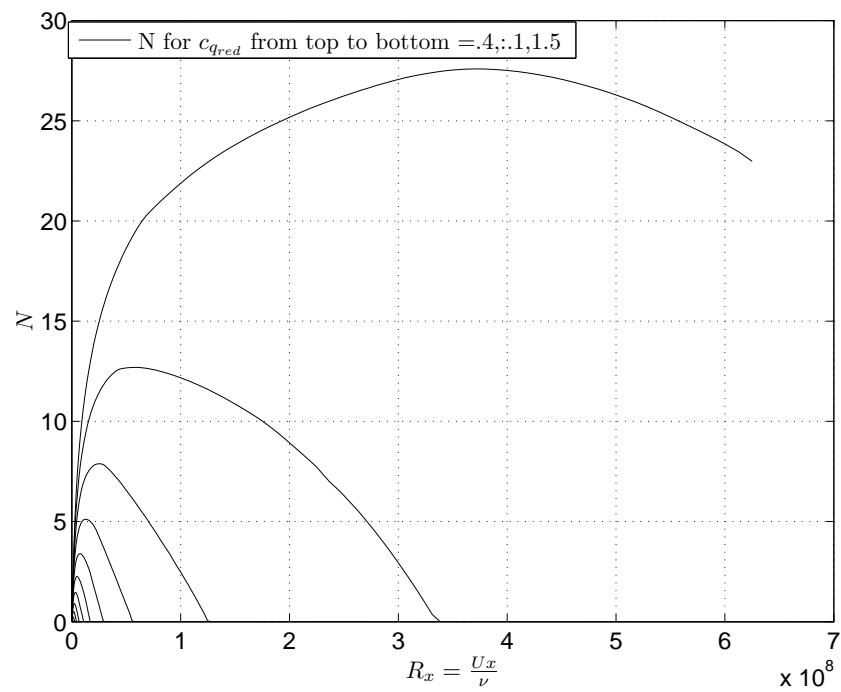
Figure 12.23: N vs $Re_x = \frac{Ux}{\nu}$ for for the Iglisch boundary layer at various values of $c_{q_{red}}$
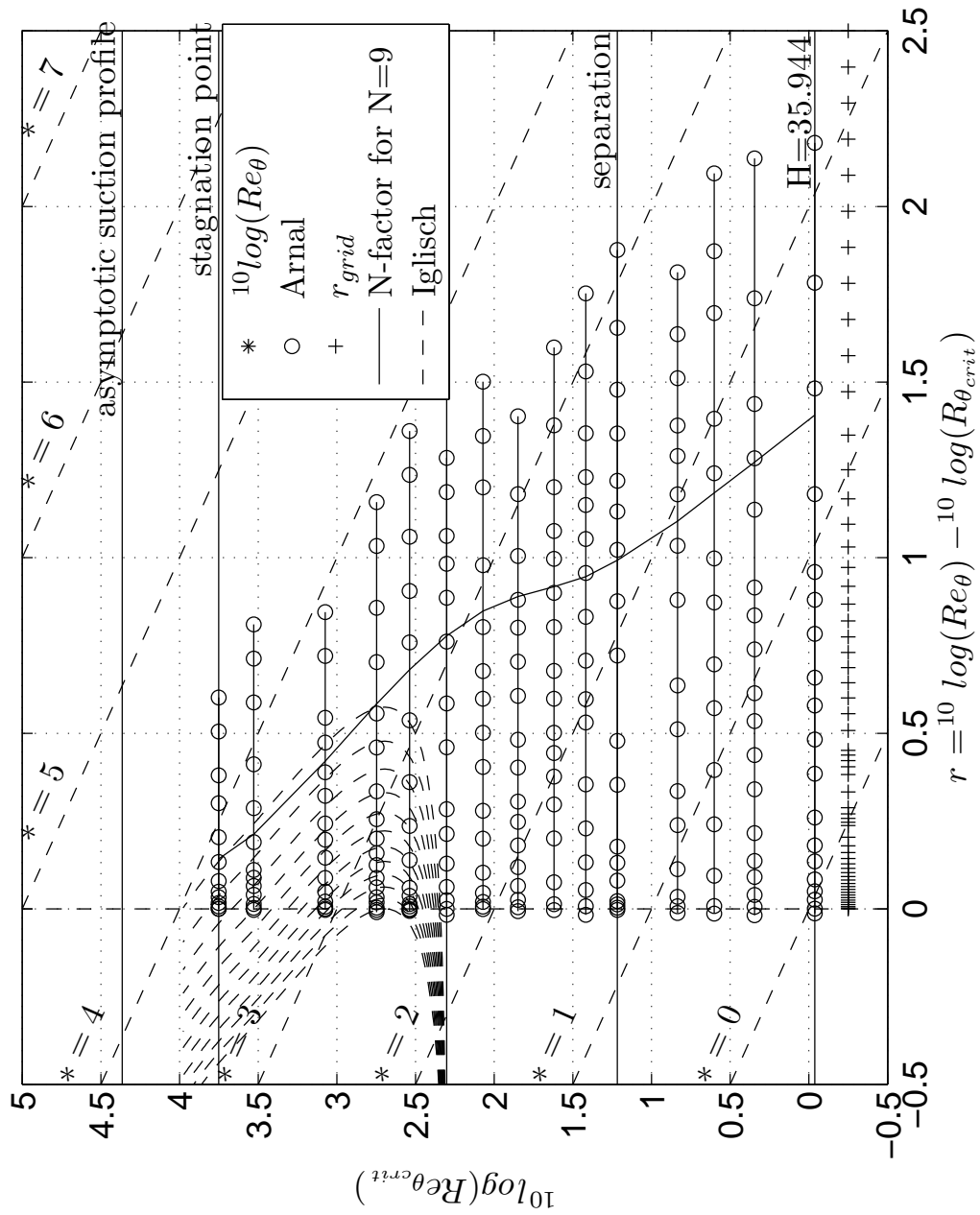
Figure 12.24: Traces for the Iglisch boundary layer in the roadmap
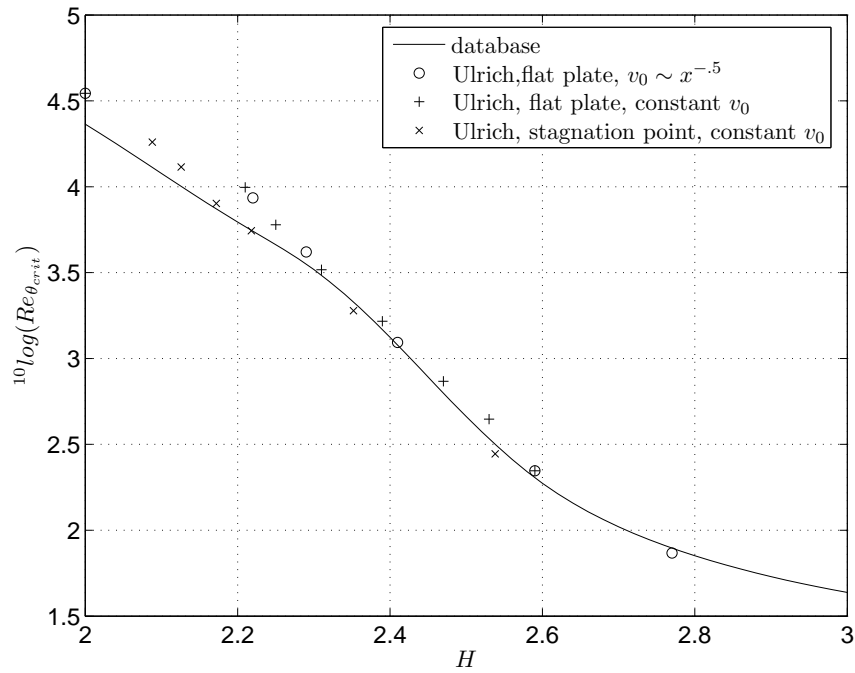
Figure 12.25: $^{10}log(Re_{\theta_{crit}})$ for some flows according to Ulrich compared to database
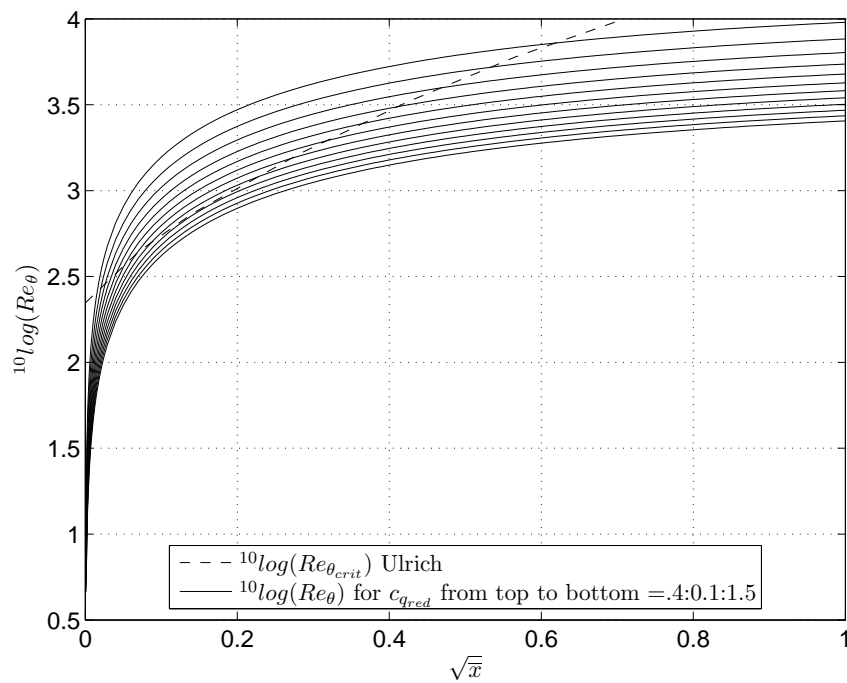
Figure 12.26: $^{10}log(Re_{\theta})$ for Iglisch flow at various c_q and $^{10}log(Re_{\theta_{crit}})$ according to Ulrich

12.8   Example 7: The simulated rooftop airfoil

This example will be discussd in section 12.9.

12.9   Comparison of the two versions of cross_cut

The examples that were discussed in the preceding sections of the present chapter have been repeated with a version of "amplification.m" in which the results of the two versions of "cross_cut"could be compared. The various flow parameters have been kept equal. In addition to the earlier figures we also show plots of H vs x.

Finally we have added case 7: "the simulated rooftop airfoil". In this example H is taken equal to the flat plate value for $0 \leq \frac{x}{c} \leq 0.5$ and is allowed to increase linearly to a higher value H_{end} at $\frac{x}{c} = 1$. In the example $H_{end} = 3.9$ and hence near to the separation value. As in earlier examples we have, for simplicity, Re_θ kept equal to the basic flat plate. Again for this demonstration this is thought to be acceptable. In most cases the results from both versions appear to be rather close and sufficiently so for design calculations. Especially the result for the simulated rooftop airfoil was at first sight surprisingly close and unexpected because for $\frac{x}{c} > .5$ we have velocity profiles with an inflexion point and hence stability diagrams with Rayleigh instability at higher Reynolds numbers. On further thought this may be explained as follows. In order to prevent transition in the present no suction case the Reynolds number has to be kept low. Hence the Rayleigh instability will not show up, even for $H > 2.591$. In general we can say that in order to prevent transition we have to keep the N-factor below 9 by a proper combination of pressure gradient, suction and Reynolds number. This will automatically keep us away from the region in the roadmap where Rayleigh instability can be expected. It may therefore be concluded that the fast version of cross_section is a useful tool for design calculations.

The results of the examples are shown in the figures 12.27 through 12.39. Because the flow parameters were kept equal to those for the examples in sections 12.2 through 12.7 no further explanation of the figures is needed. Note that the traces in the roadmap do not change.
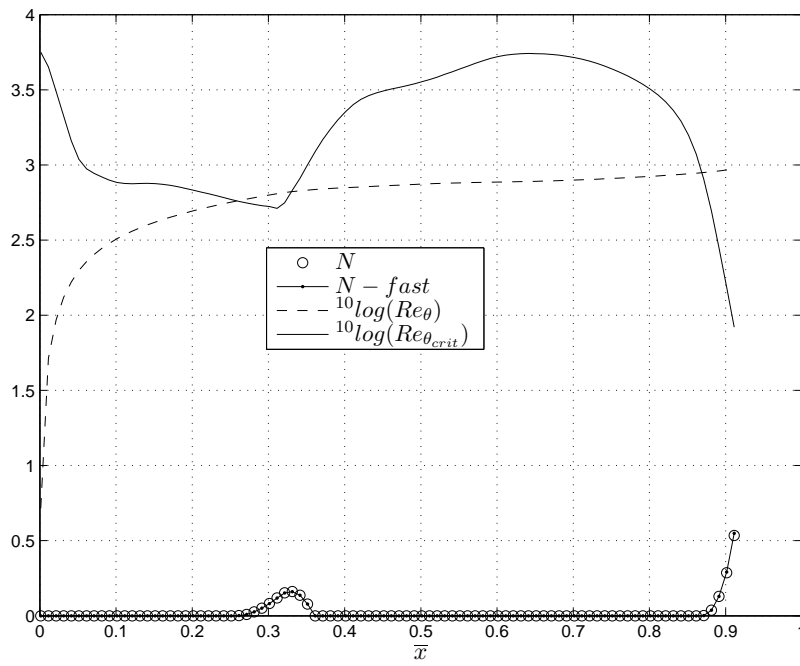
Figure 12.27: PhD case, N, $N - fast$, $^{10}log(Re_\theta)$ and $^{10}log(Re_{\theta_{crit}})$ vs $\overline{x}$
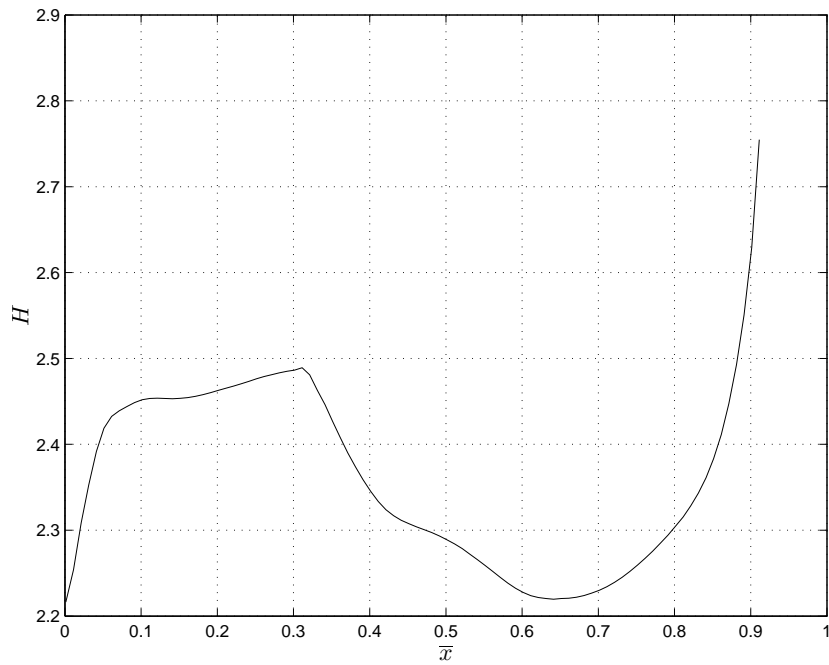
Figure 12.28: PhD case, H vs $\overline{x}$
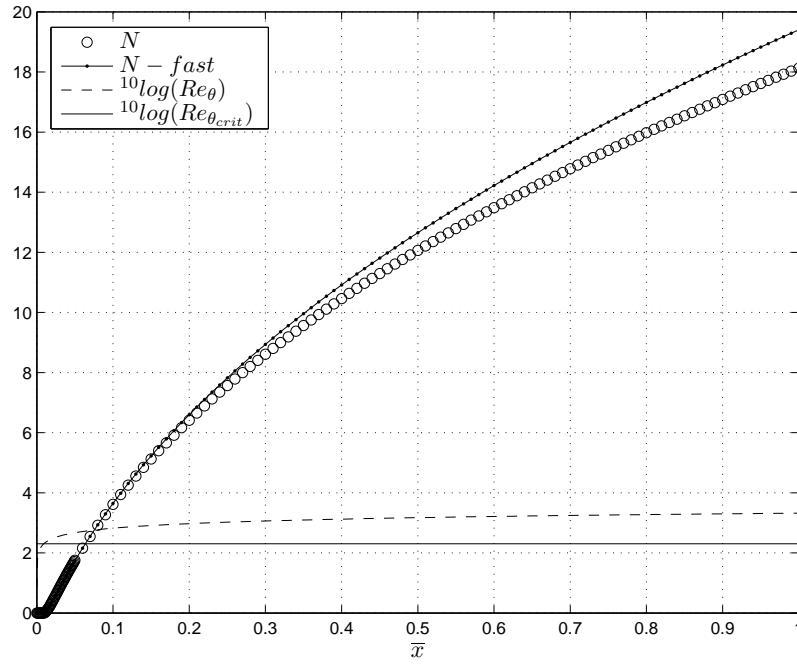
Figure 12.29: Flat plate, $R_{c_{red}} = 10$, N, $N - fast$, $^{10}log(Re_\theta)$ and $^{10}log(Re_{\theta_{crit}})$ vs $\overline{x}$
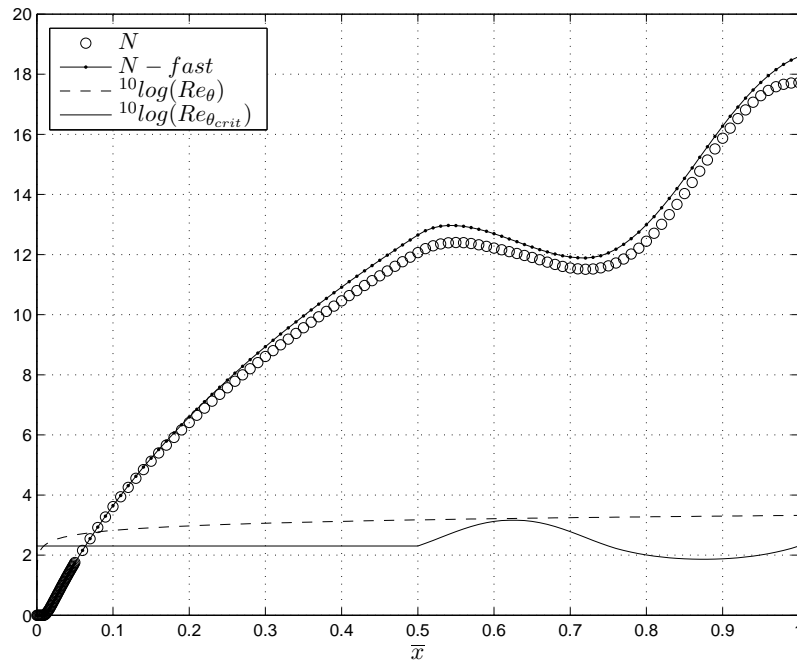
Figure 12.30: Flat plate with oscillating H superimposed with $dH = -.2$, $R_{c_{red}} = 10$, N, $N - fast$, $^{10}log(Re_\theta)$ and $^{10}log(Re_{\theta_{crit}})$ vs $\overline{x}$
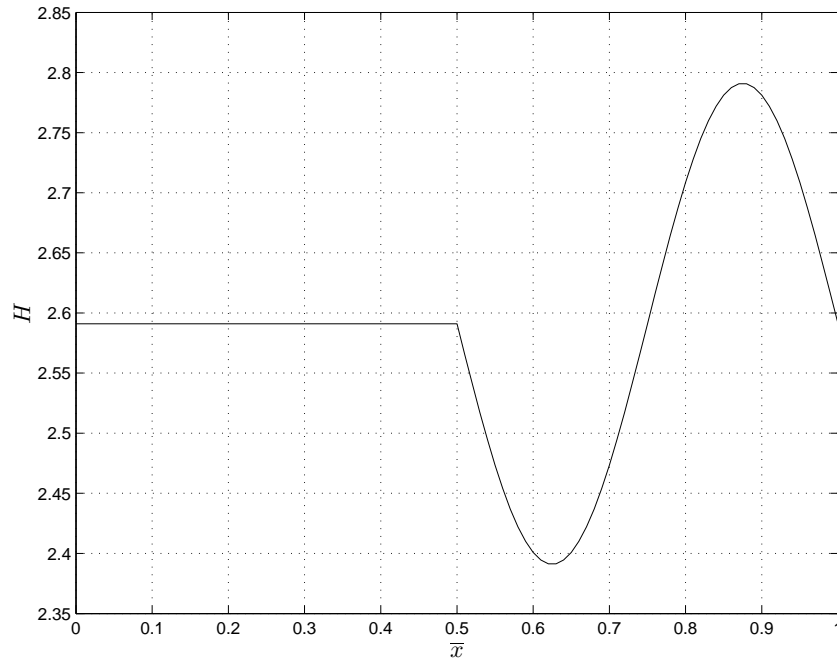
Figure 12.31: Flat plate with oscillating H superimposed with $dH = -.2$, $R_{c_{red}} = 10$, H vs $\overline{x}$
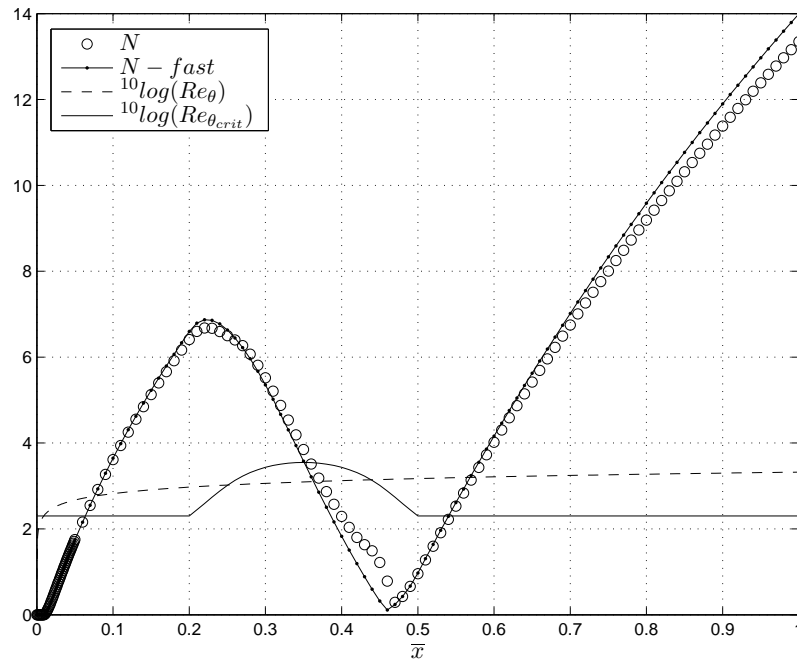
Figure 12.32: Flat plate with reduced H-region with $dH = .3$, $R_{c_{red}} = 10$, N, $N - fast$, $^{10}log(Re_\theta)$ and $^{10}log(Re_{\theta_{crit}})$ vs $\overline{x}$
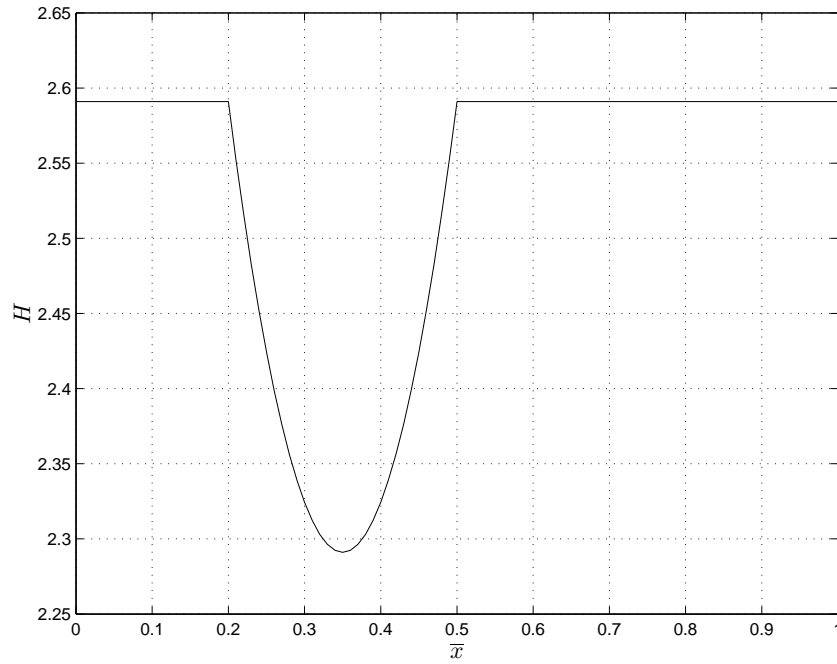
Figure 12.33: Flat plate with reduced H-region with $dH = .3$, $R_{c_{red}} = 10$, H vs $\overline{x}$
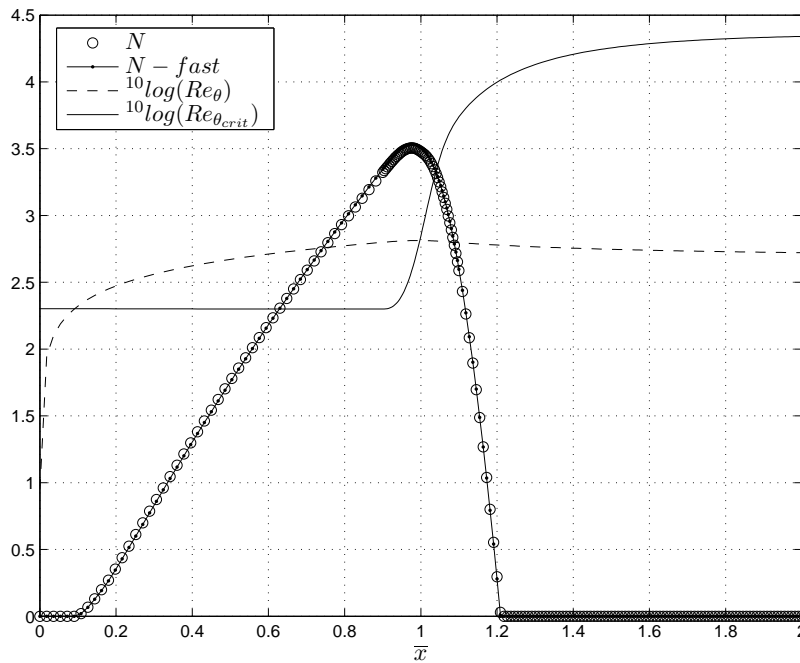
Figure 12.34: Rheinboldt's flat plate with discontinuous suction, N, $N - fast$, $^{10}log(Re_{\theta})$ and $^{10}log(Re_{\theta_{crit}})$ vs $\overline{x}$
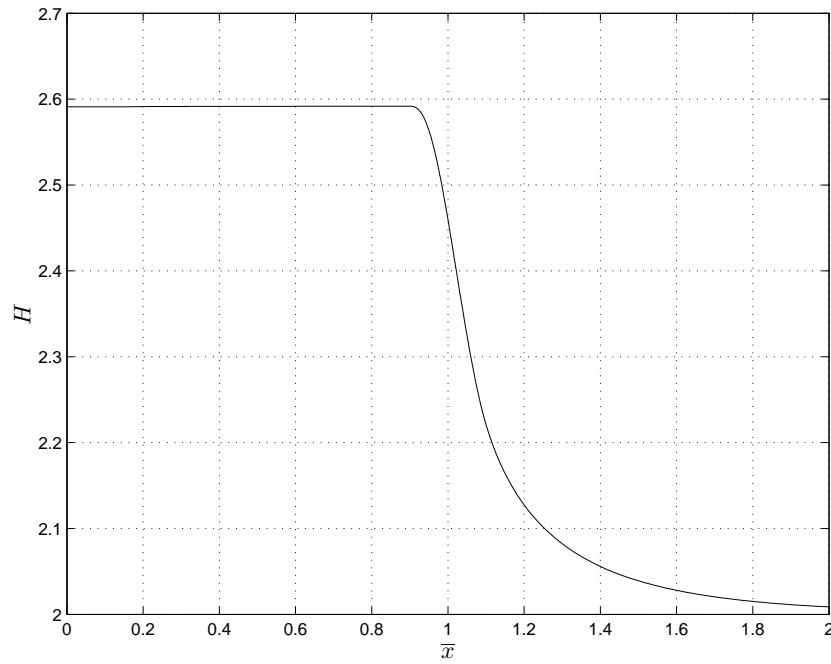
Figure 12.35: Rheinboldt's flat plate with discontinuous suction, H vs $\overline{x}$
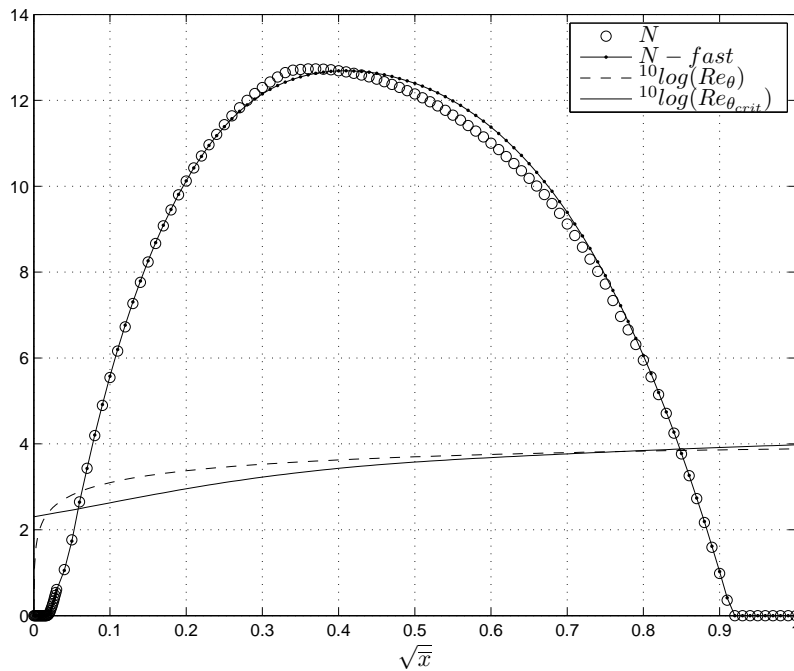
Figure 12.36: Iglisch flat plate with constant suction ($c_{q_{red}}$=.5, N, $N-fast$, $^{10}log(Re_{\theta})$ and $^{10}log(Re_{\theta_{crit}})$ vs $\sqrt{\overline{x}}$)
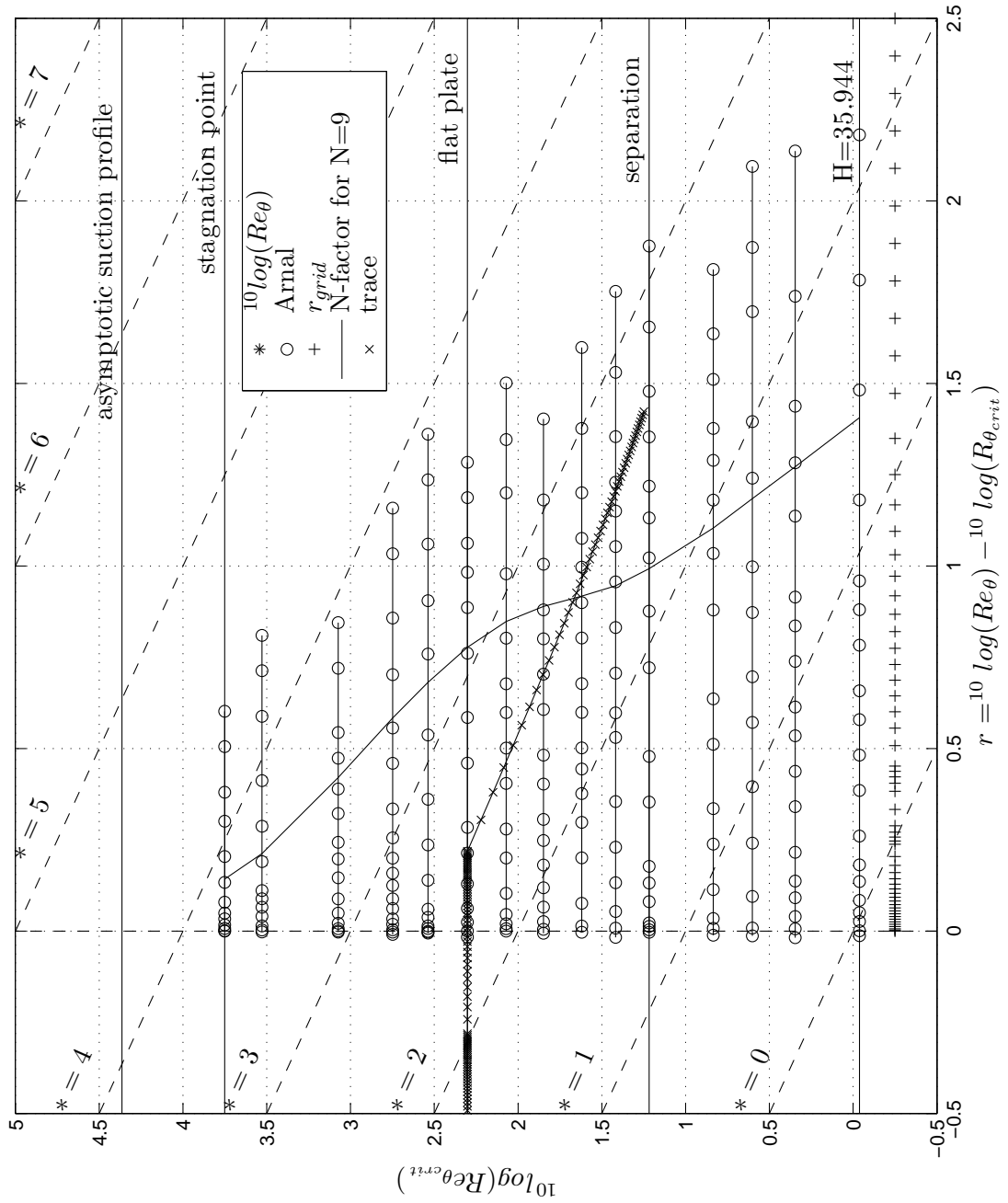
Figure 12.37: Trace in the roadmap for the simulated rooftop airfoil, $H_{end} = 3.9$, $R_{c_{red}} = .5$
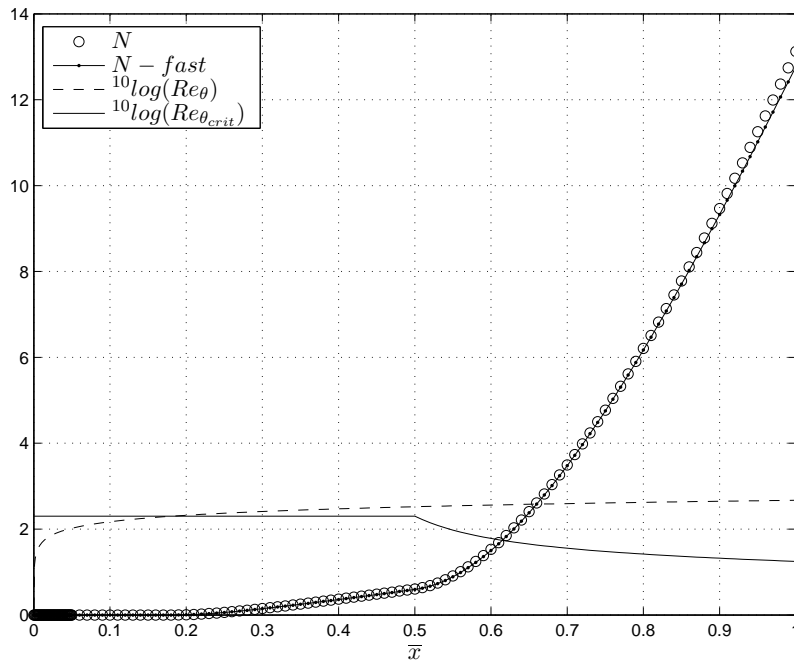
Figure 12.38: Simulated rooftop airfoil, $H_{end} = 3.9$, $R_{c_{red}} = .5$, N, $N - fast$, $^{10}log(Re_\theta)$ and $^{10}log(Re_{\theta_{crit}})$ vs $\overline{x}$
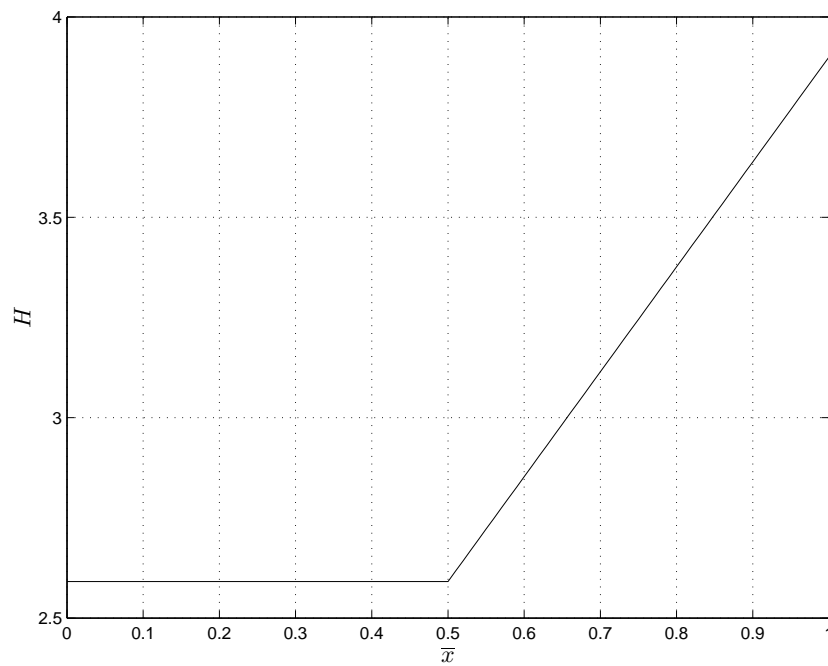
Figure 12.39: Simulated rooftop airfoil, $H_{end} = 3.9$, $R_{c_{red}} = .5$, H vs $\overline{x}$

Chapter 13

Reviewing the database method using the MATLAB program "N_factor_show"

In preceding chapters we already referred several times to the MATLAB program `N_factor_show.m`. In the present chapter we present the listing of this program to illustrate its options. In addition the MATLAB "help" information is listed for all programs (see also appendix B). For further information the reader is referred to the comment lines in the programs. No attempt has been made to optimise the MATLAB programs. For routine (design) applications you may use an optimising (e.g. C-) compiler to speed up the computation. Here we assume the laminar boundary layer to be known from a separate calculation. We have predefined some typical cases; you can easily add your own case. Practical applications inserted into XFOIL can be found in the Masters thesis by J. Bongers (Bongers, 2006, 🗐).

```
% N_factor_show.m  (CD-ROM version)
% This m-file calls on a number of other m-files as an additional illustration
% of the text and figures in the report:"A new e^N database method for transition
% prediction"
% Programs and report are on the CD-ROM
% "N-factor show" is discussed in more detail in chapter 13 of the report.
clear
close all
% ----------------------------------------------------------
want_to_go_on=input('if you want to go on give 1 else 0')
% ----------------------------------------------------------
while want_to_go_on==1
disp ('---------------------------------------------------------------------- ')
disp (' You can review a number of MATLAB programs as described in the text.  ')
disp (' The at present available options are:                                 ')
disp (' 1 =Compare Hartree profiles with and without suction/blowing          ')
disp (' 2 =Compare the data base results to the original Arnal data           ')
disp (' 3 =Principles of stability diagrams                                   ')
```

```
disp (' 4 =Review various splines                                     ')
disp (' 5 =Review Tbar (=T/TMaxMax along axis)                        ')
disp (' 6 =Review scaling                                             ')
disp (' 7 =Plot and compare stability diagrams in various formats     ')
disp ('    (classical and scaled/shifted)                             ')
disp (' 8 =Plot stability diagrams in the log(F) format               ')
disp (' 9 =Make stability diagram for arbitrary icase (especially 2:6) from ')
disp ('    icase=1 (stagnation point)using the similarity of the      ')
disp ('    shifted and scaled diagrams; especially relevant for profiles ')
disp ('    without inflexion point (icase<=6)                         ')
disp ('10 =Compose the stability diagram for the asymptotic suction profile ')
disp ('    using the similarity shown in case 9                       ')
disp ('11 =Make a stability diagram for an arbitrary value of H       ')
disp ('12 =Make a plot of the roadmap                                 ')
disp ('13 =Calculate N using "amplification.m" for a number of cases  ')
disp ('14 =You can do the same with the reduced version of nr 13 "ampli" ')
disp ('15 =See support for the choice of H as representative parameter ')
disp ('----------------------------------------------------------------------')
% ----------------------------------------------------------------------------
case_number=input('give the number of your choice                     ')
% ----------------------------------------------------------------------------
switch case_number
   case 1
      comp_Hartree_suc_nosuc
   case 2
      comp_data_base_to_Arnal
   case 3
      principles_of_stab_diagr
   case 4
      review_splines
   case 5
      review_Tbar
   case 6
      review_scaling
   case 7
      plot_stability_diagrams
   case 8
      logF_stability_diagrams
   case 9
      make_icase_from_1
   case 10
      make_asuc_diagram
   case 11
      make_diagram_for_H
   case 12
      load datafile_for_n_factor
      plot_roadmap
   case 13
      amplification
   case 14
      ampli
   case 15
      Hartree_zpg_pg
   otherwise
      disp('no valid case entered')
   end   % switch_case
   % ----------------------------------------------------------------
```

```
    want_to_go_on=input('if you want to go on give 1 else 0        ')
    % ------------------------------------------------------------
end    % while
keyboard
close all
```

1. **comp_Hartree_suc_nosuc.m** We have earlier calculated 23 Hartree velocity profiles for a flat plate with various amounts of suction and blowing.(See table 4.1 in the report). The data in the table are stored in the data file "Hartreetablezpg" Note that number 1 is for very strong suction; this boundary layer approaches the asymptotic suction profile (H=2) We now find a corresponding Hartree velocity profile with pressure gradient and no suction or blowing. This comparison profile is generated by the function "find_Hartree". The comparison can be made for equal ℓ, m_T or H. We exclude certain numbers from the table because these are outside the interesting range of H-values for attached Hartree flows. Results for Hartree velocity profiles without suction or blowing follow from the data file "Hartree_splines" Lin's approximate method is used to calculate the critical Reynolds number for the given and comparison profiles.

2. **comp_data_base_to_Arnal.m** This m-file asks to input a series of icase values and for each of the icase values a series of cross sections. At each cross section the Arnal values are compared with the data base. The user can just view the result or may choose to stop and print the figure

3. **principles_of_stab_diagr.m** This m-file generates stability diagrams in the classical form for selected cases. namely: icase=1 ($\beta = 1$); icase=6 ($\beta = 0$) and icase=11 ($\beta = -.198838$ that is separation) For the profile with an inflexion point(icase=11) the influence of Rayleigh instability shows up at the higher Reynolds numbers.

4. **review_splines.m** This m-file lets you review the various splines. You may choose to pause to view the figures or to stop and return to keyboard to print a figure.

5. **review_Tbar.m** This m-file asks for a series of icase values. First for each icase a plot is made of $\frac{T_{max}}{T_{maxmax}}$ along the axis according to Arnal. The result is compared to the analytical expression $\overline{T} = \overline{r}e^{(1-\overline{r})}$ where $\overline{r} = \frac{r}{r_{top}}$. Note that the plot is still vs r Then the results are plotted versus $\overline{r}$. On request the program will stop to allow printing a figure.

6. **review_scaling.m** This m-file shows the scalings and shiftings applied to the Arnal data to make the Tss splines for the data base

7. **plot_stability_diagrams.m** This m-file generates stability diagrams to compare the database results to the Arnal data. Note the great similarity for the scaled and shifted diagrams when icase=1:6 For these cases the velocity profiles do not have an inflexion point. For profiles with an inflexion point, that is icase > 6 the influence of Rayleigh instability starts to show up; first at the higher Reynolds numbers. We will later use the observed similarity to extrapolate to $H = 2$ (asymptotic suction profile)

8. **logF_stability_diagrams.m** This m-file generates stability diagrams in the form where frequencies are plotted as $^{10}log(F)$ where $F = \frac{\omega\nu}{U^2}$ This form is better suited for extrapolations to higher Reynolds numbers For profiles with an inflexion point (icase > 6) the

influence of Rayleigh instability starts to show up; first at the higher Reynolds numbers. When Rayleigh instability occurs the slope=-1 for the upper branch and for the axis. Note that this form can not be used for the lower branch at the higher Reynolds numbers for icase > 6 because here $\omega < 0$ and $^{10}log(F)$ becomes complex. Also small irregularities near $\omega = 0$ tend to be exaggerated when using the log scale; we accept these irregularities; they seem to be harmless. You can specify a series of values for icase to be viewed. An option is to superimpose the various scaled diagrams to better show their similarity.

9. **make_icase_from_1.m** This m-file composes the stability diagram for an arbitrary icase ($2 \leq$ icase ≤ 6) from the diagram for icase=1 (stagnation point). It is assumed that the scaled and shifted diagrams are equal for both cases.This only applies to icase=1:6 because these are all without inflexion point. For icase= 7:15 there is an inflexion point and the result is not useful. By de-scaling and de-shifting with the scales for the chosen icase,we find the diagram The results of this program suggested the making of the asymptotic suction diagram.

10. **make_asuc_diagram.m** This m-file is based on the results of `make_icase_from_1.m` It is now assumed that the scaled and shifted diagram for the asymptotic suction profile is also equal to that for the Hartree stagnation point profile. By de-scaling and de-shifting with the extrapolated values (using the appropriate splines)we find the diagram.

11. **make_diagram_for_H.m** plots a stability diagram for arbitrary H using the database

12. **plot_roadmap.m** is used to trace the path of a boundary layer in the $^{10}log(Re_{\theta_{crit}})$ vs r path where $r =^{10} log(Re_\theta) -^{10} log(Re_{\theta_{crit}})$ For each Arnal case the points representing the cross sections through the stability diagram are shown by "o" on a horizontal straight line The program `Amplification` plots the boundary layer trace in this road map The various regions used in the function `cross_cut` are indicated in the road map Also values for $^{10}log(Re_\theta)$ are shown as straight lines

13. **Amplification.m** To calculate the N-factor for a given distribution of x, U, H and Re_θ. In this program we just calculate the N-factor. You may later introduce an "effective" turbulence level Tu to define the critical N-factor N_{crit} to stop the calculation and switch to turbulent flow. In that case you may want to do the N-factor calculation step by step together with the laminar boundary layer calculation; it should not be difficult to adjust the program to your needs. The present version of the program allows you to use either:

    (a) cross_cut

    (b) cross_cut_fast

    (c) both versions in parallel

14. **Ampli.m** This is a companion program to amplification.m. The present version of the program allows you to use either:

    (a) cross_cut

    (b) cross_cut_fast

Also the detailed plots at each x-station that were provided in amplification have been removed in the present version. Therefore it is advised that, when you experience problems with ampli.m you rerun the case with amplification.m.

15. **Hartree_zpg_pg.m** M-file to find the values of "el", m_T and H for a Hartree profile with pressure gradient (but without suction/blowing) with the same vale of "el", m_T or H as for the flat plate with suction/blowing. The results of this program give support to some conclusions made in chapter 4 of the report.

Appendix A

The MATLAB 5 spline format and its transformation to other systems

Note that all 885 T_{ss} splines in the MATLAB 5 format have a constant part that contains the identification numbers, the number of polynomials, the standard series of breakpoints in $\overline{\omega}$, etc. (for details see below). This constant part could have been stored only once and after the interpolation been added again. We refrained from this and did not try to save some storage space in order to keep the programming simple. It has to be observed that due to using the MATLAB 5 student version the maximum allowable array size is 16384 elements while all Tss splines together contain 150450 elements.. Therefore we have used cell arrays to store the T_{ss} splines. Another subject of attention is that later versions of MATLAB than the one we used or other programming languages may use different spline formats. Therefore we describe below a procedure to extract from our splines the original data so that users can redefine the splines in their own preferred format.

In MATLAB 5 a so-called pp-form of the spline is used which contains all data in a single vector. Although also a MATLAB procedure is available to de-compose this vector in its various elements we will make our further description independent of MATLAB. For a cubic spline over N intervals we have N third degree polynomials and $N+1$ breakpoints. The first two numbers in the pp-vector are "1" and "10" which are used by MATLAB 5 to recognise the vector as a spline representation. Each polynomial is of the form

$$y = ax^3 + bx^2 + cx + d \tag{A.1}$$

where x is taken zero at the start of the interval. The pp-vector then is composed as follows:

- 10 (constant integer(!) identification number).

- 1 (constant integer(!) identification number).

- N = number of polynomials.

- All x-values of the $(N + 1)$ breakpoints.

- 4 = number of coefficients for a third degree polynomial.

- All (N) coefficients a

- All (N) coefficients b

- All (N) coefficients c

- All (N) coefficients d

In total then we have 5 $N+5$ elements in the vector. The values for y at the first N breakpoints follow from the d coefficients; the value for y at the last breakpoint follows from the last values for a, b, c and d and equation (A.1). For all T_{ss} points we used the same series of 34 breakpoints in $\overline{\omega}$ (see equation (6.6)) given below:

$\overline{\omega}$ = -2.0000 -1.8000 -1.6000 -1.4000 -1.2000 -1.0000 -0.8000 -0.6000 -0.4000 -0.2000 -0.1600 -0.1200 -0.0800 -0.0400 0 0.0400 0.0800 0.1200 0.1600 0.2000 0.4000 0.6000 0.8000 1.0000 1.2000 1.4000 1.6000 1.8000 2.0000 2.2000 2.4000 2.6000 2.8000 3.0000

For the Tss splines we have N=33 and hence the length of the vector is 170. The spline format is illustrated in table A.1 for $T_{ss}(6, 8)$, that is the spline for icase=6 and the r_{grid} point 8.

MATLAB users who have advanced to version 7 already should note that this version does still recognise and accept the MATLAB 5 spline format, hence a translation is not yet necessary. The author will try to follow future developments of MATLAB and will report possible changes on the website that was mentioned at the end of the Preface.

Table A.1: Example of a T_{ss} spline, namely $T_{ss}(6,8)$=spline for icase = 6 at r_{grid} point number 8

Element number	content
1	10 = identification
2	1 = identification
3	33 = number of polynomials
4-37	34 breakpoints, namely
	-2.0000 -1.8000 -1.6000 -1.4000 -1.2000 -1.0000 -0.8000 -0.6000
	-0.4000 -0.2000 -0.1600 -0.1200 -0.0800 -0.0400 0.0000 0.0400
	0.0800 0.1200 0.1600 0.2000 0.4000 0.6000 0.8000 1.0000
	1.2000 1.4000 1.6000 1.8000 2.0000 2.2000 2.4000 2.6000
	2.8000 3.0000
38	4 = 4 coefficients per polynomial
39-71	The 33 coefficients (a); note that the first and the last one are
	and should be zero to make the tail of the spline straight
	0.0000 -0.0025 0.0125 -0.0498 0.2313 -1.8893 -0.0182 0.0707
	-0.0462 -0.6001 -0.1527 0.1090 0.2125 0.3099 -0.2139 -0.3895
	-0.2914 -0.0376 1.2279 -0.7687 -0.0677 2.6784 -0.8262 0.8618
	-0.2869 0.0828 -0.0211 0.0055 -0.0019 0.0008 -0.0003 0.0001
	0.0000
72-104	33 coefficients (b) ; again the first and last one=0
	0.0000 0.0000 -0.0015 0.0060 -0.0239 0.1149 -1.0186 -1.0295
	-0.9871 -1.0148 -1.0868 -1.1052 -1.0921 -1.0666 -1.0294 -1.0551
	-1.1018 -1.1368 -1.1413 -0.9940 -1.4552 -1.4958 0.1112 -0.3845
	0.1326 -0.0396 0.0101 -0.0025 0.0008 -0.0003 0.0001 -0.0001
	0.0000
105-137	33 coefficients (c)
	1.8088 1.8089 1.8086 1.8095 1.8059 1.8241 1.6434 1.2338
	0.8304 0.4301 0.3460 0.2583 0.1704 0.0841 0.0002 -0.0831
	-0.1694 -0.2590 -0.3501 -0.4355 -0.9253 -1.5155 -1.7924 -1.8471
	-1.8975 -1.8789 -1.8847 -1.8832 -1.8836 -1.8835 -1.8835 -1.8835
	-1.8835
138-170	33 coefficients (d)
	-2.8266 -2.4648 -2.1030 -1.7413 -1.3795 -1.0174 -0.6631 -0.3753
	-0.1692 -0.0430 -0.0274 -0.0153 -0.0068 -0.0017 0.0000 -0.0017
	-0.0067 -0.0152 -0.0274 -0.0432 -0.1762 -0.4200 -0.7615 -1.1222
	-1.5001 -1.8765 -2.2532 -2.6299 -3.0066 -3.3833 -3.7600 -4.1367
	-4.5134

Note that the numbers above are given in the "short" format but that in storage the full MATLAB number of digits is available of course. In the function `cross_cut` the interpolation is performed on the complete pp-vectors . After that it has to be made sure that the integers have retained the classification "integers" and that the straight tails of the spline are maintained. For that we use the function `rectify_Tss.m` that is reprinted below. The comment lines explain its working.

function pp_out=rectify_Tss(pp_in)

```
function pp_out=rectify_Tss(pp_in)
% function to rectify the Tss spline after interpolation.
% It is called with pp_in=the Tss spline obtained from the  interpolation
% in cross_cut.m.
% Note that the function can only be applied to the spline format of Tss
% -----------------------------------------------------------------------
 h=.2; h2=h*h;                   % the first and last interval have length .2
% -----------------------------------------------------------------------
% The coefficients for the first interval are:
a=pp_in(39);
b=pp_in(72);
c=pp_in(105);
% d=pp_in(138)does not change; c is corrected to make sure that
% after putting a=0 and b=0 the y-value at the end of  the interval is kept equal
c=a*h2+b*h+c; % This is the corrected c
% now input the corrected a, b and c into pp
pp_out=pp_in;
pp_out(39)=0;
pp_out(72)=0;
pp_out(105)=c;
% Now we do the same for the last interval
a=pp_in(71);
b=pp_in(104);
c=pp_in(137);
% d=pp_in(170)does not change;
c=a*h2+b*h+c;
pp_out( 71)=0;
pp_out(104)=0;
pp_out(137)=c;
% Now we restore the integers
pp_out(1)=10;
pp_out(2)=1;
pp_out(3)=33;
pp_out(38)=4;
% end of function rectify_Tss
```

Arbitrary MATLAB 5 splines can easily be tranferred into other formats by extracting the original x and y values using the function `[x_out, y_out]=extract_from_spline(pp_in)` as listed below:

```
function [x_out,y_out]=extract_from_spline(pp_in)
% This function extracts the original x and y data from an
% arbitrary cubic spline in MATLAB 5 format
% The function does not use specific MATLAB spline commands
% Therefore it is easy to derive a new spline in any other format
N=round(length(pp_in)/5-1);
x_out=pp_in(4:N+4);
% find length and polynomial coefficients for last interval
h=pp_in(N+4)-pp_in(N+3);
a=pp_in(2*N+5);
```

```
b=pp_in(3*N+5);
c=pp_in(4*N+5);
d=pp_in(5*N+5);
last_y=a*h^3+b*h^2+c*h+d;
y_out=[pp_in(4*N+6:5*N+5) last_y];
```

Appendix B

Overview of MATLAB m-files

This appendix gives an overview of the various Matlab m-files discussed in the report. All programs are available on the CD-ROM. Below we print the first lines of each file; the text is in general equal to what you get when typing "help filename" in the MATLAB Command Window.

These programs have been developed during various sessions over a prolonged period. In hindsight the author noted that some of them could have been more efficient and clear. If need arises improved versions may be made available on the website that is mentioned on the CD-ROM. Questions and reports on errors from users will be highly appreciated.

Amplification

To calculate the N-factor for a given distribution of x, U, H and R_θ. In this program we just calculate the N-factor. You may later introduce an "effective turbulence level" Tu to define the critical N-factor (N_{crit}) to stop the calculation and switch to turbulent flow. In that case you may want to do the N-factor calculation step by step together with the laminar boundary layer calculation; it should not be difficult to adjust the program to your needs. We have predefined some typical cases; you can easily add your own case. Here we assume the laminar boundary layer to be known from a preceding calculation. After having built up experience with this program you may want to reduce the range of frequencies, and/or the number of frequencies within that range, to be used. At present this range is rather wide to accommodate applications in the upper right-hand corner of the roadmap area. Please observe the used frequencies in the detailed plots (figures 2 and 3). As soon as edge maxima for the n-factor as function of frequency occur you need to adjust the frequency range. We will denote the amplification factor as function of the frequency by n and the maximum amplification factor as function of x by N. For further explanations see chapter 12 of the report. Practical applications inserted into XFOIL can be found in the Masters thesis of J. Bongers (see report on the CD-ROM). No attempt has been made to optimise the MATLAB program. For routine (design) applications you may use an optimising (e.g. C-) compiler to

speed up the computation. The present version of the program allows you to use either:

1. cross_cut

2. cross_cut_fast

3. both versions in parallel

At each x-station detailed plots of $T \cdot U$ vs frequency and n-factor vs frequency are provided on request. Also the trace of the boundary layer in a "roadmap" and the growth of N with x may be followed. A companion program "ampli" lets you run either cross_cut or cross_cut_fast without the detailed plots.

Ampli

Companion program to amplification.m (see that m-file for explanation). The present version of the program allows you to use either:

1. cross_cut

2. cross_cut_fast

Also the detailed plots at each x-station that were provided in amplification have been removed in the present version. Therefore it is advised that when you experience problems with ampli you rerun the case with the extensive version.

Arnal_table_01 through Arnal_table_15

The lay-out of all these files is the same as for Arnal_table_01

Arnal_table_01

Arnal table for $icase = 1$ ($H = 2.216$) The tables were scanned from Arnal's publication as described in the report. Note that from the array t3 we only used the data in columns 2 and 3. Therefore only these data were checked for scanning errors! Column 5 is equal to $\frac{column3}{Re_{\delta*}}$. While reducing the tables to the final T_{ss} splines the Arnal tables were run through several programs. Each time with a different program for the actual step in the reduction process. For our analysis we inserted m-files at various places to perform the calculations that were needed in that step of our analysis

comp_data_base_to_Arnal

This m-file asks to input a series of *icase* values. At each cross section the Arnal values are compared with the T_{ss} data base using "cross_cut". Also a comparison is made with the parabolic fast approximation. by using "cross_cut_fast" The user can just view the result or may choose to stop and print the plot.

comp_Hartree_suc_nosuc

We have earlier calculated 23 Hartree velocity profiles for a flat plate with various amounts of suction and blowing. Results are in "results" in "Hartreetablezpg" See also table 4.1 in the report. Note that number 1 is for very strong suction; this boundary layer approaches the asymptotic suction profile ($H = 2$). We now find a corresponding Hartree velocity profile with pressure gradient and no suction or blowing. The comparison can be made for equal l, m_T or H; the restrictions mentioned in the m-file should be observed. Otherwise an error message may result. See chapter 4 of the report for details. Results for Hartree velocity profiles without suction or blowing follow from the function "find_Hartree"

cross_cut

Function to find the cross section in T_{ss} form of the stability diagram for arbitrary values of H (and hence of $R_{\theta_{crit}}$) and Re_{θ}. The m-file interpolates in a dataset that was derived from Arnal's tables by scaling and shifting in such a way that interpolation becomes easy and accurate. See chapters 6 and 10 of the report. The value of $^{10}log(Re_{\theta_{crit}})$ is found from a spline in $^{10}log(H)$. In this way T can be determined for a series of frequencies at a certain x-station. Repeating this procedure at a number of x-stations allows to compute the n-factor for each frequency. At each x-station the maximum n-factor gives N. A trace of the stability characteristics of the boundary layer can be plotted in a "road map" by the calling program. Sometimes the trace leaves the region covered by the Arnal data. It is advised to check this roadmap to keep an eye on the credibility of the extrapolated stability data. The roadmap shows a curve for N-factor=9 for the Hartree-Stewartson similar flows. These flows trace horizontal lines in the road map. Observe that the curve for $N = 9$ is not necessarily valid for non-similar flows. Make sure that in the main program the necessary stability data were loaded by executing "load datafile_for_n_factor" Re_{θ} should be given as a value for "Rt" in the calling program. Also the value of the shape factor H should be provided. The global statement may contain more variables then are really needed for the present function because we kept the globals the same for most m-files.

cross_cut_fast

Function to find the cross section in parabolic form of the stability diagram for arbitrary values of H (and hence of $R_{\theta_{crit}}$) and Re_θ. See chapter 11 of the report. The value of ${}^{10}log(Re_{\theta_{crit}})$ is found from coefs for a spline in ${}^{10}log(H)$. In this way T can be determined for a series of frequencies at a certain x-station in the calling program. Repeating this procedure at a number of x-stations allows to compute the n-factor for each frequency. At each x-station the maximum n-factor gives N. A trace of the stability characteristics of the boundary layer can be plotted in a "road map" by the calling program. Sometimes the trace leaves the region covered by the Arnal data. It is advised to check this roadmap to keep an eye on the credibility of the extrapolated stability data. The roadmap shows a curve for N-factor=9 for the Hartree-Stewartson similar flows. These flows trace horizontal lines in the road map. Observe that the curve for $N = 9$ is not necessarily valid for non-similar flows. Make sure that in the main program the necessary stability data were loaded by executing "load datafile_for_n_factor". Re_θ should be given as a value for "Rt" in the main program. Also the value of the shape factor H should be provided. The global statement may contain more variables then are really needed for the present function because we kept the global statement the same for a number of m-files.

extract_from_spline

This function extracts the original x and y data from an arbitrary cubic spline in MATLAB 5 format. The function does not use specific MATLAB spline commands. Therefore it is easy to derive a new spline in any other format.

find_Hartree

Find_Hartree determines the (attached) Hartree velocity profile for given values of beta, eta-max, bign and f'(0). These values should be taken from pre-calculated splines or tables so that no shooting process is required.

Hartree_zpg_pg

The Hartree_zpg_pg.m M-file finds 'the values of "el", m_T and H for a Hartree profile with pressure gradient (but without suction/blowing) with the same vale of "el", m_T or H as for the flat plate with suction/ blowing. The results of this program give support to some conclusions made in chapter 4 of the report. We will be using two datafiles namely Hartreetablezpg and Hartree_pg. Hartreetablezpg contains the results for the flat plate with suction/blowing. See chapter 4 of the report. Hartree_pg contains the values of beta and $f''(0)$ for the comparison profiles for equal "el", m_T or H.

lagrange

```
function p=lagrange(x)
x=[x1 x2 x3 xi]
The function lagrange determines the quadratic interpolation coefficients p for 3 points
(x1,y1), (x2,y2) and  (x3,y3); the points need not be equally spaced
The result y4 at xi is y4=p1*y1+p2*y2+p3*y3
```

lagrange_2d

lagrange_2d calculates the factors for quadratic interpolation in a set of 3 x-values for 3 different y-values. x and y come from a call in cross_cut where x stands for r and y for $^{10}log(Re_{\theta_{crit}})$.

logF_stability_diagrams

This m-file generates stability diagrams in the form where frequencies are plotted as $^{10}log(F)$, where $F = \frac{\omega \cdot \nu}{U^2}$ This form is better suited for extrapolations to higher Reynolds numbers. For profiles with an inflexion point ($icase > 6$) the influence of Rayleigh instability starts to show up; first at the higher Reynolds numbers. Rayleigh instability shows a slope=-1 for the upper branch and for the axis. Note that this form can not be used for the lower branch at the higher Reynolds numbers for $icase > 6$ because here $omega < 0$ and $log(F)$ becomes complex. Also small irregularities near $\omega = 0$ tend to be exaggerated when using the log scale; we accept these irregularities; because they seem to be harmless. You can specify a series of values for icase to be viewed. For the horizontal axis we use $r = ^{10}log(Re_{\theta}) - ^{10}log(Re_{\theta_{crit}})$.

make_asuc_diagram

This m-file is based on the results of "make_icase_from_1.m" It is now assumed that the scaled and shifted diagram for the asymptotic suction profile is equal to that for the Hartree stagnation point profile. By de-scaling and de-shifting with the extrapolated values (using the appropriate splines)we find the diagram.

make_diagram_for_H

make_diagram_for_H.m plots a stability diagram in classical form for an arbitrary value of H using the database.

make_icase_from_1

This m-file composes the stability diagram for an arbitrary *icase* from the diagram for *icase* = 1 (stagnation point). It is assumed that the scaled and shifted diagrams are equal for both cases. This is a very good approximation for icase=1:6, because these are all profiles without inflexion points. For *icase* = 7 : 15 there is an inflexion point and the approximation is less good. By de-scaling and de-shifting with the scales for the chosen icase, we find the diagram The results of this program suggested the making of the asymptotic suction diagram by "make_asuc_diagram.m". There you may also find some additional information.

make_table_for_H

This program generates stability data in tables for arbitrary values of H and Reynolds number. Results may be presented in terms of δ^* or θ. When using δ^* a comparison with the Arnal tables is easy. The program uses the m-file function cross_cut.m $H = 2$ generates results for the asymptotic suction profile as presented in chapter 9 of the report.

N_factor_show

This m-file calls on a number of other m-files as an additional illustration of the text and figures in the report:" A new e^N database method for transition prediction" Programs and report are on the CD-ROM "N-factor show" is discussed in more detail in chapter 13 of the report.

plot_roadmap

plot_roadmap.m is used to trace the path of a boundary layer in the $^{10}log(Re_{\theta_{crit}})$ vs r plane, where $r = ^{10} log(Re_\theta) - ^{10} log(Re_{\theta_{crit}})$. For each Arnal case the points representing the cross sections through the stability diagram are shown by "o" on a horizontal line. The programs "Amplification" and "ampli" plot the boundary layer trace in this road map Values for $^{10}log(Re_\theta)$ are shown as straight dotted lines. Also the r_{grid} is shown along top and bottom by +++++++. Note: in an external program "datafile_for_n_factor" should have been loaded In a separate program we calculated the values of r (rN9) at which the N-factor reaches the value 9 for the Hartree similar flows for which icase=constant and hence also H and $^{10}log(Re_{\theta_{crit}})$ are constant This $N = 9$ curve is not necessarily valid for non-similar boundary layers.

plot_stability_diagrams

This m-file generates stability diagrams to compare the database results to the Arnal data. Note the great similarity for the scaled and shifted diagrams when $icase = 1:6$. For these cases the velocity profiles do not have an inflexion point. For profiles with an inflexion point, that is $icase > 6$. the influence of Rayleigh instability starts to show up; first at the higher Reynolds numbers. At the lower Reynolds numbers there is still a reasonable similarity. We have used the observed similarity to extrapolate to $H = 2$ (asymptotic suction profile) and to make a fast version of cross_cut.

principles_of_stab_diagr

This m-file generates stability diagrams in the classical form for 3 selected cases namely: $icase = 1$ ($\beta = 1$); $icase = 6$ ($\beta = 0$) and $icase = 11$ ($\beta = -.198838$; that is separation) For the profile with an inflexion point ($icase = 11$) the influence of Rayleigh instability shows up at the higher Reynolds numbers. Although the program text is largely the same for the three cases, we just repeated these parts for ease of programming, because the location for the texts in the figures, titles, etc. are different.

rectify_Tss

function pp_out=rectify_Tss(pp_in)

Function to rectify the T_{ss} spline after interpolation. It is called with pp_in=the T_{ss} spline obtained from the interpolation in cross_cut.m.

review_scaling

This m-file shows the scalings and shiftings applied to the Arnal data to make the T_{ss} splines for the data base

review_splines

Shows the various splines for the Arnal data and in addition the data for the asymptotic suction profile that are known or extrapolated.

$$H = 2 \tag{B.1}$$

$$Re_{\delta^*_{crit}} = 46270 \tag{B.2}$$

(from Hughes and Reid (1965))

$$Re_{\theta_{crit}} = 23135 \tag{B.3}$$

$$MaxMaxT = .041 (extrapolated) \tag{B.4}$$

$$^{10}log(MaxMaxT) = -1.3872 \tag{B.5}$$

$$^{10}log(F_{top}) = -6.7507 (extrapolated) \tag{B.6}$$

Note that F_{top} is F at axis for the average top taken at $r_{grid}(27) = \frac{1}{3}$ With "log" we always mean ^{10}log.

review_Tbar

First for all 15 *icase* values a plot is made of $\frac{T}{TMaxMax}$ along the axis according to Arnal. The result is compared to the analytical expression $\overline{T} = \overline{r} \cdot e^{(1-\overline{r})}$ where $\overline{r} = \frac{r}{r_{top}}$. Note that all $\overline{T}$ vs r are very similar and very well represented by the simple analytical expression. The similarity is nearly perfect if we plot vs $\overline{r} = \frac{r}{r_{top}}$.

Appendix C

Overview of MATLAB data files

This appendix gives an overview of the various MATLAB data files used in the m-files that are listed in appendix B. All files are available on the CD-ROM. Some files may contain more data than used in the present report. These have been used by the author in other programs. When in the future a more detailed explanation of the files would be requested this may be provided on the web site that is mentioned on the CD-ROM.

Table C.1: datafile_for_n_factor

Name	Size	Bytes	Class
ArH	1x15	120	double array
ArMaxMaxT	1x15	120	double array
ArNumberofReynolds	1x15	120	double array
ArRdstarcrit	1x15	120	double array
ArRtcrit	1x15	120	double array
ArTbar	15x19	2280	double array
Arbeta	1x15	120	double array
Ardomega	1x17	136	double array
ArlogFax	15x19	2280	double array
ArlogH	1x15	120	double array
ArlogRtcrit	1x15	120	double array
Arr	15x19	2280	double array
Arrtop	1x15	120	double array
Arscomega	1x15	120	double array
T_Arnal	15x19	69524	cell array
Tbar	15x59	7080	double array
Tss	15x59	1285020	cell array
coefs_log_Ftop	300x4	9600	double array
coefs_log_MaxMaxT	300x4	9600	double array
coefs_logcrit_vs_logH	300x4	9600	double array
coefs_rtop	300x4	9600	double array
coefs_scale	300x4	9600	double array
coefs_slope_left	300x4	9600	double array
domega_saved	1x34	272	double array
logF_neutral_high	15x19	2280	double array
logF_neutral_low	15x19	2280	double array
logFax	15x59	7080	double array
logH_vs_logcrit_spline	1x500	4000	double array
logMaxMaxT_vs_logcrit_spline	1x100	800	double array
log_Ftop_spline	1x135	1080	double array
logcrit_vs_logH_spline	1x85	680	double array
neutr_Tss_high	15x59	7080	double array
neutr_Tss_low	15x59	7080	double array
ome_ax	15x19	2280	double array
ome_neutral_high	15x19	2280	double array

Table C.2: Hartree_pg

Name	Size	Bytes	Class
fsk_beta	23x3	552	double array
fsk_fpp0	23x3	552	double array

Table C.3: Hartreetablezpg

Name	Size	Bytes	Class
arbighzpg	1x23	184	double array
ardstarzpg	1x23	184	double array
arelzpg	1x23	184	double array
aretamaxzpg	1x23	184	double array
arf0zpg	1x23	184	double array
arfpp0zpg	1x23	184	double array
armTzpg	1x23	184	double array
arthetazpg	1x23	184	double array
results	23x6	1104	double array

Table C.4: results_Iglisch_501_10

Name	Size	Bytes	Class
H_plot	1x127	1016	double array
Iglischtable	18x5	720	double array
N_factor_array_Iglisch	15x127	15240	double array
bigh	1x144	1152	double array
rootx	1x144	1152	double array
rootx_plot	1x127	1016	double array
tau	1x144	1152	double array
theta	1x144	1152	double array
theta_plot	1x127	1016	double array

Table C.5: results_PhD_case

Name	Size	Bytes	Class
Rc	1x1	8	double array
Rtetatemp	105x1	840	double array
Utemp	105x1	840	double array
bightemp	1x105	840	double array
stop_station	1x1	8	double array
xtemp	105x1	840	double array

Table C.6: results_Rheinb

Name	Size	Bytes	Class
N Rc	1x1	8	double array
Rcred	1x1	8	double array
Rteta	1x202	1616	double array
U	1x202	1616	double array
bigh	1x202	1616	double array
x	1x202	1616	double array

Bibliography

All pagenumbers in blue (in the electronic version of the report) are hyperlinks that will take you to the page on which the reference to the publication is mentioned. iii

D. Arnal. Diagrammes de stabilité des profils de couche limite auto-semblables, en ecoulement bidimensionnel incompressible, sans et avec courant de retour. Technical Report OA Nr. 34/5018, ONERA, 1986. iv, 1, 51

H. Blasius. Grenzschichten in Flušsigkeiten mit kleiner Reibung. *Z. Angew. Math. Phys.*, vol.56, 1908. 19, 21

L.M.M. Boermans. The airfoils designed by Boermans are only published in confidential internal reports (and therefore not publicly available). The profiles designed by L.M.M. Boermans are present in high performance gliders such as the: ASW-24, ASH-25, ASH-26, ASW-27, ASW-28, ASG-29, Ventus-2B, DG-800, Antares, Concordia, and the motorplanes: Extra 400, Extra 500, Euro-Enair Eaglet and the Impuls. Some more information on the work of Boermans is mentioned in van Ingen (2008). iii

J. Bongers. Implementation of a new transition prediction method in xfoil. Master's thesis, Delft University of Technology, 2006. iv, 109, 139

M. Drela. XFOIL, An Analysis and Design System for Low Reynolds Number Airfoils. Technical report, University of Notre Dame, 1989. 16

V.M. Falkner and S.W. Skan. Some approximate solutions of the boundary-layer equations. *A.R.C., R and M 1314*, 1930. See also Solutions of the boundary-layer equations, Phil. Mag. 7, 12 p. 865-896 (1931). 19

S. Goldstein. On laminar boundary-layer flow near a position of separation. *Quart. J. Mech.*, 1:43–69, 1948. 21

H. Görtler. A new series for the calculation of steady laminar boundary layer flows. *J. Math. Mech.*, vol.6, 1957. 21, 23

D. R. Hartree. On an equation occuring in Falkner and Skan's approximate treatment of the equations of the boundary layer. *Proc. Camb. phil. Soc.*, vol.19, 1937. 19

K. Hiemenz. Die Grenzschicht an einem in den gleichförmigen Flüssigkeitsstrom eingetauchten geraden Kreiszylinder. *Dingl. Polytech. J. 326, 32*, 1911. 19

L. Howarth. On the solution of the laminar boundary layer equations. *Proc. Roy. Soc. A.*, 164:547–579, 1938. 21

T.H. Hughes and W.H. Reid. On the Stability of the Asymptotic Suction Boundary Layer Profile. *J. Fluid Mech.*, 23:715–735, 1965. xvii, 20, 26, 51, 87, 158

R. Iglish. Exakte Berechnung der laminaren Grenzschicht an der längsangeströmten ebener Platte mit homogener Absaugung. *Schr. dtsch. Akad. Luftfahrtf. 8B pl-51*, 1944. See also N.A.C.A. T.M. 1205 (1949). 16, 121

D.C. Leigh. The laminar boundary-layer equation: a method of solution by means of an automatic computer. *Proc. Camb. Phil. Soc.*, 51:320–332, 1955. 21

L.M.M. Mack. Aerodynamic analysis requiring advanced computers,paper nr 4. Technical Report SP-347, NASA, 1975. 10

L.M.M. Mack. Transition prediction and linear stability theory, paper 1. Technical Report 1, AGARD, 1977. 10

L.M.M. Mack. Rand corporation transition workshop ii. Technical report, Rand Corporation, 1978. 10

L.M.M. Mack. Boundary layer stability theory: special course on stability and transition of laminar flow. Technical Report report 109, AGARD, 1984. Paris, France. 10

F.W. Meredith and A.A. Griffith. The possible improvement in aircraft performance due to boundary layer suction. Technical Report 2315, Rep. Aero. Res. Coun., 1936. 16

H.J. Obremski, M.V. Morkovin, M. Landahl, A.R. with contributions from Wazzan, T.T. Okamura, and A.M.O. Smith. A Portfolio of Stability Characteristics of Incompressible Boundary Layers. Technical Report AGARDOGRAPH no. 134, NATO, 1969. 10, 35

K. Pohlhausen. Zur näherungsweisen Integration der Differentialgleichung der laminaren Grenzschicht. *Z.A.M.M.*, 1:252–268, 1921. 21

L. Prandtl. Über Flüssigkeitsbewegung bei sehr kleiner Reibung. *Proc. Third Internat.Math. Cong. Heidelberg*, 1904. Translation published under NACATechnical Memo. 452. 19

J. Pretsch. Die Stabilität einer ebenen Laminarströmung bei Druckgefälle und Druckanstieg. *Jb. dtsch. Luftfahrtforsch.*, 1:158–175, 1941. 26

J. Pretsch. Die Anfachung instabilier Störungen in einer laminaren Reibungsschicht. *Jb. dtsch. Luftfahrtforsch.*, pages 154–171, 1942. 26

J. Pretsch. Berechnung der Stabilitäsgrenze von Grenzschichtprofilen und der Anfachung von Störungen. *Göttinger Mongraph.*, Part. 3.2, 1945. 26

W. Rheinboldt. Zur Berechnung stationärer Grenzschichten bei kontinuierlicher Absugung mit unstetig veränderlicher Absaugegeschwindigkeit. *J. Rat. Mach. Anal.*, 5:539–604, 1956. 119

L. Rosenhead. *Laminar Boundary Layers.* Oxford University Press, 1961. 16, 21, 31

H. Schlichting. *Grenzschichtteorie.* G. Braun-Verlag, 1978. 3, 13, 16, 17, 21, 22, 23

P.J. Schmid and D.S. Henningson. Stability and transition in shear flows. *Applied Mathematical Sciences*, 142, 2000. Springer. 3

A.M.O. Smith. Transition, Pressure Gradient and Stability Theory. *Proc. 9th Int. Con. of Appl. Mech.*, vol.4:234–244, 1956. iii

A.M.O. Smith and D.W. Clutter. Solution of the Incompressible Boundary Layer Equations. *AIAA J.*, 1:2062–2071, 1963. 21, 23

A.M.O. Smith and N. Gamberoni. Transition, Pressure Gradient and Stability Theory. Technical Report ES-26388, Douglas Aircraft Company, 1956. iii, 8

K. Stewartson. Further Solutions of the Falkner-Skan Equation. *Proc. Camb. Phil. Soc.*, 50: 454–465, 1954. 19, 21

H.W. Stock. On laminar boundary layers with blowing and suction. *Z. Flugwiss. Weltraumforsch.*, 4:93–100, 1980. 31

H.W. Stock and E. Degenhart. A simplified e^N method for transition prediction in two-dimensional incompressible boundary layers. *Z. Flugwiss. Weltraumforsch.*, 13:16–30, 1989. 31

I. Tani. On the solution of the laminar boundary layer equations. *Journ. Phys. Soc. Japan*, 4:149–154, 1949. 21

R.M. Terrill. Laminar boundary-layer flow near separation with and without suction. *Phil. Trans. A 253*, pages 55–100, 1960. 21, 42

A. Ulrich. Theoretische Untersuchungen über die Widerstandsersparnis durch Laminarhaltung mit Absaugung. *Schr. dtsch. Akad. Luftfahrtf.*, 83:53, 1944. See also N.A.C.A. TM 1121 (1947). 29

J.L. van Ingen. A suggested semi-empirical method for the calculation of the boundary layer transition region. Technical Report VTH-74, Delft University of Technology, 1956a. iii, 8, 26

J.L. van Ingen. Een semi-empirisch methode voor de bepaling van de ligging van het omslaggebied van de grenslaag bij onsamendrukbare tweedimensionale stromingen. Technical Report VTH-71, Delft University of Technology, 1956b. iii

J.L. van Ingen. *Theoretical and Experimental Investigations of Incompressible Laminar Boundary Layers with and without Suction.* PhD thesis, Delft University of Technology, 1965. 3, 9, 16, 19, 26, 29, 31, 112, 121, 123

J.L. van Ingen. Transition, Pressure Gradient, Suction, Separation and Stability Theory. 1977. AGARD CP-224, Copenhagen. 9, 10

J.L. van Ingen. Transition, Pressure Gradient, Suction, Separation and Stability Theory. Januari 1978. Rand corp., Eds. William S. King and Mari Yokota. 9

J.L. van Ingen. Research on Laminar Separation Bubbles at Delft University of Technology. In V.V. Kozlov and A.D. Dovgal, editors, *Separated Flows and Jets*, 1990. IUTAM Symposium, Novosibirsk. 9

J.L. van Ingen. Prandtl Memorial Lecture. *Zeitschrift Angewandte Mathematik und Mechanik (Z.A.M.M.)*, 78:3–20, 1998. 2, 16

J.L. van Ingen. The eN method for transition prediction, Historical review of work at TU Delft. *AIAA*, 2008. AIAA-2008-3830. 35

A.R. Wazzan, C. Gazley Jr., and A.M.O. Smith. The $H - R_x$ method for predicting transition. *Rand Paper*, 1981. P-6581. xii, 14, 45, 48, 49

F.M. White. *Viscous Fluid Flow*. 2006. 3rd edition, McGraw-Hill. 3

K. Wieghardt. Zur Berechnung ebener und drehsymmetrischer Grenzschichten mit kontunuierlicher Absaugung. *Ing. Arch.*, 22:368, 1954. 26

F.J.M. Wubben, D.M. Passchier, and J.L. van Ingen. Experimental Investigation of Tollmien Schlichting Instability and Transition in Similar Boundary Layer Flow in an Adverse Pressure Gradient. In *Laminar-Turbulent Transition*, september 1989. IUTAM Symposium, Toulouse. 10